Final Report

THE DESIGN OF AN EXPERIMENT TO DETERMINE THE LIMITATIONS IMPOSED ON A MULTIPLE-APERTURE ANTENNA SYSTEM BY PROPAGATION PHENOMENA

Prepared for:

NATIONAL AERONAUTICS AND SPACE ADMINISTRATION
GODDARD SPACE FLIGHT CENTER
GREENBELT, MARYLAND

CONTRACT NAS 5-3974

STANFORD RESEARCH INSTITUTE

MENLO PARK, CALIFORNIA *SRI

STANFORD RESEARCH INSTITUTE
MENLO PARK, CALIFORNIA

June 1965

Final Report

THE DESIGN OF AN EXPERIMENT TO DETERMINE THE LIMITATIONS IMPOSED ON A MULTIPLE-APERTURE ANTENNA SYSTEM BY PROPAGATION PHENOMENA

Prepared for:

NATIONAL AERONAUTICS AND SPACE ADMINISTRATION
GODDARD SPACE FLIGHT CENTER
GREENBELT, MARYLAND

CONTRACT NAS 5-3974

Edited by: CHARLES H. DAWSON

SRI Project 5067

Approved: DEAN F. BABCOCK, MANAGER
RADIO SYSTEMS LABORATORY

D. R. SCHEUCH, EXECUTIVE DIRECTOR
ELECTRONICS AND RADIO SCIENCES

Copy No. 4

BLANK PAGE

ABSTRACT

Work on the design of an experiment to determine propagation limitations on multiple-aperture antennas is reported for the entire period of Contract NAS 5-3974. RF, meteorological, and ionospheric instrumentation, and a satellite-borne signal source are described. Data collection and processing are outlined and expected accuracies are estimated. The recommended instrumentation includes:

(1) A satellite in a 10-hour-period polar orbit capable of transmitting at 2, 4, 8, and 16 Gc with a power of at least 1 watt and preferably more. Only one frequency need be transmitted at a time unless separation of tropospheric and ionospheric effects is part of the experiment. The phase and amplitude stability of the transmissions is critical.

(2) Two or more antennas with diameters of 4 meters or more, with monopulse feeds and antenna-mounted preamplifiers. At least the error channel preamplifiers must be low noise.

(3) Two or more three-channel receivers with some special circuitry.

(4) Data conversion and multiplexing equipment with a tape recorder capable of 40 kilobits/second in computer-compatible format.

(5) Conventional meteorological instruments and preferably surface and airborne refractometers.

(6) A magnetometer to measure variations of the earth's magnetic field and possibly an ionosphere backscatter system.

Experiments on phase and angle-of-arrival fluctuations are of primary interest and importance to the design of an operational multiple-aperture array. Minor additions to the instrumentation for these two experiments are needed for the experiments on noise correlation and amplitude. Major additions are needed for the antenna-gain-vs.-size experiment, for the separation of ionospheric and tropospheric effects, and for the path bandwidth experiment.

Both partial and complete programs of meteorological and ionospheric data acquisition are described. The minimum meteorological program is fundamental to the determination of the usefulness of an operational multiple-aperture array. Complete omission of the meteorological program will greatly decrease the value of any results obtained from other portions of the experiment. However, the ionosphere is expected to be of minor significance.

The phase, angle-of-arrival, and meteorological experiments should be run and the resulting data analyzed before an operational multiple-aperture array is designed. The experimental site should be selected to provide a variety of meteorological conditions.

CONTENTS

ABSTRACT iii

LIST OF ILLUSTRATIONS ix

LIST OF TABLES xi

I INTRODUCTION 1

A. Purpose of Experiment 1

B. Format of Report 3

C. Personnel 3

II DESCRIPTION OF EXPERIMEN 5

A. General 5

B. RF Instrumentation 7

1. Phase, Amplitude, and Angle of Arrival 7
2. Noise 10

C. Meteorological Instrumentation 13

D. Ionospheric Instrumentation 14

E. Event Sequence for a Data Run 14

III DESCRIPTION OF EQUIPMENT 17

A. Signal Source and Platform 17

B. Antennas and Antenna Feeds 18

C. Antenna Pointing and Satellite Tracking System 20

1. General 20
2. Antenna Mounts 21
3. Drive System 23
4. Control System 25

a. Positioning System 25
b. Command Input 27
c. Closed-Loop Tracking 29

D. Antenna Configurations 31

E. Receiver Structure for Phase, Amplitude, and Angle-of-Arrival Measurements 34

CONTENTS (Continued)

1. Difference-Signal Demodulation 40
2. Amplitude and Phase Measurements 42
3. Recommended Measurements 44

F. Processing of Side-Band Signals 45

G. Noise and Boresighting Receiver 46

H. Meteorological Instrumentation 49

1. Introduction 49
2. Meteorological Data Acquisition 50

a. Refractometry 50
b. Measurement of Rain, Clouds, and Humidity . . . 51
c. Conventional Meteorological Instrumentation . . 52
d. Additional Instrumentation 53
e. Synopsis 54

3. Implementation of a Practical Observation Program 55

a. Minimum Program 57
b. Optimum Program 58
c. Ideal Program 58

I. Ionospheric Measurements 58

1. General 58
2. Recommendations 60

a. Minima Type Description 60
b. Ionospheric Classification 60
c. Magnetic Aspect Angle 62
d. Geomagnetic Storms and Other Disturbances . . . 62
e. Backscatter Measurements 63
f. Monitoring Measurements 64

J. On-Site Computer 65

IV EXPERIMENTAL SITE 67

A. Location 67

B. Layout 69

V DATA COLLECTION 71

A. RF--Phase, Amplitude, and Angle-of-Arrival Data 72

B. Noise Data 73

C. Meteorological Data 74

D. Ionospheric Data 75

E. Operator Data 75

CONTENTS (Continued)

VI DATA PROCESSING 77

A. Frequency and Phase 77

B. Angle of Arrival 78

1. General 78
2. Data Correction 78
3. Computed Orbit 80
4. Data Comparison 82

C. Amplitude 83

D. Noise 84

E. Correlation and Spectra 84

F. Meteorological Data 86

VII EXPECTED ACCURACIES 89

A. Phase and Amplitude 89

1. Discussion 89
2. Error Budget--Phase 92
3. Error Budget--Amplitude 93

B. Angle of Arrival 94

1. General 94
2. Nature of the Data 94
3. Measurement of Time 96
4. Measurement of Angle of Arrival 96

a. Measurement of Antenna Pointing Angle 97

1) Encoder Misalignment 97
2) Mount Misalignment 98
3) Antenna Sag 99
4) Antenna Warpage 99
5) Load Disturbances 100

b. Measurement of Pointing-Angle Error 101

5. Conclusion 103
6. Error Budget--Angle of Arrival 104

C. Noise 105

VIII SUMMARY 109

IX CONCLUSIONS AND RECOMMENDATIONS 113

CONTENTS (Concluded)

Appendix A	EFFECTS OF AIRCRAFT FLYING IN THE VICINITY	A-1
Appendix B	USE OF NATURAL RADIATORS AS SIGNAL SOURCES	B-1
Appendix C	PLATFORM MOTION CONSIDERATIONS	C-1
Appendix D	TIME IN VIEW	D-1
Appendix E	OSCILLATOR STABILITY LIMITATIONS, AND PHASE JITTER OF AN OSCILLATOR FEEDING A PHASE-LOCKED LOOP	E-1
Appendix F	MONOPULSE CONSIDERATIONS	F-1
Appendix G	NOISE CORRELATION	G-1
Appendix H	METEOROLOGICAL CONSIDERATIONS	H-1
Appendix I	IONOSPHERIC MEASUREMENTS	I-1
Appendix J	NOISE-INDUCED ERRORS	J-1
REFERENCES		R-1

ILLUSTRATIONS

Fig. 1	RF Instrumentation	9
Fig. 2	Noise Receiver	11
Fig. 3	Antenna Control System	25
Fig. 4	Antenna Positioning System	26
Fig. 5	Time-Quantization Error	28
Fig. 6	Closed-Loop Tracking	30
Fig. 7	Antenna Pattern in Elevation	39
Fig. 8	Demodulation of Difference Signal	41
Fig. 9	Amplitude and Phase Measurements	43
Fig. 10	Instrumentation Receiver Structure	44
Fig. 11	Site Layout for a Medium-Cost Experiment	70
Fig. 12	Angular Deviation from Azimuth Boresight--Sum and Difference Channels	79
Fig. 13	Angle-of-Arrival Deviations--Troposphere	95
Fig. 14	Angle-of-Arrival Deviations--Ionosphere	96
Fig. 15	Angular Deviation from Azimuth Boresight--Individual Channels	101
Fig. A-1	Propagation Paths	A-3
Fig. C-1	Path Geometry	C-9
Fig. C-2	Three-Path Processing	C-15
Fig. D-1	Satellite-Station Geometry	D-4
Fig. D-2	Intersection of Orbital and Tangent Planes for Various Values of θ	D-5
Fig. D-3	Solutions of $\cos\theta \sin\varphi + \tan\alpha \cos\varphi = \frac{r}{a \sin\alpha}$ for $r = 6371$, $a = 23{,}690$, $\alpha = 33.4^\circ$, and lines of $\Phi = 2.4(\theta - \theta_0)$	D-7
Fig. D-4	Time Above Horizon vs. θ_0	D-9
Fig. E-1	Oscillator Phase Spectra	E-9
Fig. G-1	Young's Interference Experiment	G-4
Fig. G-2	Visibility vs. Separation for a Circular Source	G-9

Fig. H-1	One-Way Degradation Due to Rain at 4 Mc and 10-Degree Elevation	H-5
Fig I-1	Geometric Considerations of Signal Fluctuation Character for Line-of-Sight Propagation Through an Ionospheric Layer	I-9
Fig. I-2	Propagation Zones for E-Region Blob Structure	I-10
Fig. I-3	Propagation Zones for F-Region Blob Structure	I-11
Fig. I-4	Trajectory Profile for Predicting Magnetic Aspect Angle: Typical Polar Circular Orbit Overhead, Altitude $\approx$ 17,000 km	I-15
Fig. I-5	Correlation of Signal Fluctuation Character at Space Frequencies	I-20
Fig. I-6	Correlation Between Amplitude and Phase Fluctuation Data	I-22
Fig. I-7	Power Spectra of Radio Star Scintillation	I-24
Fig. I-8	Typical Jonospheric Storm Record	I-34
Fig. J-1	Assumed Phase Autocorrelation Function	J-8
Fig. J-2	Noise-Induced Error Spectra, $\sigma_\varphi^2 = 1$	J-9
Fig. J-3	Noise-Induced Error Spectra, $f_\varphi/f_n = 1/4$	J-10

TABLES

Table	I	RF Equipment Requirements	8
Table	II	Typical Ionospheric Classification	61
Table	III	Phase Errors	92
Table	IV	Amplitude Errors	93
Table	V	Angle-of-Arrival Errors	103
Table	VI	ΔT in ^{o}K	105
Table	F-1	Sum Channel S/N	F-5
Table	I-1	Parameters Important to the Characterization of the Ionosphere	I-6
Table	I-2	Signal Fluctuation Character for Line-of-Sight Propagation Through an Ionospheric Layer	I-8
Table	I-3	Typical Telemetry Parameters	I-26
Table	I-4	Radar Parameters for Typical Backscatter Experiments	I-30

BLANK PAGE

I INTRODUCTION

This document reports on the work performed by Stanford Research Institute under Contract NAS 5-3974 during the entire contract period. SRI has studied the design of an experiment to determine propagation phenomena in the 1-to-20-Gc frequency range for a space-to-earth path.

A. Purpose of Experiment

The purpose of the proposed experiment is to obtain data from which the following can be determined for a space-to-earth propagation path using signals in the 1-to-20-Gc frequency range for a variety of meteorological and ionospheric conditions:

(1) The spectrum of the phase fluctuations received at a single antenna

(2) The space correlation of the phase fluctuations received at separated antennas

(3) The spectrum of the amplitude fluctuations received at a single antenna

(4) The space correlation of the amplitude fluctuations received at separated antennas

(5) The spectrum of the angle-of-arrival fluctuations received at a single antenna

(6) The space correlation of the angle-of-arrival fluctuations received at separated antennas

(7) The noise received at a single antenna

(8) The space correlation of noise received at separated antennas

(9) The variation of antenna gain with antenna diameter

(10) The bandwidth of the propagation path.

In order that the above characteristics can be later correlated with meteorological and ionospheric conditions, data must also be taken from which these conditions can be characterized.

Earlier studies (Refs. 1, 2, 3)* have shown that operation of an array of parabolic antennas is feasible under certain combinations of signal strength and path effects. This experiment will correlate path conditions and path effects and hence allow determination of those meteorological and ionospheric conditions and signal characteristics under which various possible modes of array operation are feasible.

An array of parabolic antennas will deliver its full equivalent aperture only if the phase-locked loops of the individual receivers are able to remain in lock. As the phase perturbations imposed by the propagation path increase, a greater loop bandwidth is required to allow the loop to track. This greater loop bandwidth increases the noise power and an increase in signal power is required to maintain the required signal-to-noise ratio. Thus, for a given signal power level, the array performance will be satisfactory only when the tropospheric and ionospheric phase perturbations are below a certain level. Since the correlated part of the phase perturbations can be handled by a separate, common phase-locked loop, the time and space correlation of phase under various tropospheric and ionospheric conditions must be determined.

Various modes of pointing control for the antennas of an array are discussed in Ref. 3. When monopulse control of each antenna is used, the error-angle channel bandwidths required increase with the angle-of-arrival perturbations induced by the troposphere and the ionosphere. When some antennas are slaved to other antennas, the degree to which angle-of-arrival perturbations are correlated in space becomes important. When open-loop control is used, the magnitude of angle-of-arrival perturbations is critical, particularly at the larger diameters and higher frequencies. Thus the time and space correlation of angle-of-arrival under various tropospheric and ionospheric conditions must also be determined.

The increased knowledge of path effects that is expected to result from this experiment should facilitate many of the decisions involved in

---

* References are listed at the end of the report.

the design of an operational array and should allow a minimum cost design consistent with the desired performance.

B. Format of Report

Section II describes the experiment in relatively general terms and discusses the effects on equipment requirements of decreasing the scope of the experiment. Section III describes the equipment requirements in greater detail. Section IV discusses the location of a desirable experimental site. Section V describes the data to be taken that the recording of such data. Section VI outlines data-processing procedures, and Sec. VII the accuracies that can be anticipated. Section VIII summarizes the study. Section IX contains conclusions and recommendations.

Appendices contain supporting and peripheral matter.

C. Personnel

Seven of SRI's engineering departments have contributed to this study. Footnotes have been used to credit the authors of particular sections of this report wherever possible. R. B. Battelle and J. H. Bryan have been primarily concerned with signal sources and platforms; W. H. Foy, Jr. and J. R. Woodbury with receivers; L. A. Robinson with noise correlation; E. C. Fraser with antenna drives and angle-of-arrival measurements; J. E. Alder, R. T. H. Collis, A. S. Dennis, and F. G. Fernald with meteorological instrumentation; and J. A. Martin with ionospheric instrumentation. M. Baron has served as a consultant; C. H. Dawson was Project Leader.

Table I

RF EQUIPMENT REQUIREMENTS

	Phase		Amplitude		Angle of Arrival		Noise		Antenna Gain	Path Bandwidth	Separation of Iono and Tropo Eff.
	Time Correlation	Space Correlation	Time Correlation	Space Correlation	Time Correlation	Space Correlation	Temperature	Space Correlation			
Receiver φ Stability	x	x									
Accurate Doppler Input	x	x									
Transmitter φ Stability	x										
Receiver Amplitude Stability			x	x							
Transmitter Amplitude Stability			x								
Wind Protection (Radomes)	x	x			x	x					
Accurate Satellite Angle Input					x	x					
Accurate Range-Rate Input	x	x									
Sidebands on Signal										x	
Reception at 2 frequencies											x
Reception at 2 antennas		x		x		x		x	x		
Antennas of Various Diameters									x		
φ-Measuring Receiver	x	x									
Amplitude Measuring Receiver			x	x							
Monopulse Capability					x	x					
Radiometer					x	x	x	x			
Low-Noise Preamplifier					x	x	x	x			

II DESCRIPTION OF EXPERIMENT

A. General*

The proposed experiment is expected to determine various parameters of the earth-to-space propagation path in the 1-to-20-Gc frequency range. Most of the quantities to be measured are small, and precision equipment is required. Data obtained from instrumentation less precise than that recommended herein or obtained without concurrent accurate and reasonably complete meteorological data will be essentially meaningless, and such an experiment cannot be recommended. On the other hand, if the scope of the experiment is reduced without any compromise of the remaining parts of the experiment, the data on those phenomena considered can still be meaningful. None the less, design of an operational array should not be undertaken until the full experiment has been performed.

A phase time-and-space-correlation experiment is of primary importance in determining the conditions under which a multiple-aperature array will be able to operate. Thus a phase and minimum meteorological experiment constitutes the most basic experiment. The measurement of time and space correlations of amplitude requires only minor additions to the receiver. Note that the antennas can be pointed open-loop for the phase and amplitude experiments, or a relatively simple monopulse system can be used.

The second and almost equally important parameter for the multiple-aperture array is the space correlation of the angle of arrival, since this will determine which of the several methods of array antenna pointing are feasible. The performance of this experiment requires monopulse feeds, precision pedestals, antenna protection, boresighting on radio stars, receiver angle-error channels, and a radiometer receiver. Since

---

* This section was prepared by C. H. Dawson.

the noise-induced errors must be kept small, either increased satellite power or low-noise preamplifiers may be required.

Addition of generally available ionospheric inputs plus some simple local measurements make possible the attempt to correlate the RF data with the ionospheric signatures as well as with the meteorological classes. However, the effect of the ionosphere is expected to be minimal at 2 Gc and entirely negligible at the higher frequencies. With the satellite transmitting on two frequencies simultaneously, with additional antenna feed complications, and with additional receiver channels, the contributions to phase, amplitude, and angle-of-arrival fluctuations by the troposphere and the ionosphere can be separated since these two contributions have different frequency dependence.

Although the space correlation of noise received by the antennas is expected to be very small (Ref. 2), once the angle-of-arrival experiment is implemented a noise correlation experiment requires only minor additions to the radiometer.

The path bandwidth experiment requires sideband transmissions by satellite, possibly increased preamplifier bandwidth, and some additions to the receivers.

Finally, the antenna gain experiment requires a variety of antenna diameters. Since an antenna of 4-meter diameter is considered to be a minimum for the other experiments, the added diameters will be larger and therefore appreciably more expensive.

In summary, before proceeding with the design of an operational array, the phase and angle-of-arrival measurements with at least a minimum meteorological program are essential. The amplitude and noise experiments are valuable and are available at little additional cost. The separation of ionospheric and tropospheric contributions, the path bandwidth determination, and the antenna gain determination are, however, peripheral and could be omitted. Omission of ionospheric data is probably also not serious.

B. RF Instrumentation

1. Phase, Amplitude, and Angle of Arrival*

Table I relates the RF equipment capabilities to the various desired experiment outputs. This table can be used to determine the resulting equipment changes corresponding to various reductions in the scope of the experiment--e.g., if antenna gain is not to be studied, all antennas can be of one size.

The experiment has been designed under the following assumptions:

(1) All data will be recorded in computer-compatible digital form on-line.

(2) All data reduction will be performed off-line.

(3) The phenomena of interest have no significant frequency components above 100 cps.

(4) The frequency components below 1 cps are not of particular importance in the operation of an antenna array, and their determination requires excessive run lengths.

(5) The 1-to-20-Gc frequency range will be adequately covered by experiments in the neighborhood of 2, 4, 8, and 16 Gc.

(6) A satellite source in a polar orbit with a period of 10 hours or more will be used.

(7) A signal-to-noise power ratio of at least 20 db will be available in an RF bandwidth of 200 cps without the use of low-noise preamplifiers.

(8) Boresighting on radio stars will be needed to calibrate the antenna pointing system for angle-of-arrival measurements.

(9) The essential highly accurate satellite pointing angles and range-rate will be furnished to the experimental site.

A block diagram of the RF instrumentation required for each antenna for receiving one carrier is shown in Fig. 1. If two frequencies are to be received simultaneously, all or part of this instrumentation must be duplicated.

---

* This section was prepared by C. H. Dawson.

BLANK PAGE

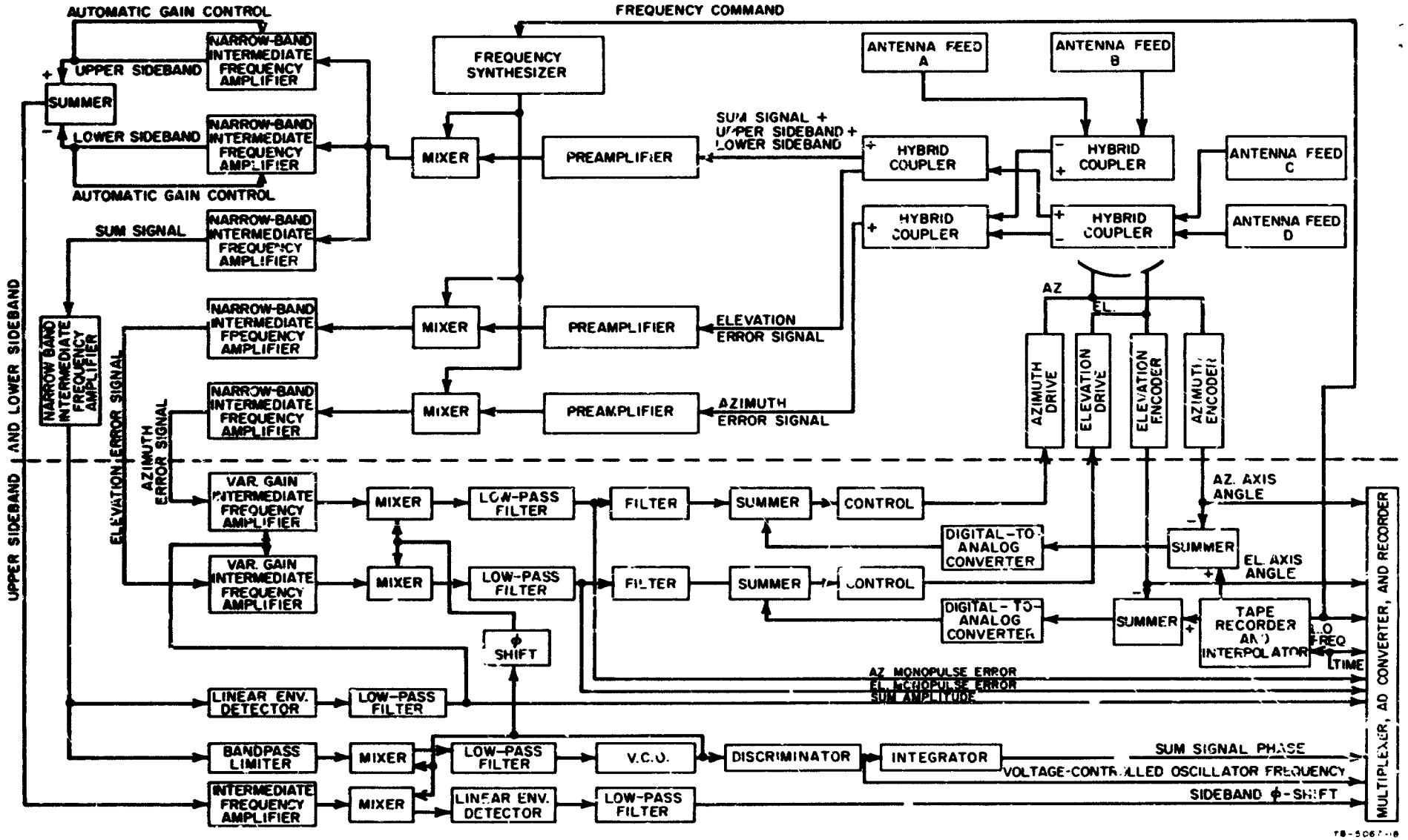

FIG. 1 RF INSTRUMENTATION

2. Noise*

Any source of radiated noise has some degree of coherence in at least two dimensions--time and angular direction. The extent of coherence in the time domain is related to the width of the frequency spectrum of the noise source. The extent to which the waveforms radiated in two different directions are coherent is related to the source size measured in wavelengths at the frequency of interest. The larger the size of a distributed source, the smaller is the angular region over which there is high coherence--i.e., the radiated waveforms are nearly identical as a function of time. It is this spatial coherence that is to be measured by the experiments described here. Specifically, with zero relative time delay between the noise waveforms received at two points on the earth, what fraction of the noise is correlated between the two channels? Uncorrelated noise will add as power at the summing junction of an array, but correlated noise adds as voltage and thus can degrade the signal-to-noise ratio of the system to a greater extent.

The experiment to determine the degree of correlation of the noise in the receiver channels of an antenna array is based on the measurement of the time average of the sum of the power output from two channels with the antennas receiving only noise (i.e., no signal from man-made sources). This time average is measured as a function of the relative phase shift introduced into one of the receiver channels. The time average is independent of the phase shift if the noise in the two channels is uncorrelated (statistically independent). The time average does vary with the phase shift if there is partial correlation of the two noise waveforms, since the correlated components add in phase and out of phase. In principle, the degree of correlation can be determined by simply observing the maximum and minimum values of the time average for many settings of the phase shifter. In practice, however, improved system resolution will be obtained by the use of a Ryle phase-switched receiver, an adaptation of which is outlined in Fig. 2. One

* This section was prepared by L. A. Robinson.

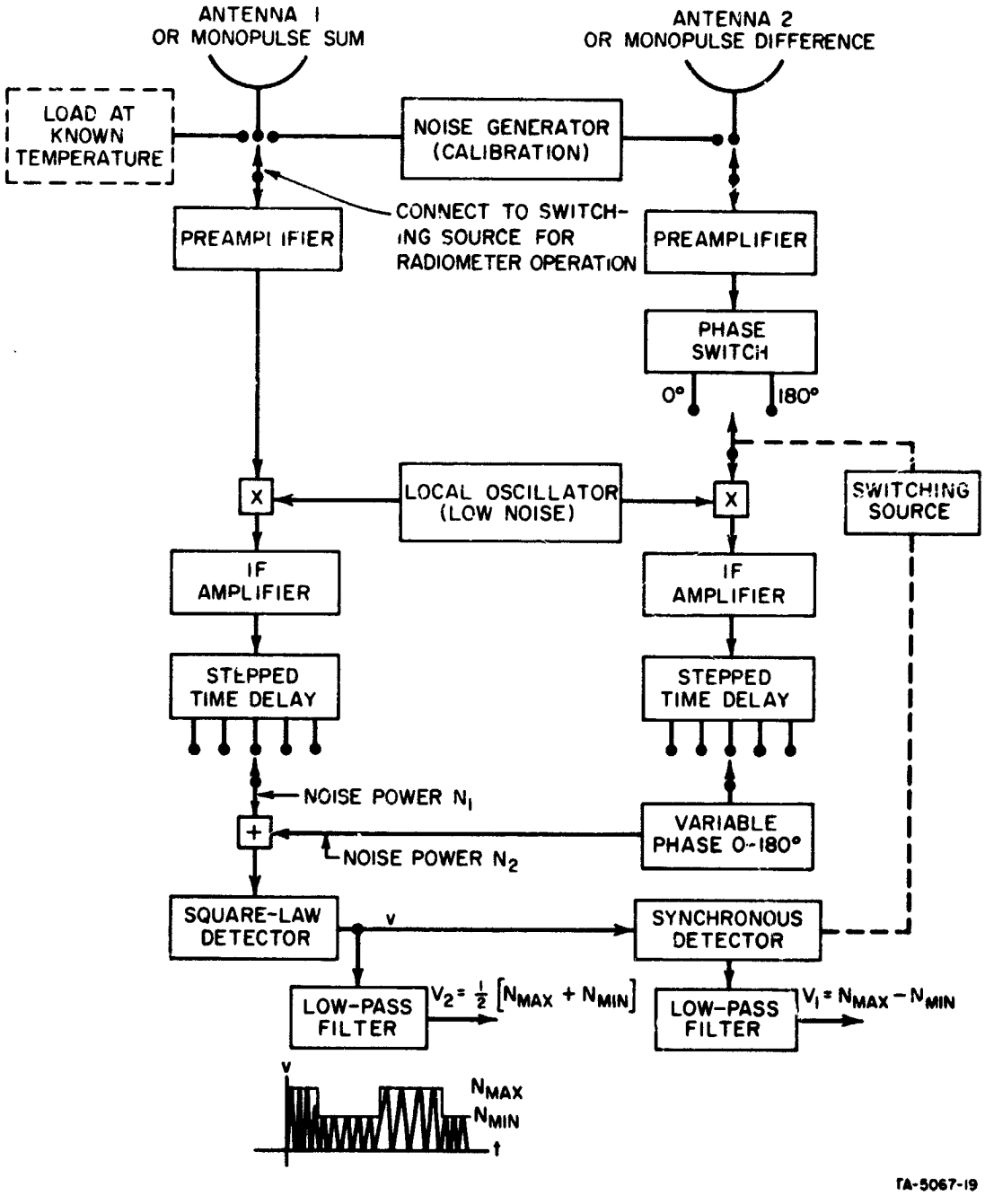

FIG. 2 NOISE RECEIVER

of the outputs of this receiver is directly proportional to the correlated component of noise power, as will be discussed in more detail in Sec. III-G.

The noise sources that might produce some degree of correlated noise in the channels of an array are those sources external to the array system, such as atmospheric-absorption, galactic, earth, and sun noise. For measurements on all but the last source, low-noise receiver front ends and low-spill-over-lobe antennas should be used to prevent these noise sources from obscuring small correlation of signals from the sources to be measured. Atmospheric-absorption noise should be measured at a frequency high in the 1-to-20-Gc range of interest, and with the antennas pointed a few degrees above the horizon (5 to 10 degrees), but pointed away from the galactic center and the sun. Galactic noise should be measured at a frequency low in the 1-to-20-Gc band of interest, and with the antennas pointed near the galactic center, but pointed away from the horizon and the sun. The earth noise should be measured with the two antennas pointed at a common area on the ground, and at any convenient frequency in the 1-to-20-Gc band. The sun noise should be measured with both antennas pointed at the sun. The sun noise is highest at the lower frequencies, but there will be sufficient sun noise at any frequency in the 1-to-20-Gc band. In interpreting the earth and sun data it should be recalled that this noise will normally be picked up in the antenna side lobes, and thus will be correspondingly lower than that measured in this experiment.

The degree of correlation of noise in the two channels due to each of the noise sources should be measured as a function of the separation between the antennas. The spacing should be varied from effectively side by side to about 1 km, to correspond with the range of spacings that might be expected to show correlation. In the case of the atmospheric-absorption noise, it might also be useful to measure the correlation as a function of the difference in pointing direction of the two antennas. Changing the relative pointing will change the volume of atmosphere seen in common by the antennas, and it is only in this common volume that correlated noise could arise.

The same basic receiver structure can also be used as a radiometer to measure noise power in a single channel and as an error-signal processor for boresighting on a radio star.

C. Meteorological Instrumentation*

The extent of the meteorological data to be collected will depend upon the funds available for this part of the multiple-array experiment. It should be stressed that atmospheric factors are determining factors in the feasibility of the proposed antenna system. Inadequate meteorological data will greatly reduce the value of the experiment. Due weight should be given this fact in designing the experiment, for without good meteorological data it will be difficult to assess the validity of the results in the actual experiment and impossible to extrapolate the results to other sites and conditions with any confidence.

The data to be collected can be grouped into (1) that absolutely required, (2) that extremely desirable, and (3) that which, while not absolutely essential, would result in a complete program from the radio meteorological viewpoint. The basic meteorological data requirements under these heads, therefore, would be:

Group 1--Surface temperature, pressure, humidity, wind, and precipitation. Upper-level temperature, pressure, humidity, and winds. The distribution of precipitation in the vicinity of the experiment from PPI and RHI radarscope photographs.

Group 2--A limited number of refractivity profiles (corrected for liquid water content) collected with airborne instruments. Surface refractometer data. Record of cloud cover by visual observations, or more preferably by use of photographic records.

Group 3--Record of the sky noise temperature recorded with a microwave radiometer. More extensive refractometer data--in particular, of conditions along the beam.

Group-1 data are routinely available or obtainable by special arrangement with the U.S. Weather Bureau or military meteorological

---

* This section was prepared by F. G. Fernald and R. T. H. Collis.

services, although additonal records would be desirable from the experiment site if the nearest Weather Bureau or military installation is more than a mile or so away. Group-2 data involves instrumentation specifically for the proposed experiment and represents only a modest investment, except for the airborne refractometry data which will be collected for only a limited number of selected runs. (For an experimental program of limited duration it is believed that much of the instrumentation--airborne and surface refractometers, for example--could be obtained on a loan basis.) The radiometer measurements of the Group-3 data are essentially already incorporated in the experiment, as the sky noise will be monitored (see Sec. II-B-2) and represents no additional meteorological instrumentation.

D. Ionospheric Instrumentation*

Although ionospheric factors are expected to have only minor effects on the experiment due to the frequency range involved, a large amount of information about the ionosphere is available from sources outside the proposed experiment when interpreted with experimental data required for other purposes. The use of such existing data represents the minimum ionospheric effort.

At the next level, variations in the local magnetic field can be determined by a magnetometer. The older instruments, using torsion-mounted bar magnets, are relatively inexpensive. Newer instruments utilizing nuclear magnetic moments offer increased precision.

Finally, a backscatter sounder at the experimental site could be used to give some direct information about the part of the ionosphere lying on the propagation path.

E. Event Sequence for a Data Run*

In the proposed experiment, there will be three distinct types of data runs. For Type I, the movable antenna and one of the fixed

---

* This section was prepared by C. H. Dawson.

antennas will be used, and space and time correlations of phase, amplitude, and angle of arrival will be determined. For Type II, two of the fixed antennas will be used, and gain as a function of antenna diameter and time correlation of phase, amplitude, and angle of arrival will be determined. For Type III, the movable antenna and one of the fixed antennas will be used, and the magnitude and the space correlation of noise will be determined.

The first step is to determine the type of run, the antennas to be used, the location of the movable antenna, the pass and elevation angle to be used, and the desired frequency or frequencies. These decisions must be documented.

The second step is to notify the satellite command station of the desired frequency or frequencies and the times the transmitter should be turned on and off.

The third step is to set the movable antenna at its selected location, select and install the appropriate antenna feeds and preamplifiers, and connect the appropriate cables. The antenna drive inputs required for satellite acquisition must be prepared.

The fourth step is to calibrate and check out all equipment and instruments to be used in the run. Note that ionospheric instrumentation and the satellite source are not required for Type III runs. The RF equipment checks must include delay measurements on the signal cables and on the cables distributing the local oscillator frequency.

The fifth step is to obtain the data required to characterize the state of the ionosphere, if such data are to be taken. Since the ionosphere probably changes rather slowly, this step can precede the RF data step by 10 to 20 minutes, except possibly near sunrise and sunset.

The sixth step is to obtain the data required to characterize the meteorological conditions, both in general and specific to the antenna-pointing angles to be used. This step can precede the RF data step by 15 to 30 minutes.

The seventh step is to record the following RF data for a period of 5 to 10 minutes (see Sec. II-B of Ref. 4): phase, amplitude, angle-of-arrival, and/or noise power.

The eighth step, in case of rapidly changing metorological conditions, might be a repetition of the sixth step. It might also be desirable to repeat the delay measurement phase of the fourth step.

The ninth step is to document the operators' and observers' comments on the run and the equipment performance. The presence of any aircraft in or near the antenna beam should be noted (see Appendix A).

The seventh step may be repeated several times in succession during a pass if data are desired at several elevation angles or if the experimental configuration can be changed rapidly enough to accommodate a new frequency or frequencies, a new spacing, an antenna of different diameter, or a change in Type from I to II or vice versa.

It is assumed that preventative maintenance procedures will be scheduled between data runs and that station time will be kept continuously, with periodic synchronization to external time signals.

III DESCRIPTION OF EQUIPMENT

A. Signal Source and Platform*

Although other possibilities were considered (see Appendices B and C), the only platform found suitable for the proposed experiment is a satellite. The orbital period (see Sec. II-A of Ref. 5 and Sec. II-A-2 of Ref. 6) should be 10 hours or more, so that the propagation path during a data run of 6 to 8 minutes will traverse relatively narrow regions of the troposphere and ionosphere. A polar orbit (see Appendix D) has been shown to have desirable time-in-view characteristics for the recommended experimental site. If the satellite is spin-stabilized along an axis perpendicular to the plane of the orbit, a set of dipole antennas can be constructed as a series of cylinders extending from the satellite along its spin axis; the 2-Gc dipole would be next to the satellite and would contain coaxial feeds to the other dipoles. Such an antenna would provide peak gain toward the center of the earth; the transmitted signal would be linearly polarized parallel to the satellite axis. However, the polarization of the received signal would depend on the aspect angle; therefore the receiving antennas should be circularly polarized.

The required transmitter frequencies are 2, 4, 8, and 16 Gc. If the path bandwidth experiment is performed, there must be coherent upper and lower sidebands separated from the carrier by 100 Mc. If separation of ionospheric and tropospheric effects is required, the satellite must transmit two carrier frequencies simultaneously.

The transmitter phase fluctuations in the 1-to-100-cps frequency range must have a small rms value; this can be accomplished by a crystal oscillator driving a phase-locked loop with a very small loop bandwidth (see Appendix E). If the loop bandwidth were set at 0.25 rad/sec, the rms phase variation would be 0.017 radians, but more importantly the bulk of this variation would lie in the very-low-frequency portion of

* This section was prepared by C. H. Dawson.

the spectrum. If, by the time of the experiment, even more stable sources are available, they should be used.

The stability of the amplitude of the transmitted signal is important in the amplitude experiment. If the received amplitude variations of 2% are to be measured, the transmitter stability should be at least 1% or 0.04 db over periods of 10 minutes or more.

Section II-A-2 of Ref. 6 shows that a minimum signal-to-noise power ratio of 30 db results when a dipole antenna is used on a satellite having a 10-hour period and a transmitter power of 1 watt. The receiver has an IF bandwidth of 200 cps and a noise temperature of 600°K; a 4-meter receiving antenna is used. Signal-to-noise ratios for other cases are easily determined.

Since receiver noise limits the accuracy of the phase and angle-of-arrival experiments, as much transmitted power and as low a receiver temperature as possible should be used. When sidebands or simultaneous transmission on two carrier frequencies are required, the satellite power must be increased accordingly.

B. Antennas and Antenna Feeds*

For the complete experiment, four sizes of parabolic antennas should be available: 4-, 8-, 16-, and 32-meter diameters. The surface accuracy must be compatible with 16-Gc operation. The design of an appropriate feed for a parabolic antenna is a complex subject. Several alternatives must be considered in such a design, including:

(1) The choice of focus-to-diameter (F/D) ratio and feedhorn separation to maximize either boresight sum-channel gain or difference-channel cross-over gain;

(2) The mechanical feedhorn structure-overlapping apertures with their associated complex combining circuits or non-overlapping apertures with the resulting large F/D and resulting low efficiency and high noise level;

* This section was prepared by C. H. Dawson.

(3) The possible use of the helical or tapped ring feed structures under development by Radiation Systems, Inc., Alexandria, Virginia, in place of the conventional horn structure.

It may be desirable to employ different feeds for each type of experiment. The particular feed best suited to the needs of a particular experiment would be used rather than a compromise design not optimum for any of the experiments. To facilitate the interchangeability of feeds for various experiments and frequencies, the same F/D ratio and the same feed mounting arrangements should be provided on all antennas. For 4- and 8-meter antennas, the blockage of a Cassegrain reflector would be severe but a strut-mounted feed should present no problem. For the larger antennas, the Cassegrain system may be preferable.

In order to prevent feed-horn motion which would affect the phase and angle-of-arrival experiments and wind-induced and temperature-gradient-induced shape distortions, which in turn would affect the angle-of-arrival experiment, radomes* are required. For the phase experiment alone, sufficiently rigid feed-horn mountings may suffice; however, radomes are mandatory for a meaningful angle-of-arrival experiment.

Because of the varying aspect angle of a satellite dipole antenna, the ground antennas must be equipped to receive circular polarization. Monopulse feeds (see Appendix F for details) must be available for the four carrier frequencies. If two carrier frequencies are to be received simultaneously, monopulse is required only at the lower frequency, and a single horn feed can be used for the higher frequency (see Sec. II-C of Ref. 4).

* For 4-meter antennas, rigid-foam construction can replace radomes.

C. Antenna Pointing and Satellite Tracking System*

1. General

The antennas suggested for use in this experiment consist of a set of parabolic reflectors, illuminated by either primary focus or Cassegrain feeds. Since such antennas have relatively narrow beams, it is important that the antenna be pointed accurately in the direction from which the signals of interest are arriving. During various aspects of the experiment, it will be desirable to operate the antennas in one of the following modes:

(1) Point one or more of the antennas in a given direction, the axes of the several beams being parallel.

(2) Point two or more antennas such that their beams intersect in a common volume of the atmosphere. This may be referred to as "squinting" of the beams.

(3) Point one or more antennas in such a way that their beams describe a particular path through the sky.

(4) Track, with one or more antennas, an active radio source aboard an artificial earth satellite. Such a satellite may have an altitude between 1000 and 24,000 km.

The first three of these modes indicate that the antennas must be capable of being accurately pointed in a given direction; while the fourth indicates that they must be capable of precision tracking as well. The remainder of this section is devoted to a discussion of the factors that must be considered in the design of antenna drive and control systems to satisfy these requirements. It is assumed throughout that the systems employed for each of the antennas are identical in that they accept the same form of command input, and produce output information in a common format. Adherence to this principle will provide complete flexibility in the selection of the combination of antennas to be used for a particular experiment.

---

* This section was prepared by E. C. Fraser.

2. Antenna Mounts

There are three mount configurations presently employed to support parabolic reflector antennas. These are: the azimuth-elevation mount (az-el), the x-y mount, and the equatorial mount. Each has its own unique advantages and disadvantages.

Equatorial mounts are not particularly well suited for tracking near-earth satellites where azimuth velocities can become fairly high, since the entire structure is moved in the azimuth plane. The equatorial mount is usually used for observing celestial sources, which move at sidereal rates.

The x-y mount is used in those instances in which it is essential to follow an object as it passes directly overhead. To date there have been very few x-y mounts built since their construction is quite expensive, requiring the very accurate machining of large structures.

The az-el mount is by far the most widely used mount. Since there have been a great number of this type built, considerable experience is available with the result that for a reflector of given size, the cost of an az-el mount will be less than that of the other two. In addition, the az-el configuration requires a relatively compact support structure (such as a truncated conical pedestal) which, it will be pointed out later, is advantageous for this experiment. One disadvantage of the az-el mount is that it is incapable of following an object that passes directly overhead. For the purposes of this experiment, however, this is not considered to be a serious shortcoming since the percentage of usable satellite passes directly overhead will be very small. It is therefore recommended that azimuth-elevation mounts be employed for the antennas to be used in this experiment.

At least one of the four-meter antennas should be made movable to permit correlation measurements over various baselines. Two possibilities exist for accomplishing this. First, the antenna* and pedestal can

---

* Rigid-foam construction rather than radomes is recommended for the movable 4-meter antennas.

be constructed on a track-mounted vehicle similar to a railroad flat car. The antenna could then be positioned anywhere along a set of rails, thus providing a continuous choice of baseline distance. However, unless several tracks and the ability to switch between them are provided, only one baseline orientation is provided by this technique. The alternative possibility is to determine those baseline distances and orientations most likely to yield meaningful data, and to construct a foundation at each of these points. The antenna and pedestal would then be designed with a special vehicle that could lift the entire unit and transport it from one foundation to another.

Inherent in any movable antenna system is the problem of leveling and alignment. This must be considered in each of the alternatives mentioned above. In the case of a track-mounted antenna, it cannot be assumed that the track and ballast provide a sufficiently firm footing to ensure proper leveling and alignment of the antenna. It will therefore be necessary to level and align (set the azimuth readout such that the reference direction coincides with true north) the antenna prior to each use. Spirit levels and optical surveying techniques can be used to accomplish this to within a few seconds of arc, but precision leveling and alignment can only be done by means of radio star tracks. This latter procedure is altogether too time-consuming to be considered as a routine procedure prior to each use of the antenna.

On the other hand, it is not unreasonable to expect that a properly prepared concrete foundation would maintain its positional stability over a long period of time. Hence, if a system of indexing pins and vernier position adjustments are provided, whereby the movable antenna would be positioned exactly the same way every time it is mounted on a particular foundation, then the antenna need be leveled and aligned only once for each of the foundations. This may take the form of either adjustments to correct for misalignments, or calibration curves, which are used to compensate the input and output data for that antenna.

On the basis of the relative simplicity of alignment, and a probable lower total cost, it is recommended that a variable baseline be achieved by means of a transportable four-meter antenna and pedestal, and a set

of permanently installed foundations located at the separation distances and orientations of interest. The extremely high pointing accuracy indicated here and elsewhere throughout this report is required for the angle-of-arrival experiment only. The other parts of the experiment do not require pointing accuracies of this order.

3. Drive Systems

Two alternative types of power sources are commonly used to drive large antennas--dc motors and hydraulic gear motors. The output torque of the dc motor is controlled by regulating its armature current, whereas the output torque of the hydraulic gear motor is controlled by regulating the pressure drop across the motor by means of a servo valve. Of the two, the dc motor is probably more convenient as it results in an all-electrical system. However, the hydraulic gear motor, which generates no RF noise, is more desirable for this experiment where very high signal-to-noise ratio must be achieved. In addition, a hydraulic system generally exhibits a wider bandwidth (25 to 30 cps), smoother low- and high-speed performance, and a greater torque-to-inertia ratio than a corresponding electrical system. For these reasons a hydraulic drive system is recommended.

The torque required of the drive system is the sum of the torques required to accelerate the antenna, counteract the effective wind torque, and overcome friction torques. Similarly, the output power required is the product of this torque and the required slewing speed. For a typical 60-foot reflector (Ref. 7) and a somewhat severe set of requirements, the following values are obtained:

Inertia	=	0.5×10^6 lb ft sec^2
Wind Torque	=	70,000 lb ft
Required Velocity	=	20 deg/sec = 0.35 rad/sec
Required Acceleration	=	5 deg/sec = 0.088 rad/sec
Friction Torque	=	2000 lb ft

Acceleration Torque = $J\alpha = 0.5 \times 10^6 \times 0.088$

= 44,000 lb ft

Total Torque = 44,000 + 70,000 + 2,000

= 116,000 lb ft

Power Required = TW = 116,000 X 0.35 X 1/550

= 74 horsepower.

Since these figures represent severe conditions, the values obtained represent upper bounds on the required power levels. These results would be correspondingly larger and smaller for larger and smaller reflectors.

Two major mechanical problems that affect the precision pointing and tracking capabilities of large antennas are gear backlash and static or coulomb friction. The first gives rise to small-amplitude, high-frequency limit-cycle oscillations about the equilibrium point while the second results in "cogging," motion in small steps rather than continuous motion when the antenna is being moved at slow speeds.

The problem of gear backlash can be eliminated by the use of a preloaded gear system. This may be done by employing two hydraulic motors each geared to the same bull gear. At zero velocity the motors produce equal but opposite torques, resulting in full gear-tooth loading but no net torque to the antenna. As the torque output of one motor is increased and the other is decreased, a net torque is provided to rotate the antenna while the gear-tooth loading is maintained constant. This constant gear tooth loading results in a zero backlash condition.

The problem of coulomb friction becomes significant for large, heavy antennas where the bearings are heavily loaded. There are at least two possible methods for alleviating this difficulty. The first is the use of very-low-friction bearings such as the hydrostatic bearing. A hydrostatic bearing has been successfully employed by North American on a 120-foot az-el mount for the Haystack Project. The Rohr Corporation has investigated the application of air bearings to the support of large antennas (Ref. 8). An alternative approach is the use of antenna reflectors that are constructed of a very light material, thus reducing

the loading on the bearings. An example of such construction is the rigid plastic foam reflectors* presently being built on an experimental basis by Sylvania Electronic Systems-West. These reflectors exhibit electrical and structural properties equal or superior to a comparable conventionally constructed reflector at considerably less weight and cost. The recommendation of a particular bearing system should be left to the antenna designer and should be based on a detailed structural analysis.

4. Control System

In order to satisfy the requirement that the antennas be capable of both accurate pointing and accurate tracking, and to facilitate the acquisition of signal sources, it is recommended that the control system be divided into two parts--a positioning system for accurately pointing the antenna, and a tracking system to supply corrected pointing information to the positioning system. This division is illustrated in Fig. 3.

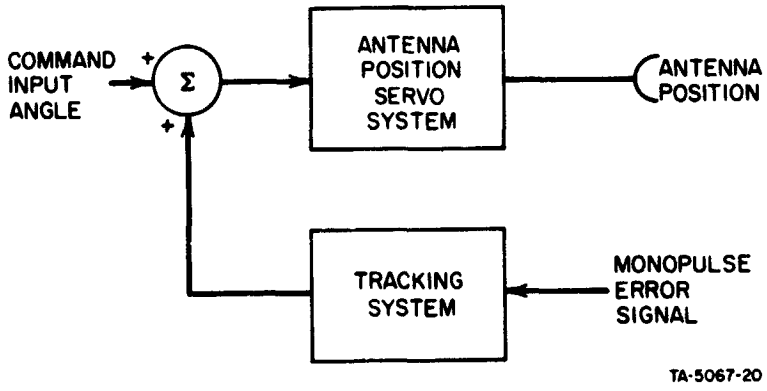

FIG. 3 ANTENNA CONTROL SYSTEM

a. Positioning System

To obtain the pointing accuracies required for this experiment it will be necessary that the antenna position servo system, which positions the antenna in response to a command input angle, employ

* See Appendix X of Ref. 3.

digital input and feedback information. Digital feedback information, indicating the actual pointing angles of the antenna, may be obtained by the use of digital shaft position encoders directly connected to the principal axes of the antenna. These encoders are available in digital word lengths up to 20 bits, thus providing an angular resolution and accuracy of 6 μr. As illustrated in Fig. 4, the digital angular position

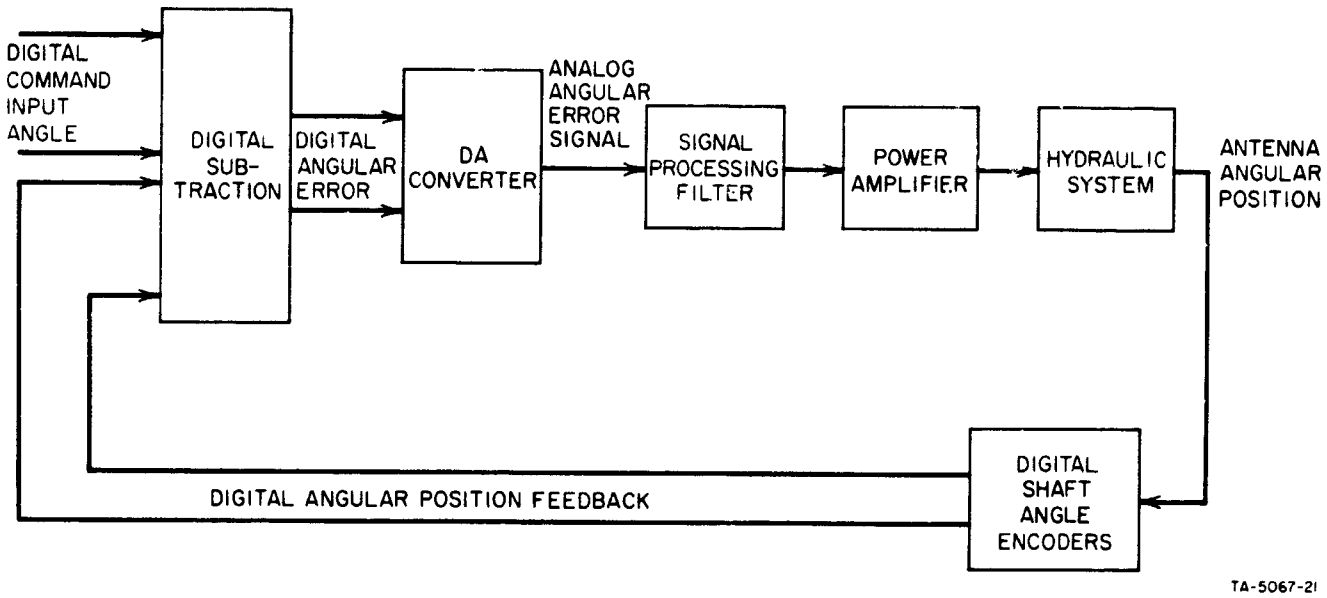

FIG. 4 ANTENNA POSITIONING SYSTEM

feedback signal is subtracted from the digital command input angle to produce a digital angular error. A digital-to-analog convertor is used to produce a signal proportional to the angular position error.

The angular error signal is applied, through a signal-processing filter, to the power amplifiers and hydraulic drive motors. The signal processing filter serves two purposes. First, it provides an integration of the input signal, which, together with the integration inherent in the hydraulic drive motors, causes the positioning system to behave as a Type II system. This insures that the positioning system will follow a constant position or constant velocity command input angle with zero steady state following error. The steady state following error for an accelerating input is a function of the system gain and bandwidth.

The second function of the signal-processing filter is to limit the bandwidth of the positioning servo system. This is necessary to prevent the inherently wide-bandwidth electronic and hydraulic systems from exciting the mechanical resonances of the antenna mount and reflector. Exciting these resonances would seriously impair the accuracy of the system and may cause structural damage as well. On the other hand, the bandwidth of the system should be maintained as high as practicable in order to minimize the effects of disturbances such as wind torques. The upper frequency limit of this filter will typically be about 0.1 to 0.5 cps for reflector diameters of 16 to 32 meters, and may be as high as 2 to 5 cps for reflector diameters of 4 meters.

b. Command Input

For manual pointing of the antenna, the digital command input angles may be readily obtained from a digital shaft position encoder driven by the operator's handwheel.

For programmed pointing of the antenna, the digital command input angles may be obtained either from a pre-prepared digital tape or directly from an on-site computer. In either case, the command input angles must be synchronized with the station time standard. For the reading of prepared tape this may be accomplished by using the time standard to generate read command pulses. In the case of a digital computer the station time can be used to pace the program.

The rate at which updated command input angles are supplied to the antenna positioning system is limited by the speed of the digital tape unit or computer being used. Several currently available photoelectric punched paper tape readers and several digital magnetic tape readers are capable of delivering at least 100 points per second. (This assumes that a point consists of three 20-bit words: one for azimuth pointing angle, one for elevation pointing angle, and one for the calculated Doppler frequency. This latter information is required for setting the local oscillator frequency. Most of the presently available digital computers would also be capable of computing updated input

information at at least this rate. To evaluate the suitability of this input rate, consider the following worst-case situation:

Antenna diameter	=	32 m
Operating frequency	=	16 Gc
Effective beamwidth (3 db)	=	1.33 mr
Satellite altitude	=	1000 km
Satellite zenith angle	=	85°
Maximum angular rate of change	=	84.4 mr/sec (azimuth).

At a sample rate of 100 points per second, and at this maximum rate of change, each input command angle differs from the previous one by 0.845 mr. As a result the input command angle differs from the previous one by 0.845 mr. As a result the input command angle contains a maximum time quantization error as shown in Fig. 5

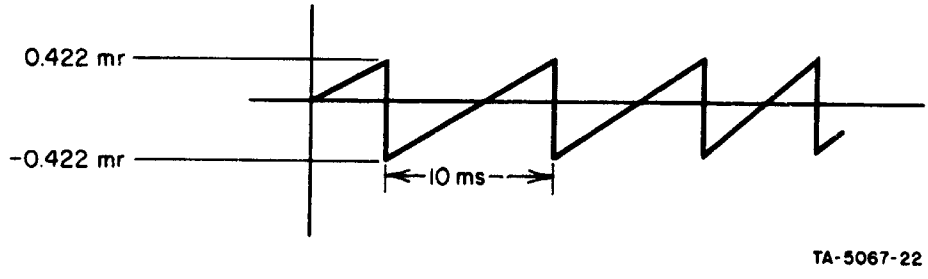

FIG. 5 TIME-QUANTIZATION ERROR

The fundamental (100 cps) Fourier component of a signal of this nature has a peak value of 0.36 mr. Since the bandwidth of the antenna positioning system for a 32-meter reflector is certainly no greater than 1 cps, the system response to an input of this frequency will be attenuated by a factor of at least 100. (This assumes that the attenuation characteristics of the system beyond its cutoff are those of a first-order filter. This assumption is certainly conservative.) The higher harmonics will experience correspondingly greater attenuations. The result is that an input error component as large as that shown in Fig. 5 can be expected to produce an antenna beam position

disturbance no greater than 3.3 μr. This quantity is entirely negligible when compared to the 1.33-mr antenna beamwidth.

The conclusion that may be reached is that, even under very severe conditions, a command input rate not greater than 100 points per second results in negligible pointing error due to quantization. This data rate is well within the capabilities of presently available digital equipment. For satellites in higher orbits or with lower zenith angles, or for smaller antennas operating at lower frequencies, this rate could conceivably be reduced to as low as 1 to 10 points per second without materially affecting performance.

c. Closed-Loop Tracking

In the previous section it was assumed that the antenna is pointed solely on the basis of predicted signal source positions. For many portions of the experiment, closed-loop signal-source position tracking will be possible. For this purpose a monopulse feed structure is used to illuminate the antenna reflector. This feed structure, together with its associated electronics, develops two signals that are proportional to the azimuth and elevation components of the offset angle between a line to the signal source and the electrical axis of the antenna. For closed-loop tracking these signals are used to correct the antenna pointing angles and thus to eliminate any pointing errors.

The specific configuration recommended for implementing closed-loop tracking is shown in Fig. 6. (The figure shows the configuration for azimuth only. The elevation channel is identical.) This configuration exhibits several desirable properties. First, the system does not depend exclusively on feedback information for tracking but uses this information only to compensate for the difference between the observed position of the signal source and the predicted positions being used as the command inputs. The result is that short-term disruptions of the received signal will not seriously affect the continuity of tracking. A second property is the automatic acquisition of the signal source. Before any pointing-angle feedback is available the antenna will follow the predicted position of the signal source exactly.

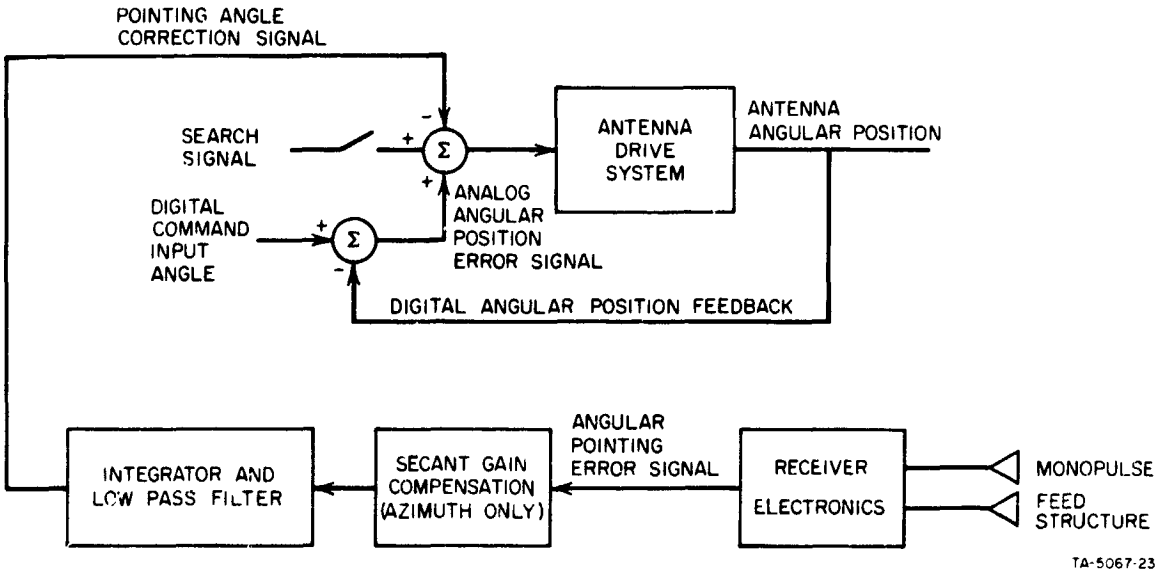

FIG. 6 CLOSED-LOOP TRACKING

As soon as the source is acquired, sufficient correction signal will automatically be generated to eliminate any pointing error that may exist. This is done without any deliberate change in the mode of the system operation. In the case of large-diameter reflectors operating at high frequencies, with their correspondingly narrow beam patterns, the situation may arise in which the predicted pointing angles are not sufficiently accurate to insure that the signal source will be located within the antenna beam. In this event it will be necessary to insert a search signal into the system, that causes the antenna beam to oscillate about the predicted source trajectory. Once acquisition has been effected, this search signal would be disconnected.

Referring to Fig. 6, the "Secant Gain Compensation" block shown must be included to compensate for the effective decrease in azimuth pointing error sensitivity with increasing elevation. To compensate for this, a variable gain element, whose gain is proportional to the secant of the antenna elevation angle, is included in the azimuth channel. The integrator serves to ensure that the steady-state pointing error due to bias errors and very-low-frequency effects such as prediction errors, dish and feed structure sag, and uncompensated steady-state effects of the atmosphere are reduced to essentially zero. The low-pass

filter is included to reduce the effective bandwidth of the pointing-error feedback channel from the 100-cps bandwidth of the receiver electronics. Doing so will reduce the disturbing effects of the receiver noise and enhance the signal-to-noise ratio of the feedback channel. In instances where the received signal-to noise ratio is very low, and the source is moving at very low angular rates (i.e., a high satellite or a celestial source), the upper frequency cutoff of this filter may need to be set considerably lower than the bandwidth of the antenna positioning system in order to obtain reasonably smooth tracking. It has been suggested (Ref. 7) that this filter be made adjustable and its cutoff frequency set for each tracking operation on the basis of expected angular rates and signal-to-noise ratios.

D. Antenna Configurations*

The proposed experiment involves the determination of (1) the space correlation of signal phase, amplitude, and angle-of-arrival (2) the space correlation of noise, and (3) the variation of antenna gain with diameter. Purpose 3 clearly requires the use of several different antenna sizes; small separations would increase confidence that the same signal was being received at all the antennas. However, larger separations should not greatly affect the results. Conversely, Purpose 1 would be more easily implemented using several antennas of a single size and will require a variety of effective separations. Since larger antennas will not receive the higher-frequency components of the phase, amplitude, and angle-of-arrival fluctuations, the upper frequency of spectrum measurements will be limited by the size of the largest antenna in use.

Thus Purposes 1 and 3 are basically incompatible and require essentially distinct sets of antennas. However, the smallest antenna certainly can be used for both purposes.

The effective separations for Purposes 1 and 2 should vary from the minimum consistent with negligible blockage of one antenna by

---

* This section was prepared by C. H. Dawson.

another* to a maximum in excess of the correlation distance† of the tropospheric effects; a 1000-meter maximum should be satisfactory (see Ref. 3). However, the correlation distance will frequently be less than 200 meters and the acquisition of data at effective separations of 200 meters or less should be emphasized.

The desired variations in effective separation can be obtained by using fixed antenna locations and depending entirely on the azimuth and elevation angle variations existing during the same or different satellite passes. This effect of various satellite angles will always be present, but more flexibility will be provided when the available antennas can be moved to secure different physical separations.

There are two distinct methods of providing movable antennas: either several pads can be provided at predetermined separations or an antenna can be used at any point along some track on which it can be moved. If pads are provided, alignment of the antenna is facilitated, but there are only a relatively small number of separations possible. If a rail system is used, alignment becomes relatively more difficult and time-consuming but any separation within the system's limits can be obtained.

The use of fixed antennas or of pads allows permanent installation§ of cables to carry incoming signals to the receiver house and control signals to the antenna; when pads are used, cables at an unused pad may be patched through to a more distant pad that is in use. When an antenna is moved along a track, the cabling cannot be permanently installed and, in fact, microwave links may be a more suitable solution.

---

* The experiment could be easily adapted to explore blocking.

† Perturbations experienced by two paths separated by this distance are essentially uncorrelated.

§ It may be desirable to bury cables to minimize the temperature variation to which they are subjected.

In the following it will be assumed that:

(1) No more than two antennas will ever be used simultaneously.

(2) Four-meter-diameter rigid-form antennas will be standard.

(3) Eight-meter-diameter antennas will cause only negligible low-pass effects.

(4) The cost of facilities to move an antenna between pads will be appreciably less than the cost of the antenna.

(5) The cost of pads will be much less than that of a rail system which, in turn, will still be less than that of an antenna.

(6) Only 4-meter antennas will be moved from pad to pad or along a rail system.

The minimum installation would then consist of two, fixed 4-meter antennas. No gain data (Type 3 experiment) would be obtained. A baseline of 200 meters would provide effective separations in the range of principal interest; correlations for effective separations above 200 meters could not be obtained. At moderate additional cost, one 4-meter and one 8-meter antenna could be used to give limited gain data.

A fixed 4- or 8-meter antenna and a 4-meter antenna used at either of two preset pads could provide separations of, say, 200 and 1,000 meters. If three pads were used and both 4-meter antennas were movable, separations of 200, 800, and 1,000 meters along a straight line would be available.

Still at costs near the minimum, a fixed 8-meter antenna and a pad-mounted 4-meter antenna for separations of 50, 100, 250, and 500 meters would provide nearly all desirable effective separations and very limited gain data. This is the recommended configuration in the low-cost range.

In the medium-cost bracket, the recommendation is fixed 8- and 16-meter antennas at the ends of a 1,000-meter baseline with a rail-mounted 4-meter antenna to run from 20 to 500 meters from the 8-meter antenna along the baseline. Alternatively, the 4-meter antenna could be moved between pads located 30, 60, 120, 240, and 480 meters from the 8-meter antenna (see Fig. 11). When the 16-meter antenna is used, some

loss of high-frequency detail could be expected; however, the 16-meter antenna would be used only for separations in excess of 500 meters where only the lower-frequency components of the fluctuations would be expected to correlate. If this baseline were located approximately along the east-west direction and the satellite were in a polar orbit, the effective separation would approximate the actual separation for a portion of every satellite pass.

If complete antenna gain data is to be obtained, a 32-meter antenna would be added to the configuration described above. Since the loss of high-frequency detail at this diameter would not be negligible, it could not be used except for the gain studies and its location would be determined entirely by convenience.

A configuration to provide complete flexibility would consist of a cluster of fixed 4-, 8-, 16-, and 32-meter antennas at the minimum separations to avoid blockage, and a rail-mounted 4-meter antenna capable of motion in either of two orthogonal directions with respect to the cluster out to distances approaching 250 meters on one leg and 1,000 meters on the second leg.

Fixed and pad-mounted movable antennas will, at least initially, require boresighting, while rail-mounted antennas will require boresighting after each move. If suitable receiver configurations are available, strong radio stars could be used. Alternatively, a boresight tower can be used. Unless this tower can be demounted, its presence will raise the possibility of multipath reception for certain satellite positions. The towers proposed for meteorological instrumentation must also be considered potential sources of multipath.

E. Receiver Structure for Phase, Amplitude, and Angle-of-Arrival Measurements*

The purpose of the receiver channels in this experiment is to take the signals from an antenna and to develop voltage measurements of the amplitude fluctuations, phase fluctuations, and angle-of-arrival

* This section was prepared by W. H. Foy.

fluctuations induced by the atmosphere. These measurements should be independent, and the effects of noise should be minimized. The channels must accomplish a frequency translation of the signals from RF (1 to 20 Gc) down to workable IF range (around 100 Mc), and must amplify them to reasonable analog voltage levels. It was concluded, in order to reduce the digital data-processing load, that analog operations should perform as much of the data-processing as possible consistent with measurement accuracy; the signals should be demodulated prior to conversion from analog to digital form.

Previous studies[3] indicate that the maximum bandwidth of the fluctuations of interest here is about 100 cps, so this value will be used in the following discussion when channel bandwidths and data-sampling rates need to be considered.

The initial step in receiver channel design is to choose an antenna pickup ("feed") configuration, the basic criterion being the need to develop angle-of-arrival indications. It is proposed that an "amplitude monopulse" structure be used; this consists of four pickup horns mounted in the focal plane of the antenna. The signals from the individual horns are summed in pairs and then both summed and differenced, as shown in Fig. 1, to yield a sum signal and two orthogonal difference signals. We assume that the pickup patterns are identical except for offset angles, so the resulting sum signal is insensitive (to first order) to angles-of-arrival, and by synchronous demodulation the effects of phase fluctuations do not appear in the demodulated difference signals. This configuration thus offers the possibility of measurement separation. Other antenna structures and configurations were also considered for this application. For instance, a single pickup head in conical scan could replace the amplitude-monopulse pickups. However, conical scan gives (roughly) one angle sample per scan cycle. Our maximum bandwidth of about 100 cps for angle fluctuations implies that the scan rate must be about 200 rev/sec which seems impracticably high. Another technique involves the use of two single-pickup antennas located some distance apart (i.e., the interferometer or the phase-comparison monopulse methods).

However, the signals from the two antennas will have experienced slightly different paths and time delays, so we could find no way (neither by mixing nor by differencing) to separate any of the effects of interest here, even to first order. In short, the amplitude-comparison antenna offered the only significant separation of measurements we could find, and so we rejected the other configurations from further consideration.

The next tasks of the receiver are voltage amplification and frequency translation. Conventional methods should be adequate--each channel would consist of a microwave preamplifier, a mixer with a local oscillator signal common to all channels, and a band-pass IF amplifier. It will be useful to eliminate the Doppler frequencies and the predictable transmitter frequency variations, so the first mixer reference should be a signal of frequency

$$\omega_4 = \left\{\omega_o + \hat{\omega}_1\right\}\left\{1 - \frac{\hat{\dot{r}}}{c}\right\} + \omega_5$$

where

ω_o = Average (constant) transmitter frequency (assumed known)

$\hat{\omega}_1$ = Predicted transmitter frequency drift

$\hat{\dot{r}}$ = Predicted range rate

c = Velocity of light

ω_5 = IF frequency.

It will be assumed that the prediction errors (e.g., difference between $\hat{\dot{r}}$ and the true range rate at any time) are small enough for the expressions to be linearized. The sum and two difference signals out of the IF amplifiers of their respective channels (see Fig. 1), can now be written as follows:

$$\begin{aligned}
\Sigma(t) &= A_s \cos(\omega_5 t + \varphi) + n_s \\
\Delta_A(t) &= A_A \cos(\omega_5 t + \varphi + \varphi_{\Delta A}) + n_{\Delta A} \qquad (1) \\
\Delta_E(t) &= A_E \cos(\omega_5 t + \varphi + \varphi_{\Delta E}) + n_{\Delta E} .
\end{aligned}$$

In these we have assumed that the amplitude-monopulse pickups are located at the focal plane of the antenna and the patterns of the individual pickups are identical; the difference signals will then be in phase (i.e., no quadrature components) with the sum signal, so $\varphi_{\Delta A}$ and $\varphi_{\Delta E}$ are the phase angles of the difference channels as compared with the sum channel; φ is the received phase. Further, we can write

$$
\begin{aligned}
A_s &= a_o A_p \qquad\qquad A_p \simeq A_t K_o (1 + k_a + k_p) \\
A_A &= A_p b_{oA} (\psi_{aA} + \alpha_{pA} - \alpha_{eA}) \\
A_E &= A_p b_{oE} (\psi_{aE} + \alpha_{pE} - \alpha_{eE}) \qquad (2) \\
\varphi &\simeq \theta_o + \int dt \left(\frac{\omega_o}{c} \dot{d} + \hat{\omega}_\Delta + \frac{\omega_o}{c} \hat{\dot{r}}_\Delta \right)
\end{aligned}
$$

where

A_p = Amplitude of the received signal at one pickup for arrival along the main-lobe axis

A_t = Average amplitude of the transmitted signal

K_o = Average path gain

k_a = $k_a(t)$ = Fractional fluctuations of transmitter signal amplitude

k_p = $k_p(t)$ = Fractional fluctuations of path gain

a_o = Voltage gain of the summing hybrids with respect to one pickup

b_{oA}, b_{oE} = Voltage-per-unit-angle gain of the differencing hybrids with respect to one pickup

ψ_{aA}, ψ_{aE} = Average angles-of-arrival measured with respect to an earth-fixed reference

α_{pA}, α_{pE} = $\alpha_{pA}(t)$, $\alpha_{pE}(t)$ = Angle-of-arrival fluctuations induced by the atmosphere path

α_{eA}, α_{eE} = $\alpha_{eA}(t)$, $\alpha_{eE}(t)$ = Antenna Position angle errors

θ_o = $\theta_o(t)$ = Phase fluctuations of the transmitter

$\int dt \frac{\omega_o}{c} \dot{d}$ = Phase fluctuations induced by the atmospheric path

$\hat{\omega}_\Delta = \hat{\omega}_\Delta(t)$ = Transmitted frequency prediction error

$\hat{\dot{r}}_\Delta = \hat{\dot{r}}_\Delta(t)$ = Range-rate prediction error.

$\dot{d}$ = Rate of change of electrical path length.

The angles may be visualized more readily by referring to Fig. 7, which shows the elevation pattern. The fluctuation and error quantities are assumed to be small. No channel gains have been written into these expressions; we shall reference the powers of the noise terms [n_s, $n_{\Delta A}$, and $n_{\Delta E}$ in Eqs. (1)] to the preamplifier inputs and therefore will be able to neglect the channel gains. Since the channel operations as far as the IF outputs are nearly linear, we can take n_s, $n_{\Delta A}$, and $n_{\Delta E}$ to have power-density spectra determined by the filter shapes of the IF amplifiers. The three noise terms will be somewhat correlated if external noise is significant compared to receiver noise, but we shall make the assumption that they are statistically independent. Quantities that will be useful in what follows are the ratio of maximum available ($a_o = 4$) sum-channel signal power to sum-channel noise power,

$$\eta_s = \frac{\langle 4A_p \rangle^2}{2\langle n_s^2 \rangle} = \frac{(4A_t K_o)^2}{2\langle n_s^2 \rangle}$$

and the similar ratio to a difference channel noise,

$$\eta_{\Delta A} = \frac{\langle 4A_p \rangle^2}{2\langle n_{\Delta A}^2 \rangle} \qquad \eta_{\Delta E} = \frac{\langle 4A_p \rangle^2}{2\langle n_{\Delta E}^2 \rangle} \quad .$$

The $\langle\ \rangle$ brackets indicate an average. In the following discussion only one difference signal will be considered; demodulation of the other will be identical. Note that the quantities in Eqs. (2) that the experiment is intended to measure, are $K_o\,[1 + k_p(t)]$, $\alpha_{pA}(t)$, $\alpha_{pE}(t)$, and $\int dt\, \frac{\omega_o}{c}\, \dot{d}$. In order to get these we must develop measurements of sum-signal amplitude, difference-signal amplitudes, and sum-signal phase.

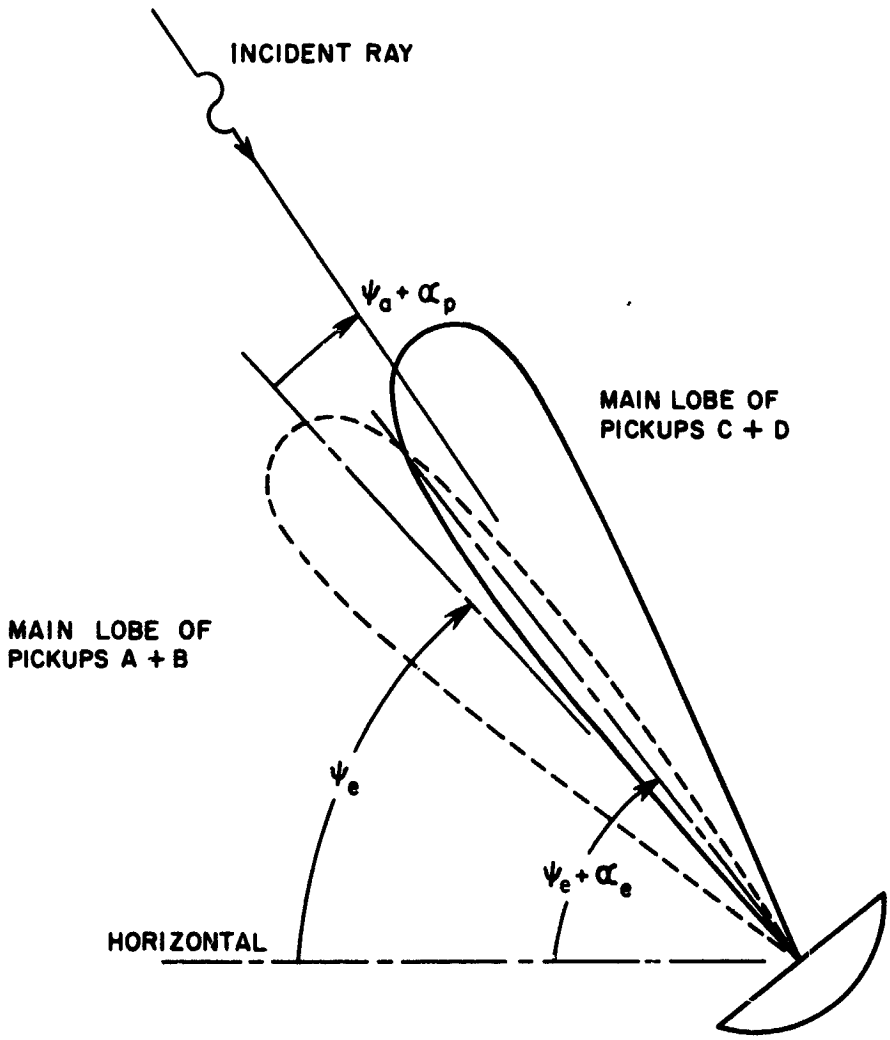

ψ_e = COMMANDED ANTENNA ELEVATION ANGLE

α_e = VARIATION OF ANTENNA ELEVATION ANGLE FROM ψ_e

ψ_a = AVERACE ANGLE SHIFT OF INCIDENT RAY FROM ψ_e

α_p = ANGLE-OF-ARRIVAL FLUCTUATIC .S

RA-5067-3

FIG. 7 ANTENNA PATTERN IN ELEVATION

1. Difference-Signal Demodulation

A natural step is to use the sum signal as reference for coherent demodulation of the difference signal. This requires removal of the amplitude fluctuations of $\Sigma(t)$, which conceivably could be accomplished by hard-limiting, fast automatic gain control, a phase-locked loop, or some combination of these. Figure 8 shows block diagrams of the hard-limiter and phase-locked loop methods. A phase-locked loop has the desirable properties of being able to deliver out of its voltage-controlled oscillator (VCO) a wave of constant amplitude with some of the phase-noise cleaned off the incoming signal; it exhibits, for good signal-to-noise ratios, a very desirable nonlinear lock-on effect. The loop, however, suffers from the fact that its effective closed-loop bandwidth is a function of input signal strength. As several authors have noted, this latter disadvantage will be removed if the loop is preceded by a hard band-pass limiter which will remove most of the envelope variations. This combination should be superior in performance to either method alone. Normalization of the $\Sigma(t)$ amplitude by use of fast AGC was also considered; a cursory examination suggested that this might introduce undesirable signal-noise product terms and that the hardware requirements might exceed those of a band-pass limiter, but no firm conclusions could be drawn. This should be considered an alternate and competitive method to the use of a hard limiter. With either structure the reference signal for the mixer with $\Delta(t)$ as input in Fig. 8 will be of the form

$$V_s = \cos(\omega_5 t + \varphi + \varphi_{ns}) \tag{3}$$

where

$\varphi_{ns} = \varphi_{ns}(t; n_s, a_o)$ = phase variations induced by the effect of noise n_s on $\Sigma(t)$

and so the result of difference-signal demodulation will be an output

$$\psi_m(t) = \frac{1}{2} A_p b_o (\psi_a + \alpha_p - \alpha_e) \cos(\varphi_\Delta - \varphi_{ns}) + n'_\Delta \tag{4}$$

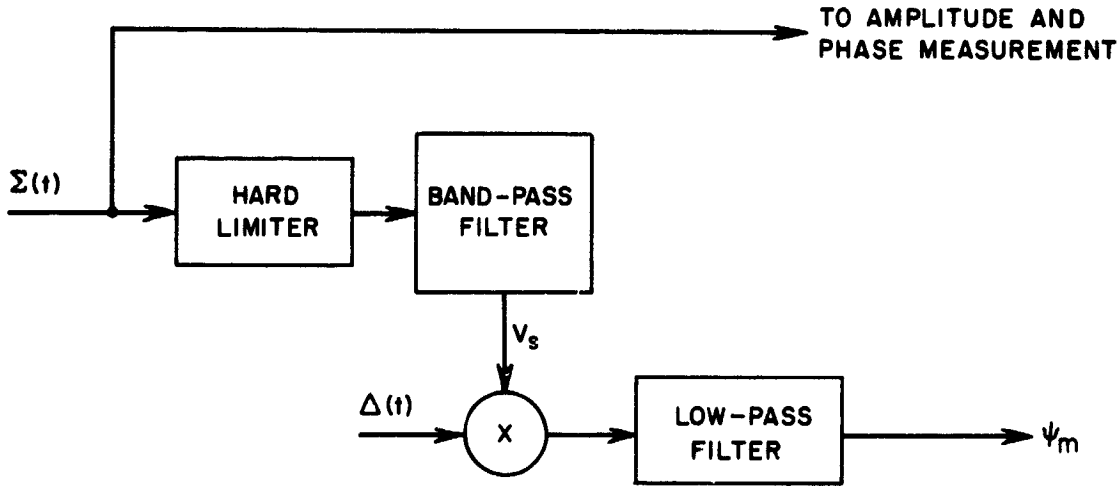

(a) LIMITER METHOD

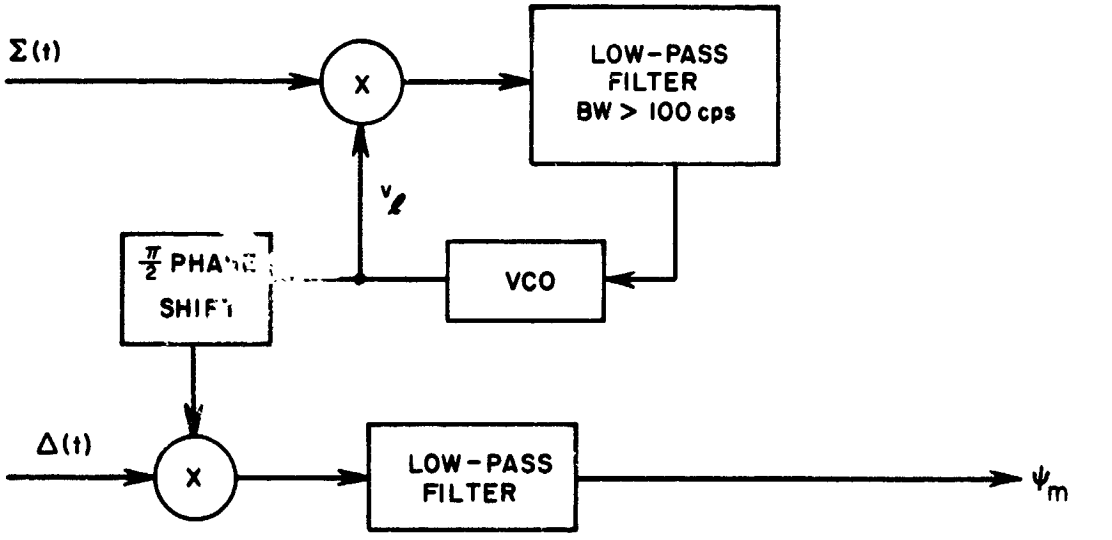

(b) PHASE-LOCKED LOOP METHOD

RA-5067-2

FIG. 8 DEMODULATION OF DIFFERENCE SIGNAL

with n'_Δ the result of mixing noise $n_\Delta(t)$ with the reference signal V_s. The dc voltage $\psi_m(t)$ has the phase fluctuations $\varphi(t)$ eliminated; it only remains to eliminate the amplitude fluctuations A_p in order to obtain an angle-of-arrival measurement.

2. Amplitude and Phase Measurements

The most direct method of extracting the amplitude fluctuations and the phase fluctuations from the sum signal is to use a conventional nonsynchronous envelope detector and a phase detector. Again, the amplitude fluctuations should be removed prior to phase detection. Figure 9(a) illustrates this technique, where for phase detection reference a signal of known frequency ω_5 and set phase φ_r is used.

A second possibility involves use of a phase-locked loop. The output of the phase-locked voltage-controlled oscillator will supply a useful reference signal with which the envelope of $\Sigma(t)$ can be synchronously demodulated. This method is illustrated in Fig. 9(b). An analysis was made of the effects of sun-channel noise, n_s, on these measurements. It indicated that the noise-induced error on the envelope measurement with the scheme of Fig. 9(b) would be greater than that with simple envelope demodulation, so conventional envelope detection was chosen. For phase measurement, the proper choice is a cascade of a hard limiter (or fast AGC) followed by a phase-locked loop. Use of a conventional phase detector, as in Fig. 9, however, introduces the difficulty of resolving ambiguities in the phase-angle measurement when the $\varphi(t)$ variation is greater than a 360-degree range. This problem is examined in Sec. II-D-2 of Ref. 6, and the recommended solution is use of an accurate frequency discriminator followed by an analog integrator.

In addition to these techniques, a demodulator employing quadrature detection was considered. This method would involve mixing $\Sigma(t)$ with the sine and cosine components of a reference signal of frequency ω_5; low-pass filters would then give the amplitudes of the in-phase and out-of-phase components of $\Sigma(t)$ from which the envelope and phase could be calculated. It turns out that this method produces signal-noise product terms that would probably cause a severe decrease in the measurement

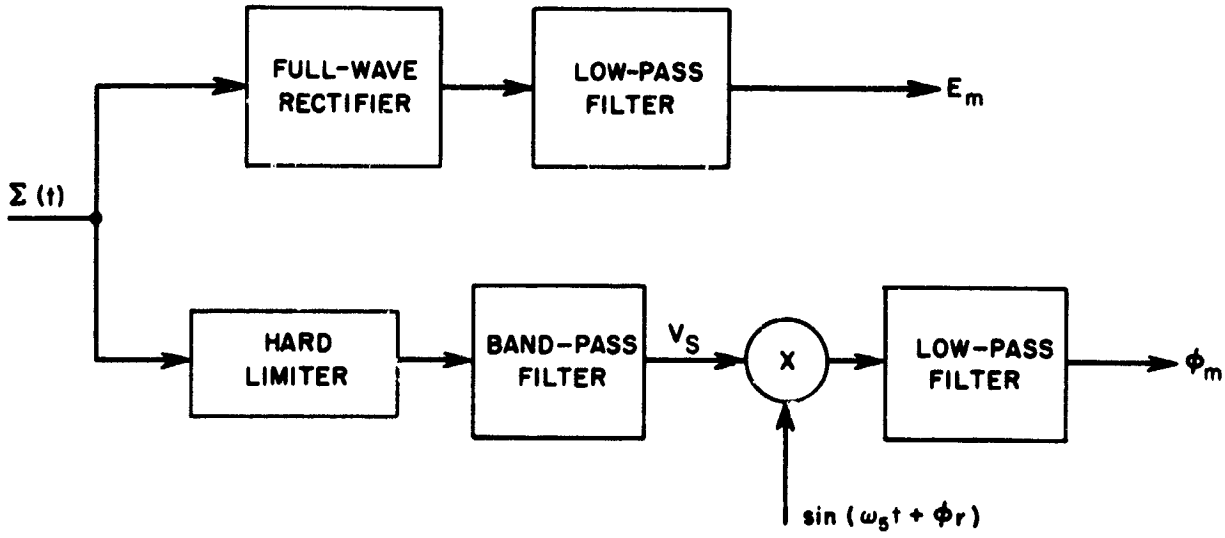

(a) CONVENTIONAL DETECTION

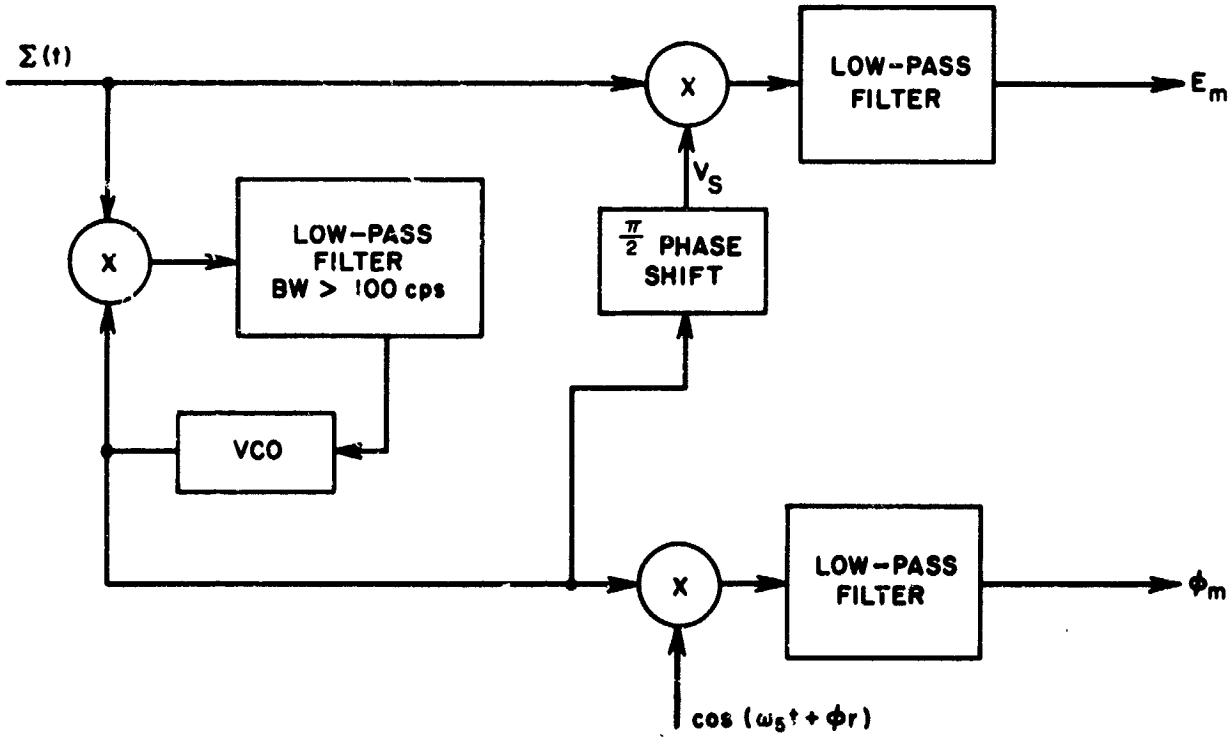

(b) DEMODULATION BY PHASE-LOCKED LOOP

RA-5067-4

FIG. 9 AMPLITUDE AND PHASE MEASUREMENTS

accuracies as compared with the other methods discussed. We therefore rejected the quadrature detection method.

3. Recommended Measurements

The remaining step in the analog processing is to remove the effect of amplitude fluctuations on the angle-of-arrival signals. This can be accomplished by dividing the demodulated difference signal, ψ_m of Eq. (4), by the detected sum-signal envelope. The resulting receiver structure is shown for the sum channel and one difference channel in Fig. 10. The output dc voltages will be

$$\varphi_M(t) = \theta_o + \int dt\left(\frac{\omega_o}{c}\dot{d} + \hat{\omega}_\Delta + \frac{\omega_o}{c}\dot{\hat{r}}_\Delta\right) + \varphi_{ns}$$

$$g_M(t) = K_o\left[1 + k_a(t) + k_p(t)\right] + \frac{N_s(t)}{a_o A_t} \qquad (5)$$

$$\alpha_M(t) = \frac{(\psi_\alpha + \alpha_p - \alpha_e)\cos(\varphi_\Delta - \varphi_{ns}) + \frac{2}{b_o A_p} n'_\Delta}{1 + \frac{1}{a_o A_p} N_s}$$

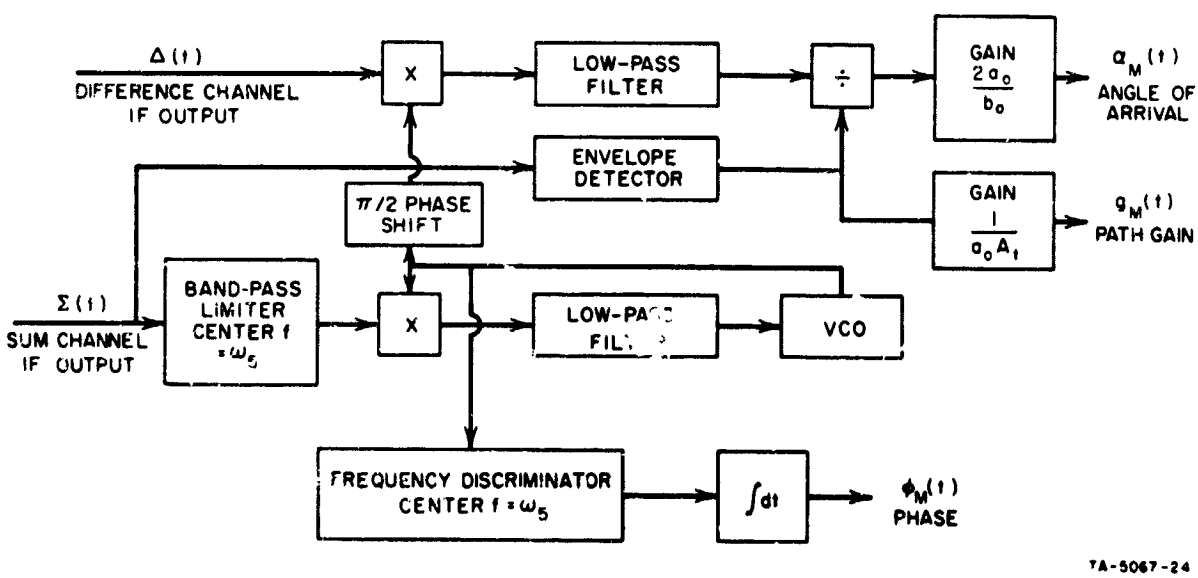

FIG. 10 INSTRUMENTATION RECEIVER STRUCTURE

where

$N_s = N_s(t;n_s)$ = error induced on the sum-signal envelope measurement by sum-channel noise, n_s.

Equations (5) display, in addition to the desired quantities, the various error terms that will corrupt the final measurements.

F. Processing of Side-Band Signals*

An indication of the bandwidth limitation due to phase distortion introduced by the propagation path is the amount by which the phase characteristic departs from a straight line through the phase shift at midband over a bandwidth B. When the sum of the two components (above and below the carrier) of this departure reach $\pi/2$ radians (90^0), the extreme frequency components add in quadrature to give a 3-db loss; thus the bandwidth may be defined as the frequency range at the extremes of which the departure from a linear phase characteristic is $\pi/2$ radians.

Consider a sounding signal consisting of a carrier component $\cos \omega_o t$ and two sidebands $a_2 \cos(\omega_o - \omega_1)t$ and $a_3 \cos (\omega_o + \omega_1)t$. When this composite signal passes through the system and the phase shift at ω_o is considered to be zero, these components become:

$$v_2 = a_2 \cos [(\omega_o - \omega_1)t - k\omega_1 + \theta_1]$$

$$v_3 = a_3 \cos [(\omega_o + \omega_1)t + k\omega_1 + \theta_2]$$

where k is the slope of the best linear phase characteristic. For a straight line, $\theta_1 = -\theta_2$ or $\theta_1 + \theta_2 = 0$.

The desired measurement is $|\theta_1 + \theta_2|$. If this angle is less than $\pi/2$, then $B \geq 2\omega_1$; if larger than $\pi/2$, then $B \leq 2\omega_1$.

---

* This section was prepared by C. H. Dawson.

The recommended technique* involves automatic gain control applied to v_2 and v_3 separately to make $a_2 = a_3 = a$ as shown in Fig. 1. Then the sideband voltages are added to give

$$v_4 = v_2 + v_3 = 2a \cos\left[\omega_o t + \left(\frac{\theta_1 + \theta_2}{2}\right)\right] \cos\left[\omega_1 t + k\omega_1 + \left(\frac{\theta_2 - \theta_1}{2}\right)\right] .$$

This sum signal is mixed with the output of the existing voltage-controlled oscillator, $v_1 = \sin \omega_o t$, and the low-frequency component is retained, giving

$$v_5 = \text{low frequency component of } v_4$$

$$= a \sin\left(\frac{\theta_1 + \theta_2}{2}\right)\left[\cos \omega_1 t + k\omega_1 + \left(\frac{\theta_2 - \theta_1}{2}\right)\right] .$$

This component is then envelope-detected and low-pass-filtered to give

$$v_6 = a \sin\left(\frac{\theta_1 + \theta_2}{2}\right)$$

or

$$\theta_1 + \theta_2 = 2 \sin^{-1}\left(\frac{v_6}{a}\right) .$$

G. Noise and Boresighting Receiver†

The receiver that appears most promising for the measurement of the correlation of noise between channels is a phase-switched interferometer of the Ryle type used in radio astronomy (Refs. 9, 10). This receiver is connected to two antennas, and uses two separate channels down to a summing junction, as was shown previously in Fig. 2. Between the antenna and the first mixer in one channel, an increment of 180 degrees phase shift is switched into and out of the channel at a convenient audio rate

---

* For an alternative, see Sec. II-F of Ref. 4.

† This section was prepared by L. A. Robinson.

that is compatible with the bandwidth of the IF stages and with the integration time at the system output. The signals in the two channels, consisting of internal and external noise, are combined in a linear summing junction and then square-law-detected so that the output voltage is proportional to total noise power. The correlated noise at the summing junction adds as voltage, and thus has a modulation component at the switching rate of the 180-degree phase switch. A phase shifter continuously adjustable over a 180-degree range is provided in one channel to adjust this correlated noise for maximum amplitude modulation of the output of the summing junction. A phase-sensitive detector is driven in synchronism with the phase switch to measure the amplitude-modulated component of the summing junction output. A second output is also provided that measures the average output of the summing junction. Time delay units are provided in the IF strip of each channel to compensate for the difference in arrival time at the two antennas of the external noise. These delays can be manually set to values calculated from the known antenna spacing and pointing direction.

With the adjustable time delays and the variable phase shifter set as described above, the ratio of the correlated noise power, N_{cor}, at the summing junction to the total noise power, N_{total}, can readily be determined from the receiver output voltages V_1 and V_2, as follows:

$$\frac{N_{cor}}{N_{total}} = \frac{N_{cor}}{N_{uncor} + N_{cor}} = \frac{N_{max} - N_{min}}{N_{max} + N_{min}} = K\frac{V_1}{2V_2}$$

where

N_{max} = Maximum output noise power from the summing junction, which is obtained when the correlated noise adds in phase

N_{min} = Minimum output noise power from the summing junction, which is obtained when the correlated noise adds out of phase

K = A constant of proportionality correcting for any differences in gain beyond the square-law detector.

The origin of this equation is given in Appendix G. The total noise power at the junction will include a significant contribution from the receiver pre-amplifiers even if these are of low-noise design. Separate measurement may be made of the receiver contribution.

Although the basic block diagram is the same for all noise-correlation measurements, some specific details will vary according to what noise source is being measured. These differences arise in order to emphasize the source of interest compared to the other sources. Atmospheric-absorption noise increases with frequency in the 1-to-20-Gc band, and thus the receiver should be set to receive at some high frequency such as 16 Gc. Atmospheric-absorption noise also is greater for antenna look angles near the horizon. Thus the antenna beam should be pointed just far enough above the horizon that neither the main beam or the higher side-lobes near the main beam pick up significant noise from the warm surface of the earth.

Galactic noise, on the other hand, decreases approximately as f^{-2} in the 1-to-20-Gc band. Thus the receiver front end should be set to receive a frequency near the lower band edge. To maximize the ratio of galactic noise to atmospheric-absorption noise, the antennas should be pointed near the galactic center and away from the earth horizon. These two requirements are in conflict for sites very far north of the equator.

The receiver designed for noise-correlation measurements can also readily be modified to perform two other functions. To measure absolute noise temperature distribution of the sky, one antenna and receiver channel could be used as a Dicke radiometer (Refs. 11, 12). In this application, the receiver would be alternately switched between the antenna and a load of known equivalent noise temperature, which is shown in dotted lines in Fig. 2. The phase-sensitive detector would be driven in synchronism with the switch, then the output voltage V_1 would be proportional to the difference in equivalent noise temperatures of the sky and the load. This receiver could also be used for boresighting the individual antennas on a radio star. In this application, the unswitched receiver channel would be connected to the sum output of the monopulse feed network, and the switched channel connected to one of the

error-channel outputs. The two receiver channels would be adjusted for equal time delay and phase shift. As the radio-star drifted through the null of the monopulse difference pattern, the output voltage V_1 of the receiver would go to zero.

H. Meteorological Instrumentation*

1. Introduction

Tropospheric phenomena are the determining factors in the utility of the proposed antenna system. Appendix H reviews the controlling factors upon the performance of large antenna arrays, with special emphasis on the contribution of the liquid water content of the atmosphere (cloud and rain drops) to the refractive index fluctuations. On the basis of these factors, details of a meteorological support program for the conduct of the proposed experiments and the extrapolation of its results are now described.

It will be necessary to carry out a comprehensive observational program to monitor:

(1) The atmospheric parameters of direct significance to the radio reception experiments

(2) The more general meteorological conditions, with which the direct parameters can be related systematically.

Thus, the observation of the temporal and spacial variations in dielectric inhomogeneities, with related wind motion, mainly to be acquired by refractometer measurements, will be available for correlation with the radio measurements. Comparisons can then be made between results obtained under comparable meteorological conditions, the better to isolate the effects of other factors. The degree of significance of meteorological factors can be assessed and, hopefully, related objectively to phase interference effects, signal fluctuations, etc.

Ideally, the aim should be to describe the refractive index variations in terms that could be applied directly in numerical formulations

---

* This section was prepared by R. T. H. Collis and F. G. Fernald.

of the experimental data. Failing this, it is expected that it will be possible to divide the significant conditions into a limited number of classes.

The object of relating such direct parameters to the more general meteorological conditions is to make it possible to extrapolate the results of the radio experiments to other locations and climates. For, although it is unlikely that the variability of refractive conditions will be known for other situations, standard meteorological data are usually fairly readily available. If correlations can be established between the broader meteorological factors and phase interference, the latter can be readily assessed for most locations.

The design of the meteorological data-acquisition program is now discussed and a method of processing and applying the data is described.

2. Meteorological Data Acquisition

a. Refractometry

Radio refractivity reflects the sum effects of atmospheric pressure, temperature, and humidity on the propagation velocity of radio waves through the atmosphere. For rain or cloudy atmospheres, allowances also have to be made for the effects of liquid water.

For reasons of simplicity as well as accuracy in data processing, in this experiment refractivity will be measured directly by monitoring the resonant frequencies of microwave cavities, as opposed to the indirect method of computing refractivity from individual recordings of temperature, pressure, and humidity (see Ref. 13, for a complete review of the various methods of measuring refractivity).

The proposed array will be capable of compensating for phase variations of approximately 1 cps or less; therefore, the meteorological instrumentation must be capable of recognizing parameters that will induce high-frequency fluctuations of greater than 1 cps. Surface refractometers sensitive to fluctuations of up to 100 cps and airborne refractometers with resolution down to a few feet can be obtained. As the variations over the array will, for the most part, result from

components in the turbulence spectrum comparable to or smaller than the receiver separation, two refractometers mounted at suitably exposed surface locations will be separated by a distance equivalent to the maximum separation between the fixed and movable antennas of the test array (approximately 1 km). With this arrangement, comparison of the output of the two refractometers might possibly give some information on the turbulence spectrum affecting the array near the earth's surface.

The airborne refractometers provide the most effective means of monitoring the actual eddy spectrum of refractivity through the troposphere up to 20 to 30,000 feet and are, therefore, of prime importance for comparison with the phase fluctuations over the array. The data will be collected while the aircraft is descending on a path coinciding as closely as possible to the array in time and space. The aircraft refractometers are mounted to exclude all cloud and rain drops; therefore, a liquid-water-measuring device (such as paper tape or hot wire instruments) must be included since, as shown in Appendix H, liquid water can induce large, rapid fluctuations in refractivity that would otherwise go undetected. The refractometer data, corrected for liquid water content, will then yield information on the refractive conditions and inhomogeneities therein. Such data are somewhat limited in that the conditions prevailing along the path of the relatively slowly descending aircraft will not be exactly representative of conditions in the radio beam; even so, the results should be reasonably representative of the atmosphere at the time of the experiment.

b. Measurement of Rain, Clouds, and Humidity

In order of importance, high-frequency fluctuations will be associated with the presence of (1) rain, (2) clouds, and (3) a humid atmosphere. It is, therefore, necessary to monitor the distribution of rainfall with a C- or S-band radar. Military or Weather Bureau radars in the vicinity of the experiment can be utilized. RHI, PPI, and possibly A-scope displays should be recorded on film. The distribution of precipitation along the satellite-to-earth path can be determined from these radarscope photographs. A simple yes-no correlation of precipitation

with phase jitter, possibly broken down for different layers through the atmosphere, can then be established.

Similarly, for daytime operations either by use of a whole-sky camera or two individual cameras, one slaved to the movable antenna and the other to the central fixed antenna of the array, a yes-no correlation can be established with the presence of, or lack of, clouds along the path. The humidity data collected during rawindsonde ascents will describe the moist and dry layers through the atmosphere in sufficient detail to enable a simple correlation, similar to those mentioned above, to be performed for varying levels throughout the atmosphere.

Sky-noise temperature is lowest under clear skies and increases with increasing humidity and cloud cover, and is greatest when precipitation is present. The tendency for high-frequency phase jitter, therefore, is directly proportional to the sky-noise temperature, and thus presents a simple quantity with which the phase jitter should be correlated. Therefore, a receiver-antenna system to monitor the sky noise along the satellite-to-earth propagation path would be a desirable addition to the instrumentation. It would not replace the radar, sky camera, and radiosonde humidity measurements, in that the sky-noise temperature represents a quantity integrated along the entire path through the troposphere. As the detrimental phase jitter will not extend through the entire troposphere, but more likely be limited to a few layers throughout the troposphere, the range resolution of these other instruments (the radar in particular) negates any replacement by a simple microwave radiometer.

c. Conventional Meteorological Instrumentation

The instrumentation discussed above covers the recording of parameters that can be directly related to the expected phase jitter. Conventional surface and rawindsonde measurements will be required to describe the meteorological state of the atmosphere at the time of the experiment. A comparison of the phase jitter with the several meteorological conditions is necessary so that the results of the multiple

array experiment can be extrapolated to other climatic regimes for which only standard meteorological records are available.

Rawindsondes, on ascending through the atmosphere, record temperature, pressure, humidity, and the wind velocity. Hopefully, the test array will be located near a Weather Bureau station at which these measurements are recorded routinely at 0000 GMT and 1200 GMT. If these ascents are more than an hour or two from the time of the array experiment, special ascents to coincide with the experiment should be requested. The temperature, pressure, and humidity sensors respond too slowly to produce a refractivity profile of the resolution desired for this experiment. The wind data are most important and must be considered when comparing the refractivity spectrum to the phase jitter. Also, devices located adjacent to the refractometers to record surface pressure, temperature, humidity, wind, and precipitation will be needed to complete the meteorological instrumentation. In the event of refractometer failure, both the radiosonde and surface measurements could be used to compute radio refractivity, but the resolution of the resultant values would be appreciably degraded.

Aside from the data collected at the test site and the special radiosonde ascent simultaneous with the experiment, the standard U.S. Weather Bureau 3-hourly surface charts and twice-daily upper-air charts along with the standard 0000 GMT and 1200 GMT radiosonde data from the nearest facility should be available both during the experiment and for reference purposes at a later date.

d. Additional Instrumentation

For the past two years, the Aerophysics Laboratory at SRI has been probing the atmosphere with a ruby lidar (laser radar). This instrument can determine the range of all types of visible clouds, plus receiving echo returns from particulate matter in clear air.

Although the height and range of clouds would be a useful input, this would probably not justify the use of the lidar as part of the multiple array experiment. On the other hand, clear-air returns from a stratified atmosphere (Ref. 14) along with the accompanying

rawindsonde data, would be a valuable aid in describing the structure of these stratified layers. Possibly the lidar's most valuable contribution would be the determination of the eddy spectrum near the surface within a turbulent mixing atmosphere (Ref. 15). More work, though, is necessary to perfect these methods and to determine their limitations.

e. Synopsis

The ideal meteorological instrumentation outlined above would therefore consist of:

(1) Two radio refractometers, one at the site of the antenna of the experimental array, and the other at the most remote position of the movable antenna of the array.

(2) One airborne refractometer plus a device to measure the liquid water content when clouds and rain are encountered.

(3) One whole-sky camera or two wide-angle cameras slaved to the main antenna and the movable antenna of the experimental array.

(4) One C- or S-band radar capable of recording PPI and RHI data of precipitation during the experiment.

(5) One microwave radiometer to record the sky-noise temperature.

(6) Instrumentation in the vicinity of the two surface refractometers to record wind speed and direction, atmospheric pressure, temperature, humidity, and rainfall rate.

(7) A rawindsonde ascent concurrent (± 1 hour) with the performance of the experiment.

The C- or S-band radar and the cloud cameras are an important part of the instrumentation, as the ability to state whether or not rain and clouds are in the earth-satellite link will be lost without them. The microwave radiometer* is of less importance in that it duplicates other instrumentation to some extent, but should be included, if possible, in that sky noise itself would be a valuable record in the

* The Ryle receiver recommended for noise correlation studies and boresighting on radio stars can also be operated as a radiometer.

evaluation of the proposed array. If a radar and/or cameras cannot be obtained for the experiments, the radiometer should definitely be included so that an indication of the sky conditions will be available when the analysis of the phase jitter is performed.

Surface refractometers are of limited value in that refractivity fluctuations at only one end of a long radio path would not be expected to correlate well with phase jitter due to refractive variations extending along the entire path through the troposphere. At least one surface refractometer, though, would be desirable. If the array experiment is in the vicinity of a Weather Bureau station, no surface meteorological data need be collected. Otherwise, instrumentation to record surface temperature, pressure, humidity, wind, and rainfall rates is necessary.

At least a limited number of airborne refractometer soundings should be made if anything other than a strictly empirical refractivity-phase jitter relationship is to be studied. Rawindsonde data should definitely be included, as they will give the winds aloft; and for those cases where an aircraft is not available, humidity, pressure, and temperature data will be essential. If the rawindsonde were not available, some other method such as pilot balloon measurements or utilization of an airborne Doppler navigation system would be required in order to determine the winds aloft.

3. Implementation of a Practical Observational Program

A complete program of observations employing the full range of instrumentation described above would be a major undertaking and, although it would result in extremely valuable data of fundamental importance in radio meteorology, it is probable that a less ambitious program is indicated. It should be re-emphasized, however, that atmospheric factors are all-important in the realization of this concept and accordingly the experiment would suffer seriously if the meteorological data collection program were inadequate.

In terms of cost and operational effort, the situation is more encouraging than it might appear. This is because in the ordinary course of events a considerable number of meteorological observations are made routinely and could provide (either unchanged or with minor additional effort) much of the needed data. Also, the experimental instrumentation that would be required for special observations would possibly be available for short-term use on a loan basis in the investigations of the type proposed.

By using existing observational programs and, wherever possible, collaboration with other investigational programs, it is probable that the cost of the necessary meteorological support would be distributed between a relatively small instrumental-observational program and the cost of the meteorological analysis and interpretation.

Upper-air data are collected at 0000 GMT and 1200 GMT over an extensive network of Rawindsonde stations covering the United States and can be used unless the experiment is performed in a location quite remote from one of these stations Also, special soundings at times other than the standard hours can be arranged at a nominal cost of less than $100 per data run. An extensive network of weather radars covers the East, South, and Midwest; therefore, almost any site in these parts of the country will be within range of one of the existing weather radar facilities. At these stations, records of precipitation incidence are made routinely, often by radarscope photographs, and it is probable that special coverage of selected areas could be obtained by arrangement.

A number of experiments have been performed by the Air Force, Army, and National Bureau of Standards using airborne and surface refractometers (see, for example, Refs. 16-19), and an attempt should be made to borrow this equipment. Surface refractometers, exclusive of recording equipment, cost approximately $6000 to $7000, while airborne refractometers prior to installation will cost approximately $9000 to $10,000; an additional $3000 for a tape recorder is required. Unless a prolonged program is envisioned, it should not be necessary to purchase this equipment, as it might possibly be available on loan for short periods. The National Bureau of Standards has extensive experience with this equipment,

and it is possible that they would be prepared to collaborate with this part of the meteorological program.

The minimum and optimum meteorological program can now be outlined. The basic minimum system would rely on the existing weather and military meteorological networks. The data available from these systems, though, will at best allow only an empirical correlation between the phase jitter and meteorological conditions to be established. The optimum working system (a compromise between the minimum and ideal systems) would rely on additional surface and airborne instrumentation, and by employing a limited number of relatively highly instrumented data runs, the atmospheric parameters of direct significance to the radio reception could be monitored on selected occasions.

A complete program of observations comprising an ideal meteorological support program would extend the optimum working program described above to include further refractivity data and observations of sky noise temperature. The additional refractive data would be obtained by a more comprehensive airborne data-collection program. Sky-noise data, which would cover clear sky, cloudy sky, and precipitation effects, would be obtained directly by a microwave radiometer having directional properties.

a. Minimum Program

The minimum program would require no additonal instrumentation. A meteorologist would be necessary to analyze the data collected from the nearest available Weather Bureau and/or military facilities. These data would consist of:

(1) Surface temperature, pressure, humidity, wind, and rainfall measurements

(2) PPI and RHI radarscope photographs when there is precipitation during the experiment

(3) The standard rawindsonde data plus any special rawindsonde ascents that might be required.

b. Optimum Program

The minimum program outlined above would remain the basic part of this program with the following additional requirements:

(1) A limited number of soundings with an aircraft equipped with a radio refractometer and liquid-water sensor

(2) A surface refractometer

(3) A sky camera

(4) Instrumentation to record surface pressure, temperature, humidity, wind, and rainfall rate if the existing Weather Bureau or military weather stations are not adjacent to the test site.

c. Ideal Program

The optimum program above would be extended as follows:

(1) Item 4 extended to include more frequent and comprehensive airborne soundings of refractivity fluctuations

(2) Addition of a directional microwave radiometer.

I. Ionospheric Measurements*

1. General

The ionosphere is expected to be relatively unimportant in the frequency range of interest. The initial recommended program uses data from outside this experiment supplemented by a magnetometer. However, the components of a more complete ionospheric program are described herein for possible later implementation.

A measurement program is investigated in Appendix I to relate characteristics of the ionosphere with the amplitude and phase fluctuations measured in the communications experiment. The contributions of the ionosphere to the total signal description at frequencies above 1 Gc appears to be unimportant relative to tropospheric effects. Therefore, consideration is given to meaningful data correlations and minima-type ionospheric descriptions.

*This section was prepared by J. A. Martin.

Correlation of ionospheric phenomena with radio wave propagation is difficult for a number of reasons. A quantitative description of the ionosphere involves both physical and mathematical approximations. The approximations are governed in a complex manner by a variety of parameters such as plasma structure, propagation mechanism, radio wavelength, and geometry. During large-scale disturbances a number of measurable events occur simultaneously, so that it is not clear if direct cause-and-effect relations exist among the observed phenomena.

The static character of the ionosphere (the gross electron density profile) has no direct effect on the fluctuation character of a radio wave. Therefore, measurements of integrated electron density over ionospheric paths, $\int_{path} N_e dZ$, are unimportant for correlation with the communication experiment signal. Only the dynamic character of the ionosphere, $\int_{path} (\partial N_e/\partial t) dZ$, is important. The measureable dynamic character of the ionosphere is limited by low and high filtering limitations in the receiving and data-processing stages. The time variation in electron density as sensed by the receiver can be caused by transmitter-receiver motion as well as by motions of the electron structure.

It is especially important to recognize that an ionospheric description may differ for different multi-aperture configurations and signal source characteristics. Due to the complexity of the ionosphere and the number of parameters involved, a complete description of the ionosphere is unlikely. (Parameters important to the characterization of the ionosphere are listed in Table VIII in Appendix I).

The investigation described in Appendix I reveals that ionospheric models and measurements are qualitative and are capable of explaining only gross features and changes. Predictions of the ionosphere are limited to time periods longer than correlation periods measured in the communication experiment. Fluctuation phenomena are only known to an order of magnitude based on a particular statistical model. Repeatability of measuring similar ionospheric conditions also appears to be limited by order of magnitude accuracies.

Until ionospheric effects are proven significant to signal fluctuations and their correlation characteristics in the communications experiment, only a minima type ionospheric description appears to be feasible.

2. Recommendations

a. Minima Type Description

A program is recommended to assign signatures to the communication experiment data output that relate the state of the ionosphere to the fluctuation character of the communication experiment signal. It is suggested that signatures apply to the following parameters:

(1) Magnetic aspect angle (angle between the communication experiment signal line of sight and the normal to the earth's magnetic field)

(2) Disturbed conditions (geomagnetic storms, solar variations, aurora, ionospheric storms).

Other relevant data such as pointing aspects of the communication experiment (receiving antenna elevation and bearing) and time variables (real time, day of month, season of year, sunspot cycle) are normally recorded. The position of the satellite transmitter is defined by the pointing angles of the receiving antenna.

It is also recommended that the variations in the magnetic field be recorded at the experimental test site. These variations in magnetic field would be useful in monitoring geomagnetic storms. Magnetic-field-measuring equipment at the experimental test site is especially advantageous in regard to accessibility of storm data.

Measurements of backscatter and the monitoring of signal character below 2 Gc are considered in Appendix I. The facilities required for these measurements are considerable, and implementation of these measurements at the experimental test site are not recommended at the present time.

b. Ionospheric Classification

Classification of the ionosphere with a single signature, such as a range of magnetic aspect angles, may be meaningless. Proper classification of the ionosphere requires a number of signatures. The

number of ionospheric classifications is arbitrary and depends upon the number of signatures assigned to each parameter set. This is illustrated in Table II, where 1296 classifications are suggested. This high figure

Table II

TYPICAL IONOSPHERIC CLASSIFICATION

Parameter	Signatures in parameter set	
	Number	Description
Magnetic Aspect Angle	3	$\pm 10^{o}$ transverse, $\pm 10^{o}$ longitudinal, other
Antenna Pointing Elevation	2	0 - 10^{o}, other
Antenna Pointing Bearing	3	Northern latitudes, equatorial latitudes, southern latitudes
Real Time	3	Midnight, midday, other
Geomagnetic Activity	3	Normal, sudden storm commencement, storm main phase
Solar Variations	2	Normal, high (solar flares and cosmic noise bursts)
Aurora Activity	2	None, aurora present (visual or radar sensing)
Ionospheric Storms	2	None, storms present (spread-F and sporodic-E)

Possible Number of Classifications = 1296

could be reduced to 162 if classification with solar variations, aurora activity, and ionospheric storms is neglected. A minimum number of classifications would be 9 where only magnetic aspect angle and geomagnetic activity data are use.

It is apparent that an effort toward a large number of ionospheric classifications may prove meaningless if ionospheric effects are negligible. However, important data for ionospheric descriptions can be stored or recorded separately from the communication experiment data. Subsequent data correlation could be confined to times when communication signal fluctuations are severe.

c. Magnetic Aspect Angle

Magnetic aspect signatures would provide a measure of the sensitivity of the 2-Gc signal fluctuations to blob anisotropy along the magnetic field. The magnetic aspect can be computed from antenna pointing or satellite trajectory data and from existing isomagnetic data or a dipole model of the earth's magnetic field. Magnetic aspect signatures would be useful only if signatures of ionospheric disturbances were also available.

d. Geomagnetic Storms and Other Disturbances

The use of geomagnetic storm, aurora activity, solar variation, and ionospheric storm data is important in possibly predicting subsequent periods of severe signal-fluctuation character. The availability and geographic extent of information requires further investigation. An effort of this type would require an engineer well versed in ionospheric phenomena. In this respect, geomagnetic storm and aurora data would be most useful and probably easier to obtain on an economical basis. The monitoring of magnetic storms at the experimental test site is a minimal effort in this direction.

Disturbed conditions in the ionosphere could also be correlated with subsequent gross changes or disturbances in the troposphere. Solar energy incident on the atmosphere creates disturbances in the ionosphere and subsequent changes in the meterological characteristics of the troposphere. The processes involved are not yet fully understood and have not been measured.

Equipment to measure variation in the earth's magnetic field are not costly. A magnetometer (a small bar magnet suspended on a quartz fiber) is used at many magnetic observatories. This instrument does not fix the total magnetic field but measures variations in field components. Newer instruments (Ref. 20) of higher precision are also in operation. The operation of these instruments is based on Larmor precession in the magnetic field of the magnetic moments of nuclei and atoms. Measured fluctuations may be transformed immediately into

digital form and can either be fed concurrently into the communication-signal data processor or can be stored on magnetic tape for ease in data processing.

e. Backscatter Measurements

A backscatter experiment operating at frequencies of ≈ 10 to 100 Mc could measure the smallest blob structure sensed in the communication experiment. However a meaningful equal-beamwidth experiment would require an excessively large aperture at the experimental site. Thus a feasible backscatter experiment at the experimental site would involve a broad-beam antenna installation subject to measurement limitations (namely range and resolution).

A narrow- or equal-beam experiment could be performed from existing facilities at common latitudes. In this respect, the use of VHF and UHF radars that normally explore aurora are limited in that blob sizes measured may be an order of magnitude less than blob sizes sensed in the communication experiment. The VHF and UHF radars would however, give a measure of auroral activity. A rhombic array at Stanford University offers a narrow HF beam. However, the viewing time in conjunction with the communications experiment would be limited and the geometry would be broadside to communication experiment geometry.

Backscatter measurements would add more signatures and more classifications to ionospheric descriptions. Additional backscatter signatures would include: scattering level, scattering range, and scattering direction.

A simple form of backscatter signature is included in Table II as indicating aurora activity.

The discussion in Appendix I suggests that ionospheric backscatter correlation with communication experiment phase fluctuations will not exceed 0.6. Backscatter correlation with amplitude fluctuations should exist only for large, slowly varying irregularities in the ionosphere (Fresnel scattering). Thus backscatter is useful for predicting gross effects rather than precise and rapid fluctuation characteristics.

f. Monitoring Measurements

Monitoring of the fluctuation character of the telemetry signal from the communications experiment satellite could be more useful than a backscatter measurement. The telemetry signal propagates through the same general irregular structure as the communication experiment signal. The propagation path effects on the two signals become more equal as the signal frequency separation decreases.

An alternative to monitoring the telemetry signal of the communication experiment satellite (≈100 Mc) is to add a UHF frequency (≈700 Mc) to the communication experiment.

The monitoring of the telemetry frequency (≈100 Mc) and the UHF (≈700 Mc) signals requires modifications to the communication experiment configuration. The monitoring of the 100-Mc satellite telemetry signal requires no modification to the satellite system. However, a large receiving antenna installation would be required at the ground terminal. The 700-Mc signal would require an additional package in the satellite. Receiving facilities at the ground terminal could be used in common with the communications experiment. Use of data monitored at 100 Mc would be limited in scaling and correlation by multiple scattering effects. Multiple scattering does not appear to be a problem to scaling between and correlation of 700-Mc and 2-Gc signals.

The usefulness of monitoring the line-of-sight character of the ionosphere (other than basic research in correlation and scaling) is that satellite monitors could be used to assign an ionospheric signature to signals received from deep space. Assuming the monitoring and deep-space signals are correlated, the receiving configuration could be adjusted to the signature of the stronger monitoring signal. The monitoring signature could also be used as a measure of reliability.

The monitoring process should be reserved for future experiments if ionospheric effects are shown to be significant.

J. On-Site Computer*

The digital data equipment required on site for the operation of the tracking equipment consists, in the simplest case, of a digital tape reader (either punched paper or magnetic), a shift register equal in length to the total number of bits per point (60), and three 20-bit buffer registers. These items, together with appropriate synchronizing and control equipment, are all that is required to drive the antennas on the basis of predicted angles.

The data rate indicated in Sec. III-C-4-b (100 points per second) may be reduced by using more widely spaced data points and employing linear interpolation between them. To do this would require two additional words of input--azimuth and elevation rates--which adds to the size of the shift register and buffer registers. In addition, two relatively simple digital-to-analog convertors and two resettable integrators will be required. However, employing velocity input information and linear interpolation permits a reduction of the required input data rate to no more than 10 points per second.

No on-site computer requirements other than those described above are needed since all data processing can be done off-line.

---

* This section was prepared by E. C. Fraser.

BLANK PAGE

IV EXPERIMENTAL SITE*

A. Location

The most likely permanent location for a phased array intended for deep-space tracking would be in a region where tropospheric variations of those factors effecting radio refractive index (temperature, pressure, and humidity) are minimal and where clouds and precipitation affecting signal attenuation are scarce. Such a location will probably be in a region outside the path of frequent storms throughout the year, such as the desert areas in the southwestern part of the U.S. However, selection of an exact site in this region will require careful examination of all available climatological records to determine which specific area experiences minimum cloudiness and precipitation because of a sporadic influx of upper-level moisture from the south during the summer and fall, as well as passage of an occasional cyclone during the winter and spring.

On the other hand, the test site should be located where there is a high probability that a wide variety of tropospheric variations in temperature, pressure, humidity, clouds, and precipitation will occur during the test period. Test operation at such a location will enable evaluation of array performance under the tropospheric conditions experienced in most parts of the U.S., and should produce operating criteria such as initial antenna pointing angles and estimated array performance for a number of specific synoptic conditions. In turn, these criteria should be very useful in the operation of a permanent array, wherever it may be located, under similar synoptic conditions.

In order to obtain data under a broad spectrum of tropospheric variations in temperature, pressure, humidity, clouds, and precipitation, the test site should be located in a path of frequent storms, as well as in

---

* This section was prepared by J. E. Alder.

an area exposed to a maximum number of the types of air masses that are characteristic of different parts of the U.S. An examination of Figs. 12 and 13 of Ref. 4 (which appeared originally in Refs. 21 and 22) indicates that the central Oklahoma-Texas panhandle area best meets these requirements. Figure 12 of Ref. 4 showing monthly mean frequency distributions of migratory cyclones in the U.S. reveals that this region is, on the average, within or very close to a path of frequent storms each month of the year. Figure 13 of Ref. 4 indicates monthly average distributions of tropospheric water vapor, expressed in centimeters of precipitable water, over the U.S. Note that the area is also, on the average, within or along the edge of a considerable gradient in this parameter throughout the year. Aside from some terrain height effect, this condition is largely due to the fact that the area is near the boundary between dry desert air to the southwest and west, and moist tropical air from the Gulf of Mexico to the southeast; furthermore, these two air mass types often alternate over the region as the migratory cyclones mentioned above traverse the area. Cold polar and arctic air masses also alternate over the region with the warm moist Gulf air as migratory cyclones pass by during the winter.

Another consideration of importance in test site selection is the availability of an existing radiosonde facility and other instrumentation that could be used during this experiment. The U.S. Weather Bureau operates radiosonde stations at Oklahoma City and Amarillo, Texas; therefore, it would be very desirable to locate the test site as close as possible to one of these facilities. Also, the National Severe Storms Project (NSSP) mesoscale meteorological network is presently in operation in northern Texas, Oklahoma, and Kansas (see Ref. 23). In this network, all stations are within 50 miles of each other and are equipped with barographs, while several of the stations also include hygrothermographs, recording rain gauges, and recording wind instruments. All such instruments are serviced by U.S. Weather Bureau cooperative observers. Information from this network should permit the tracking of weather features such as fronts and squall lines in the vicinity of the test array with an accuracy much greater than would be possible with the normal synoptic-scale network of stations.

A site near Oklahoma City is our first choice because it would be more centrally located in the NSSP network and would allow detailed meteorological tracking of fronts and squall lines approaching from the west and northwest (the most common cases) for a longer period than at Amarillo. Also, Fig. 13 of Ref. 4 indicates that somewhat less water vapor is present, on the average, over Amarillo than over Oklahoma City throughout the year. This means that drier air masses originating from the west and north are over the Amarillo area more often than they are over the Oklahoma City area.

Considering the variety of tropospheric conditions, the availability of comprehensive meteorological instrumentation, and a relatively low expected density of aircraft, Oklahoma is recommended as an experimental site. This site recommendation has not considered cost, availability, accessibility, or convenience. Such considerations may well result in another choice for the experimental site with probably only a very minor decrease in the utility of the experiment.

B. Layout*

Figure 11 displays a possible site layout for a medium-cost experiment. The three towers are specified as demountable since their presence would distort the antenna patterns for certain azimuth angles. Except when such angles are to be used, the towers can remain in place. Either telescoping towers or towers hinged at the base should be satisfactory.

Living quarters may be necessary if a remote site is chosen. Since the magnetometer may be sensitive to nearby metal, it may require a separate shelter well removed from all other equipment. As noted elsewhere, the 4-meter antenna would be moved from pad to pad but would require alignment and calibration only once for each pad. A reasonably well graded road along the line of antennas would facilitate the movement of the antenna.

* This section was prepared by C. H. Dawson.

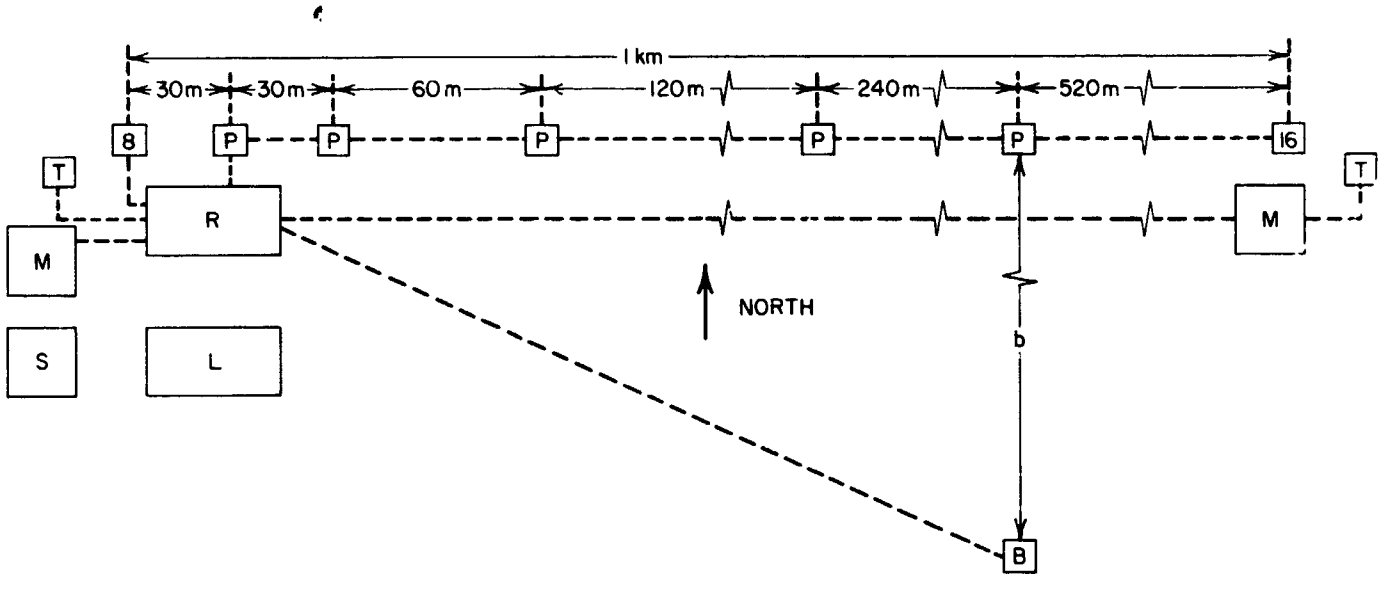

8 8-meter antenna and radome
16 16-meter antenna and radome
P Mounting pad for 4-meter rigid foam antenna
T Demountable meteorological instrumentation towers
M Meteorological instrumentation shelter
(Magnetometer mounted in eastern shelter)
R Receiver house: RF equipment, recorders, clock
S Equipment storage
---- Buried cables
L Living quarters (if required)
B Demountable boresight tower
(b should be as large as possible)

TA-5067-25

FIG. 11 SITE LAYOUT FOR A MEDIUM-COST EXPERIMENT

V DATA COLLECTION

As discussed in Sec. II-B of Ref. 4, the data of interest are in the 0-to-100-cps range and are essentially zero above 200 cps. Therefore, a sampling rate of 150 cps will be satisfactory.

While exact determinations of the appropriate number of levels and hence of bits will be a function of the final design, the following estimates can be made:

Signal	Peak Value	Resolution	Number of Bits
Time	3600 sec	1/1000 sec	22
Local Oscillator Offset*	16 kc	1 cycle	14
Azimuth Encoder	1 rev.	6.28 μr	20
Elevation Encoder	1/4 rev.	6.28 μr	18
Azimuth monopulse error	10 mr	10 μr	10
Elevation monopulse error	10 mr	10 μr	10
Sum signal amplitude	Peak	1/100 peak	7
VCO frequency	512 cps	1 cps	9
VCO phase	8 cycles	10 mr	13
	Total of common data		36
	Total of data per antenna		87

Hence, for N antennas in use, the required recording rate is approximately (36 + 87N) 150 = 5400 + 13100N bits/sec. For two antennas, this is 31.5 kilobits/sec.

* The maximum Doppler shift at 16 Gc for a 10-hour orbit is ±6 kc. The remaining 4 kc allows for satellite oscillator drift.

A. RF--Phase, Amplitude, and Angle of Arrival Data*

For each antenna in use during a given run of Type I or II (see Sec. II-E), both analog and digital data will be generated. After analog-to-digital conversion of the analog data, all data will be recorded in computer-compatible digital format. Data originally in digital form may require format conversion before recording.

The local oscillator signal for the first mixer is common for all antennas in use and is produced at each antenna by a frequency synthesizer that accepts a digital input. Hence the local oscillator frequency is available in digital form and need be recorded only once, regardless of the number of antennas in use. The station time signal is, obviously, also digital and common.

The remaining digital data are the mechanical axis pointing angles of each antenna. These are sensed by shaft encoders directly in digital form. There is an azimuth and an elevation angle encoder for each antenna.

Each antenna and associated receiver will also generate the following analog voltage inputs:

(1) Azimuth monopulse error
(2) Elevation monopulse error
(3) Received sum signal amplitude
(4) Voltage-controlled-oscillator frequency
(5) Voltage-controlled-oscillator phase.

With the possible exception of the two monopulse error voltages, these outputs will be directly proportional to the quantities of interest. However, each monopulse error voltage is, except for very small angles, a non-linear function of both the error angles. Hence analog prccessing to obtain the error angles is impractical.

* This section was prepared by C. H. Dawson.

B. Noise Data*

The peak readings of noise temperature for various noise sources are known from available data. The correlated fraction of the noise can be estimated, using reasoning such as in Appendix G, to be less than approximately 15 percent. The equivalent temperature of the atmospheric-absorption noise at 16 Gc, and at an elevation angle of 5 degrees is about 60°K (Ref. 24); thus the expected correlated noise temperature is less than approximately 9°K. The galactic center has an equivalent temperature of 60°K at 0.91 Gc (Ref. 25), which can be extrapolated to about 12°K at 2 Gc. The expected correlated noise at 2 Gc is thus less than approximately 1.8°K. The noise temperature also falls off rapidly away from the galactic center. The equivalent temperature of the earth is 200 to 300°K, but since a given area of the earth will be viewed from considerably different angles by the two antennas, the correlated fraction of noise will be appreciably less than 15 percent. All that can be said at this time is that the correlated earth noise will be appreciably less than 30°K when viewed in the antenna main beams, and correspondingly less when viewed in the side-lobes. The equivalent noise temperature of the sun in the 1-to-20-Gc band is several thousand degrees Kelvin; thus there will be no problem in obtaining sufficient system sensitivity. The system gain will have to be reduced considerably over that used for measurements on the other noise sources.

The resolution of the Ryle phase-switched receiver can approach the theoretical limit of the minimum detectable increase in noise (Ref. 9), provided that care is taken in the design and construction of the equipment. This minimum detectable increase (Ref. 9) is†

$$\Delta T = 2 \frac{T_{total}}{\sqrt{B_T}}$$

* This section was prepared by L. A. Robinson.

† Ryle's result does not include the factor 2 although the presence of such a factor is generally accepted.

where T_{total} is the equivalent temperature of the total output power, B is the receiver predetection bandwidth, and τ is the post-detection integration time constant. Taking as an example some values that might be typical, assume $T_{total} = 500^{\circ}K$ referred to the receiver input, B = 1 Mc, and τ = 200 sec, then $\Delta T = 0.05^{\circ}K$, which would be adequate for the purposes of this experiment.

The sampling rate for the noise measurements will be considerably slower than for the other measurements. The parameters to be measured are not expected to change with time, and relatively long integration times are required to get good resolution. One measured data point every few minutes would be a typical sampling rate.

C. Meteorological Data*

In Sec. II-C, meteorological measurements were grouped into (1) absolutely required, (2) extremely desirable, and (3) desirable.

Group 1 includes surface temperature, pressure, wind and precipitation; upper-level temperature, pressure, humidity and wind; and precipitation distribution (radarscope photograph). None of these variables need be sampled more than once per minute and probably one or two readings during a 5-to-10-minute run would suffice. All can be handled with standard meteorological accuracy. While automatic logging is desirable, the data rate involved is low.

Group 2 includes airborne refractivity profiles and liquid water measurements, surface refractivity, and cloud cover (photograph). It is expected that the airborne instruments include suitable recorders.† Surface refractivity should be sampled at a rate of 10 per second. A resolution of one N unit and a peak of 350 N units requires 9 bits. One cloud photograph every five minutes should suffice.

---

* This section was prepared by F. G. Fernald and C. H. Dawson.

† Nine-bit refractivity samples are required at a rate of 10 per second.

Group 3 includes additional airborne refractometer data and sky-noise temperature measurement. The later measurements could be taken with the radiometer receiver about 10 minutes or less preceding or following a data run. Since long integration times are required and only one value is required, the amount of data generated is very small.

D. Ionospheric Data*

Much of the data required to characterize the ionosphere will be taken for the RF experiment and need not be repeated. Other data will be obtained elsewhere at a rate of once per day or less.

The output of the magnetometer measuring the local magnetic field can be graphically recorded (see Fig. 34) for later interpretation, or alternatively digitized and recorded. In the latter case, the resulting data rate will be low.

If backscatter instrumentation is used, the various displays should be photographed at least once per run. These displays include A-scope, PPI, and height.

The equipment receiving the 100- or 700-Mc beacon should detect the phase variations of the signal and these variations can be graphically recorded for later interpretation.

E. Operator Data*

In order to make the experiment as meaningful as possible, it is important that the personnel manning the equipment be required to document each run in as much detail as time permits. A voice recorder might be an appropriate medium.

In addition to such environmental factors as an aircraft in or near the beam and unusual temperatures in the receiver house, calibration

---

* This section was prepared by C. H. Dawson.

procedures and results, equipment performance and required maintenance, and identification of the equipment actually in use should be noted.

Since the effect of factors external to the experiment are in general unknown, any unusual circumstance should be noted in order to facilitate interpretation of the experimental results.

VI DATA PROCESSING*

Regardless of the extent of the meteorological and ionospheric experiments actually performed, whatever data is available for each run should be used by appropriately trained personnel to classify the states of the troposphere and the ionosphere. Possible classifications of the ionosphere are described in Sec. III-I.

Data from the RF experiment will be classified as indicated in the following sections.

Correlations can then be sought between these three classifications where each data run constitutes one item of reduced data. Standard statistical techniques can be used. Alternatively, the mass of parameters accumulated for each run can be clustered by techniques (Ref. 26) now being developed for such multi-dimensional problems.

Note that, in general, the meteorological and ionospheric data will not all be taken concurrently with the RF data and therefore no fine-scale correlation should be attempted.

A. Frequency and Phase

Since the local oscillator frequency is programmed to include the expected range-rate variations and the predicated transmitter frequency, the average, over the run, of the VCO frequency represents primarily the error in transmitter frequency prediction. Hence the average over the run of the VCO frequency should be computed and used as follows:

(1) To predict the transmitter frequency for the next data run

(2) To remove the corresponding linear trend from the phase record.

The remaining phase fluctuation record will then be ready for the processing described in Subsection E below.

---

* This Section was prepared by C. H. Dawson.

B. Angle of Arrival*

1. General

The purpose of data reduction is to extract from the experimentally obtained raw data, meaningful results for the angle-of-arrival experiment. The principal results desired for this experiment are amplitude and frequency distributions of the angular deviations of the angle of arrival away from line of sight. In order to determine these distributions, the instantaneous deviation must be determined continuously from the raw data. This may be done by first correcting the raw data to compensate for errors that can be calibrated, and then subtracting the most reliable computed orbit data from the experimental data. The difference is, to within the accuracy limitations of the various contributions, the instantaneous-angle-of-arrival deviation. The following subsection discusses some of the considerations attendant to the question of data reduction for this experiment.

2. Data Correction

The data as recorded during an experimental run consists of two variables for each axis: the antenna pointing angle as indicated by the shaft position encoders, and the angular pointing error signal from the monopulse receiving equipment. In the absence of errors the angle of arrival is just the sum of these two quantities. However, several data-processing operations should be performed on each of these quantities before they are added, to ensure that the sum obtained contains the least possible error.

There are several factors that cause the boresight axis of the antenna to differ from the position indicated by the digital encorders (see Sec. VII-B-4-a). It was also indicated that techniques are available for obtaining calibration curves that describe the effects of these factors. Storing these curves in the memory of the data-processing

---

* This section was prepared by E. C. Fraser.

computer will permit the raw position-encoder data to be corrected to remove (or significantly reduce) the errors contained in this measurement.

The error contained in the angular pointing error signal resulting from RF front-end noise cannot be compensated by calibration techniques. However, a calibration curve is necessary in order to obtain the angular pointing error from the angular pointing error signal. As shown in Fig. 12, the relationship between angular pointing error and angular

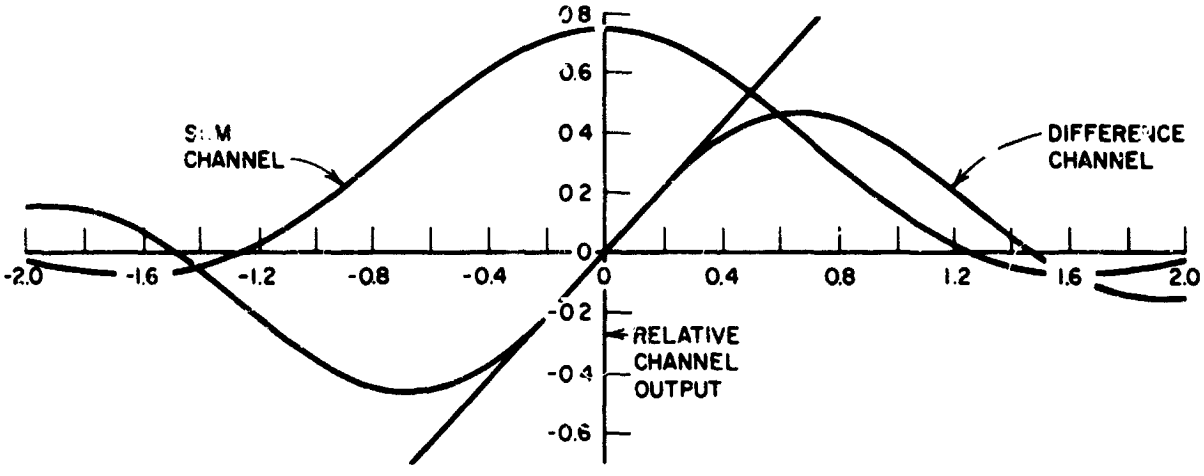

FIG. 12 ANGULAR DEVIATION FROM AZIMUTH BORESIGHT — SUM AND DIFFERENCE CHANNELS

pointing error signal is nonlinear and is defined by the shape of the antenna beam pattern. Since the beam pattern shape cannot be precisely defined a priori, it is not possible to accurately predict the curves shown in Fig. 12. It is therefore necessary to measure these curves and employ the resulting calibration curves in all subsequent data processing. Furthermore, the curve shown in Fig. 12 is somewhat misleading in that it tends to indicate that the output of the azimuth

difference channel due to an angular pointing error in azimuth is independent of the value of angular pointing error in elevation (and vice versa). This is not strictly true, the shape of the curve varies slightly as a function of pointing error in the orthogonal axis. For most applications this effect may be neglected (and usually is) but here it is necessary to compensate for it in order to obtain maximum possible accuracy. Hence it will be necessary to measure and store in the computer memory the calibration curve relating the output of each difference channel to the azimuth and elevation pointing errors. By the use of this curve and the raw-data pointing-error signals, the best possible values of the instantaneous-pointing-angle errors can be obtained.

Once the appropriate corrections have been made to the antenna pointing-angle data and the pointing-error data, these two quantities can be added to produce a "best" value for the observed instantaneous angle of arrival. If all of the indicated corrections are made, the rms measurement error is estimated to be of the order of 50 μr.

3. Computed Orbit

If the angle-of-arrival deviations are to be obtained by comparing the observed values with those derived from a computed orbit, consideration must be given to the determination of this computed orbit; since any errors introduced at this point will be directly reflected in the end results of the experiment.

The procedure most frequently employed for modeling the orbit of an earth satellite is that of specifying the set of six coupled first-order differential equations that govern the motion of the satellite. In the case where the forcing functions for these equations derive solely from a homogeneous $1/r^2$ gravitational force field, the equations yield the classic Keplerian ellipse as the closed-form solution for the orbit of the satellite. However, there are a number of additional factors that also contribute to the differential equation forcing functions, thus producing a more complex result. Included among these factors are the following:

(1) Since the gravitational force field of the earth is neither symmetric nor homogeneous, it cannot be expressed by a simple closed form expression but rather is usually expressed in terms of zonal and tesseral harmonics. Each of these harmonics contributes a forcing term to the differential equations.

(2) The effect of solar pressure,

(3) The effect of the sun, moon, and other planets,

(4) The effects of atmospheric drag.

Several solutions have been derived by various investigators (Refs. 27-33), that take into account some or all of the effects mentioned above. Each of these solutions yields an orbit description in terms of a set of defined parameters.

When it is desired to determine the orbit of a particular satellite on the basis of observed tracking data the procedure is to find a set of values for the parameters associated with the particular solution or formulation being used, such that the curve resulting from the orbit model fits the tracking data in some optimal fashion. The customary measure of fit is that of least square residual. In this case the quality of fit is given by the average value of the square of the difference between the observed value and that given by the model. When adjusting a model to fit observed data it is good practice to include, as parameters to be determined, the location coordinates of the tracking stations, since topological surveys are not capable of determining these coordinates with sufficient accuracy. It has been found by experience that the optimal amount of tracking data to consider in the determination of an orbit is on the order of one week. This value yields the minimum residual errors.

The orbit, as determined by the methods just described, may be used to interpolate (make a best estimate of where the satellite was at a given time), or to extrapolate (make a best estimate of where the satellite will be at some future time). Of these two, the first is most appropriate to this experiment. By transforming from the space coordinates--in which the differential equations were solved to obtain the computed orbit--to the azimuth, elevation, and range coordinates

centered at the tracking station, the computed orbit is obtained in a format allowing direct comparison with the observed angle-of-arrival data. A second output of this coordinate transformation is information on range and range rate. This will be valuable in reducing the data from the phase-fluctuation experiment.

The accuracy of a computed orbit (i.e., how closely it corresponds to the true path of the satellite) can be discussed only in terms of the accuracies of the tracking data from which it was determined, and the residual errors associated with the fit of the model to the data. Most tracking data used at present for scientific satellites is obtained from the NASA Minitrack network. These tracking stations operate on the interferometer principle and have a reported accuracy of 0.9 mr of arc. Several of the tracking stations are equipped with parabolic reflector tracking antennas that have reported accuracies in the order of 0.3 to 0.6 mr. Utilizing this data, the residual error over a period of a week ranges from 0.126 to 1.63 mr, depending on the particular satellite and the sophistication of the model used to describe its orbit.

The most accurate orbit determinations that have been made to date utilized data from the optical tracking network maintained by the Astrophysical Observatory of the Smithsonian Institution. These site employ Baker-Nunn tracking cameras that photograph the satellite against the star field background. Using the stars as a reference, most of the errors attendant to other sources of tracking data are avoided. The Baker-Nunn camera is reported to have an accuracy of 14.5 μr. The residual errors, over a one-week period of data, that have been achieved using optical tracking data, are in the order of 14 μr.

4. Data Comparison

It was stated in Sec. 1 that the angle-of-arrival deviation is obtained by subtracting the computed points on the satellite orbit from the observed value at that time. Considering the expected magnitude of the deviations (in the order of 0.3 mr), it is seen that an accurate computed orbit must be used in the computation if any degree of confidence in the result is to be preserved. It is recommended that as a

minimum the tracking data from the Minitrack network be used in determining the computed orbit. The most sophisticated orbit model available (i.e., one that takes into account the greatest number of contributions to the differential-equation forcing functions) should be employed to minimize errors due to model imperfections. The tracking data on which the model is adjusted should be evenly divided in time on either side of the experimental data to be reduced. The total span of data used should be in the order of 7 to 10 days. Following this procedure will lead to a computed orbit with an estimated error variance in the order of 50 to 100 μr.

For a measured data standard deviation of 50 μr, the resulting angle-of-arrival standard deviation will have to be of the order of 75 to 110 μr.

To achieve a smaller variance in the angle-of-arrival deviation information, it is recommended that the computed orbit be determined on the basis of optical (Baker-Nunn) tracking data. The standard deviation of the computed orbit will then be in the order of 15 μr, leading to a standard deviation in the resulting angle-of-arrival deviation information in the order of 53 μr.

The angle-of arrival fluctuation record as derived above is then ready for the processing described in Sec. E below.

C. Amplitude*

Depending on the accuracy desired and the variation of range† during a data run, it may be desirable to correct the received amplitude for the effect of range. After such correction, the amplitude should be averaged over the run. This average would then be used to:

---

* This section was prepared by C. H. Dawson.

† The maximum change in range during a 10-minute period for a 10-hour orbit is 4%.

(1) Determine antenna gain as a function of diameter

(2) Normalize the path gain fluctuation data with respect to antenna diameter and sum channel receiver gain.

If x is the amplitude data, the normalization is

$$y = \frac{x - \bar{x}}{\bar{x}}$$

where $\bar{x}$ is average of x over the run.

The amplitude data, y, will then be ready for the processing described in Sec. E below.

D. Noise*

The processing of the noise-correlation data is very simple. The ratio of the correlated noise to the total noise is just the ratio of two output voltages from the receiver of Fig. 2: $K(V_1)/(2V_2)$. Separate measurements of the receiver noise figure and gain will provide data on the internal noise (which is uncorrelated between channels), so that this can be subtracted from the total external plus internal noise. The final result will be the ratio of the correlated noise to the total external noise.

E. Correlation and Spectra†

For each of the reduced fluctuation variables--phase, amplitude, and angle of arrival--described in Secs. A, B, and C, there is available a record of length ≥ 400 seconds for each antenna used during the run. These records consist of samples taken at a rate of 150/second. Following the procedure described in Sec. II-B of Ref. 4, the autocorrelation is computed for shifts up to 0.2 second at intervals of 1/150 second and, after additional low-pass filtering, for shifts from

---

* This section was prepared by L. A. Robinson.

† This section was prepared by C. H. Dawson.

0.2 to 2 seconds at intervals of 1/15 second. Fourier transformation then yields spectral estimates every 0.5 cps from 0 to 10 cps and every 5 cps from 10 to 100 cps. Finally the Hamming window is applied to give the smoothed power spectrum of the variable.

An entirely analogous procedure applied to data from a pair of antennas will yield the crosscorrelation* and the smoothed crosspower spectrum. These crossfunctions are the autocorrelation and smoothed power spectrum of the part of the variable that is the same at two antennas--i.e., the correlated component.

For purposes of classification, the peaks of the autocorrelation and crosscorrelation functions measure the mean square fluctuation and the correlated component of the mean square fluctuation respectively. The ratio of the correlated component to the square root of the product of the peaks of the two autocorrelations is the correlation coefficient for the 0-to-100-cps range. Correlation coefficients for other frequency intervals can be obtained by dividing the area under the smoothed crosspower spectrum for the frequency interval of interest by the square root of the product of the corresponding areas of the two smoothed power spectra.

Each spectrum can be further classified by its low-frequency value, its break frequencies and its slopes. Since the noise contributions in the power spectra are expected to be flat with frequency, and since the fluctuations should decrease with increasing frequency, the level of the spectra near the upper frequency of 100 cps can be expected to measure the noise level.

The correlation results for various antenna spacings might be presented as one or the other of the following:

(1) Plots of correlation coefficient vs. effective spacing with the frequency interval as parameter.

(2) Power spectral density vs. frequency with effective separation as a parameter.

---

* Since these crosscorrelations are actually autocorrelations, they are even functions of the shift variable.

Finally the RF data for each run (phase, amplitude, angle-of-arrival) will be classified by the characteristics of the spectra (total area, low frequency value, break frequencies, slopes, correlation coefficients).

F. Meteorological Data*

The details and extent of the data-processing task will depend upon the scope of the instrumental observations and how much use is made of existing facilities.

The most powerful tool for examining and correlating the variability of the significant parameters is undoubtedly power spectrum analysis (see Sec. II-B of Ref. 4). The key parameter is refractivity in the beam, particularly at the lower levels, and spectra should be computed for a series of height intervals for unit periods during the collection of radio signal data.

There is clearly no point in carrying out the analysis with unnecessary refinement. The order of spatial inhomogeneity of refractive index which will be signigicant is of the order of 30 meters and above. Lag intervals to cover wave numbers appropriate to say, twice this value should thus be adequate. It is important to recognize the part played by wind velocity in relating spatial fluctuations to observed temporal fluctuations at a fixed point. In reducing the refractometer and hygrometric observations, the wind velocity should be taken into account.

If it is found that the spectra can be adequately described by a relatively simple expression (i.e., the -5/3 power law or the Bessel function found by Gossard), it would be convenient to use such an expression in describing the observations in each case. If, however, the power spectra are irregular, so that comparisons between one series of observations and another can only be made in general terms, then it would be convenient to classify the various forms of spectra observed

---

* This section was prepared by F. Fernald.

into as few representative classes as possible and to use this classification as a basis for comparison and extrapolation of the radio observations.

It would also be necessary to correlate the refractive index data with the general meteorological data. For purposes of extrapolation, a fairly broad classification according to weather types would probably suffice. It would be much better, however, to establish more quantitative relationships, and attempts should be made to find correlations between refractive index power spectra and factors combining such parameters as wind velocity and absolute humidity.

The ultimate aim of the analyses should be to establish a sound practical technique for interpreting the radio data and applying the results of the experiment to subsequent operations. As a minimum it would be valuable to be able to distinguish clearly between those occasions when tropospheric conditions were a negligible factor and those occasions when such conditions severely affected propagation. Hopefully, the atmospheric conditions could be assessed with sufficient precision to permit identification of the separate occasions when the atmospheric effects were strictly comparable. Ideally, we would hope to describe the propagation conditions quantitatively with sufficient precision for comparisons of other aspects of the experimental results on occasions when the atmospheric conditions were dissimilar.

BLANK PAGE

VII EXPECTED ACCURACIES

A. Phase and Amplitude*

1. Discussion

The expressions obtained for the output measurement voltages in Sec. III-E-3 on the receiver structures permit us to list the major error sources and to examine in some detail the way in which these sources contribute to total measurement error. The error list for angle-of-arrival measurement is given in Subsection B, below, so in this section only the other measurements are considered. Equations (5), Sec. III-E, or, more directly, their linearized approximations, Eqs. (J-5), Appendix J, give the gain and phase measurements as

$$\varphi_M(t) = \theta_o + \int dt \left(\frac{\omega_o}{c} \dot{d} + \hat{\omega}_\Delta + \frac{\omega_o}{c} \dot{\hat{r}}_\Delta \right) + \varphi_{ns}$$

$$g_M(t) \simeq K_o \left(1 + k_p \right) + K_o k_a + \frac{N_s}{a_o A_t} \quad .$$

The quantities in these we desire to measure are the atmosphere-induced phase fluctuations, $\int dt (\omega_o/c)\dot{d}$, and the path gain fluctuations, $K_o \left(1 + k_p \right)$. The error terms in phase and gain, then, are

$$\varphi_e(t) = \theta_o + \int dt \left(\hat{\omega}_\Delta + \frac{\omega_o}{c} \dot{\hat{r}}_\Delta \right) + \varphi_{ns} \tag{6}$$

$$g_e(t) \simeq K_o k_a + \frac{N_s}{a_o A_t}$$

---

* This section was prepared by W. H. Foy.

where θ_o and k_a enter because of phase and amplitude (fractional) variations of the transmitted signal, $\hat{\omega}_\Delta$ and $\hat{\dot{r}}_\Delta$ are errors in the prediction of transmitted signal frequency and of range rate, and φ_{ns} and N_s enter because of sum-channel receiver noise. Constants ω_o, c, K_o, a_o, and A_t have been defined in Sec. III-E-3. The different error sources are statistically independent, at least in the first-order approximation for which Eq. (6) is valid, so the power density spectra for the error terms are

$$G_{\varphi e}(f) = G_{\theta o}(f) - \frac{1}{(2\pi f)^2} G_{\omega\Delta}(f) - \frac{\omega_o^2}{c^2 (2\pi f)^2} G_{\dot{r}\Delta}(f) + \frac{G_e(f;\, \sigma_s^2,\, f_{ns})}{a_o^2 \langle A_\mu^2 \rangle}$$

$$G_{ge}(f) \simeq K_o^2 G_{ka}(f) = \frac{G_e(f;\, \sigma_s^2,\, f_{ns})}{a_o^2 A_t^2} \qquad (7)$$

where, for example,

$$G_{\theta o}(f) = \int_{-\infty}^{\infty} dt \exp\,(i_{2\pi f\tau}) \langle \theta_o(t)\theta_o(t+\tau) \rangle \quad .$$

Here, $G_e(f;\sigma^2, f_n)$ is the spectral function defined in Eq. (J-5), Apendix J, and gives the power density spectrum of a noise-induced error term. The terms $G_{\theta o}$ and G_{ka} in Eq. (7) can usually be evaluated from test data on the transmitter. The spectra $G_{\omega\Delta}$ and $G_{\dot{r}\Delta}$ are very difficult to evaluate; they depend on orbit prediction errors for which comprehensive data are not easy to find. The noise-induced errors have been estimated analytically in Appendix J. The function $G_e(f;\, \sigma_s^2,\, f_{ns})$ depends on the variance and bandwidth of the signal phase fluctuations as well as on the noise power and noise bandwidth; shapes of this spectral function for various parameter values are shown in Figs. J-2 and J-3.

The variances of the total errors, φ_e and g_e, are the sum of the variances of the individual terms in Eqs. (6). Equations (7) thus

provide a basis for the construction of an error budget in which the contribution of each individual error term to the overall mean-squared error can be assessed. Only the noise-induced error terms have been treated analytically. In Eqs. (J-9) and (J-10), Appendix J, we find

$$\left\langle \varphi_{ns}^2 \right\rangle \simeq \frac{1.961}{\eta_s} \tag{8}$$

$$\left\langle \frac{N_s^2}{a_o^2 A_t^2} \right\rangle \simeq \frac{1.961}{\eta_s} K_o^2$$

for the phase noise-induced mean-squared error and the gain noise-induced mean-squared error, respectively; here we have taken $a_o = 2.02$ for a reasonable value of summing hybrid gain. The ratio (η_s) of maximum available sum-signal power to sum-channel noise is defined in Sec. III-B-3. These show that an increase in transmitter power or a decrease in receiver noise temperature will decrease these error variances proportionately; a decrease in average path length (i.e., an increase in K_o) will decrease the rms phase error but will leave the gain rms error unchanged.

There is a possibility that one might be able to eliminate the noise-induced terms in Eqs. (7) by running a "calibration" noise spectrum on a receiver channel with no received signal and then subtracting this calibration spectrum (weighted properly) from the signal fluctuation spectra calculated from later runs. Such an operation is of doubtful usefulness since the G_e spectra that should be subtracted depend not only on the signal's presence but also on its phase fluctuations. Further, the spectrum of the sample of noise available for calibration may be significantly different from the spectrum of the noise during the data run because of errors due to finite time of observation and local non-stationarity. The more profitable course would be to increase the experimental signal-to-noise ratio so that the rms noise-induced errors would be made small.

In any case, since one would expect the error of the noise "calibration" spectrum to be some significant fraction of the noise power, the variances given by Eqs. (8) provide useful design limits for the other

error-contributing terms. For example, the designer would surely specify that the variance of the transmitter phase fluctuations be less than $\langle \varphi_{ns}^2 \rangle$, but it will be a waste of effort to make it less than $\langle \varphi_{ns}^2 \rangle /10$ since all the squared error contributions are added and the square root of the sum taken to give rms overall error. Equations (8) thus provide a sort of design reference level for the various error terms.

2. Error Budget--Phase*

The rms phase fluctuation of the transmitter output (see Appendix E) is expected to be 17 mr. The range-rate is expected to be sufficiently accurately known from orbit prediction that the resulting uncertainty will not contribute significant phase error. While the transmitter frequency may not be exactly known from previous runs, its uncertainty will contribute only a linear term to the phase, which will be removed in processing. The noise-induced phase error is given by

$$\varphi_n^2 = \frac{1.961 \times 10^6}{\eta_s} (\text{mr})^2$$

where η_s is the signal-to-noise power ratio for the ideal sum channel.

Then the total rms phase error is given by Table III.

Table III

PHASE ERRORS

η_s (db)	Mean Square Errors $(\text{mr})^2$			Total rms error (mr)
	Transmitter	Noise	Total	
20	289	19,610	19,899	141
30	289	1961	2250	47
40	289	196	485	22

* This section was prepared by C. H. Dawson.

The minimum rms fluctuation in phase due to the propagation path is expected to be about 75 mr. Therefore an ideal sum S/N of 40 db will be sufficient to give meaningful results under all conditions.

3. Error Budget--Amplitude*

The rms amplitude fluctuation of the transmitter output has been specified as 1%. It is assumed that the fluctuation in the gain of the receiver sum channel can also be held to 1%. The gain variations due to mispointing of the antenna are expected to be negligible. The noise-induced fluctuations at the output of the amplitude circuit expressed in percent of the average output are given by

$$\left(\frac{1.961 \times 10^4}{\eta_s}\right)^{1/2}$$

where η_s is the signal-to-noise power ratio for the ideal sum channel.

Then the total rms amplitude error in percent is given by Table IV.

Table IV

AMPLITUDE ERRORS

η_s (db)	Mean Square Errors $(\%)^2$				Total rms error (%)
	Transmitter	Receiver	Noise	Total	
20	1	1	196	198	14.6
30	1	1	19.6	21.6	4.6
40	1	1	1.96	3.96	2.0

No definite information has been found on the magnitude of attenuation changes to be expected along a propagation path. However, it is known (page 40 of Ref. 3) that reception of non-planar phase fronts causes antenna gain reductions that increase with frequency and antenna diameter. This may be the primary effect measured by the amplitude experiment.

* This section was prepared by C. H. Dawson.

If various antenna diameters are used simultaneously, the rms errors of Table IV would be correlated only due to the contribution of the transmitter. Suppose a 4-meter and an 8-meter antenna were used; assume that η_s for the 4-meter antenna was 20 db; then η_s for the 8-meter antenna would be 40-db, giving variances of $\sigma_4^2 = 198$ and $\sigma_8^2 = 3.96$ and a covariance $\sigma_{4-8}^2 = 1$. Hence the correlation coefficient would be

$$\frac{1}{\sqrt{198 \times 3.96}} = 0.035 \quad .$$

Since the correlation coefficient is very small, the error in determination of the gain ratio would be very closely approximated by the square root of the sum of the individual mean square errors. For the example above, this would be

$$(198 + 3.96)^{1/2} = 14.9\% \quad .$$

B. Angle of Arrival*

1. General

The purpose of the angle-of-arrival experiment is the measurement of the amplitude and frequency distributions of the angular deviation between the observed direction of arrival of a radio signal from a known source and the straight-line path joining the receiver and the source. To accomplish this objective it is necessary to accurately measure and record the signal arrival angle (in a convenient coordinate system, such as azimuth and elevation) versus time. This section is devoted to a discussion of the method for collecting this data and the errors to be expected in each of the measurements.

2. Nature of the Data

Before discussing the measurement of an experimental variable it is well to consider the nature of the variable to be measured. In the

---

* This section was prepared by E. C. Fraser.

case of angle-of-arrival deviations, some feel for the expected magnitude of the variable to be measured may be obtained from the work of previous investigators. Smyth Research Associates (Ref. 34) measured angle-of-arrival deviations resulting from the action of the troposphere over a three-year period at Fairbanks, Alaska. The average of the maxima and minima are shown in Fig. 13. It is stated that for any given short

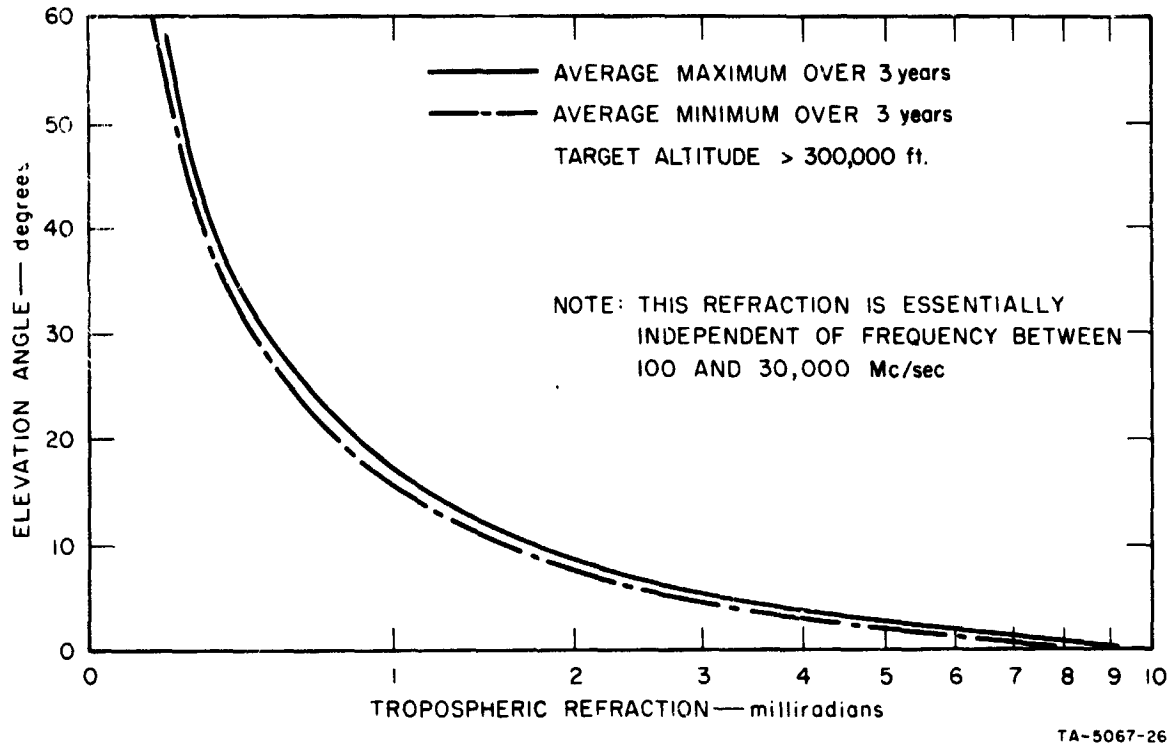

FIG. 13 ANGLE-OF-ARRIVAL DEVIATIONS — TROPOSPHERE

interval, fluctuations of the deviation about its mean value were in the order of 0.2 mr for a 5-degree elevation angle, decreasing to 5 μr at the vertical. Deviations due to the troposphere were found to be essentially independent of frequency up to at least 30 Gc.

Similar data for angle-of-arrival deviations resulting from the effects of the ionosphere are shown in Fig. 14. Ionospheric effects are dependent on frequency; the magnitude of the effect for two representative frequencies is shown in the figure.

The conclusion that may be reached from these data is that except for elevation angles less than 10 degrees, the magnitude of angle-of-arrival deviations will be less than 1.0 mr. Even at zero elevation it

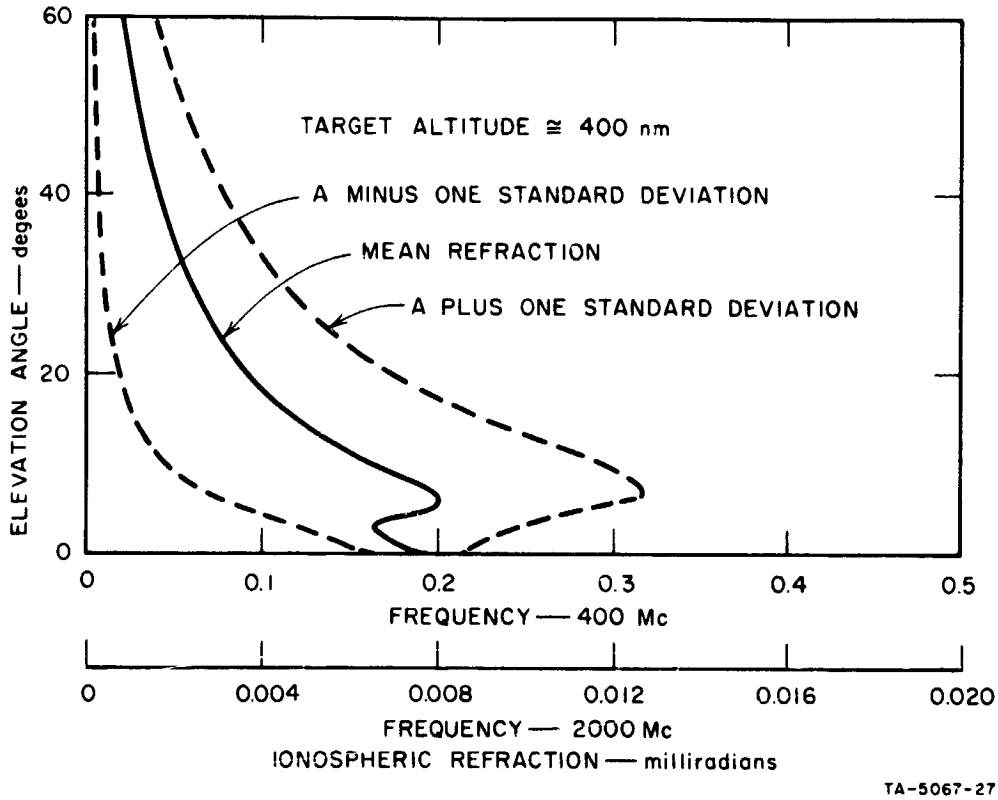

FIG. 14 ANGLE-OF-ARRIVAL DEVIATIONS — IONOSPHERE

is unlikely that any measurement would exceed 10 mr. The predominant contributions to these deviations take the form of steady-state or very-low-frequency fluctuations. In order to provide meaningful data, the measuring equipment must be able to provide accuracy and resolution considerably better than 0.9 mr. This implies that the total measurement error should be no greater than perhaps 40 μr. In addition the measurement equipment should be capable of measuring fluctuations that occur at rates up to at least 10 cps and preferably 100 cps.

3. Measurement of Time

It is assumed that the station time standard will be a WWV receiver capable of supplying timing signals accurate to at least 1 millisecond.

4. Measurement of Angle of Arrival

The angle of arrival of a radio signal is the apparent direction from the receiving site to the signal source. This angle may be expressed as the sum of two angles: the antenna pointing angle, and the pointing angle correction as determined by the monopulse system. These two quantities for each of the azimuth and elevation axes, together with time,

comprise the net data to be recorded. The antenna pointing angles, as read by the digital shaft position encoders may be recorded directly on digital tape. The pointing angle corrections will be in the form of analog voltages and hence must be digitized before being recorded in a digital format. A sampling rate of several hundred samples per second will be sufficient to retain all of the information contained in the 100-cps bandwidth of the receiver electronics output. Since time will most likely be available as a digitally encoded quantity, it may be directly recorded on digital tape.

a. Measurement of Antenna Pointing Angle

The pointing angles of the antenna are measured by means of digital shaft position encoders mounted on the azimuth and elevation axes. Such encoders, employing optical position readout techniques, are available in sizes up to 20 bits (e.g., Wayne-George Corp., Newton, Mass.). An encoder of this size provides a resolution of 6 μr and a peak error of ± 3 μr. These values are sufficiently small for the purposes of the experiment.

In addition to the errors inherent in the shaft position encoders, there are a number of other sources of error in the measurement of antenna pointing angle. For mechanical reasons the shaft angle encoders are mounted on the axes of the antenna; yet they are intended to measure the angular orientation, with respect to an absolute coordinate system, of the axis of the radiation beam pattern of the antenna. Therefore anything that acts to disturb the relationship between these two quantities introduces an error into the measurement. Several such contributing factors are described below.

1) Encoder Misalignment

This error is the result of mounting the encoder in such a way that its readout does not coincide with the true pointing angle of the antenna. Normal care during the assembly of the antenna should permit the initial value of this error to be held below 0.18 mr. Further reductions in this error may be made by calibrating the combination of antenna and encoder by sighting on orbital or celestial radio sources

whose positions are accurately known. The encoder misalignment errors may then be corrected either by repositioning the encoders or by incorporating the appropriate corrections in the subsequent data processing. The Jet Propulsion Laboratory has been successful in using radio stars to calibrate their 85-foot DSIF antennas to an accuracy of 18 μr (Ref. 36). It is to be expected that for smaller antennas, accuracies of this order cannot be achieved due to increased beamwidth with its attendent loss of angular resolution, and due to decreased signal-to-noise ratio as a result of the smaller energy-collecting aperture.

2) Mount Misalignment

This error arises if the axis about which the antenna rotates in azimuth is not vertical with respect to the local coordinate system. A second form of mount misalignment is the nonorthogonality of the azimuth and elevation axes. Each of these will cause the encoder readout to differ from the true pointing angles. As in the case of encoder misalignment, the errors introduced by mount misalignments may be measured by calibration of the antenna with a source of known location. Errors in the vertical axis (leveling errors) could conceivably be removed by the use of leveling jack screws, whereas no such convenient adjustment is usually available to correct orthogonality errors. In either case it is usually more convenient to establish a calibration function for these errors and to compensate the data during subsequent processing. The total error, before compensation, due to mount misalignment will rarely exceed 0.3 mr for a well designed mount positioned on a properly prepared foundation.

The problem of mount misalignment will be aggravated in the case of a movable antenna; the more so since it will be a small antenna for which highly accurate calibrations cannot be obtained. If the antenna is made portable by moving it from one prepared foundation to another, then it is not unreasonable to expect that, if a system of keying is provided to insure that the antenna is repositioned exactly the same every time it is placed on a particular foundation, an initial calibration of the antenna and mount on that foundation would be valid

for each subsequent use of the antenna at that location. Due to the difficulties of calibrating a small antenna, it is probably not reasonable to expect calibration accuracies better than 50 μr for the movable antenna.

3) Antenna Sag

As a result of its continuously varying aspect relative to the earth's gravitational field, the reflector and feed structure will be continually flexing, resulting in small perturbations of the antenna beam pattern. This phenomenon is usually referred to as antenna "sag." The effect of sag is to cause the principal axis of the antenna beam to deviate from the direction of this axis indicated by the encoders. The magnitude of this deviation varies from 10 μr or less at the zenith to as much as 600 μr when the antenna is pointed at the horizon. (Sag effects are most predominant in the elevation axis.) To the extent that the sag of the antenna is repeatable and may be measured by calibration procedures, this error may be compensated for in subsequent data processing. It is expected that these errors can be measured and thus compensated to within 10 μr.

4) Antenna Warpage

As distinguished from antenna sag, antenna warpage results from non-constant and unpredictable effects such as differential heating due to solar radiation, and distortion of the reflector and feed structure as a result of wind loading. [This latter effect must be distinguished from rigid-body wind-load effects which will be discussed in Subsection 5 below.] The effective deviation of the antenna beam pattern as a result of antenna warpage could become as large as 30 mr under severe conditions. Under normal conditions a reasonable value is in the order of 50 μr.

Since these effects are neither constant nor accurately predictable, it is futile to attempt to compensate for them by calibration. The only alternative is to eliminate, or significantly reduce, the source of the problem. Two possibilities exist for eliminating the effects of both thermal distortions and wind-load distortions. The first is the use of either rigid or inflatable radomes. In either case the

temperature of the environment inside the radome can be maintained constant, thus eliminating thermal distortions of the antenna. A radome will also eliminate wind effects on the antenna itself; however, in the case of an inflatable radome the wind could cause distortion of the radome shape. No data are as yet available to indicate the effect of radome shape distortion on the antenna beam pattern. Rigid radomes have been found to produce boresight deviations of less than 0.1 mr. (Ref. 37). This, however, is a systematic error whose effect can be reduced by calibration.

The second possibility involves the use of rigid shell structure antennas made of plastic foam rather than the conventional truss construction. These antenna construction techniques are described in Appendix X of Ref. 3. The shell construction is inherently more rigid than truss construction and would thus be less subject to wind-induced distortion. In addition, the smooth airfoil-like outer surface of a shell antenna is considerably less subject to wind induced differential forces which give rise to antenna distortions. The extremely low coefficient of thermal expansion and thermal conductivity of the plastic foam reduce the effects of solar heating to an unmeasurable quantity.

5) Load Disturbances

Load disturbances are those effects which cause the axis of the antenna to deviate from the command input pointing angles. These effects include the component of the wind that tends to move the antenna as a rigid body (as opposed to the component that distorts the antenna), and the effects of pointing servo system dynamics. The effect of wind gusts of 50 mph can cause angular deviation of up to 1 mr for a 30-foot-diameter reflector. Similarly, the maximum pointing error for an antenna with a pointing system bandwidth of 10 rad/sec (1.6 cps) tracking a satellite whose altitude is 200 miles with a zenith angle of 86^0, is 1 mr. For satellites at higher altitudes or lower zenith angles this value is only about 10 μr.

The errors produced by load disturbances are unlike the previously listed errors in that they produce a deviation of the axis

of the antenna beam away from the radio source, the amount of this deviation being indicated by a change in the readings of the antenna position encoders. This is in contrast to the errors that caused the antenna beam to point in a direction different from that indicated by the encoders. Since any deviation of the axis of the antenna beam from the direction of the radio source gives rise to an error signal in the monopulse pointing-error feedback channel, this type of pointing error will be automatically compensated for by the data-processing techniques suggested in Sec. VI-B.

b. Measurement of Pointing-Angle Error

As a result of the monopulse feed structure, the antenna exhibits two patterns for each of the azimuth and elevation axes. These are illustrated in Fig. 15 for the azimuth axis.

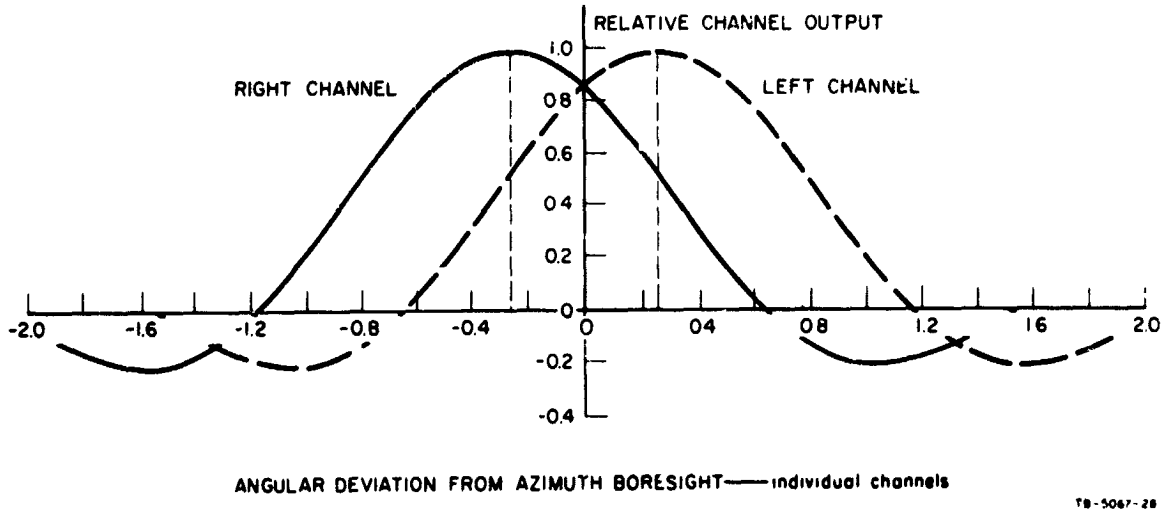

FIG. 15 ANGULAR DEVIATION FROM AZIMUTH BORESIGHT — INDIVIDUAL CHANNELS

The outputs of the left and right channels are combined in a hybrid junction to produce a sum and a difference signal. The resulting effective antenna beam patterns for the sum and difference channels are shown in Fig. 12.

It is evident from Fig. 12 that the output of the difference channel provides a measure of both the magnitude and direction of any

angular deviation between the radio source and the azimuth boresight. As discussed in Sec. III-E-1, the output signal of the difference channel is divided by the output of the sum channel. The effect of this operation is to remove the dependence of the output of the difference channel on the amplitude of the received signal. The result is that the magnitude of the angular pointing error signal is dependent only on the magnitude of the angular pointing error.

Since the bandwidth of the angular pointing error signal at the output of the receivers is limited only by the information bandwidth of the receiver electronics, it will contain information on angle-of-arrival deviations occurring at frequencies up to 100 cps. (Note that this bandwidth is not required for tracking purposes; hence further filtering is employed before the angular-pointing-error signals are fed into the tracking system.)

It can be noted from Fig. 12 that the relationship between angular-pointing-error signal and the angular pointing error is multi-valued if the error signal is taken as the independent variable and used to determine the error. To avoid this problem the maximum angular pointing error must be kept less than the values corresponding to the peaks of the difference curve. For antenna diameters D in meters and frequency f in gigacycles, the angular deviation corresponding to this peak is approximately

$$\psi = \frac{300}{fD} \text{ milliradians} \quad .$$

Hence for a 4-meter reflector operating at 2 Gc, unambiguous data will be obtained for pointing-error angles less than 38 mr, whereas for a 32-meter reflector operating at 16 Gc, the error angles can be no greater than 0.6 mr.

In addition to the measurement of angular pointing error, the angular-pointing-error signal will contain error terms from two additional sources: phase and amplitude unbalance in the RF combining hybrids, and RF noise generated at the front end of the receivers.

The phase and amplitude unbalance cause a loss of sensitivity in the difference channel and also a shift in the apparent boresight location. Since both the phase and amplitude unbalances are steady-state effects, they may be measured and corrected by insertion of appropriate RF phase shifters and gain adjustments, or their effects may be calibrated and compensation made during data processing.

The effect of RF noise generated at the front ends of the receivers is to add a spurious increment to the observed angular pointing error. The mechanism for this perturbation is analyzed in Sec. III-E-3.

The conclusion reached is that if the angular pointing error is to be measured with an error not exceeding 30 μr (a figure commensurate with the other uncompensatable errors) input signal-to-noise-ratios in the range of 26 to 56 db will be required depending on the reflector diameter and operating frequency.

5. Conclusion

It is recommended that during a tracking operation the output of the shaft-angle encoders and the angular-pointing-error signals be recorded versus time. Digital recording techniques should be employed, using A to D convertors for the pointing-error signals. Both variables should be recorded to a resolution of 5 μr (20 bits for a full 360 degrees). Most of the errors associated with the antenna and mount can be calibrated to an accuracy in the order of 15 to 30 μr. The use of radomes or plastic foam construction will materially reduce the size of the errors that cannot be calibrated, such as wind and thermal warpage. The most serious source of error is the front-end RF noise corrupting the angular pointing error signal. Considerable care must be taken to obtain RF signal-to-noise ratios sufficient to insure that this error contribution is made small (see Table V).

It may be concluded that if state-of-the-art equipment is employed and all the indicated calibrations carefully performed, the angle-of-arrival data can be obtained for which the rms error will be in the order of 50 μr.

6. Error Budget--Angle of Arrival*

The rms error in knowledge of satellite position is expected to be about 50 μr if Minitrack tracking data are used and about 15 μr if optical data are used. The encoder errors due to quantization are about 2 μr and are therefore negligible. The rms error due to wind and thermal distortions of the antenna is expected to be about 300 μr for an unprotected antenna, decreasing to 20 μr if a radome is used or to 50 μr for a rigid-foam 4-meter antenna. Calibration errors are estimated at 10 μr and are therefore negligible.

The error in the monopulse angles due to thermal noise is given by

$$\psi^2 = \frac{5.83 \times 10^9}{(fD)^2 \eta_s} (\mu r)^2$$

where f is the frequency in Gc, D the diameter in meters, and η_s the signal-to-noise power ratio for the ideal sum channel.

If fD is taken at its minimum value of 8 and the noise-induced error is equal to the remaining errors, then the results for the six cases of interest are as given in Table V.

Table V

ANGLE-OF-ARRIVAL ERRORS

	Minitrack			Optical		
	Unprotected	Foam	Radome	Unprotected	Foam	Radome
Tracking $(\mu r)^2$	2,500	2,500	2,500	225	225	225
Distortions $(\mu r)^2$	90,000	2,500	400	90,000	2,500	400
Monopulse $(\mu r)^2$	92,500	5,000	2,900	90,225	2,725	625
η_s	985	18,200	31,400	1,010	33,400	146,000
η_s (db)	30	43	45	30	45	52
rms error (μr)	430	100	76	424	74	25

* This section was prepared by C. H. Dawson.

The minimum rms angle-of-arrival fluctuation due to the propagation path is expected to be about 300 μr. Hence either a rigid-foam 4-meter antenna or a radome is required if meaningful data are to be secured under all environmental conditions.

Larger diameters and higher frequencies will decrease the required signal-to-noise ratio. With larger diameters the distortion error in a rigid-foam antenna can be expected to increase and only antennas with radomes can give meaningful data.

C. Noise*

Tiuri (Ref. 38) and Manasse (Ref. 39) have summarized the properties of receivers intended for noise measurements. In the proposed experiment, such receivers will be used for three purposes: (1) temperature measurements of the receiver noise, galactic noise, atmospheric noise, and earth noise; (2) correlation coefficient determination of the noise received by separated antennas referenced to both total noise and noise originating outside the receiver; and (3) boresighting on radio stars for antenna pointing system calibration.

For the first two purposes, Tiuri (Ref. 38) quotes the relation

$$\Delta T = 2 \frac{T_N}{\sqrt{B\tau}}$$

where ΔT is standard deviation of the receiver output, T_N is the system noise temperature, B is the RF bandwidth, and τ is the integration time. The factor 2 is theoretical and will probably be larger in an actual system. When switching is used, great care is required to equalize insertion losses for the two switch positions and to equalize the impedance seen by the receiver for the two switch positions since the receiver temperature can vary with impedance (Ref. 12).

---

* This section was prepared by C. H. Dawson.

For the temperature measurements, the rms error is ΔT. When the receiver temperature is subtracted from total temperature to give the received noise temperature, the rms error will be $\sqrt{2}\ \Delta T$. Since the correlation coefficient is given (see Sec. III-G) by $KV_1/2V_2$, the rms fractional error in its determination will be $\sqrt{2}\Delta T/V_1$ for total noise and $\sqrt{3}\Delta T/V_1$ for noise external to the receiver.

For system noise temperatures of $500^{\circ}K$ and $50^{\circ}K$, and for RF bandwidth integration time products of $(2 \times 10^6)\ 50 = 10^8$ and $(10^6)\ 1 = 10^6$, the resulting ΔTs are given in Table VI.

Table VI

ΔT IN $^{\circ}K$

		System Noise Temperature ($^{\circ}K$)	
		500	50
B_T	10^8	0.1	0.01
	10^6	1	0.1

For boresighting, Manasse (Ref. 39) gives the rms noise-induced angular error for a parabolic antenna as

$$\Delta\psi = \frac{\sqrt{2}}{\pi}\left(\frac{\lambda}{D}\right)\frac{\sqrt{1+\rho}}{\rho\sqrt{B_T}} \text{ radians}$$

Where λ and D are the wavelength and antenna diameter in the same units, and ρ is the power ratio of the star to the system temperature.

One of the brighter radio stars, Cassiopeia A, delivers a flux at the earth's surface of approximately 2×10^{-23} watts/m^2/cps at 2 Gc. This flux varies approximately inversely with frequency. The corresponding signal temperature seen by a 4-meter antenna with 0.55 efficiency at 2 Gc is

$$T_s = \frac{0.55\ \frac{\pi}{4} \cdot 4^2}{1.38 \times 10^{-23}}\ 2 \times 10^{-23} = 9^{\circ}K \ .$$

If the system noise temperature is $500^{\circ}K$, $\rho = 0.018$; if it is $50^{\circ}K$, $\rho = 0.18$. For these parameters,

$$\Delta\psi_{500} = \frac{\sqrt{2}}{\pi}\left(\frac{0.15}{4}\right)\frac{\sqrt{1 + 0.018}}{0.018\sqrt{B\tau}} = \frac{9.09}{\sqrt{B\tau}} \times 10^5 \ \mu r$$

or

$$\Delta\psi_{50} = \frac{\sqrt{2}}{\pi}\left(\frac{0.15}{4}\right)\frac{\sqrt{1 + 0.18}}{0.18\sqrt{B\tau}} = \frac{1.018}{\sqrt{B\tau}} \times 10^5 \ \mu 4 \ .$$

Thus, to keep the rms calibration error below 10 μr, for $500^{\circ}K$,

$$B\tau = \left(\frac{9.09 \times 10^5}{10}\right)^2 = 8.28 \times 10^9$$

and for $50^{\circ}K$,

$$B\tau = \left(\frac{1.018 \times 10^5}{10}\right)^2 = 1.04 \times 10^8 \ .$$

Thus a low-noise system is essential; B = 1 Mc and τ = 100 seconds would be suitable. Since the antenna will be tracking the star during the 30-second integration time, the calibration determination will be an average for the angle traversed by the star during that interval.

It is of interest to note that T_s and hence ρ varies as D^2 while $\Delta\psi$ varies inversely with D and ρ. Hence, for a given $\Delta\psi$, $B\tau$ is inversely proportional to D^3. On the other hand T_s and ρ vary approximately inversely with frequency or directly with λ. Hence $\Delta\psi$ does not vary with frequency.

BLANK PAGE

VIII SUMMARY*

A study has been made of the design of experiments to determine the effects of propagation phenomena on the operation of a multiple-aperture antenna array and to relate these effects to the states of the troposphere and ionosphere. Experiments to determine other, less closely related effects of propagation phenomena were considered.

In the frequency range of interest, the characteristics of the propagation path are primarily determined by the troposphere. Hence, the collection of meteorological data is an essential part of the proposed experiment. Three successively more complex programs for collecting the meteorological data are described, of which the first uses primarily data available from existing instrumentation. If the classifications of the troposphere on the basis of such data are found not to correlate with the observed path characteristics, it is recommended that the second, more complete program should be implemented. The third, very extensive program would provide data of great interest to radio meteorology but is not essential for the proposed experiment.

The characteristics of the propagation path are also determined by the ionosphere but, in the frequency range of interest, ionospheric influences are expected to be small. However, a great amount of gross ionospheric data is available from existing sources, and it is recommended that an attempt be made to correlate classifications of the ionosphere based on such data with the observed path characteristics. More extensive ionospheric programs are described and their implementation is discussed.

A variety of possible transmitter platforms and the use of natural sources have been investigated, but only for satellites with periods of

---

* This section was prepared by C. H. Dawson

ten hours or more can the position, velocity, and acceleration be determined with the accuracy required in the proposed experiment. The position of the satellite has to be known to within 50 μr if the errors in angle-of-arrival measurement are to be held to the order of 100 μr. Tracking accuracies of 15 μr are required if the position errors are to be of the order of 50 μr. The frequency stability (3×10^{-5} radians/sec rms for a 5-Mc crystal) and amplitude stability (0.04 db for a 10-minute interval) required are believed to be available in satellite-borne oscillators.

Measurement of phase fluctuations imposed by the path is the most important experiment that should be conducted. The carrier phase variations must be tracked by the individual phase-locked receivers of an operational multiple-aperture array. As these variations become more severe, the loop bandwidth must be increased with a corresponding reduction in the carrier-to-noise ratio. It is, therefore, of primary importance to determine the time and space correlations of phase under a variety of tropospheric and ionospheric conditions. An experiment to determine phase correlation is discussed and the sources of error investigated. A specific phase-locked receiver configuration is described and meaningful results can be expected using existing precision techniques to minimize the sources of phase error. Highly accurate antenna-pointing instrumentation and calibration is required only for the angle-of-arrival experiment.

The selection of a system for pointing the antennas of a multiple-aperture array depends upon the determination of the time and space correlations of angle of arrival. Thus, the angle-of-arrival experiment is second only to the phase experiment in its importance to the design of an operational array. Since angle-of-arrival variations are expected to be small, precision techniques must be used and all sources of error kept as small as possible. These error sources are identified and techniques for their control are described. The precision required for the angle-of-arrival experiment is believed to be attainable if the state of existing techniques are carefully used (e.g., use of radomes,

precision encoders, and precise orbital parameters); however, this experiment is both complex and expensive. Monopulse feeds are recommended; calibration of these feeds and all other pointing-angle instrumentation by boresighting on radio stars using a Ryle receiver is recommended. Highly accurate actual satellite position data are required for meaningful reduction of the resulting angle-of-arrival data. Discussions of antenna drives, rigid foam construction, rail- and pad-mounted movable antennas, and angle-error receivers are included. It was found that radomes are necessary to eliminate the effects of wind for the angle-of-arrival measurement.

Determination of the time and space correlations of signal amplitude is not critical in the design of a multiple-aperture array. The amplitude experiment requires only minimum additions to the receiver used for the phase experiment.

From theoretical analyses, the external noise received by separated antennas is expected to be essentially uncorrelated. However, since the amount of such correlation is important to the multiple-aperture concept, the theoretical conclusion of low correlation should be verified. The Ryle receiver is suitable for the noise-correlation experiment. This receiver can also supply sky-noise temperature for use in tropospheric classification.

The modulation bandwidth limitation imposed by a propagation-path phase characteristic non-linear with frequency is of interest not only to a multiple-aperture system but to all types of receiving systems. The implementation of this experiment requires the addition of two coherent sidebands, extra satellite power, and a small modification of the receiver.

Antenna gain is expected to increase more slowly than the theoretical second power of diameter when the received phase fronts are non-planar. No changes in receiver structure are necessary for the gain-versus-size experiment. Investigation of gain phenomena requires that a variety of antenna sizes be available. All other experiments require only one antenna size; a diameter of four meters is recommended.

The separation of tropospheric and ionospheric effects is discussed only briefly since the tropospheric effects are expected to be strongly predominant in the frequency range of interest. Simultaneous operation at two suitably separated frequencies is necessary to discriminate between these effects.

Methods of data collection, recording, and reduction are described together with site selection considerations and the events of a typical data run. Three types of data runs were specified. The maximum recording rate required is 32 kilobits per second.

IX CONCLUSIONS AND RECOMMENDATIONS*

The variables to be measured in the proposed experiment are small, and difficult to measure accurately. Hence, precision apparatus carefully operated is essential. While the scope of the experiment can be reduced, any reduction in the quality of the instrumentation will seriously decrease the value of the resulting data. The use of non-satellite sources has been considered (see Appendices B and C) but the characteristics of such sources cannot be measured with sufficient accuracy. Therefore, the use of a satellite source is recommended.

While the entire experiment is valuable in the design of an operational multiple-aperture array and in increasing understanding of propagation phenomena, the phase and angle-of-arrival fluctuation measurement programs together with at least the minimum meteorological program and their resulting data are essential to the proper design of the operational array.

Minor additions to the instrumentation required for the phase and angle-of-arrival programs will allow the performance of amplitude fluctuation and noise correlation programs. Prior analytical work indicates strongly that noise will not be correlated to a degree significant to an operational array.

The early phases, using only 4-meter antennas, of an actual experiment might be:

(1) The phase experiment with minimum meteorological (Group 1) and ionospheric programs would be implemented.

(2a) If the phase is found to correlate with the available meteorological data, the angle-of-arrival experiment would be implemented.

---

* This section was prepared by C. H. Dawson.

(2b) If the phase is found not to correlate with the meteorological data, a more extensive meteorological (Group 2) program would be implemented.

(3) The amplitude, angle-of-arrival, and noise-correlation experiments would be implemented.

Programs to determine antenna gain as a function of diameter and the bandwidth of the propagation path require relatively major equipment additions and modifications. The results of these programs are not essential to proper design of an operational array.

Experimental separation of tropospheric and ionospheric effects is of somewhat doubtful value since tropospheric effects are expected to predominate in the frequency band of interest. Similarly, ionospheric measurements may not prove useful; however, a modest ionospheric program requiring minor additional instrumentation is recommended.

Selection of a site having a variety of meteorological conditions and access to as much existing instrumentation as possible, and implementation of the phase and angle-of-arrival measurement programs with at least a minimum meteorological program are strongly recommended.

Appendix A*

EFFECTS OF AIRCRAFT FLYING IN THE VICINITY

* This appendix was prepared by R. B. Battelle.

BLANK PAGE

Appendix A

EFFECTS OF AIRCRAFT FLYING IN THE VICINITY

Because it may be impractical to restrict flying of aircraft through the area in which the propagation measurements are being made, it is important to take into consideration the effects that aircraft might produce on the measurements. Although an aircraft is too complex in its geometrical shape to permit analysis of its wave scattering characteristics in any great detail, it is possible to suggest the order of magnitude of the effects of an aircraft as a scatterer using a simple analytical model.

Consider the configuration of propagation paths shown in Fig. A-1. The incident wave at the plane through BC is scattered by an aircraft located at C, which is at an angle φ off the receiving antenna boresight and at a distance h from the receiving antenna at A. Thus, the antenna receives not only the desired signal over path AB, but also a multipath signal component over path AC.

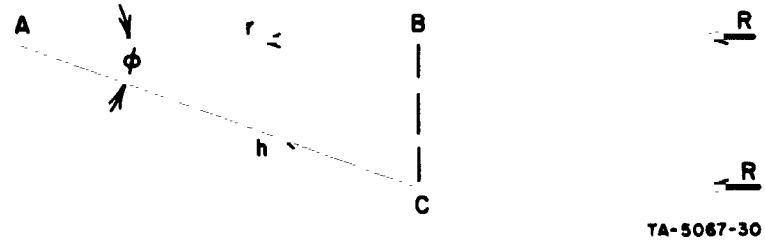

FIG. A-1 PROPAGATION PATHS

The relative amplitudes of the direct and multipath signal components can be estimated. The direct ray produces a signal at the receiver of power

$$P_d = \frac{P_t G_o}{4\pi(R + r)^2} \frac{\lambda^2}{4\pi} \qquad (A\text{-}1)$$

where

P_t = Effective radiated power from the RF source

R = Range from the source to the plane through BC

r = Direct path distance to the plane through BC

G_o = Receiving antenna gain in the $\varphi = o$ direction (G measured with respect to isotropic gain)

$\lambda^2/4\pi$ = Effective area of an isotropic antenna.

The power P_s received due to scattering of the incident signal from the aircraft is

$$P_s = \frac{P_t}{4\pi R^2} \frac{\sigma(\pi - \varphi) G_\varphi}{4\pi h^2} \frac{\lambda^2}{4\pi} \qquad (A\text{-}2)$$

where

$\sigma(\pi - \varphi)$ = Scattering cross section of the aircraft in the direction $\pi - \varphi$ from the direction to the incident signal source

G_φ = Receiving antenna gain in the φ direction

h = Distance from the receiving antenna to the aircraft.

The ratio of the scattered signal power to the direct signal power is thus

$$\frac{P_s}{P_d} = \sigma(\pi - \varphi) \frac{G_\varphi}{G_o} \frac{(R + h)^2}{4\pi R^2 h^2} \qquad (A\text{-}3a)$$

which for $R \gg h$ becomes

$$\frac{P_s}{P_d} \cong \sigma(\pi - \varphi) \frac{G_\varphi}{G_o} \frac{1}{4\pi h^2} \quad . \tag{A-3b}$$

In the frequency range of concern here, an aircraft will be very large in terms of wavelengths. Such large bodies will always have a forward-scattering cross section $\sigma(\pi)$ that is much larger than its back-scattering cross section $\sigma(0)$. Although the geometrical complexity of an aircraft makes the calculation of its forward-scattering cross section impractical, approximations can be made on the basis of calculations for simple geometrical shapes. For a sphere (Refs. 40-42), the value of $\sigma(\pi)$ has been determined to be

$$\sigma(\pi) = \frac{4\pi A^2}{\lambda^2} \tag{A-4}$$

where

A = geometrical cross section, and $\lambda^2 \ll A$.

At angles off the forward direction, the scattering cross section is less than it is in the forward direction. It has been found that $\sigma(\pi - \varphi_1) \approx (1/2)\sigma(\pi)$ at an angle

$$\varphi_1 \approx \frac{1.6\lambda}{2\pi r} \tag{A-5}$$

where

r = radius of the sphere, and $2\pi r > \lambda$.

At angles further off the direct path, the scattering cross section is independent of frequency and essentially equal to the geometric cross section of the scatterer. Equations (A-4) and (A-5) can be used to obtain an order-of-magnitude estimate of the cross section and forward-scattering beamwidth of an aircraft.

For example, a large transport aircraft might present a geometrical cross-sectional area A of 300 m^2. From Eq. (A-4), its forward-scattering cross section $\sigma(\pi)$ would thus be expected to be of the order of $10^9 m^2$ at 10 Gc and $10^7 m^2$ at 1 Gc. If the geometric surfaces of the aircraft can be assumed to have an equivalent radius of 2 m, the half-power angle φ_1 of the forward-scatter pattern, from Eq. (A-5), would be of the order of 4×10^{-3} radians at 10 Gc and 4×10^{-2} radians at 1 Gc. These angles are comparable with the angles to the half-power points of the antennas being considered for use on the experiment (e.g., a 4-meter-diameter parabolic antenna has a gain 3 db below maximum gain at an off-axis angle of about 2.5×10^{-3} radians at 10 Gc, and 2.5×10^{-2} radians at 1 Gc). From a "worst-case" point of view, Eq. (A-3b) can be applied to the condition for a large aircraft passing through the beam of the receiving antenna. The ratio of direct to scattered power would then be as follows:

$G_\varphi/G_o \simeq 1/2$, and h = 6000 meters,

$$\frac{P_s}{P_d} \simeq \frac{(1/2)10^9}{4\pi(6000)^2} \times 1/2 \simeq 5.5 \times 10^{-1} .$$

For $\varphi \simeq 0$, and the other conditions as above,

$$\frac{P_s}{P_d} = \frac{10^9}{4\pi(6000)^2} = 2.2 .$$

At 1 Gc, $\lambda = 3 \times 10^{-1}$ m, $\varphi \simeq 2.5 \times 10^{-2}$, $\sigma = 1/2 \times 10^7$, $G_\varphi/G_o \simeq 1/2$, and h = 6000 m,

$$\frac{P_s}{P_d} = \frac{1/2 \cdot 10^7}{4\pi(6000)^2} \times 1/2 = 5.5 \times 10^{-3} .$$

For $\varphi \simeq 0$,

$$\frac{P_s}{P_D} = \frac{10^7}{4\pi(6000)^2} = 2.2 \times 10^{-2} .$$

Therefore, in the worst case, moderate to severe interference will be expected to result from aircraft scattering.

While the power in the scattered beam can be as much as 2 to 3 times the power in the direct beam, the frequency of the scattered signal will be shifted by Doppler phenomena and may well fall outside the passband of the receiver. Let v_t be the component of aircraft velocity perpendicular to the line from the antenna to the aircraft and θ be the angle between the boresight and the line to the aircraft. Then it can be shown that the Doppler shift is given by

$$f_d = \frac{1}{\lambda} v_t \sin \theta \quad .$$

Doppler shifts of 200 cps or more will occur at 10 Gc whenever

$$v_t \sin \theta \geq \frac{3 \times 10^8}{10^{10}} \times 200 = 6 \text{ meters/sec.}$$

For a v_t of 100 knots $\simeq$ 50 meters/sec., there will be no interference for

$$\theta \simeq \sin \theta \geq 6/50 = 0.12 \text{ radians} = 6.9^\circ \quad .$$

Radial velocities are much less effective in shifting frequency since the aircraft receives a signal shifted one way and retransmits with the opposite shift. If v_r is the radial velocity component,

$$f_d = \frac{1}{\lambda} v_r(1 - \cos \theta) \simeq \frac{1}{\lambda} v_r \frac{\theta^2}{2} \quad .$$

For a v_r of 100 knots, there will be a shift of 200 cps or more for

$$\theta \geq (2 \times 200 \times 3 \times 10^8)^{1/2} = (0.24)^{1/2} = 0.49 \text{ radians} = 28^\circ \quad .$$

However, aircraft velocity will be primarily radial only for ranges considerably greater than the 6-km case described above and therefore the signal will be weaker.

When the aircraft is not in the beamwidth, the scattering cross-section will be decreased by from 10 to 20 db from its peak value and the antenna gain will be decreased by from 20 to 30 db. At 10 Gc and 6 km range, the ratio of scattered to direct power will be at most 2.2×10^{-3} and will probably be about -40 or 10^{-4} db in power, or 10^{-2} db in voltage.

While a multipath signal 1/100 of the main signal voltage is certainly not negligible, the probability of this signal magnitude and a simultaneous Doppler shift less than 200 cps is very small. At lower carrier frequencies, the Doppler shift will be less but the scattered signal magnitude will also be reduced.

In conclusion, it appears that aircraft flying in the vicinity of the experiment site will probably have no significant effect on the measurements except possibly when the flight path passes through the beam of a receiving antenna. During the short interval of time that the aircraft is in the beam, moderate to severe interference (large errors) may be experienced. Such intervals must be identified either by monitoring aircraft movements in the area or by careful checks of the consistency of the measured data.

Appendix B*

USE OF NATURAL RADIATORS AS SIGNAL SOURCES

*This appendix was prepared by J. H. Bryan.

BLANK PAGE

Appendix B

USE OF NATURAL RADIATORS AS SIGNAL SOURCES

1. Introduction

For several years radio astronomers have been receiving and processing radio signals from the heavenly bodies, and a growing body of literature is developing around the measurements performed on these signals and the implications of these measurements. A number of papers in this literature have reported measurements of fluctuations or scintillations in high-frequency signals that are attributed to tropospheric perturbation of the signals, and analytical tools for interpretation of measurement data have been developed (Ref. 43), suggesting that information of the kind desired about such atmospheric effects might be available from published work or from an experimental program making observations over a period of time. It appeared at the outset of the study to be worthwhile to review available material to find out what has been done and to estimate what might be done in the future using these sources. This section summarizes the results of the resulting investigation.

2. Signals and Measurement Techniques

The signals used by radio astronomers have one characteristic that differs basically from the signal obtainable from a stable CW transmitter: they are characterized as generated by a random process and have a broad, relatively flat spectrum rather than the line spectrum of the signal from a stable CW transmitter. The waveform of a narrowband-limited signal of this kind (bandwidth a small fraction of the center frequency) appears on display to be a sinusoidal wave whose frequency is at the band center with fairly slowly varying envelope (amplitude) and phase. The rate of variation of this envelope (although not of the phase) is determined, of course, by the bandwidth of the receiver and display.

Since the fluctuations of such a signal before it impinges on the troposphere are not known and are not fully predictable, the perturbing effects of the atmosphere on the signal arriving at a single receiving antenna cannot be fully determined.* However, signals from the same source that pass through different portions of the atmosphere will generally be affected somewhat differently, and a comparison of such signals should in principle reveal the differences in effects along the two paths, at least for sources that are small (in angle) and adequately resolved. To use these signals, then, for measurement of atmospheric effects, a pair of receiving antennas is needed. This is not a major system drawback in considering an experiment to determine atmospheric effects on microwave signals, however, since a principal question to be answered by the experiment is that of decorrelation; a pair of antennas, one movable, is needed. If the paths are sufficiently separated that the atmospheric effects along the paths are essentially uncorrelated, inferences about the magnitude of the total effects can be drawn. The required separation to accomplish decorrelation is not known in advance, but is one of the parameters to be determined by experiment; it would appear from a simple physical model of the phenomenon (blobs of many sizes being blown by the wind) to depend not only on the RF wavelength but also on the fluctuation rates that are of concern--i.e., longer correlation distances would be associated with lower rates. The correlation distances of signal perturbations that are observable at the earth's surface can be shown (Ref. 43) from scattering theory to depend not only on the dimensions of the blobs that are responsible for the effects, but also on the distance from the blobs to the region of observation. The statistical description of these blobs and their aggregate effects on microwave extraterrestial signals appears from the available literature to be far from complete;

* Amplitude scintillations largely attributed to atmospheric effects because of characteristic magnitudes and rates can indeed be recognized in the output of a microwave radiometer. But the phase perturbation on the signal cannot in general be inferred from the magnitude of the amplitude perturbation (Ref. 43).

its further development appears to depend on the development and systematic use of more advanced measuring equipment.

The comparison of signals arriving from distant sources over paths that are very nearly parallel suggests interferometry, and it is basically interferometric technique that is applicable to the estimation of the tropospheric effects on these signals and the variation of these effects with separation between the two receiving antennas. If the atmospheric effects on the two signals are negligible, or if they are identical, the interferometer basically measures a time difference between the times of arrival of the identical waveforms at the two receiving antennas. This time difference is a strong function of the angle of arrival in the plane containing the source and the baseline between the antennas. If a signal along one propagation path suffers more or less delay because of difference in the mean propagation speed along the two paths, these differential delays are also measurable. For our present purposes, this measurement contains the information of concern.

The measurability of phase perturbations produced by the atmosphere depends upon the magnitude of these perturbations compared with those produced by system noise. The signal flux densities at the earth from the brightest of the radio stars (other than the sun) at microwave frequencies are weak by usual standards--of the order of 10^{-23} w/m^2/cps, yielding a signal power at the terminals of a 30-foot paraboloidal antenna (linearly polarized) of 50% efficiency, of about 25 x 10^{-23} watts/cps, equal to the noise power of a receiving system with an effective noise temperature of about 18°K. For a system of noise temperature 700°K, a large integrating factor is needed to be able to measure the interferometer fringe phase to 18-mr accuracy. For 1 second of post-detection integration time, followed by averaging over a fringe period of several seconds, a pre-detection bandwidth of tens of megacycles is needed.* The constraints on design and development of a system to make useful measurement of atmospheric effects using these signals are severe.

---

* Based on system parameters in Ref. 44

The simplest picture of interferometry using a single frequency, point source, and point receiving antennas needs to be modified for considering actual measurements if one or more of the following is important: the finite (non-zero) bandwidth of the signal accepted by the receiver; the angular extent of the source; and the dimensions of the receiving antennas. The angular extent of a source limits the practical interferometer baseline length because as the baseline increases, the spatial angular width of a fringe of the interference pattern shrinks down to that of the source, and the signal output of the interferometer drops* like the function $J_1(ka)/ka$, where a is the angular width of the source (in radians) and k is π times the baseline length in wavelengths (Ref. 2). Moreover, fluctuations in radiation over the surface of a source as large as the sun will produce fluctuations in the net direction of arrival of the radiation from the source, producing fluctuations in the interferometer output. Although in principle the effects of such fluctuations could be resolved from those due to the atmosphere on the basis of spatial correlation (with a 3-element system) or elevation-angle dependence (requiring much data processing), these fluctuations in the centroid of the brightness distribution for a 2-element system may exceed atmospheric effects considerably in magnitude, and tend to obscure them.

Although system sensitivity using these sources varies inversely with the square root of the bandwidth, system complexity must be increased to accommodate signals of increasing bandwidth. The effects of non-zero bandwidth and non-zero antenna size are similar to each other (Refs. 46, 47) in that they tend to blur the cancellation of identical time-displaced waveforms, since the interferometer baseline is not a single fixed number of wavelengths but varies over the band and over the antenna aperture, and only the center-frequency component will cancel perfectly at nulls corresponding to a path length difference between the aperture centers of n = 1,2,3...wavelengths at the center frequency. Cancellation of other components is increasingly poor as n increases, expecially so as

---

* For a circularly symmetrical source like the quiet sun (Ref. 45).

the band is widened. By use of compensating sections of transmission line to make n small for all elevation angles and by judicious choice of pre-detection bandwidth and post-detection integration times, however, it appears (Ref. 48) that the perturbing effects of these system characteristics can be held within reasonable bounds.* The choice of post-detection integration time, of course, limits the highest fluctuation frequencies that can be measured. For well designed microwave antennas, the finite size of the aperture does not appear to be a matter of practical concern.

3. Solar Observations and Interpretation

A number of pertinent radio-astronomical observations of the sun can serve to frame our speculation about the use of the sun for measuring atmospheric effects on microwave signals. In 1956, Aarons, Barron, and Castelli (Ref. 50) found that radiometrically-measured amplitude scintillations in solar radiation at 3.2-cm and 8.7-mm wavelengths (average scintillation periods: 15 to 22 sec at X-band and 33 to 55 sec at K-band) were sometimes well correlated and sometimes not. In October 1959, Aarons and Castelli (Ref. 51) found that such scintillations from the partially eclipsed sun at 1300 and 3000 Mc were well correlated. Such correlation implies (Ref. 43) that the "shadow pattern" on the earth's surface caused by atmospheric scattering irregularities has the same spatial dimensions at the two frequencies, and that the rms phase deviation suffered by the wave in passing through the atmosphere under the conditions of observation was less than one radian at these frequencies (Refs. 43, 44).

The spatial decorrelation of 3-cm solar signal amplitude fluctuations has been measured by Kazes and Steinberg (Refs. 51,52) using a pair of radiometers at variable spacing (up to at least 460 meters) and measuring the cross-correlation coefficient of their output. The zenith angles for their observations were between 80 and 85 degrees, and the cross-correlation coefficient fell to 0.5 at 125 meters, and to 1/e at 170 meters. [From

---

* The fringes observed with a finite bandwidth are analogous to the white-light fringes observable in optical interference for short optical path length differences (Ref. 49).

a reproduced illustrative plot in a secondary source (Ref. 52), it appears that fluctuation rates up to a few cycles per minute were measurable; the fractional fluctuation magnitude cannot be estimated from the plot. It is of major concern for prediction of such distances for phase fluctuations at other frequencies and other elevation angles, to develop a coherent theory that can link all such observations. It may be observed here that whereas from Booker's model (Ref. 43) the inferred size of the tropospheric irregularities is at least as large as the correlation distance at the earth's surface, Steinberg and Lequeux (Ref. 53) have concluded that diffraction effects due to blobs of the order of a few meters in size produce the observed microwave signal scintillations, while Aarons and Castelli (Ref. 51) prefer a large-blob refraction model to explain their data.

Zolnay (Ref. 45) at Ohio State University in 1962, using a 2.2-Gc interferometer of 7.6-meter baseline to observe the apparent motion (presumed to be due largely to effects of the atmosphere) of the sun's centroid of brightness at 60-degree elevation, succeeded in specifying a bound based on difference-signal phase fluctuations of period between 4 seconds and 4 minutes: these components he found to have amplitudes corresponding to less than 0.6 mr in elevation angle, about 1/15 of the solar diameter, for at least 60 percent of the time. Over this baseline, the corresponding difference-signal phase fluctuation bound is about 0.1 radian.

The inferences about signal phase deviation made from data in Refs. 50 and 51 tend to be confirmed by a preliminary measurement of rms phase scintillation of about 0.1 radian, of an S-band signal from an airborne transmitter made by Cornell Aeronautical Laboratories (Ref. 54). Unfortunately, under the conditions of these measurements, the fluctuations in signal phase produced by the atmosphere could not be resolved from fluctuations in phase due to transmitter platform motion; the overall fluctuations estimated from the experimental data can serve, however, as a bound on atmospheric effects under the conditions of observation.

In considering the possible use of the sun as a natural signal source for detecting atmospheric effects, one is struck by the fact that the sun's angular extent (about 9 mr) is of the order of 10^3 times greater than the apparent angular distortion of the wavefront expected to be produced by the atmosphere (over a 100-meter baseline at 1 Gc) on the basis of the preliminary measurements by Cornell Aeronautical Laboratory. This implies that a random angular shift in the centroid of the sun's brightness distribution, of 1/100 of its diameter, could mask quite thoroughly the anticipated atmospheric effects, provided the rates of these random effects are not sufficiently different to allow them to be separated by filtering. As observed above, random motion of the centroid, if not of such a magnitude as to overwhelm atmospheric effects, could be distinguished if sufficient data and data processing could be used.

It is possible that if random wander of the centroid of brightness over intervals of a minute or less (in time) is significant, a double-baseline, three-element interferometer system might be needed to suppress its effects and to measure the atmospheric phase perturbations.

There are no measurement data known to the author to serve as a better basis for estimating the random motion of the sun's centroid of brightness at microwave frequencies than the bounding data obtained by Zolnay.* Tracking radiometers like that described in Ref. 55 have had too little angular accuracy to detect the small motions of concern. Stanford University's 32-dish interferometer† (Ref. 56) (with crossed arms, each of length 375 feet) at 9.1 cm has an angular resolution in two dimensions of about 0.75 mr--about 1/12 of the solar diameter--and requires about an hour to scan the entire face of the sun and measure the brightness

---

* Because of the short baseline that was used in this work, the atmospheric effects on the two paths would be expected to be well correlated, so that the difference-signal phase perturbation does not give a good basis for estimating the atmospheric phase perturbations along a single path.

† Similar arrays used for scanning the sun are located at the Meudon Observatory in France and at the Radiophysics Laboratory, CSIRO, Sidney, Australia.

distribution. These mappings are currently made once each day. Thus, although it provides a possible source of data for estimating drifts of the centroid of brightness from day to day, and potentially perhaps from hour to hour, it does not lend itself to measurement of random fluctuations over intervals of the order of a second. The drifts from day to day can be computed from Stanford Heliographic data, and the magnitude of one sample calculation indicates that the drift over 24 hours is very large compared to the anticipated apparent fluctuation of angular position of a point source due to the atmosphere, for interferometer baseline lengths of interest.

One means for estimating the motion of the centroid of brightness in one dimension would be to use a phase-swept interferometer to scan the entire solar disk rapidly at short intervals. This technique has been used to detect motions of short-lived bright regions over the face of the sun (Ref. 53). Such measurements would also of course include atmospheric effects, but motions of the centroid could at least be bounded in this manner. Measurements of this kind at microwave frequencies may have been made and the results published, but are unknown to the author.

The solar spectroheliograms at microwave frequencies present graphically a daily record of the locations and relative brightness of small regions of intense radiation distributed over the solar disk. These regions often coincide in location with visual sunspots, and the total radiation from the sun at 1200 and 2800 Mc has been found (Ref. 46) to correlate well (over a range of about 2:1 in power) with observed sunspot area. The resolution of the Stanford instrument, about 1/12 of the sun's diameter, is somewhat larger than the size of visual sunspots, which probably would set a limit on the smallest intense microwave source detectable against the back ground of the remainder of the solar surface.

The fact that for a considerable portion of the time a sizable fraction of the sun's radiated microwave power [as much as 2/3 or more at times, according to several observers (Refs. 45, 57)] comes from regions of diameter 1/10 or less of the solar diameter suggests the possibility of using individual sunspots as radio sources for estimating the atmospheric

effects on microwave signals. A 3-cm interferometer with 450-μr angular resolution at Nancay has been used to measure the size, intensity, and brightness distribution of bright regions (of the order of 0.03 to 1.5 mr in diameter) associated with amplitude scintillations observed by radiometers in solar radiation (Ref. 52). No details of interferometric study of these sources for extraction of atmospheric phase perturbation information are known to have been reported. An important advantage to be gained by using a source of smaller angular extent is in permitting useful measurements to be made with greater antenna separation than was permitted Zolnay (7.6 meters) when he used the entire solar disk as a source (Ref. 45). The increase in fringe signal amplitude relative to receiver noise level (assumed fixed) due to the angular reduction from solar diameter to sunspot diameter for a baseline of 76 meters,* for example, could be enough to reduce phase fluctuation measurement errors by a factor of about 28. If there is more than one region of high intensity at a given time, the resulting distribution might still be useful, depending on the stability and spacing of these regions. One possible problem would arise if fluctuations in amplitude of radiation from the regions should cause excessive wander of the centroid of brightness. If one such region could be resolved angularly from the remainder of the solar surface, this possible problem could be avoided. However, to resolve an angle of 0.9 mr at, say, 5 Gc, thereby discriminating against radiation from other portions of the sun, would require an aperture for each element of an interferometer of the order of 60 meters. This is impractically large for the experiment under consideration. A long-baseline system using antennas of smaller size (perhaps a few meters in diameter) would be useful, however, under conditions in which a single strong bright spot on the sun dominates the total radiation in the frequency range of concern, provided its random wander and that of the background brightness distribution do not exceed certain limits.

* At the frequency used by Zolnay, 2 Gc.

Under these conditions, the bright spot is the signal source, and the radiation from the remainder of the sun contributes only background noise. It is of interest to determine the phase accuracy that could be expected from an interferometer system that measures the fringes arising from the bright-spot radiation in the presence of this noise from the rest of the sun. The flux density available (Ref. 57) to a linearly polarized antenna from the quiet sun at 3 Gc is about 3.3×10^{-21} w/m^2/cps, and during periods of activity this level can increase for hours to a level of about 1.2×10^{-20} w/m^2/cps. If all of the incremental radiation from the "active sun" comes from a single bright region, and assuming the angular width of the bright spot is less than one fringe lobe, the ratio of effective source temperature to effective background temperature can be assumed to be about 3. This effective background temperature for a 30-foot-diameter paraboloidal antenna of 50% efficiency would be about 23,000°K, and would probably dominate the system effective noise temperature.

To measure fringe phase to an accuracy of 18 mr, the system must yield a voltage S/N of 57.3 in the relative amplitudes of fringe waveform and noise waveform in the interferometer output. We assume here that the antenna spacing has been chosen so that the quiet-sun background radiation produces no fringe pattern (Ref. 45). The question of system measurement feasibility depends on achieving a useful output data rate without prohibitive complexity. The post-detection S/N is given approximately for an interferometer system with equal gain in its two elements by (Ref. 10)

$$S/N = k(B\tau)^{1/2} \frac{T_s}{T_b + T_r}$$

where

B = Pre-detection bandwidth

τ = Post-detection integration time

T_s = Effective temperature of the sunspot radiation

T_b = Effective temperature of the noise background

T_r = Effective noise temperature of the receivers

k = a constant of order unity.

If $T_s/(T_b + T_r) = 3$, only moderate integration (a factor of order 20) is needed to achieve a phase measurement accuracy of 18 mr. Thus only a moderate pre-detection bandwidth is needed to provide a usefully high data rate for the purposes of the experiment of concern. Therefore, considering the signal and noise effects under these idealized conditions (a point-source sunspot and uniformly bright solar disk), it appears to be feasible at times to use sunspot radiation in the microwave band to measure atmospheric phase perturbations.

It is of interest to estimate the capabilities of such a system at 3 Gc using a longer baseline to obtain a useful estimate of correlation distance and the magnitudes of the uncorrelated phase fluctuations. If the baseline length is extended to the order of 1000m, the fringe signal from a bright-spot source 0.9 mr in angular width will have a maximum amplitude about 0.008 that of a point source, and a drift period of about 2 to 6 seconds per cycle, depending on the hour elevation angle of the sun. For a receiver bandwidth of 40 Mc, a ratio $T_s/(T_b + T_r)$ of 3, and appropriate processing of fringe signal data, the phase fluctuations should be measurable with an accuracy of 18 mr using post-detection integration times of a fraction of a second.

This leaves open the question of the random wander of the sunspot region over the face of the sun, and the random fluctuation in the centroid of brightness of the quiet-sun background. Both of these effects might importantly affect the phase measurements and might have to be compensated by the use of a three-element interferometer. Even large fluctuations due to this wander could be attenuated in the output of such a system to insignificant levels, as may be shown by considering the magnitudes of the error terms corresponding to tangential and radial motion of the signal source as developed in Appendix C. In the calculations below, it is of concern to compare the magnitudes, calculated on the basis of

two 1-km baselines* separating the elements at 3 Gc for illustrative purposes, with the rms atmospheric phase fluctuation estimated from Cornell Aeronautical Laboratories' preliminary data to be about 0.1 radian:

Error due to Tangential Velocity:

$$\Delta\varphi_{v_t} = \frac{4\pi\ell^2}{\lambda r}(\sin\theta\cos\theta)\dot{\theta}\tau = 3.9 \times 10^{-6} \text{ rad.}$$

Error due to Tangential Acceleration:

$$\Delta\varphi_{a_t} = \frac{4\pi\ell^2}{\lambda r}(\sin\theta\cos\theta)\frac{\ddot{\theta}\tau^2}{2} = 2 \times 10^{-8} \text{ rad.}$$

These errors correspond to a limiting situation--motion of the signal source across the entire solar disk within one post-detection integration period, 0.01 sec. The numerical values indicated assume that sin θ cos θ has magnitude of approximately 0.5. The radial motion bounds are somewhat harder to estimate, but as an illustrative case it is assumed that the source moves outward from the surface of the sun at a rate equal to 3×10^8 m/sec for the integration period, 0.01 sec. The value for phase error due to radial acceleration assumes that the radial velocity changes this entire quantity within 0.01 sec. On this basis, these errors are computed as follows:

Error due to Radial Velocity:

$$\Delta\varphi_{v_r} = \frac{2\pi\ell^2}{\lambda r^2}(\cos^2\theta)\, v_r\tau = 3.7 \times 10^{-9} \text{ rad.}$$

Error due to Radial Acceleration:

$$\Delta\varphi_{a_r} = \frac{2\pi\ell 2}{v^2}(\cos^2\theta)\frac{a_v\tau^2}{2} = 1.9 \times 10^{-9} \text{ rad.}$$

---

* The error terms will be smaller for shorter baselines.

In making the numerical estimates, the following values are assumed:

The distance ℓ between antennas is 1000 meters

The angular motion $\dot{\theta}\tau$ in τ sec is 0.01 radian;
$\tau = 0.01$ sec; $\ddot{\theta} = 1$ rad/sec^2

The distance r from the source is 1.6×10^{11} meters

The wavelength λ is 0.1 meter

The numerical values assume that $\cos^2\theta$ has the magnitude 0.5.

Use of a three-element system with its added complexity, may not be worth the additional information obtained. One might choose, as an alternative, to measure the total fluctuation in the apparent direction of arrival of the signal from the sun, confident that the atmospheric effects can be no greater than this magnitude. As indicated above, the magnitude of the component due to the source itself could be estimated from analysis of the independence of the total fluctuation on elevation angle. Its possible importance might be evaluated, as suggested above, from a series of one-dimensional interferograms of the kind displayed in Ref. 11, but measured at intervals as short as the measurement process will allow.

Additional information about changes in microwave solar radiation brightness distribution over short periods of time may become available independently if and when the Haystack Radiometric equipment (Ref. 58) is used to examine the sun. With its 120-foot aperture, it should have sufficient angular resolution (3-db beamwidth of 0.9 mr, at 10 Gc) to resolve portions of the sun, track individual bright regions on its surface in a matter of seconds. The tracking accuracy of the radiometer should be a small fraction of its 3-db beamwidth--perhaps approaching its precision limit of 13 μr, about 1/700 of the solar diameter. This is the expected order of magnitude of centroid wander that, if it took place over short intervals of time, would be comparable to the atmospheric perturbation phenomena expected to be measured by interferometers having useful baselines. Thus the Haystack radiometric equipment may be able to provide information useful in evaluating the sun as a signal source for observing atmospheric phenomena; but its availability for measurements

of the kind suggested is questionable because of the many projects for which its use is planned.

In summary, then, the available observational data on the solar radiation at microwave frequencies do not permit a confident conclusion that the sun can be readily used as a signal source for measuring atmospheric effects with great accuracy and high data rate with a two-element interferometer system. It can, however, be used by such a system particularly during intervals when most of its microwave radiation originates from a small, bright region on its surface, to obtain bounds on the magnitudes of such effects, within the limits set by system noise and unknown short-term random fluctuations in the angular location of the bright region or the disk's centroid of brightness. The effects of this random wander can in principle be made negligible by the use of a collinear-baseline, three-element interferometer receiving system of the kind discussed in Appendix C in connection with the use of an airborne transmitter. The magnitude of these effects could be estimated by means of a (probably extensive) measurement program to resolve them from atmospheric effects on the basis of spatial correlation and elevation-angle dependence. Such a program would also (if successful) yield extensive data on the atmospheric effects themselves.

4. Star Observations

A number of observations of amplitude scintillation of stellar radio signals have been reported in the literature. Most are at frequencies below L-band, but a few observations of microwave signals have also been reported. The strongest radio galaxy, Cygnus A, which is almost as strong as Cassiopeia, and which has the advantage for interferometry work of having smaller angular dimensions (about 0.6 mr long by 0.15 mr wide), appears (Ref. 47) to be a favorite signal source. Allen, Aarons, and Whitney (Ref. 59) during 1961-62 measured scintillations of 1200 and 2980 Mc radiation from Cynus A during its periods of rising and setting. "Considerable day-to-day variations" but "no correlation with obvious gross weather characteristics" were reported.

A number of microwave signal measurements of marginal interest in the present study have been made using this signal source. Ko (Ref. 60) in 1957-58 used a 915-Mc radiometer to measure scintillation amplitudes and rates of signals from Cygnus A over a wide range of elevation angles. Lequeux and Heidmann measured the east-west radiation profile of Cygnus A interferometrically at 21 cm, and Jennison and Rowson did so at 10 cm. Mayer, McCullough, and Sloanaker measured the polarization of radiation from Cygnus A at 10 cm and at 3 cm.

The only attempt known to the author to measure phase perturbations of the microwave signal from a radio star has been made recently by Stanford University's Radioscience Laboratory (Ref. 44), using a pair of 30-foot antennas in a two-element interferometer at 3075 Mc with a 105m baseline. This baseline length was limited by loss of S/N through resolution of the source, Cygnus A. Processing of the Stanford data averaged fluctuations over (fringe period) intervals of 20 to 60 seconds, thus attenuating components of higher frequency, as well as those of periods greater than a few fringe periods. A series of observations at angles of elevation greater than 30 degrees yielded measured fluctuations of 18 to 90 mr in phase, compared with fluctuations due to system noise of the order of 18 to 36 mr (noise output is a function of averaging time, which is a function of fringe width, and hence a function of source elevation angle).

The estimate of the cross-correlated phase fluctuations attributable to atmospheric effects at these elevation angles, based on ten hours of observation at intervals during January and February, 1965, is 25 mr. Terrain features at the Stanford site make low-elevation measurements questionable and difficult to interpret. Because of some uncertainties about instrumental effects and the relatively small quantity of data, some qualifications as well as detailing of the observational data so far obtained may be needed. Lack of knowledge of the correlation distance under the conditions of measurement introduces an important uncertainty into interpretation of the data. The reported measurements at a single spacing do not permit an experimental estimation of the spatial correlation of the phase fluctuations. Because of the S/N limitation that constrains

the useful baseline, the correlation function at greater antenna separations would be difficult to measure without larger antennas or lower-noise amplifiers than the TWT's used (these yielded a 700°K effective system noise temperature). The cross-correlated phase fluctuations at smaller separations could in principle be measured to estimate the functional form and parameters of the spatial correlation function, unless these parameters are sensitive functions of atmospheric conditions that are changeable and difficult to measure. However, because of the increased correlation of atmospheric effects at shorter distances, the detectability of these effects by interferometric means becomes more difficult as the difference-signal phase fluctuations drop toward the level of those produced by system noise. [Preliminary observations were made (Ref. 44) at short antenna spacings with the Stanford equipment in 1964, but apparently yielded no data of help in estimating correlation distance].

As indicated above, the processing of the Stanford Cygnus A data estimated phase perturbation on the basis of averaging over one fringe period, an interval of about 20 to 60 seconds. To distinguish atmospheric phase perturbations from those due to noise over shorter intervals, of the order of one second or less, would require a higher S/N ratio. Given sufficient signal power, a method of measuring phase over fractions of a fringe period at lower frequencies using phase-tracking techniques has been developed by NBS (Ref. 10). An estimate of the difficulties that would be encountered in attempting to achieve accurate measurements of rapid phase fluctuations by improving the Stanford equipment may be instructive. To measure phase perturbations having a frequency of 100 cps to an accuracy of 18 mr using Cygnus A as the signal source would require an improvement (Ref. 10) in S/N power ratio of about 20, if the baseline distance remained 105 meters. If a 70°K effective system noise level could be achieved using maser preamplifiers, and if a receiver bandwidth of 40 Mc is used, paraboloidal antennas about 43 feet in diameter would be needed to gather the required signal power. Alternatively, if receiver bandwidth could be increased somewhat, the required increase in antenna size could be lessened. These figures suggest that information on rapid phase fluctuations measured over baseline distances sufficiently

great to decorrelate the fluctuations at the two antennas (perhaps a few hundred meters) cannot be expected to be readily obtained by modest improvements in the measurement equipment used at Stanford using radio stars as signal sources. Such improvements, however, can be expected to yield important increments of information on atmospheric phase perturbations of stellar radiation by drawing firmer bounds on the magnitudes of the effects. To gain a comprehensive understanding of the spatial and temporal fluctuations in signal phase produced by the atmosphere, using measurement equipment of the cost and complexity of the Stanford equipment, a source more powerful and/or smaller in its angular dimensions than the radio stars appears to be necessary.

Appendix C*

PLATFORM MOTION CONSIDERATIONS

* This appendix was prepared by R. B. Battelle.

Appendix C

PLATFORM MOTION CONSIDERATIONS

1. Sources of Phase Measurement Error

Although measurements of the fluctuations in signal phase produced by atmospheric turbulence have been carried out by a number of investigators in the past, their data have only limited applicability to an understanding of turbulence effects on the signals of deep-space probes. The primary shortcoming of the available data is that they apply, in nearly all cases, to near-horizontal propagation paths at low altitudes. Measurements of turbulence effects on probe signals must be made for propagation paths through the atmosphere along lines of sight at angles more than four degrees above the horizontal. Only once have such measurements been attempted in the past. Under Air Force sponsorship, the Cornell Aeronautical Laboratory (Ref. 61) made phase-fluctuation measurements for a propagation path between an aircraft and a ground terminal, for which the line of sight was at an angle of 6 to 12 degrees above the horizon. The objective of this section is to examine the requirements of the experiment with respect to signal source and platform stability.

If measurements of phase fluctuations due to the atmosphere are to be made, all other sources of signal phase fluctuations must be either made negligibly small or removed by suitable signal processing. Hopefully a combination of these two techniques can be applied to this experiment. The sources of instability of concern are:

(1) Phase variations of the RF source itself (oscillator phase jitter and frequency drift)

(2) Phase variations of the receiver used for measurements (local oscillator phase jitter and frequency drift)

(3) Geometrical path length variations (Doppler variations) caused by platform velocity and acceleration effects

(4) Geometrical path length variations (Doppler variations) caused by ground antenna motion.

The tolerances on these sources of instability will be examined in terms of the alternative designs for the experiment.

The phase fluctuations due to the atmosphere itself establish the tolerances on other phase instabilities. As a reasonable model of the atmosphere-induced phase fluctuations under "normal" conditions, assume a spectral distribution of phase approximating the function

$$\Phi^2(\omega) = \frac{0.2}{20\omega^2 + 1} \text{ rad}^2/\text{rad/sec}, \qquad (C\text{-}1)$$

which has an rms phase variation σ_φ of

$$\sigma_\varphi = 0.26 \text{ radian}, \qquad (C\text{-}2)$$

where the source wavelength is assumed to be 0.036 meters (i.e., about 8.4 Gc). Although a complete analysis should, of course, consider the frequency spectrum of the errors, it will be assumed here only that the contribution from each source of phase instability must individually be less than approximately 10% of the path variation, or 0.03 radians.

2. Errors for a Simple Single-Path Measurement

Consider first a simple experiment using an RF source on an elevated platform (e.g., an aircraft, balloon, or satellite) and a phase measurement receiver on the ground. In this case, phase jitter in the source and in the receiver local oscillator will appear directly in the phase measurement.

Oscillator phase jitter is analyzed in Appendix E. Of the various sources of jitter normally involved, the noise due to amplifier (and multiplication) stages is dominant at high fluctuation frequencies, while shot noise in the oscillator is dominant at low fluctuation frequencies. If a high-stability RF source is used, the amplifier and

multiplier noise might be expected to produce an rms phase fluctuation of at least 5×10^{-2} radians at 8 Gc, but the spectrum of this noise will be quite broad. The phase-measuring receiver can be expected to incorporate a low-pass filter, which will greatly reduce the rms phase jitter from this source, so that errors in the measurement will be negligible. Shot noise can be expected to produce an rms phase fluctuation in 10 seconds, of about 5×10^{-3} radians at 8 Gc. Therefore, errors from this source should also be negligible. Oscillator drift should not be a problem if the receiver local oscillator is readjusted periodically to match the source frequency. A frequency drift of 10^{-10} parts per day would result in a phase error of only 4×10^{-3} radians per minute, which would imply a requirement to make frequency corrections at least every few minutes during the measurements. Thus, it appears that oscillator phase jitter and frequency drift will produce negligible errors, at least for an experiment incorporating high-stability components. However, it is also clear that any techniques that would reduce the dependence of the results on the use of high-stability equipment would be quite desirable.

The stability of the platform carrying the RF source must also be examined. The phase of the received signal will be a function of the propagation path length r, as indicated below:

$$\varphi_s = \omega t + \varphi_j(t) - \frac{2\pi}{\lambda}\left(r + v_r t + A_r \frac{t^2}{2} + \ldots\right) + \varphi_a(t) \qquad \text{(C-3)}$$

where

ω = Signal frequency, rad/sec

λ = Signal wavelength

r = Path length from the platform

v_r = dr/dt = Platform radial velocity

a_r = d^2r/dt^2 = Platform radial acceleration

$\varphi_j(t)$ = Signal phase jitter or drift due to source instability, radians

$\varphi_a(t)$ = Phase fluctuation due to the atmosphere, radians.

Measurement of $\varphi_a(t)$ might be carried out by mixing this signal with a local oscillator of frequency ω. The mixing process (using a balanced modulator or product detector) followed by a low-pass filter results in an output voltage of the form

$$V_{out} = K \cos(\varphi_s - \varphi_{\ell o})$$

$$= K \cos \left[\varphi_j'(t) - \frac{2\pi}{\lambda}\left(r + v_r t + a_r \frac{t^2}{2} + \ldots\right) + \varphi_a(t)\right] \quad \text{(C-4)}$$

where

K = Constant depending on receiver characteristics

$\varphi_j'(t)$ = Phase jitter due to combined source and receiver local oscillator jitter and drift.

Thus, the receiver output in this case is a voltage, distorted from a simple cosine form by pnase jitter and geometrical path length variations as well as by atmospheric turbulence effects. If phase jitter (and ground antenna motion) is assumed to be negligible, the error is due entirely to the uncertainty in the knowledge of r, v_r, a_r, etc. The tolerance on these parameters of the platform motion depends upon the time intervals over which continuous measurement of $\varphi_a(t)$ must be made. The atmosphere-induced phase fluctuations will have spectral components virtually to zero frequency, but from a practical standpoint, extremely low-frequency fluctuations can be overlooked. For example, one might decide that fluctuations that occur at frequencies below 1.0 cps are of no concern. Then $\varphi_a(t)$ can be analyzed from measurements made over intervals τ = 10 seconds. The tolerances on the platform motion parameters are then related to the phase instability tolerance of 0.03 radians established earlier by

$$\frac{2\pi}{\lambda}\left(r + v_r\tau + a_r\frac{\tau^2}{2} + \ldots\right) < 0.03 \text{ radians} , \qquad (C\text{-}5)$$

and for $\tau = 10$ seconds, and $\lambda = 0.036$ meters,

$$\sigma_r < \frac{\lambda}{2\pi} \times 0.03 = \frac{0.036}{2\pi} \times 0.03 = 1.72 \times 10^{-4} \text{ meters} \qquad (C\text{-}6a)$$

$$\sigma_{v_r} < \frac{\lambda}{2\pi} \times 0.03 \times \frac{1}{\tau} = 1.72 \times 10^{-5} \text{ meters/sec} \qquad (C\text{-}6b)$$

$$\sigma_{a_r} < \frac{\lambda}{2\pi} \times 0.03 \times \frac{2}{\tau^2} = 3.44 \times 10^{-6} \text{ meters/sec}^2 . \qquad (C\text{-}6c)$$

Obviously these tolerances are unattainable with any movable platform.

Returning to the equation of received signal phase, Eq. (C-3), it is feasible to carry out a frequency-conversion process in the receiver whereby the first-order Doppler phase variations on the signal are removed. The process might be carried out manually using a plot of V_{out} as defined by Eq. (C-4). In such a process, one would find zero-crossings of V_{out} that are separated by approximately 10 seconds of time, and then assume that a constant platform radial velocity $\hat{v}_r$ existed over that time interval, which could be subtracted from the measured function. In effect, this process involves a subtraction of a phase function

$$\varphi_c = -\frac{2\pi}{\lambda}\left(\hat{r} + \hat{v}_r t\right) \qquad (C\text{-}7)$$

where $\hat{r}$ and $\hat{v}_r$ are estimates of the range and radial velocity of the platform, chosen on the basis that $(\varphi_s - \varphi_{lo} - \varphi_c) = (2n + 1)\pi/2$ at times $t = 0$ and $t = \tau$. In this way, the phase error terms that remain are due to platform acceleration and higher-order motion parameters. The tolerances on platform motion are then

$$\frac{2\pi}{\lambda}\left(a_r\frac{\tau^2}{2} + \ldots\right) < 0.03 \text{ radians} . \qquad (C\text{-}8)$$

Since the velocity assumed in this process minimizes the error at 0 and 10 seconds, the maximum error due to platform acceleration will tend to occur at $\tau = 5$ seconds. Therefore,

$$\sigma_{a_r} < 1.38 \times 10^{-5} \text{ meters/sec}^2 \quad .$$

Although the acceleration tolerance has been relaxed somewhat, it is nevertheless unattainable in any practical situation.

The above process might also be carried out automatically by introducing a frequency offset in the receiver local oscillator, which would be based on a prediction of the platform velocity. The effective frequency of the local oscillator would then be $\omega (2\pi/\lambda)v_r$, and the error in the velocity estimate must be no more than 1.72×10^{-5} meters/sec, which corresponds to 0.03 radians/sec or about 5×10^{-3} cycles/sec. Whether or not an estimate of the received signal frequency could be made to this accuracy on the basis of successive 10-second averages is doubtful.

One might further process the received signal phase function by subtracting assumed velocity and acceleration terms based upon three zero-crossing times, separated by about 10 seconds. The critical tolerance on platform motion would then be the rate of change of acceleration, and that tolerance would apply for the full 20 seconds of the measurement sample. It should be clear from this simple analysis that measurements based on a single one-way propagation path imply a necessity for an extremely stable platform, high phase-stable and frequency-stable source and receiver oscillators, and complex processing of the signal and output data.

3. Errors for a Near-Parallel Path Measurement

Consider now a phase measurement utilizing two receivers on the ground. The geometrical configuration of the platform and the receivers should be as shown in Fig. C-1, with the receivers at points P_2 and P_3 separated by a distance 2ℓ, and the platform carrying the RF source at

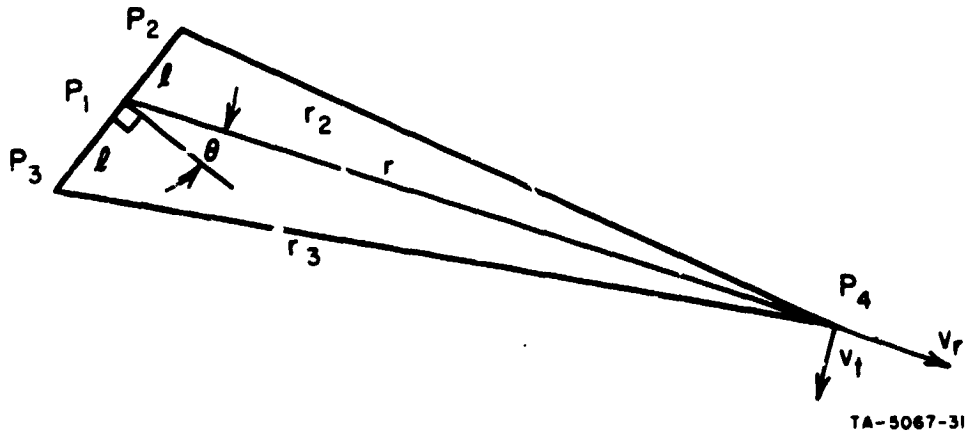

FIG. C-1 PATH GEOMETRY

P_4 at a range r from the point P_1 midway between the receivers. The azimuth angle θ is measured from the plane through P_1 perpendicular to the line $P_2 - P_3$. For the geometry shown,

$$\varphi_{s_1} = \omega t + \varphi_j(t) - \frac{2\pi}{\lambda}\left(r_1 + v_{r_1} t + a_{r_1}\frac{t^2}{2} + \ldots\right) + \varphi_{a_1}(t) \quad \text{(C-9a)}$$

$$\varphi_{s_2} = \omega t + \varphi_j(t) - \frac{2\pi}{\lambda}\left(r_2 + v_{r_2} t + a_{r_2}\frac{t^2}{2} + \ldots\right) + \varphi_{a_2}(t) \quad \text{(C-9b)}$$

$$\varphi_{s_3} = \omega t + \varphi_j(t) - \frac{2\pi}{\lambda}\left(r_3 + v_{r_3} t + a_{r_3}\frac{t^2}{2} + \ldots\right) + \varphi_{a_3}(t) \,. \quad \text{(C-9c)}$$

By straightforward but tedious calculation using series expansions and keeping only terms in (ℓ/r_1) to powers of three or less and in which the negative power of r_1 is not greater than the power of ℓ, r_2, r_3 and their derivatives, can be expressed as:

$$r_2 \simeq r_1\left(1 - \frac{\ell \sin\theta}{r_1} + \frac{\ell^2 \cos^2\theta}{r_1^2} + \frac{\ell^3 \sin\theta \cos^2\theta}{2r_1^3}\right) \quad \text{(C-10a)}$$

$$r_3 \simeq r_1\left(1 + \frac{\ell \sin\theta}{r_1} + \frac{\ell^2 \cos^2\theta}{r_1^2} - \frac{\ell^3 \sin\theta \cos^2\theta}{2r_1^3}\right) \quad \text{(C-10b)}$$

$$v_{r_2} \simeq v_{r_1}\left(1 - \frac{\ell^2 \cos^2\theta}{2r_1^2} - \frac{\ell^3 \cos^2\theta \sin\theta}{r_1^3}\right)$$

$$+ v_t\left(-\frac{\ell \cos\theta}{r_1} - \frac{\ell^2 \sin\theta \cos\theta}{r_1^2} + \frac{\ell^3 \cos^3\theta}{2r_1^3} - \frac{\ell^3 \sin^2\theta \cos\theta}{r_1^3}\right) \quad \text{(C-10c)}$$

$$v_{r_3} \simeq v_{r_1}\left(1 - \frac{\ell^2 \cos^2\theta}{2r_1^2} + \frac{\ell^3 \cos^2\theta \sin\theta}{r_1^3}\right)$$

$$+ v_t\left(\frac{\ell \cos\theta}{r_1} - \frac{\ell^2 \sin\theta \cos\theta}{r_1^2} - \frac{\ell^3 \cos^3\theta}{2r_1^3} + \frac{\ell^3 \sin^2\theta \cos\theta}{r_1^3}\right) \quad \text{(C-10d)}$$

$$a_{r_2} \simeq a_{r_1}\left(1 - \frac{\ell^2 \cos^2\theta}{2r_1^2} - \frac{\ell^3 \cos^2\theta \sin\theta}{r_1^3}\right)$$

$$+ a_t\left(-\frac{\ell \cos\theta}{r_1} - \frac{\ell^2 \sin\theta \cos\theta}{r_1^2} + \frac{\ell^3 \cos^3\theta}{2r_1^2} - \frac{\ell^3 \sin^2\theta \cos\theta}{r^3}\right) \quad \text{(C-10e)}$$

$$a_{r_3} \simeq a_{r_1}\left(1 - \frac{\ell^2 \cos^2\theta}{2r_1^2} + \frac{\ell^3 \cos^2\theta \sin\theta}{r_1^3}\right)$$

$$+ a_t\left(\frac{\ell \cos\theta}{r_1} - \frac{\ell^2 \cos\theta \cos\theta}{r_1^2} - \frac{\ell^3 \cos^3\theta}{2r_1^3} + \frac{\ell^3 \sin^2\theta \cos\theta}{r_1^3}\right) \quad \text{(C-10f)}$$

where

$\varphi_j(t)$ is assumed to have negligible phase variation in the time interval $(r_1 - r_2)/c$

$\varphi_{a_1}(t)$, $\varphi_{a_2}(t)$, and $\varphi_{a_3}(t)$ are assumed to be independent atmosphere-induced phase fluctuations

v_{r_i} = dr_1/dt, the radial velocity of the platform

v_t = $r_1(d\theta/dt)$, tangential velocity

a_{r_1} = d^2r_1/dt^2, radial acceleration

a_t = $r_1(d^2\theta/dt^2)$, tangential acceleration.

The independence of $\varphi_{a_1}(t)$, $\varphi_{a_2}(t)$, and $\varphi_{a_3}(t)$ can be assumed if P_1, P_2, and P_3 are separated by a distance greater than the correlation distance of atmosphere-induced phase fluctuations. Correlation distances may typically be of the order of 100 meters, so that site separation distances of 1000 meters should assure the independence of these phase fluctuations for sufficiently small θ.

If the signals at P_2 and P_3 are fed to a balanced modulator or product detector with a low-pass filter, the output voltage will be of the form

$$V_{out} = K \cos \left(\varphi_{s_3} - \varphi_{s_2}\right) \qquad \text{(C-11a)}$$

$$= K \cos \left\{\varphi_{a_3}(t) - \varphi_{a_2}(t) + \frac{2\pi}{\lambda}\left[(r_2 - r_3) + \left(v_{r_2} - v_{r_3}\right) t + (1/2)\left(a_{r_2} - a_{r_3}\right) t^2\right]\right\} \qquad \text{(C-11b)}$$

$$V_{out} = K \cos \left[\varphi_{a_3}(t) - \varphi_{a_2}(t) + \frac{2\pi}{\lambda} \left(- 2\ell \sin \theta + \frac{\ell^3 \sin \theta \cos^2 \theta}{r_1^2} \right) \right.$$

$$+ \left(\frac{2\ell^3 \cos^2 \theta \sin \theta}{r_1^3} \right) v_{r_1} t$$

$$+ \left(- \frac{2\ell \cos \theta}{r_1} + \frac{\ell^3 \cos^{\ell} \theta}{r_1^3} - \frac{2\ell^3 \sin^2 \theta \cos \theta}{r_1^3} \right) v_t t$$

$$+ \left(- \frac{2\ell^3 \cos^2 \theta \sin \theta}{r_1^3} \right) a_r \frac{t^2}{2}$$

$$\left. + \left(- \frac{2\ell \cos \theta}{r_1} + \frac{\ell^3 \cos^3 \theta}{r_1^3} - \frac{2\ell^3 \sin^2 \cos \theta}{r_1^3} \right) a_t \frac{t^2}{2} \right] .$$

(C-11c)

Note that phase jitter and drift in the source and receiver oscillators do not appear in the output function. Similarly, all the first-order errors due to radial motion of the platform have been eliminated. If the measurement interval is 10 seconds, the phase instability tolerance on $\varphi_{a_3} - \varphi_{a_2}$ is $\sqrt{2} \times 0.03$ radians, the range, r_1, is 2×10^5 meters, the receiver spacing, ℓ, is 5×10^2 meters, the wavelength, λ, is 0.036 meters, and only the most significant terms are retained:

$$\sigma_{v_r} \cos^2 \theta \sin \theta < \frac{\sqrt{2} \times 0.03 \times r_1^3}{2\ell^3 \tau} \cdot \frac{\lambda}{2\pi}$$

$$= \frac{\sqrt{2} \times 0.03 \times 0.036}{4\pi \times 10} \times (400)^3 = 7.78 \times 10^2 \text{ meters/sec}$$

(C-12a)

$$\sigma_{v_t} \cos\theta < \frac{\sqrt{2} \times 0.03 \times r_1}{2\ell\tau} \times \frac{\lambda}{2\pi}$$

$$= \frac{\sqrt{2} \times 0.03 \times 0.036}{4\pi \times 10} \times 400 = 4.86 \times 10^{-3} \text{ meters/sec}$$

(C-12b)

$$\sigma_{a_r} \cos^2\theta \sin\theta < \frac{\sqrt{2} \times 0.03 \times r_1^3}{\ell^3\tau^2} \times \frac{\lambda}{2\pi} = 1.56 \times 10^2 \text{ meters/sec}^2$$

(C-12c)

$$\sigma_{a_t} \cos\theta < \frac{\sqrt{2} \times 0.03 \times r_1}{\ell\tau^2} \times \frac{\lambda}{2\pi} = 9.72 \times 10^{-4} \text{ meters/sec}^2 \quad .$$

(C-12d)

The tolerances on the radial velocity and acceleration of the platform have been greatly relaxed by this use of two receivers, but the tangential velocity and acceleration tolerances are still impractical to achieve with any platform even at the 200-km range assumed above.

Signal or output data processing techniques can be applied to this measurement procedure as was suggested for the single propagation path measurement, to relieve the tolerances on platform motion. For example, the output voltage function could be examined and zero-crossings separated by approximately 10 seconds of time established. Then a constant velocity could be assumed for the platform, which upon subtraction from the measured function would eliminate the simple $v_r t$ and $v_t t$ terms. In effect, this process involves the subtraction of a phase function

$$\varphi_c = \frac{2\pi}{\lambda}(d + vt) \qquad \text{(C-13)}$$

where d and v are estimates of constant and first-order time-dependent terms of the phase error function, chosen on the basis that

$$\left(\varphi_{s_3} - \varphi_{s_2} - \varphi_c\right) = (2n + 1)\pi/2 \text{ at } t = 0 \text{ and } t = \tau \quad .$$

Since the velocity assumed in this process minimizes the error at 0 and about 10 seconds, the maximum error due to platform acceleration will tend to occur at t = 5 seconds. Therefore,

$$\sigma_{a_r} \cos^2 \theta \sin \theta < 6.24 \times 10^{2} \text{ meters/sec}^2 \qquad \text{(C-14a)}$$

$$\sigma_{a_t} \cos \theta < 3.89 \times 10^{-3} \text{ meters/sec}^2 \ . \qquad \text{(C-14b)}$$

The radial acceleration will then be a negligible factor for most experiments, though the tangential acceleration is still a serious problem.

This process could be carried out electronically instead of manually. For example, the equal and opposite phase errors due to radial and tangential velocity components of the platform might be reduced by inserting a small frequency offset in the receiver local oscillators at the two sites, the frequency of one site being offset higher and that of the other site lower than the nominal local oscillator frequency. The offset would be based on the phase error existing, say, 10 seconds after a reference zero-crossing of the output voltage, and would apply to the succeeding 10-second interval. However, the above acceleration tolerances would still apply.

The more elaborate processing involving estimates of the time and time-squared terms of the error function is possible. The principle is clear, but the feasibility of their use in an experiment appears doubtful.

4. Errors for Three Near-Parallel Path Measurements

Consider finally a phase measurement utilizing three receivers on the ground. The configuration is identical to that suggested above, but the receiver sites are at point P_1, P_2 and P_3, each of which must be separated by a distance ℓ = 1 km. In this case, the signals from pairs of receivers should be processed in such a way that their phases are subtracted, and then the resulting phase-differences are added to obtain an output voltage directly related to the desired atmosphere-induced phase fluctuations.

One method for doing this signal processing would involve the steps indicated in Fig. C-2. The signal from the receiver at P_1 is offset in frequency by mixing with the local oscillator operating at the offset frequency ω_i. This offset replica of the signal at P_1, in Fig. C-1,

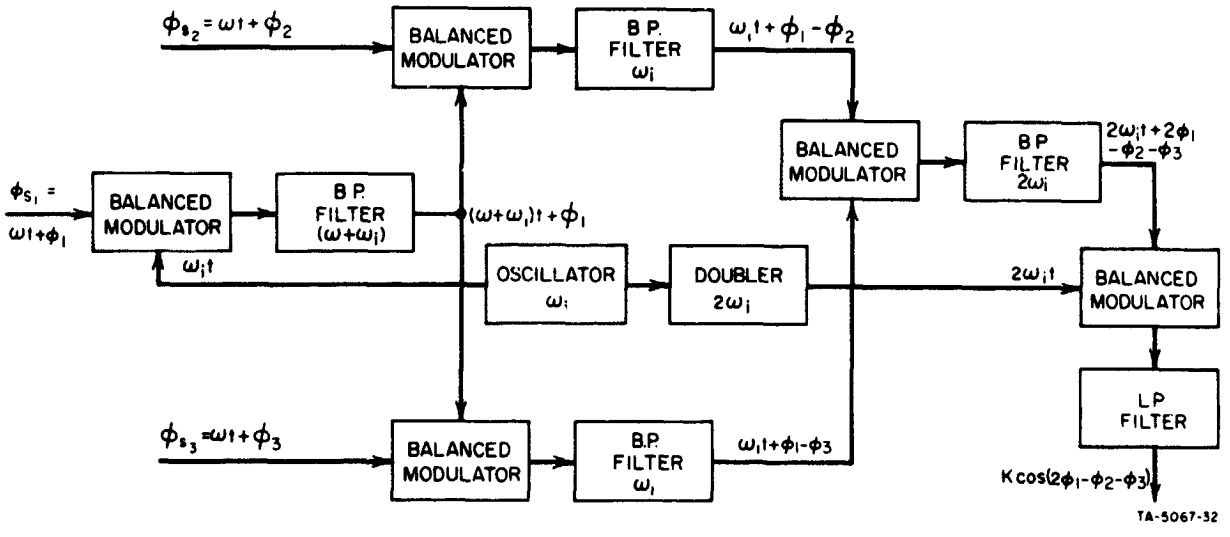

FIG. C-2 THREE-PATH PROCESSING

carries the same phase information as the signal at P_1, and therefore, when mixed with the signal at P_2 and the signal at P_3 in separate balanced modulators, the respective outputs (after suitable filtering) are signals at the offset frequency ω_i carrying the respective phases, $\varphi_1 - \varphi_2$ and $\varphi_1 - \varphi_3$. These signals can then be fed to a third balanced modulator, this one followed by suitable filters for passing the sum signal, which will be at frequency $2\omega_i$, with a phase $2\varphi_1 - \varphi_2 - \varphi_3$. A frequency doubler applied to the local oscillator output is then used to obtain a voltage at frequency $2\omega_i$, which can be mixed with the signal in a balanced modulator or product detector to obtain a voltage directly related to the desired phase fluctuations.

In equation form, the output of this signal processor is a voltage (neglecting higher order terms),

$$
\begin{aligned}
V_{out} &= K \cos (2\varphi_1 - \varphi_2 - \varphi_3) \\
&= K \cos \Bigg\{ 2\varphi_{a_1}(t) - \varphi_{a_2}(2) - \varphi_{a_3}(t) \\
&\quad + \frac{2\pi}{\lambda} \Bigg[- \frac{2\ell^2}{r_1^2} (\cos^2 \theta) r_1 + \frac{\ell^2}{r_1^2} (\cos^2 \theta) v_{r_1} t \\
&\quad + \frac{2\ell^2}{r_1^2} (\sin \theta \cos \theta) v_t t + \frac{\ell^2}{r_1^2} (\cos^2 \theta) a_{r_1} \frac{t^2}{2} \\
&\quad + \frac{2\ell^2}{r_1^2} (\sin \theta \cos \theta) a_t \frac{t^2}{2} \Bigg] \Bigg\}
\end{aligned}
\qquad \text{(C-15)}
$$

The desired output component is

$$2\varphi_{a_1}(t) - \varphi_{a_2}(t) - \varphi_{a_3}(t) \cong \sqrt{6}\varphi_a(t)$$

and the remaining terms of the output function are errors. Assuming again that measurements are made over 10-second intervals beginning at a zero-crossing of the output voltage, and that the phase instability tolerance is $\sqrt{6} \times 0.03$ radians for a range r = 200 km and a receiver spacing λ = 1 km, then

$$\sigma_{v_r} \cos^2 \theta < \frac{\sqrt{6} \times 0.03 \times r_1^2}{\ell^2 \tau} \times \frac{\lambda}{2\pi}$$

$$= \frac{\sqrt{6} \times 0.03 \times 0.036}{2\pi 10} \times (200)^2 = 1.68 \times 10^{-1} \text{ meters/sec}$$

(C-16a)

$$\sigma_{v_t} \sin\theta \cos\theta < \frac{\sqrt{6} \times 0.03 \times r_1^2}{2\ell^2\tau} \times \frac{\lambda}{2\pi}$$

$$= \frac{\sqrt{6} \times 0.03 \times 0.036}{4\pi 10} \times (200)^2 = 8.40 \times 10^{-2} \text{ meters/sec}$$

(C-16b)

$$\sigma_{a_r} \cos^2\theta < \frac{\sqrt{6} \times 0.03 \times r_1^2 \times 2}{\ell^2\tau^2} \frac{\lambda}{2\pi}$$

$$= \frac{\sqrt{6} \times 0.03 \times 0.036}{\pi 10^2} \times (200)^2 = 3.38 \times 10^{-1} \text{ meters/sec}^2$$

(C-16c)

$$\sigma_{a_t} \sin\theta \cos\theta = \frac{\sqrt{6} \times 0.03 \times r_1^2}{\ell^2\tau^2} \frac{\lambda}{2\pi}$$

$$= \frac{\sqrt{6} \times 0.03 \times 0.036}{2\pi 10^2} \times (200)^2$$

$$= 1.69 \times 10^{-1} \text{ meters/sec}^2 \quad . \qquad \text{(C-16d)}$$

Since these tolerances could not be met by any practical platform, a velocity estimate must be made for each 10-second interval (or an additional offset frequency introduced into the signal path through the processor, where the offset is determined by the phase error 10 seconds after a reference zero-crossing, to apply to the succeeding 10-second measurement interval). As was explained in the previous cases, this velocity correction tends to eliminate the phase error due to platform velocity, but acceleration errors will tend to maximize at the 5-second time after the reference zero-crossing. Therefore, the tolerances on platform acceleration become

$$\sigma_{a_r}(\cos^2\theta) < 1.35 \text{ meters/sec}^2$$

$$\sigma_{a_t}(\cos\theta \sin\theta) < 6.75 \times 10^{-1} \text{ meters/sec}^2 \quad .$$

Although these tolerances are much less severe than those resulting from any of the other experiment configurations discussed here, they are nevertheless a serious problem for any airborne platform.

5. Conclusions

The three experimental configurations discussed here represent successive attempts to relieve the stringent tolerances on platform motion imposed by the requirements of measurements of atmosphere-induced phase fluctuations. Clearly, there is no simple way to make these measurements. Tolerances can only be relaxed by adding receiver sites, signal processing capability, and phase error prediction capability. Even with the relatively complex system discussed in Sec. 4 above, the tolerances are too stringent to make measurements accurately using an aircraft or balloon as an RF source platform at 200 km range. The alternatives remaining are either to use a satellite platform at longer ranges or more complex signal processing and prediction capability.

It is quite feasible to carry out the experiment with a high-altitude satellite and a multiple receiving-site configuration, since the velocities and accelerations are then very slowly varying parameters and the ranges involved are sufficiently great to relax the tolerances on platform motion by one or more orders of magnitude from those used for illustration here.

Appendix D*

TIME IN VIEW

* This appendix was prepared by C. H. Dawson.

BLANK PAGE

Appendix D

TIME IN VIEW

Consider a receiving station at a latitude of α° north and a satellite in polar orbit with a period $T \geq 10$ hours. Let the earth's radius be $r = 6371$ km, and $\underline{a}$ be the satellite orbit radius ($a = 23{,}690$ for $T = 10$ hours). Let θ be the angle, in the x-y plane, between the projection of the station vector and the plane of the orbit. Let Φ be the satellite angle measured from the z-axis.

Then the coordinates of the station are (See Fig. D-1):

$$\begin{aligned} x_1 &= r \cos\alpha \cos\theta \\ y_1 &= r \cos\alpha \sin\theta \\ z_1 &= r \sin\alpha \quad . \end{aligned} \tag{D-1}$$

Call the vector from the origin to the station $\vec{r}$. Then the plane tangent to the earth at the station is the locus of all vectors $\vec{A}$ such that

$$(\vec{A} - \vec{r})\cdot\vec{r} = 0$$

or

$$\vec{A}\cdot\vec{r} = |\vec{r}|^2 = r^2 \quad . \tag{D-2}$$

The equation of this plane is

$$(r \cos\alpha \cos\theta)x + (r \cos\alpha \sin\theta)y + (r \sin\alpha)z = r^2 \tag{D-3}$$

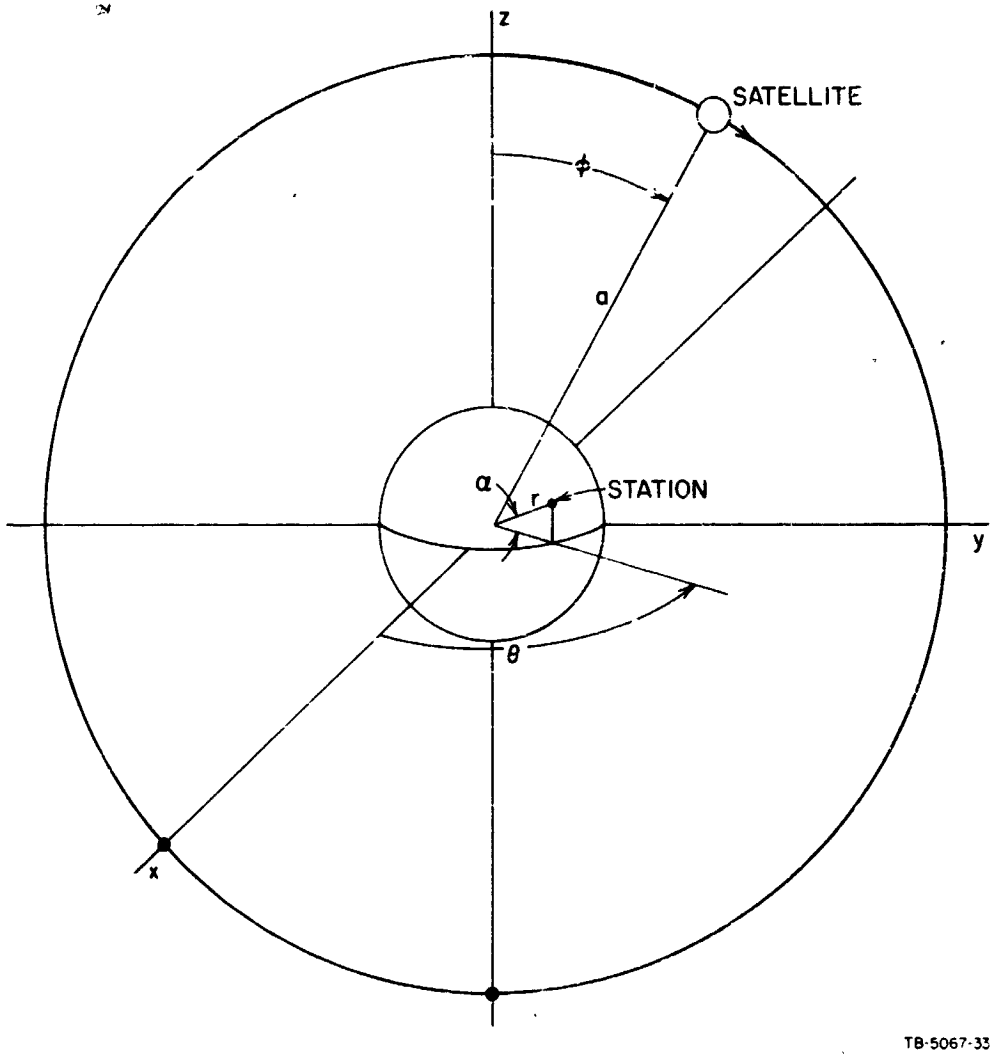

FIG. D-1 SATELLITE-STATION GEOMETRY. Orbit in X-Z Plane

The equation of the orbital plane may be taken as y = 0. Hence the intersection of the orbital plane with the tangent plane is the line (See Fig. D-2):

$$y = 0$$

$$x \cos \theta + z \tan \alpha = \frac{r}{\cos \alpha} \quad . \qquad \text{(D-4)}$$

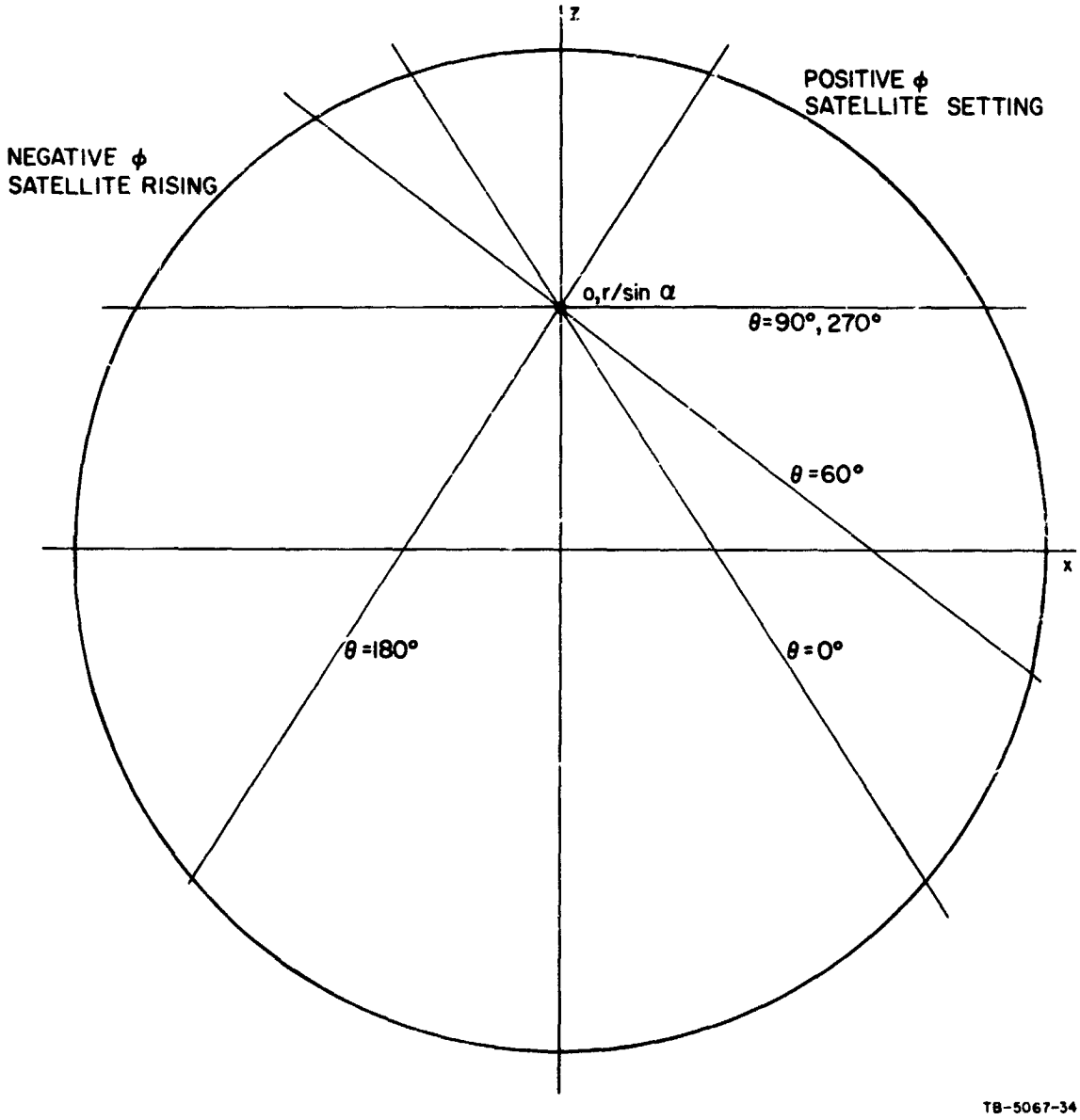

FIG. D-2 INTERSECTION OF ORBITAL AND TANGENT PLANES FOR VARIOUS VALUES OF θ

Note that this line cuts the z-axis at

$$x_2 = 0,\ y_2 = 0,\ z_2 = \frac{r}{\sin \alpha} \qquad \text{(D-5)}$$

which is independent of θ and hence, if

$$a > \frac{r}{\sin \alpha} \qquad \text{(D-6)}$$

the satellite will be visible on every orbit as it passes over the north pole.

The orbit may be written as

$$x = a \sin \theta$$

$$z = a \cos \theta \quad . \qquad \text{(D-7)}$$

When these values are substituted in Eq. (D-4), the result is

$$a \sin \theta + a \cos \Phi \tan \alpha = \frac{r}{\cos \alpha}$$

or

$$\cos \theta \sin \Phi + \tan \alpha \cos \Phi = \frac{r}{a \cos \alpha} \quad . \qquad \text{(D-8)}$$

This one equation in the two variables θ and Φ defines the intersection of the station horizon with the orbit. For each θ there exist two values of Φ, one positive and one negative (See Fig. D-2). The negative value of Φ represents the rising of the satellite; the positive value the setting.

Since

$$\cos (\pi \pm \theta) = - \cos \theta$$

and (D-8)

$$\sin (- \Phi) = \sin \Phi \quad ,$$

if θ_o and Φ_o satisfy Eq. (D-8), then so do

$$-\theta_o \ , \ \Phi_o$$

$$\pi - \theta_o \ , \ \Phi_o$$

$$\pi + \theta_o \ , \ \Phi_o \quad .$$

The solutions of Eq. (D-8) for the 10-hour orbit and a station at Oklahoma City ($\alpha = 33.4^0$) are shown in Fig. D-3.

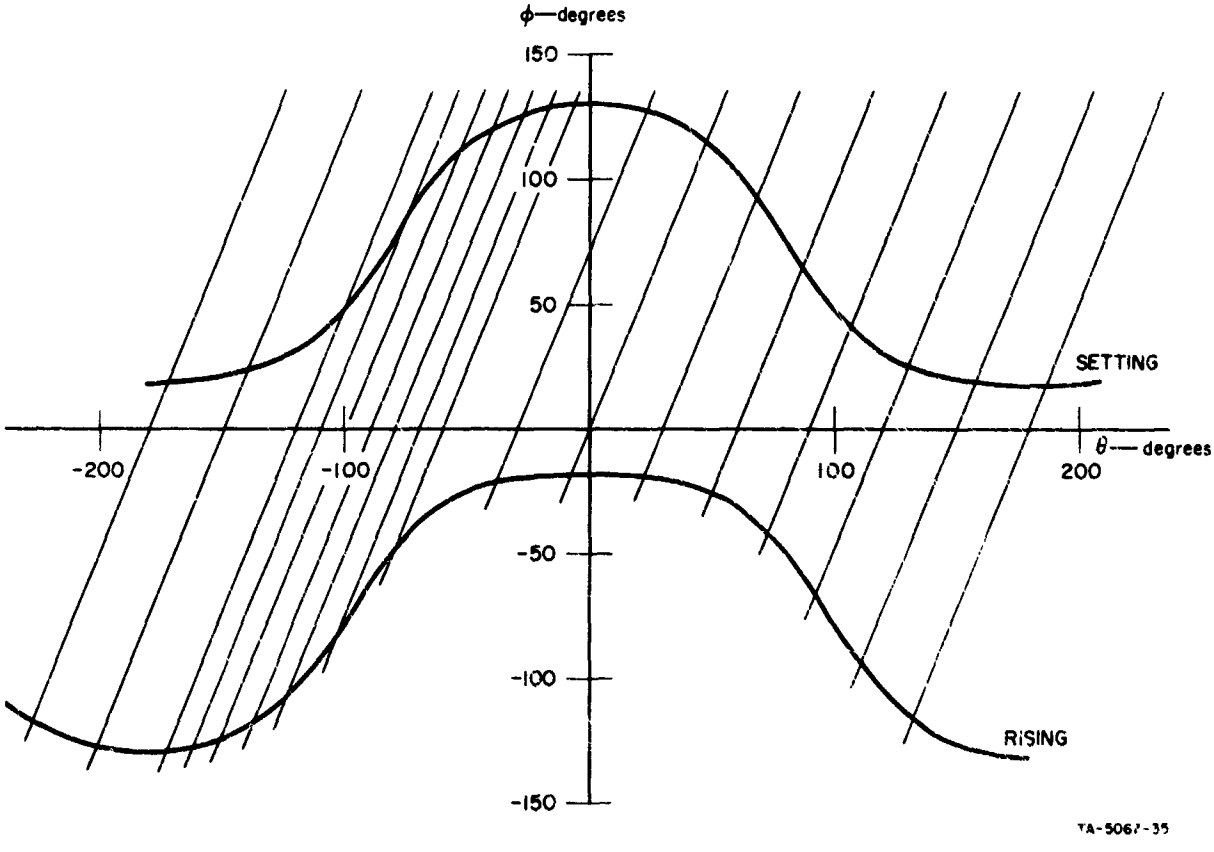

FIG. D-3 SOLUTIONS OF $\cos\theta \sin\phi + \tan\alpha \cos\phi = r/a\sin\alpha$ FOR $r = 6371$, $a = 23{,}690$, $\alpha = 33.4°$, AND LINES OF $\phi = 2.4(\theta - \theta_0)$

Since $\theta = \frac{2\pi}{24} t + \theta_o$ where θ_o is the value of θ when $\Phi = 0$ (the satellite is over the north pole), and $\Phi = \frac{2\pi}{T}t$, with $(T = 10)$, we have

$$\Phi = 2.4(\theta - \theta_o) \quad . \qquad \text{(D-10)}$$

A family of these lines have been added to Fig. D-3. The time the satellite is above the horizon is $\theta_S - \theta_R$ where θ_S is the intersection of Eq. (D-10) with the setting curve and θ_R the intersection with the rising curve. Since the satellite period will not be exactly ten hours, over a long time θ_o will be uniformly distributed.

Figure D-4 is derived from Fig. D-3 and shows that the time above the station horizon varies from a minimum of 2.26 hours when $\theta_o = 90^o$ and the station is moving away from the half of the orbital plane in which the satellite sets, to a maximum of 6.60 hours when $\theta = -90^o$ and the station is moving toward the half of the orbital plane in which the satellite sets. A rough average time in view is 3.78 hours.

When the orbital period is greater than 10 hours, the minimum, average, and maximum times above the station horizon will all increase.

Thus, if the experimental satellite is placed in polar orbit with a period of 10 hours or more, all passes will be usable, the minimum time above 0^o will be 2.26 hours, and there will be at least one pass per day.

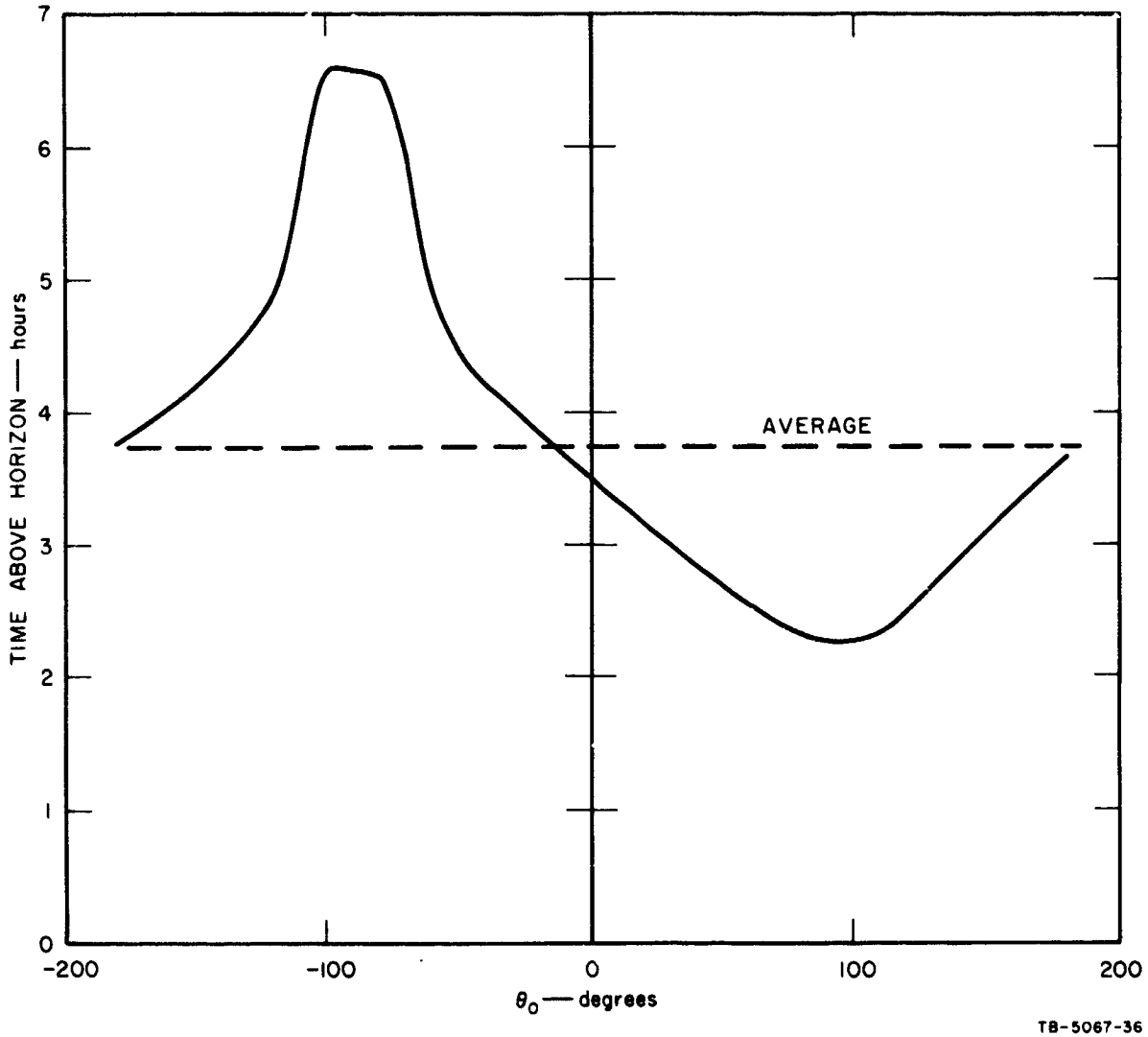

FIG. D-4 TIME ABOVE HORIZON vs. θ_0
10-hour orbit, latitude 33.4 degrees

Appendix E*

OSCILLATOR STABILITY LIMITATIONS, AND PHASE JITTER OF AN OSCILLATOR FEEDING A PHASE-LOCKED LOOP

* This appendix was prepared by R. B. Battelle.

Appendix E

OSCILLATOR STABILITY LIMITATIONS, AND PHASE JITTER OF AN OSCILLATOR FEEDING A PHASE-LOCKED LOOP

1. Oscillator Stability Limitations

There are three fundamental limitations to the stability of an oscillator:

(1) Thermal noise generated in the frequency control element and in the amplification chain following the oscillator, and shot noise in the oscillator tube or transistor

(2) Temperature, power, and load stability of the oscillator and its amplifier chain

(3) Aging of the oscillator components.

These three limitations affect primarily the short-term (i.e., $t \lesssim 10$ seconds), intermediate ($10 \text{ sec} \lesssim t \lesssim 100$ minutes), and long-term ($t \gtrsim 100$ minutes) stability, respectively, of an oscillator.

In the first category, three sources of noise affect the short-term stability of an oscillator. Consider first the thermal noise generated in the frequency control element. Following a straightforward derivation such as described by Schwartz (Ref. 62), and assuming that a simple frequency-control element such as a quartz crystal is used, the probability of a phase error in the output of the oscillator due to thermal noise in the crystal is

$$P_1(|\varphi|<|\varphi_o|) = \text{erf}\left[\sqrt{\left(\frac{S}{N}\right)_1}\,\varphi_o\right]$$

where

φ = Phase error in radians

$(S/N)_1$ = Signal-to-noise (power) ratio across the crystal

$$\text{erf}\,(x) = \frac{2}{\sqrt{\pi}}\int_o^x e^{-y^2}\,dy \quad .$$

The rms phase error is thus

$$\sigma_{\varphi_1} = \frac{1}{\sqrt{2(S/N)_1}} .$$

The signal-to-noise ratio S/N can be related to the oscillator parameters as follows:

Mean square signal voltage = P_s/G

where

P_s = Signal power dissipated in crystal

G = Equivalent shunt conductance of the crystal.

Mean square noise voltage = kT/C

where

k = Boltzman's constant

T = Absolute temperature of the crystal

C = Equivalent shunt capacity of the crystal.

Therefore $(S/N)_1 = \frac{P_s C}{kTG}$

and since $Q_c = \omega C/G$ = the quality factor of the crystal,

$$(S/N)_1 = \frac{P_s Q_c}{kT\omega_o}$$

and

$$\sigma_{\varphi_1} = \sqrt{\frac{kT\omega_o}{2P_s Q_c}}$$

For a typical crystal oscillator,

$\omega_o = 2\pi \times 5 \times 10^6$ radians/sec

$P_s = 0.5 \times 10^{-6}$ watts

$Q_c = 2.5 \times 10^6$

$T = 350^o$ K

$k = 1.38 \times 10^{-23}$ watts/cps/^{o}K

$$\sigma_{\varphi_1} \tilde{=} 2.5 \times 10^{-7} \text{ radians.}$$

Consider next the thermal noise generated in the amplifier chain following the oscillator. The same fundamental equations as those described above apply to this source of noise, but the parameters involved are different.

Thus,

$$P_2 \left(|\varphi| < |\varphi_o|\right) = \operatorname{erf}\left[\sqrt{\left(\frac{S}{N}\right)_2}\ \varphi_o\right]$$

and

$$\sigma_{\varphi_2} = \frac{1}{\sqrt{2\,(S/N)_2}}$$

where $(S/N)_2$ = Signal to noise (power) ratio at the amplifier output.

In this case,

Mean square signal voltage = $g\ P_s$

and

Mean square noise voltage = $4g\ F\ kT\ BR$

where

P_s = Amplifier input power

g = Gain of the amplifier chain

F = Noise figure of the chain

B = Equivalent bandwidth of the chain

R = Equivalent input resistance of the chain.

Therefore

$$(S/N)_2 = \frac{P_s}{4FkTBR}$$

and

$$\sigma_{\varphi_2} = \sqrt{\frac{4FkTBR}{2\ P_s}}\ .$$

For a typical oscillator-amplifier system,

$P_s = 0.5 \times 10^{-6}$ watts

$F = 5$

$T = 350^{\circ}K$

$B = 125$ cps

$R = 50$ ohms

$\sigma_{\varphi_2} = 2.5 \times 10^{-5}$ radians,

which is 100 times larger than the rms phase error due to thermal noise in the crystal. σ_{φ_2} would be smaller and σ_{φ_1} larger if P_s were increased. However, σ_{φ_2} cannot be reduced much without significantly reducing F, B, T, and R.

Consider next the shot noise generated in the oscillator tube or transistor. Following the derivation of Edson (Ref. 63), the rms phase error due to shot noise is a function of the sampling time τ; thus,

$$\sigma_{\varphi_3} = \sqrt{\frac{\omega_o^2 KT\tau}{2P_s Q^2}}$$

which, for the typical crystal oscillator parameters used above, becomes

$$\sigma_{\varphi_3} \cong 8.7 \times 10^{-7} \sqrt{\tau} \text{ radians}$$

which is much less than the thermal-noise-induced phase errors for all reasonable sampling times ($\tau < 100$ sec).

The phase error in an oscillator can be reduced, however, at the expense of circuit complexity, by applying the output of the oscillator to a phase-locked loop and using the voltage-controlled oscillator (VCO) of the loop as a phase-stable source. Typically, the VCO is itself a crystal-controlled oscillator of inherently high phase stability. A small range of phase control derived from the phase detector of the loop is added to this oscillator. The output of this oscillator has an rms phase jitter (as derived in Sec. 2 of this Appendix) of

$$\sigma_{\varphi_L} = \sigma_{\varphi} \left(\frac{6Q_c \omega_\ell}{\sqrt{2}\omega_o} \right)^{1/2}$$

where ω_ℓ and ω_o are the loop natural frequency and oscillator frequency, respectively, and Q_c is the figure of merit of the crystal unit. For values of ω_ℓ less than about $\sqrt{3}$ radians per second, the rms phase error of a typical crystal oscillator can be reduced by the addition of the loop.

In addition to thermal noise and shot noise, fluctuations in crystal drive power and oven temperature are sources of oscillator instability (Ref. 64) in the second category. Typically, the drive power P_s must be stabilized to 1 part in 10^{-10} to maintain a frequency stability of 1 part in 10^{-12} (frequency stability is sometimes defined as $\sigma_\omega/\omega_o = \sigma_\varphi/\omega_o\tau$). Variations in crystal parameters due to oven temperature changes limit the frequency stability to about 5 parts in 10^{12} per degree Centigrade, so that typical oven temperature variations result in a lower limit of frequency stability of about 10^{-12}. These two instability factors tend to have intermediate time constants of a few seconds to several minutes, and nearly always exceed the instability effects of oscillator shot noise.

The stability of an oscillator is also affected by any regeneration in the oscillator-amplifier circuits due to incomplete isolation of the crystal from the output load (Ref. 64). If a fraction of the output voltage leaks into the oscillator input, the input phase may be shifted. Thus,

$$\tan \Delta\varphi = \frac{V_f \sin \theta}{V_s + V_f \cos \theta}$$

where

$\Delta\varphi$ = Phase shift due to regeneration

V_f = Leakage voltage

V_s = Input voltage

θ = Phase difference between V_s and V_f.

For $\theta \neq 0$, the oscillator frequency must shift until θ goes to zero. The phase shift $\Delta\varphi'$ due to frequency change in a crystal is

$$\Delta\varphi' \simeq \tan^{-1} \frac{2Q\Delta\omega}{\omega} \simeq \frac{2Q\Delta\omega}{\omega} .$$

Therefore, the frequency shift resulting when the oscillator adjusts itself to make $\Delta\varphi' = \Delta\varphi$ is found by setting

$$\frac{2Q\Delta\omega}{\omega} = -\frac{V_f \sin \theta}{V_s + V_f \cos \theta}$$

If $V_s \gg V_f$, this equation reduces to

$$\frac{\Delta\omega}{\omega} = -\frac{1}{2Q}\frac{V_f}{V_s}\sin\theta \quad .$$

For a typical crystal Q of $2.5 \times 1.^6$, therefore, V_f/V_s must be on the order of 10^{-6} (120-db isolation) if the frequency shift due to load variations are to be less than 1 part in 10^{12}.

Finally, long-term aging of the crystal results in frequency changes typically of 1 part in 10^{10} per day. If slow drift must be eliminated, the oscillator can be compensated by correcting its frequency using the comparison of its output with some absolute standard such as a rubidium cell (Ref. 65).

The spectral characteristics of these phase fluctuations can be calculated (Ref. 66). The fluctuations due to thermal noise in the crystal have a power spectral density of

$$S_{\varphi_1}(\Delta\omega) \simeq \frac{\omega_1}{(S/N)_1\left(\Delta\omega^2 + \omega_1^2\right)}$$

where

$$\omega_1 = \frac{\omega_o}{2Q_c}$$

$$\Delta\omega = (\omega - \omega_o) \quad .$$

Similarly, the fluctuations due to thermal noise in a succeeding single-tuned amplifier stage have a spectral density of

$$S_{\varphi_2}(\Delta\omega) \simeq \frac{1}{(S/N)_2}\frac{\omega_2}{\left(\Delta\omega^2 + \omega_2^2\right)}$$

where

$$\omega_2 \simeq \pi B \quad .$$

The spectral density of phase fluctuations due to shot noise in the oscillator have the form,

$$S_{\varphi_3}(\Delta\omega) \cong \frac{4\pi^2\omega_1}{(S/N)_1\Delta\omega^2} \quad .$$

This latter spectral density becomes infinite at $\Delta\omega = 0$, which is due to the "random walk" of phase resulting from shot noise in the oscillator. The peak value of $S_{\varphi_3}(\Delta\omega)$ can be limited by drift compensation using an absolute frequency standard.

A plot of these spectral densities for the typical crystal oscillator and amplifier chain used to illustrate the order of magnitude of phase errors due to the basic noise sources is shown in Fig. E-1. For convenience in plotting, only one side of the spectral distribution is shown. Note that $S_{\varphi_2}(\omega)$ dominates the spectral density of the oscillator-amplifier except as $\Delta\omega$ approaches zero.

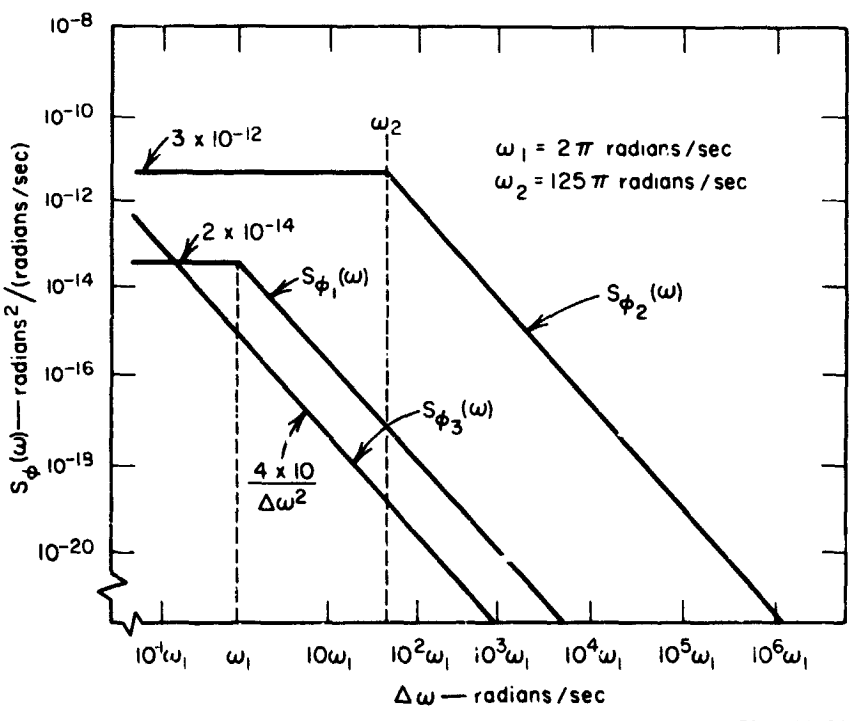

FIG. E-1 OSCILLATOR PHASE SPECTRA

In conclusion, this analysis indicates that phase errors due to thermal noise in the amplifier chain following a crystal oscillator dominate the short-term phase errors due to other causes. The order of magnitude of these phase errors is 3×10^{-5} radians rms for a 5-Mc crystal oscillator without phase stabilization from a separate phase-locked loop. This phase error multiplies to 0.06 radians rms at 10 Gc.

The rms path phase at 10 Gc for a clear troposphere is of the order of 0.075 radians at the zenith, increasing to 0.297 radians at 4 degrees above the horizon. Hence, a phase-locked loop with a bandwidth of at most 0.25 radians/second should be used to reduce the rms phase error of the transmitter to $0.58 \times \sqrt{0.25} \times 0.06 = 0.017$ radians. Such a loop would be particularly effective in reducing the spectrum of the transmitted phase in the 1-to-100-cps range of particular interest.

Since the power spectrum of the phase measurements in the proposed experiment is expected to extend to approximately 100 cycles per second, this analysis indicates that oscillator stability will not limit the accuracy of these measurements over any appreciable fraction of the spectrum. Furthermore, the lower end of the spectrum, where oscillator instability might affect measurements, is not of primary interest to the multiple-aperture concept.

2. Phase Jitter of an Oscillator Feeding a Phase-Locked Loop

Oscillator phase jitter due to differential noise component dN is

$$d\varphi^2 = \frac{dN}{A_c^2} = \frac{4kTR}{2\pi A_c^2} \left|H(\omega)\right|^2 d\omega \quad .$$

When the oscillator feeds a phase-locked loop, the loop output (VCO) phase is

$$d\varphi_o^2 = d\varphi^2 \left|F(\omega)\right|^2 = \frac{4kTR}{2\pi A_c^2} \left|H(\omega)\right|^2 \left|F(\omega)\right|^2 d\omega$$

where $F(\omega)$ = loop transfer function.

The transfer function of a second-order loop is

$$|F(\omega)|^2 = \frac{1 + \frac{2\Delta\omega^2}{\omega_n^2}}{1 + \frac{\Delta\omega^4}{\omega_n^4}}$$

$$|H(\omega)|^2 = \frac{1}{1 + (2RC\Delta\omega)^2} .$$

Let $\omega_e = \frac{1}{2RC}$

$$|H(\omega)|^2 \simeq \frac{1}{1 + \frac{\Delta\omega^2}{\omega_e}}$$

Now the loop output phase is

$$\varphi_o^2 = \int_{-\infty}^{\infty} d\varphi_o^2 = \frac{4kTR}{2\pi A_c^2} \int_{-\infty}^{\infty} \frac{\left(1 + \frac{2\Delta\omega^2}{\omega_n^2}\right)}{\left(1 + \frac{\Delta\omega^4}{\omega_n^4}\right)\left(1 + \frac{\Delta\omega}{\omega_e}^2\right)} d\Delta\omega$$

which, for $\omega_n \ll \omega_e$, gives

$$\varphi_o^2 = \frac{4kTR}{2\pi A_c^2} \frac{3\pi\omega_n}{\sqrt{2}} = \frac{6kTR\omega_n}{\sqrt{2}\ A_c^2}$$

$$\overline{\varphi_o^2} = \sqrt{\frac{6kTR\omega_n}{\sqrt{2}\ A_c^2}} .$$

The rms phase jitter of the oscillator alone was

$$\sigma_{\varphi} = \sqrt{\frac{kT}{CA_c^2}} \quad .$$

Thus, the phase-locked loop has changed the rms phase jitter by the factor

$$\left(\frac{6RC\omega_n}{\sqrt{2}}\right)^{1/2} = \left(\frac{6Q\omega_n}{\sqrt{2}\ \omega_c}\right)^{1/2} \quad .$$

For a typical crystal oscillator

$$\omega_c = 2\pi \times 5 \times 10^6 \text{ rad/sec}$$

and

$$Q = 2.5 \times 10^6 \quad .$$

The corresponding loop factor is

$$\left(\frac{6Q\omega_n}{\sqrt{2}\ \omega_c}\right)^{1/2} = 0.58\ \omega_n^{1/2} \quad .$$

Thus for $\omega_n < 1.7$ rad/sec, the phase jitter of the loop output will be less than that of the input oscillator.

Appendix F*

MONOPULSE CONSIDERATIONS

* This appendix was prepared by C. H. Dawson.

BLANK PAGE

APPENDIX F

MONOPULSE CONSIDERATIONS

Consider an antenna of diameter D meters receiving signals of frequency f Gc. Let the pattern resulting from each horn and the reflector have a half-power beamwidth (angle from peak to 0.707 of the peak voltage) θ_{HP}, and a first null at α_n.

Assume that the beam of the horn has a (sin x)/x shape for which $\theta_{HP} = 1.39$ radians. Then $\theta_{HP}/\alpha_n = 1.39/\pi$ or $\alpha_n = \pi\theta_{HP}/1.39$. However, θ_{HP} can also be expressed as 0.180/fD radians and therefore

$$\alpha_n = \frac{\pi \times 0.180}{1.39\ fD} = \frac{0.407}{fD} \text{ radians} \quad . \qquad \text{(F-1)}$$

Assume the four monopulse horns are located on the corners of a square and the beams are squinted out radially by 0.6 α_n radians. The gain for a signal arriving on boresight is then given by (sin x)/x evaluated at x = 0.6π = 1.885 radians = 108°, where sin 108° = 0.9511, cos 108° = -0.3090, and sin 108°/1.855 = 0.505. Since there are four horns, the sum channel factor is

$$a_o = 4 \times 0.505 = 2.02 \quad . \qquad \text{(F-2)}$$

Now assume that the angle of arrival moves off boresight along a line bisecting the line connecting two adjacent horns by an angle $d\psi$. The equivalent Δx is

$$\Delta x = \frac{1}{\sqrt{2}} \frac{\pi}{\alpha_n} \Delta\psi$$

where x is the angle from the horn boresight. This angle increases for two horns and decreases for the other two. Since the gain at x is $(\sin x)/x$, the horns with increased angles have gains of

$$\frac{\sin x}{x} - \frac{d}{dx}\left(\frac{\sin x}{x}\right)\Delta x$$

and those with decreased angles,

$$\frac{\sin x}{x} + \frac{d}{dx}\left(\frac{\sin x}{x}\right)\Delta x \quad .$$

Therefore the gain of the difference channel is

$$b_o = 4\,\frac{d}{dx}\left(\frac{\sin x}{x}\right)\cdot\frac{1}{\sqrt{2}}\,\frac{\pi}{\alpha_n} \qquad \text{(F-3)}$$

Since

$$\frac{d}{dx}\,\frac{\sin x}{x} = \frac{\cos x - \dfrac{\sin x}{x}}{x} = \frac{-0.3090 - 0.505}{1.885} \quad ,$$

$$b_o\alpha_n = \frac{4}{\sqrt{2}} \times \frac{0.814}{1.885}\,\pi = 3.845 \quad . \qquad \text{(F-4)}$$

Thus the voltage in the difference channel is

$$b_o A\Delta\psi + n$$

where n is noise of power N and A is the peak signal received by one horn. Hence the rms angular equivalent of the noise, σ_ψ, is $\sqrt{N}\,/b_c A$. Since the signal-to-noise power ratio in the sum channel is

$$\rho = \frac{(2.02A)^2}{2} \times \frac{1}{N} = 2.04\,\frac{A^2}{N} \quad ,$$

$$\sigma_\psi^2 = \frac{N}{(b_o A)^2}\,\frac{N}{A^2} \times \frac{\alpha_n^2}{(3.845)^2} = \frac{\alpha_n^2}{(3.845)^2} \times \frac{2.04}{\rho} \qquad \text{(F-5)}$$

$$= 0.138 \frac{\alpha_n^2}{\rho} = 0.138 \times \frac{(0.407)^2}{(fD)^2} \times \frac{1}{\rho}$$

$$= 2.28 \times 10^{-2} \frac{1}{(fD)^2} \times \frac{1}{\rho} \text{ rad}^2 \quad . \qquad \text{(F-5) Co't'd}$$

Since the path contribution to the angle-of-arrival fluctuations is predicted to be of the order of 0.3 milliradians (1 minute), it is desirable to keep $\alpha_\psi \leq 0.03$ milliradians. The corresponding requirement on sum channel signal-to-noise ratio is

$$\rho = \frac{2.28 \times 10^{-2}}{(3 \times 10^{-5})^2} \times \frac{1}{(fD)^2} = \frac{2.54 \times 10^7}{(fD)^2} \qquad \text{(F-6)}$$

which is evaluated for values of fD of interest in Table F-1.

Table F-1

SUM CHANNEL S/N RATIOS, ρ

fD	8	16	32	64	128	256
$(fD)^2$	64	256	1024	4096	16,384	65,536
ρ	3.96×10^5	9.9×10^4	2.435×10^4	6.2×10^3	1.55×10^3	3.875×10^2
ρ(db)	56	50	44	38	32	26

Appendix G*

NOISE CORRELATION

* This appendix was prepared by L. A. Robinson.

Appendix G

NOISE CORRELATION

1. Noise Correlation Between Two Channels of an Array and an Optical Analog

In the noise-correlation measurements we are concerned with the degree of correlation existing in the RF noise picked up at two elements in an array of large paraboloidal reflectors. This RF noise is radiated by an extended distribution of incoherent radiators. These radiators could be, for example, the thermally excited molecules in the atmosphere. Considerable physical insight into this situation of present interest can be gained by considering an analogous situation at another wavelength--namely, at optical wavelengths. In addition, the theoretical results in optics, which have been adequately confirmed by experiment, make it possible to estimate what degree of correlation might exist in the case of the array at microwave frequencies.

Consider now the experiment performed by Young on the interference pattern produced by two pinholes illuminated by an incoherent light source of finite spatial extent and finite but narrow frequency spectrum (see Ref. 67 and pp. 499-507 of Ref. 68). This source is represented by S in Fig. G-1. The two pinholes P_1 and P_2 in the screen A produce interference fringes in the intensity pattern observed on screen B. The fringes have maximum depth near the line that passes from the center of the source through a point midway between the pinholes. As the observation point Q moves away from that line, the depth of successive fringes decreases until the fringes cease to exist when the path length difference $(r_1 - r_2)$ divided by the speed of light becomes on the order of the reciprocal of the spectrum width. The existence of any interference fringes at all, although there is not complete cancellation at the minima, indicates that there is partial coherence of the light at the two pinholes even though this light originated at an incoherent source.

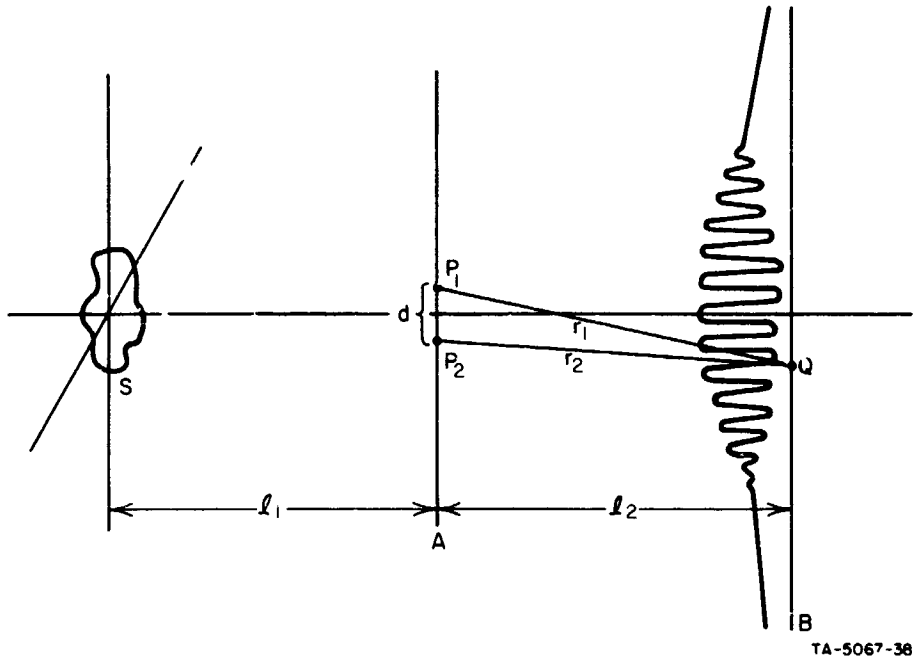

FIG. G-1 YOUNG'S INTERFERENCE EXPERIMENT

One way of describing the degree of coherence of the light at the pinholes is in terms of the visibility of the fringes. The visibility V is defined in terms of the intensity I_{max} at the central maximum, and the intensity I_{min} at an adjacent minimum:

$$V = \frac{I_{max} - I_{min}}{I_{max} + I_{min}} \qquad (G\text{-}1)$$

Starting with closely spaced pinholes, we find that the visibility decreases as the pinhole spacing is increased, going to zero at a certain spacing. Further increase in pinhole spacing causes the visibility to increase again, reach a peak, and then go to zero, with this "side-lobe" type of structure continuing with decreasing peak values. Leaving the pinhole spacing fixed and increasing the source size produces the same effect.

In the optical analogy, the light source is directly analogous to the microwave noise source, the spectral width being narrow compared to the center frequency in the microwave case due to the filtering in the receiver. The pinholes correspond to the antennas in the microwave case.

The intensity of the light fringes corresponds directly with the noise power output from the summing junction of the two-channel microwave receiver. The position of the observation point Q corresponds to a given combination of relative time delay of the microwave signal in traveling from the source to the antennas, and through the receiver channels to the summing junction. The central fringes correspond to noise arriving at an array from directions close to the same direction as the telemetry signal the array is intended to receive, since the array will be adjusted to give nearly equal delay through all channels for the telemetry signal. The smaller fringes near the edge, and the region where there are no fringes, correspond to noise arriving at an array from directions considerably different from the telemetry signal. How much different is "considerably" different depends inversely on the receiver bandwidth and antenna spacing. We will concern ourself here with the central fringes, which are the most pronounced.

The partial coherence of the light at the pinholes corresponds to the possibility of partial correlation of microwave noise in two or more channels of an array. Thus we find that a simple statement like "signals from coherent sources (man-made) will add voltage-wise at the array summing junction, and noise from incoherent sources will add power-wise at the summing junction" is not adequate to describe the physical situation. It will be shown later (Sec. 2 of this Appendix) by some examples, however, that correlation of natural noise signals between adjacent antennas in an array can be expected to be small, and that significant correlation of noise across the entire array is not expected.

Let us now consider in more detail the structure of the light fringes in Fig. G-1. Following the notation of Born and Wolf (Ref. 68), we let $I^{(1)}(Q)$ be the light intensity at observation point Q due to pinhole P_1 alone, and $I^{(2)}(Q)$ be the light intensity at Q due to pinhole P_2 alone. The light at point Q is a mixture of coherent and incoherent light. Use will be made of a complex degree of coherence (Ref. 68) μ_{12} such that the ratio of coherent to incoherent light is:

$$|\mu_{12}| = \frac{I_{coh}}{I_{incoh} + I_{coh}} = \frac{I_{coh}}{I_{total}} \qquad (G\text{-}2)$$

Restricting our consideration only to the central fringes, such that the relative time delay between arrival of the two light beams is small compared to the reciprocal of the spectrum line width--i.e.,

$$t_d = \frac{r_2 - r_1}{c} \ll \frac{1}{\Delta\nu} \quad , \qquad (G\text{-}3)$$

then μ_{12} does not have to be considered a function of t_d. Here c is the speed of light. The coherent portion of the light will add coherently, contributing the first term of Eq. (G-4), and the incoherent portion of the light will add as power, contributing the second term of Eq. (G-4), giving an intensity at point Q of:

$$I(Q) = |\mu_{12}|[I^{(1)}(Q) + I^{(2)}(Q) + 2\sqrt{I^{(1)}(Q)}\sqrt{I^{(2)}(Q)} \cos(\beta_{12} - \delta)]$$

$$+ [1 - |\mu_{12}|][I^{(1)}(Q) + I^{(2)}(Q)] \qquad (G\text{-}4)$$

$$= I^{(1)}(Q) + I^{(2)}(Q) + 2|\mu_{12}|\sqrt{I^{(1)}(Q)}\sqrt{I^{(2)}(Q)} \cos(\beta_{12} - \delta) \quad . \qquad (G\text{-}5)$$

Here β_{12} is the argument of μ_{12}, which is of no direct concern to us, and

$$\delta = 2\pi \frac{r_2 - r_1}{\bar{\lambda}} \qquad (G\text{-}6)$$

where $\bar{\lambda}$ is the average wavelength of the light. The maximum and minimum of Eq. (G-5) are:

$$I_{max} = I^{(1)}(Q) + I^{(2)}(Q) + 2\sqrt{I^{(1)}(Q)}\sqrt{I^{(2)}(Q)}\ |\mu_{12}|$$

$$I_{min} = I^{(1)}(Q) + I^{(2)}(Q) - 2\sqrt{I^{(1)}(Q)}\sqrt{I^{(2)}(Q)}\ |\mu_{12}| \qquad (G\text{-}7)$$

Thus the visibility of the central fringes is:

$$V = \frac{I_{max} - I_{min}}{I_{max} + I_{min}} = \frac{2\sqrt{I^{(1)}(Q)}\sqrt{I^{(2)}(Q)}}{I^{(1)}(Q) + I^{(2)}(Q)} |\mu_{12}| \quad . \qquad (G\text{-}8)$$

If the two beams are of equal intensity (which corresponds to equal antenna and receiver-channel gains in the microwave case), then:

$$|\mu_{12}| = V = \frac{I_{max} - I_{min}}{I_{max} + I_{min}} \quad . \qquad (G\text{-}9)$$

That is, $|\mu_{12}|$ can be experimentally determined by measuring I_{max} and I_{min}. Also for the equal-intensity case,

$$I_{max} = 2I^{(1)}(Q)[1 + |\mu_{12}|] \quad . \qquad (G\text{-}10)$$

The effect of the partial coherence is to make I_{max} greater by a factor of $(1 + |\mu_{12}|)$ than would be the intensity at point Q if there was no coherence.

In the case of two microwave antennas of equal gain with two receiver channels of equal gain, it is only necessary to replace all intensities I in the above equations by noise powers N. The magnitude of the complex degree of coherence (correlation) can be measured as outlined in Secs. II-B-2 and III-G. The maximum increase in noise power at the summing junction due to correlation is then found from Eq. (G-10).

Having thus established physical significance for the complex degree of coherence, consideration will be given as to how this function varies with separation between the pinholes. For an incoherent, quasi-monochromatic source distributed over a plane and having a small angular diameter as seen from the point of observation, the van Cittert-Zernike theorem states (pp. 508-510 of Ref. 68): "The complex degree of coherence, which describes the correlation of vibrations at a fixed point P_2 and a variable point P_1 in a plane illuminated by an extended

quasi-monochromatic primary source, is equal to the normalized complex amplitude at the corresponding point P_1 in a certain diffraction pattern, centered on P_2. This pattern would be obtained on replacing the source by a diffracting aperture of the same size and shape as the source, and on filling it with a spherical wave converging to P_2, the amplitude distribution over the wave-front in the aperture being proportional to the intensity distribution across the source." This theorem is proved by the fact that the integrals arising from the coherence problem and from the diffraction problem have identical forms.

A particular example for a source distribution will serve to give insight into what sort of degree of coherence can be expected. For a uniform-intensity, plane, circular source whose distance from the points of observation is large compared to both the source diameter and the separation between points P_1 and P_2, we have (p. 511 of Ref. 68):

$$|\mu_{12}| = 2\frac{|J_1(v)|}{v}$$

$$v = \pi \xi \frac{d}{\bar{\lambda}} \qquad \text{(G-11)}$$

where J_1 is the Bessel function of the first kind and first order, which is purely real with either positive or negative sign, and ξ is the angular diameter of the source as seen from P_1 and P_2. The degree of coherence for this source is plotted in Fig. G-2. The first zero occurs for $d = 1.22\ \bar{\lambda}/\xi$. The first lobe has a peak of only 0.132, and occurs at $d = 1.64\ \bar{\lambda}/\xi$.

Some actual noise sources that could be approximated by the distribution assumed above are radio stars, distributed galactic noise, and the sun. Noise from the warm earth and from atmospheric absorption violate the assumption of the source-to-observer distance being very large compared to source size and to separation of the antennas. Violation of this assumption, however, would be expected to decrease

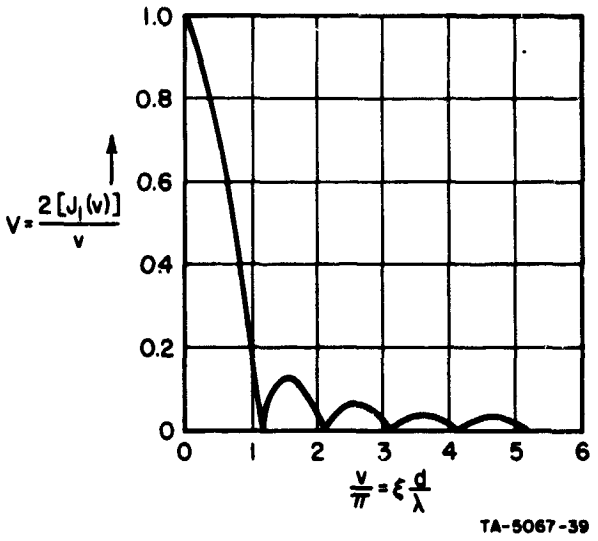

FIG. G-2 VISIBILITY vs. SEPARATION FOR A CIRCULAR SOURCE

rather than increase the correlation between noise in the array channels. Some numerical examples are given in Sec. 2 of this appendix, based on Eq. (G-11).

2. Numerical Examples Related to Noise Correlation

In this appendix some numerical examples will be presented to give a definite indication as to what antenna separations on the earth's surface will result in significant correlation of noise in the channels of an array. Also, an indication will be given of an upper bound on how much the system signal-to-noise ratio might be degraded by noise correlation. The correlation distances will be based on Eq. (G-11), which equation applies specifically for an extended uniform circular source of small angular diameter that is far from the array compared to the antenna spacing. The calculations will be made for a frequency of 2 Gc, and the distances scale inversely proportional to frequency for other frequencies.

a. Correlation Distances

1) Source Diameter of 0.08 Degrees

This source diameter is the same as that of the radio star Cassiopia A. The first null of the degree-of-coherence function occurs at an antenna spacing of

$$d = 1.22 \frac{\lambda}{\xi} = 1.22 \frac{1.5 \times 10^{-1} \text{m}}{1.4 \times 10^{-3} \text{radian}} = 130 \text{ meters.}$$

The first side-lobe peak of 13 percent occurs at an antenna spacing of

$$d = 1.64 \frac{\lambda}{\xi} = 176 \text{ meters.}$$

For larger antenna spacing, the correlation of noise from a source of this size would always be less than 13 percent. Even for this relatively small source diameter, high correlation of the noise does not extend over distances that are comparable to the overall size of an operational array.

2) Source Diameter of 0.5 Degree

This source diameter is equal to that of the quiet sun. The first null of the degree-of-coherence function occurs at an antenna spacing of

$$d = 1.22 \frac{\lambda}{\xi} = 1.22 \frac{1.5 \times 10^{-1} \text{m}}{0.87 \times 10^{-2} \text{radian}} = 21 \text{ meters.}$$

The first side-lobe peak of 13 percent occurs at an antenna spacing of

$$d = 1.64 \frac{\lambda}{\xi} = 28 \text{ meters.}$$

These distances are of the same order as the diameter of the parabolic reflectors that would be used in an operational array.

3) Source Diameter of 2.6 Degrees

This source diameter would just fill the 3-db beamwidth of a 4-meter reflector such as would be used in the experiments described in the body of this report. The first null of the degree-of-coherence function occurs at an antenna spacing of

$$d = 1.22 \frac{\lambda}{\xi} = 1.22 \frac{1.5 \times 10^{-1} \text{m}}{4.5 \times 10^{-2} \text{radian}} = 4 \text{ meters.}$$

The first side-lobe peak of 13 percent occurs at an antenna spacing of

$$d = 1.64 \frac{\lambda}{\xi} = 5.5 \text{ meters.}$$

This result can be generalized to state that when the antennas are observing a distant uniform background of noise (the effective source diameter then being set by the antenna beamwidth), the first null in the degree-of-coherence function will occur when the two antennas are approximately side by side.

b. Signal-to-Noise Ratios

The worst source of external noise that an operational array in the 1-to-20 Gc band would regularly encounter would be that due to atmospheric absorption at elevation angles near the horizon. None of the theory presented in Sec. 1 of this appendix applies to the case of a noise source extending in three dimensions, and that is relatively close to the array. On the basis of the material that has been presented, however, it would seem that the assumption of 15 percent correlation of the atmospheric absorption and galactic noise over the entire array would be extremely pessimistic. Therefore, this assumption will be used to estimate an upper bound on the degradation of system signal-to-noise ratio.

Assume first of all a receiver noise temperature of 50°K, such as might be obtained with a cooled parametric amplifier. If the antennas

are pointed such that the equivalent sky temperature due to atmospheric absorption and galactic noise is 70°K, then the assumed noise correlation could produce at the worst a system noise temperature of

$$50^\circ K + 1.15(70^\circ K) = 50 + 80 = 130^\circ K.$$

This is a fractional increase over the case of zero correlation of

$$\frac{130^\circ K}{50 + 70} = \frac{130}{120} = 1.085.$$

Therefore, the maximum degradation of signal-to-noise ratio under the assumed conditions would be only 0.35 db.

If a receiver noise temperature of 10°K is taken, as might be obtained with a maser including some ohmic transmission-line loss, the degradation comes out:

$$\frac{10 + (1.15)(70)}{10 + 70} = \frac{10 + 80}{10 + 70} = \frac{90}{80} = 1.125.$$

This is only 0.4 db.

Finally, it is of interest to compare the performance of an array of many antennas with a single large reflector having the same effective signal-capture area. Assume that the same quality of receiver is used with each antenna of the array as is used with the single large reflector. Then even if all external noise sources were completely correlated across the array, the two systems would have the same signal-to-noise ratio on any signal strong enough that the individual channels of the array could lock on the signal (see Appendix I of Ref. 3).

Appendix H*

METEOROLOGICAL CONSIDERATIONS

* This appendix was prepared by A. S. Dennis

BLANK PAGE

Appendix H

METEOROLOGICAL CONSIDERATIONS

1. Introduction

The various performance limitations imposed upon satellite-to-ground radio links by the troposphere were reviewed in Sec. III of Ref 3. The tropospheric effects are numerous, including refraction and amplitude scintillation; however, it is not the purpose of this report to consider all of them. Rather, attention will be concentrated upon the three effects that apparently will be the controlling factors in the performance of large arrays. The three effects are

(1) Attenuation

(2) Sky noise

(3) Phase instability.

Each of these effects is discussed below. The references quoted are not exhaustive, but an attempt has been made to select those which contain material in a form that is immediately applicable to the engineering problem at hand.

2. Principal Limitations on System Performance

The first two limiting effects, attenuation and sky noise, are obviously closely related. One can write the sky-noise temperature as

$$T_s = \int_o^\infty \alpha T \exp\left[-\int_o^r \alpha dr\right] dr \quad , \qquad \text{(H-1)}$$

where α is the absorption coefficient per unit length and T is the absolute temperature at range r measured along the beam from the antenna. The exponential term expresses the fact that the contribution from range r is modified by attenuation over the range interval from 0 to r. It should be noted that when particulate matter is present, there can be attenuation due to scattering in addition to that associated with the

absorption coefficient α. However, the absorption term predominates at frequencies below 10 Gc even when fog or cloud particles are present.

The attenuation and sky noise produced by the gaseous components of the troposphere, including water vapor, have been examined by numerous authors (e.g., see Ref. 69). The attenuation can generally be ignored in the 1-to-10-Gc region for elevation angles of 5 degrees or more. The sky noise they produce is negligible at elevation angles approaching 90^{0}, but it is not negligible at low elevation angles. Sky temperatures ranging from 20^{0}K at 1 Gc to 30^{0}K at 10 Gc have been calculated for the ICAO Standard Atmosphere at an elevation angle of 5 degrees (Ref. 69). Under very humid conditions, the corresponding range could be from 22^{0}K at 1 Gc to about 75^{0}K at 10 Gc (Ref. 70).

With cloud and precipitation particles present in the beam, attenuation becomes significant and the sky temperature increases (Ref. 70). The scattering and absorption due to any assemblage of spherical particles can be worked out from Mie scattering theory. Thus, tropospheric scattering and absorption can be related to rainfall rates and cloud densities through the use of observed drop-size distributions (e.g., see Ref. 71). The results are somewhat complicated by the fact that the complex refractive index of water is a function of frequency in the gigacycle range. In general, the magnitude of the effects increases with frequency.

Results based upon Mie scattering theory are of little value in assessing the impact of cloud and precipitation upon space-to-earth telemetry links until they are combined with statistics on the occurrence of these phenomena. A recent paper by Feldman (Ref. 72) is of particular value in this connection, because the author provides estimates of the probability of given amounts of attenuation and sky noise in various climatic regimes for selected frequencies.

Figure H-1 adapted from Feldman's Fig. 8 (Ref. 72), shows the degradation of the signal-to-noise ratio due to rain for one-way transmission through the troposphere at 4 Gc. The probabilities have been computed for an elevation angle of 10 degrees for a hypothetical site that combines

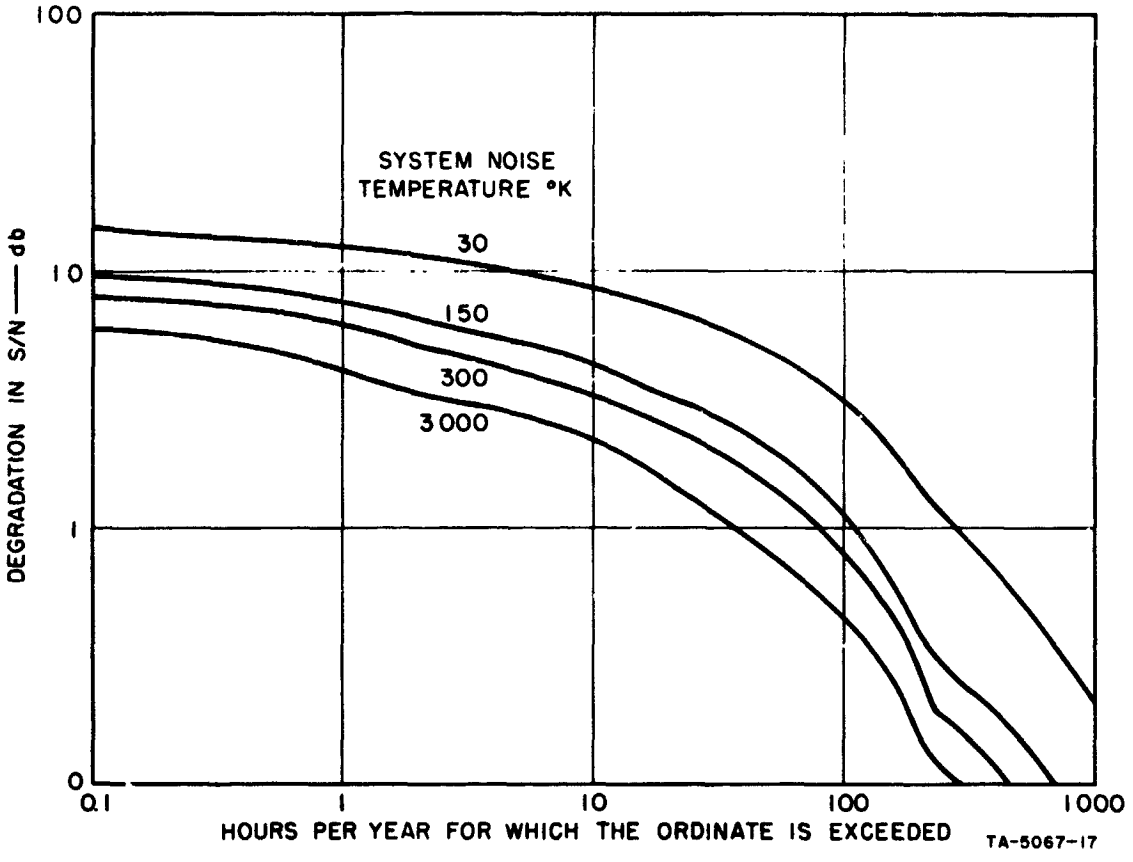

FIG. H-1 ONE-WAY DEGRADATION DUE TO RAIN AT 4 Mc AND 10-DEGREE ELEVATION

the worst features of such locations as Guam (frequent, usually light rainfall), Ceylon (frequent moderate rain), and Tokyo (relatively frequent heavy rains). The degradation is most critical when very sensitive receiver systems are used--i.e., if the receiver is noisy, sky noise becomes relatively unimportant, and only the degradation due to signal attenuation is experienced.

The generalization of Fig. H-1 to other frequencies and elevation angles is not entirely straightforward. However, the effects would certainly be much worse at 10 Gc than at 4 Gc for any assemblage of raindrops in the beam, with the sky noise increased and the attenuation (in decibels) increased by a factor of more than 10. There would be no marked reduction in the peak degradations if the elevation angle were increased, because the degradations are caused by convective storms whose heights and diameters

are comparable. However, the probability of intersecting such a storm would be reduced.

In considering noise for very sensitive receiving systems the question of interference from beyond the horizon should not be completely neglected. In particular the part played by precipitation in scattering energy from otherwise invisible sources may be significant (Refs. 73, 74). In selecting frequencies and/or sites, possible sources of interference over a considerable radius should be identified and the possibility of their causing interference, during times of precipitation, investigated.

The sky noise due to precipitation received in the various antennas of a phased array should not show any phase correlation. Marshall and Hitschfeld (Ref. 75) have considered the signals received at two antennas from randomly positioned scatterers illuminated by a single radar transmitter. Their reasoning regarding relative phases of the signals at the two antennas is applicable to the noise problem, where independent radiators replaced independent scatterers. For practical purposes, the signals received from a given range interval are statistically independent, provided that the antenna apertures do not overlap. In the proposed experiment there would be many situations in which the individual beams would not overlap below the top of the precipitation, and in such cases there could obviously be no phase correlation.

Phase fluctuations arise at the individual antennas of an array as a result of variations in electrical path length, which in turn are related directly to irregularities in radio refractivity along the path. Some treatments of the problem rely on particular models of the spatial correlation structure of the refractivity, or even on such a simple picture as that of discrete "blobs," within which the refractivity is uniform. A much more powerful and flexible approach is that of Wheelon (Ref. 76) who performs a Fourier transformation of the spatial correlation function of the refractivity, and then examines the roles of the various wave-number components in propagation phenomena. Variations in the phase difference between two receivers arise as a result of turbulence spectrum components with wavelengths comparable to or smaller than the

receiver separation. Larger-scale components tend to affect both receivers in the same fashion.

The phase instabilities likely to be met in the proposed experiment are discussed at length in a recent report by Research Triangle Institute (Ref. 1). Experimental data on refractivity fluctuations, obtained by previous authors, is summarized in terms of the variance of ΔN, the departure of N from its mean within a region small enough to be considered homogeneous, and the correlation length and correlation time of ΔN.

Reference 1 includes graphs (Figs. 5-17 and 5-18) from which the standard deviation of the difference in phase between signals recorded at two antennas can be estimated as a function of baseline separation, elevation angle, frequency, and atmospheric conditions. For example, with antennas 300m apart and an elevation angle of 15 degrees, the rms phase difference for a 10-Gc signal from a satellite is estimated to be 0.44 radians under typical fair-weather conditions. However, much of this variability in relative frequency would be contained in frequency components below 0.1 cps (Ref. 13), and so could be overcome by phase-following and phase-adjustment devices.

One point brought out by the experiments in phase stability over line-of-sight paths reported to date is that the high-frequency phase jitter increases markedly when rain falls along the path (Ref. 17). This observation has led us to examine the contributions of liquid water to the refractivity of the atmosphere, contributions that are ignored in the usually quoted formula (Ref.6) but which can be important. Since this is one of the more important findings to come out of the present study, the appropriate theory will be reviewed briefly at this point.

3. Contribution of Liquid Water to Radio Refractivity of the Troposphere

The change in refractivity imposed upon a medium by the presence of scatterers within it has been treated by many authors. Van de Hulst (Ref. 77) has examined the problem with respect to particle separation that is large compared to wavelength and has compared the results with the problem of particle separation that is small compared to the

wavelength (Lorentz-Lorenz scattering). Mason (Ref. 78) has examined radar backscattering from a cloud and has shown the equivalence of the discrete-particle and refractive-index continuum theories of scattering.

It should be noted that the power-spectrum approach to tropospheric refractivity can account for particulate matter without any difficulty. The appearance of spectral components that are related to particle spacing account for any periodicities in particle concentration. If the spacing were completely random, the droplets would contribute "white noise' to the power spectrum of the refractivity (Ref. 76).

Cloud-droplet concentrations vary widely with cloud type and even vary within individual clouds. The order of magnitude of the cloud-water contribution to refractivity can be obtained by assuming a cloud containing 250 droplets per cm^3 of radius 10μ . When this concentration is considered in the light of the wavelengths of interest (3 to 30 cm), the Lorentz-Lorenz results are shown to be applicable. Using rationalized MKS units and the simplifying assumption that $\tilde{m}$, the complex refractive index of the medium (including the scatterers), is near unity, we write

$$\tilde{\epsilon} = \epsilon_o + \frac{\alpha N_o}{V} \quad , \qquad \text{(H-2)}$$

where $\tilde{\epsilon}$ is the complex dielectric constant ($\tilde{m}^2$); ϵ_o is the complex dielectric constant in the absence of the scatterers; α is the polarizability of one scatterer; and (N_o/V) is the concentration of scatterers.

The cloud droplets act like dielectric spheres whose polarizability is given by

$$\alpha = \frac{\pi \epsilon_o}{2} \left(\frac{m^2 - 1}{m^2 + 2} \right) D^3 \qquad \text{(H-3)}$$

where m is the complex refractive index of water and D is the droplet diameter. Combining Eqs. (H-2) and (H-3), we get

$$\epsilon = \epsilon_o \left[1 + \frac{\pi N}{2V} \left(\frac{m^2 - 1}{m^2 + 2} \right) D^3 \right] \quad , \qquad \text{(H-4)}$$

where m is a function of frequency and temperature. The value applicable at 9.4 Gc and 0°C is (7.14 - 2.89 i), where $i = \sqrt{-1}$. Substitution in Eq. (H-4) shows that the real part of $(m^2 - 1)/(m^2 + 2)$ is close to unity and the imaginary part is near 0.03. We therefore estimate for the cloud model described above,

$$\epsilon = \epsilon_o [1 + (6 \times 10^{-6})] \quad .$$

Therefore,

$$\tilde{m} \doteq m_o [1 + (3 \times 10^{-6})] \quad .$$

Recalling that the definition of N, the reduced radio refractivity, is

$$N = (n - 1)10^6$$

and that n is simply the real part of m, the complex refractive index, we see that the cloud water contributes three N-units to the refractivity.

For raindrops, the treatment given on pages 32 to 34 of Ref. 77 appears more appropriate. This yields

$$\tilde{m} = 1 - iS(o) \cdot 2\pi \left(\frac{N_o}{V} \right) k^{-3} \quad , \qquad \text{(H-5)}$$

where S(o) is the amplitude scattering function in the forward direction and k is the wave number. Taking the real part, ($\tilde{m} = n - in'$),

$$n = 1 + 2\pi \left(\frac{N}{V} \right) k^{-3} \, \mathrm{Im}[S(o)] \quad . \qquad \text{(H-6)}$$

For small raindrops we can make

$$S(o) = ik^3\alpha \quad . \tag{H-7}$$

Considering a raindrop of radius 1 mm at 0^oC, we find its polarizability at 9.4 Gc to be

$$\alpha = \frac{\pi\epsilon_o}{2}\left(\frac{m^2 - 1}{m^2 + 2}\right)D^3 = \epsilon_o(0.13 - 0.004i)\,cm^3$$

$$Im[S(o)] = k^3 Im(i\alpha) = d^3(0.13\epsilon_o)\,cm^3 \quad .$$

Assuming a value of 10^{-4} cm^{-3} for (N_o/V), we find that

$$n = 1 + 2\pi(10^{-4})0.13 \doteqdot 1.0001 \quad ,$$

indicating that rain can produce changes in radio refractivity of up to 100 N-units.

Appendix I*

IONOSPHERIC MEASUREMENTS

* This appendix was prepared by J. A. Martin.

BLANK PAGE

Appendix I

IONOSPHERIC MEASUREMENTS

1. Introduction

Descriptions of the ionosphere could involve geophysical, electromagnetic, and optical measurements. Geophysical measurements would reflect upon the processes and particle fluxes that cause the irregular, time-and-space-varying structure in the refractive profile of the medium. Measurements of solar variations and of the earth's geomagnetic field and geomagnetic storms are of primary interest. Electromagnetic studies of ionization properties include radio-star measurements, satellite monitoring experiments, satellite radar sightings, moon echo studies, ionospheric profile soundings, ionospheric scatter measurements, and solar noise measurements. Optical measurements of luminosity include photographs of the aurora and measurement of electron and proton interaction by photometers. Not all types of measurements are required in the proposed experiment.

This investigation is primarily concerned with the crosscorrelation between the variation in an ionospheric parameter--e.g., x--and the variation in the signal character (phase or amplitude) measured in the communication experiment--e.g., y. The correlation function of x and y, R_{xy}, is

$$R_{xy} = \frac{\overline{XY}}{\sqrt{\overline{x^2}\,\overline{y^2}}} \quad \text{for } 0 \leq \text{time, } t \leq T_n \qquad \text{(I-1)}$$

where $\overline{x^2}$ and $\overline{y^2}$ are the variance of x and y and T_n is the time length of data analyzed. Low-frequency fluctuations are limited by finite T_n. High-frequency fluctuation measurements are limited by the sampling interval and by the response characteristics of the receiver and data sampler. Spectral characteristics of X and Y depend upon both T_n and sampling interval.

The correlation data in ionospheric studies is presented in a number of ways:

(1) Threshold designations--when $X > X_o$ during T_n, $Y > Y_o$

(2) Histograms--during N observations of X, M occurrences of Y are recorded

(3) Visual observation of time plots concerning X and Y followed by a written description.

Usually threshold designations are used in histograms. Once threshold values X_o and Y_o are determined, correlation data can be processed automatically. In predicting future activity of Y, phenomena X may be recorded with a variable time lag base.

Radio propagation characteristics through the ionosphere are usually related to frequency, zenith angle, time of day, season of year, year in sunspot cycle, geomagnetic effects, auroral effects, and a variety of disturbed phenomena.

It is intended that ionospheric data and descriptions be of such form as to allow a direct correlation (preferably automatic) with the RF experiment data. The presentations should have a common or relatable time base. The use of ionospheric characteristics as a means of forecasting severe communication signal fluctuation is also considered.

Ionospheric measurements are discussed in Sec. III-I of the main text, following discussions of the proper characterization of the ionosphere and the limitations on measurements due to communication experiment parameters.

2. Characterization of the Ionosphere

Proper characterization of the ionosphere requires description of the ionospheric effects on the character of the line-of-sight signal received in the communications experiment. Fundamental in designing an experiment is the a priori formulation of a suitable model encompassing the objectives and purposes to be accomplished (Ref. 79). Parameters important to the characterization of the ionosphere and to the character of the communication experiment signal are summarized in Table I-1.

Until recently, the irregularity or blob concept appeared adequate to describe the irregular structure of the ionosphere and to explain radio effects. During 1963 Buneman and Farley pointed out independently the possibilities that the ionospheric current system represents a "two-stream" instability described in modern plasma theory (Refs. 80-82).

Other possible energy sources for producing irregularities are listed in Item VI of Table I-1. The exact source of fluctuations is, however, open to speculation, and there is little agreement among authorities. The disagreement naturally reflects experimental and theoretical state-of-the-art limitations. The failure to designate accurately energy sources does not void an ionospheric measurement program. However an unique measurement technique and an useful correlation phenomena may be hidden as a result.

The irregularity concept presented by Hewish (Refs. 83-85), Booker, and others (see bibliography in Ref. 85) takes little account of energy mechanisms except insofar as the required phase shifts could be produced by irregularities in electron density. Most experimental results are described in connection with the irregularity concept. Therefore the irregularity concept will be used in this discussion to describe the parameters important to ionospheric characterization.

In terms of the communications experiment, the ionosphere is simply characterized by an anisotropic, heterogeneous blob or irregular structure separated into one or more scattering domains. Each blob ℓ_o in the structure has a spatial extent (spatial correlation) measured by an arbitrary per unit variation in electron density $\Delta N_e/N_e$. Each blob in the structure moves with a velocity V_o associated with the drifts and wave pattern of energy processes or with the turbulence velocity of the plasma gas molecules. Forward scattering is assumed to be the wave propagation mechanism, although diffraction theory can be used to explain identical results for thin scattering layers.

In general, the domain of an irregular, scattering ionospheric layer is occupied by numerous sets of blobs. Each set has a characteristic blob length (or blob configuration). Considering only small

Table I-1

PARAMETERS IMPORTANT TO THE CHARACTERIZATION OF THE IONOSPHERE

I. Description of Irregular Structure

- A. Scattering domains
  1. Number
  2. Statistical blob structure in each domain (time and space)
  3. Scattering mechanism in each domain (single or multiple scattering)
  4. Extent of each domain
  5. Orientation of the scatterers in each domain (relative to receiver-transmitter path, and earth's geomagnetic field)
  6. Relative level of scattering from each domain
  7. Direction and magnitude of blob motion
- B. Acoustic plasma waves
- C. Other models

II. Earth's Geomagnetic Field

- A. Variations (time and space)
- B. Orientation relative to transmitter, receiver, and the scatterers in each scattering domain

III. Solar Time

- A. Time of day
- B. Month, season, year
- C. Sunspot cycle

IV. Transmitting and Receiving Configurations

- A. Orientation relative to earth's geomagnetic field and the scatterers in each scattering domain
- B. Ranges between transmitter and receiver, transmitter and each scattering domain, and receiver and each scattering domain
- C. Direction and magnitude of transmitter and receiver motion
- D. Antenna directivity
- E. Receiver data processing

V. Disturbed Phenomena

- A. Geomagnetic storms: longitudinal and remainder components; sudden commencement; initial, main, and recovery phases
- B. Solar variations: solar energy, solar flares, cosmic noise
- C. Aurora: visible glow, polar components, temperate components, correlations with geomagnetic storms and solar variations
- D. Ionospheric storms: longitudinal and remainder components, changes in critical frequency, sporadic-E, spread-F, correlations with geomagnetic storms and solar variations

VI. Energy Sources

- A. Extraterrestrial particles
- B. Currents in the dynamo region
- C. Magneto-hydrodynamic waves
- D. Aligned ionization
- E. Vertical instability
- F. Leakage from the radiation belt.

fluctuation levels where single scattering applies, the standard deviation in fluctuation rate is predicted to be 0.13 V_o/ℓ_o to 0.22 V_o/ℓ_o. It is usually assumed that the velocity V_o is unique to a blob set. However, this assumption is not required and has not been experimentally verified. Fluctuation rates tend to increase when fluctuation level is large and multiple scattering mechanisms exist. The fluctuation rates are sensed by the receiving structure in a direction determined by the blob motion and by transmitter-receiver motion.

Important to the design of ionospheric experiments is the character of line-of-sight signal fluctuation due to the ionosphere. Models of the signal fluctuation character, though not exact, provide an insight into important characteristics of the ionosphere to be measured and important parameters relevant to the design of the experimental configuration. Table I-2, along with Fig. I-1, gives models of the variance in phase $\overline{\Delta\alpha^2}$ and in amplitude $\overline{\Delta A^2}/\overline{A^2}$.

The zone function $F(\eta)$ in Table I-2 (Fresnel zone - $\eta \to \infty$ and Fraunhofer zone - $\eta \to 0$) was obtained from work by Chernov (Ref. 86) and de Wolf (Ref. 87). Formulation of scattering cross section and integration of the scattering cross section over the scattering domain was based on work by Booker and Gordon (Ref. 88) and Muchmore and Wheelon (Ref. 89). While the actual signal character may differ from the idealized models (formulas in Table I-2 refer to one blob set and one scattering domain), the important ionospheric characteristics and experimental parameters are nevertheless indicated.

In the Fraunhofer zone [$F(\eta) \to 0$ as $\eta \to 0$], the phase and amplitude fluctuations are identical. In the Fresnel zone [$F(\eta) \to 1 - 1/3\eta^2$; as $\eta \to \infty$], amplitude fluctuations are weak and approach zero as $\ell_\perp^2/\lambda \to \infty$ $\left[\text{i.e., } \Delta A^2/A^2 \approx 0.135\left(\lambda^2 R_s^2/\ell_\perp^4\right)\right]$. Phase fluctuations seem to vary no more than a factor of two between the Fresnel and Fraunhofer zones.

The beamwidth function $F(\beta)$ is a measure of aperture smoothing at the receiving antenna. The beam-coupling function approaches $|\Omega_s/\Omega_a|$ for broad-beam receiving antennas. The function $F(\beta)$ approaches zero

Table I-2

SIGNAL FLUCTUATION CHARACTER FOR LINE-OF-SIGHT PROPAGATION THROUGH AN IONOSPHERIC LAYER

PHASE FLUCTUATIONS:

$$\overline{\Delta\alpha^2} = 2\pi^{3/2}\left(\frac{\overline{\Delta N_e^2}}{\overline{N_e^2}}\right)\frac{\lambda^2}{\lambda_N^4} R_S \varphi_o \ell_{||} [1 + F(\eta)]F(\beta)$$

AMPLITUDE FLUCTUATIONS:

$$\frac{\overline{\Delta A^2}}{A^2} = 2\pi^{3/2}\left(\frac{\overline{\Delta N_e^2}}{\overline{N_e^2}}\right)\frac{\lambda^2}{\lambda_N^4} R_S \varphi_o \ell_{||} [1 - F(\eta)]F(\beta)$$

$$F(\eta) = \eta \arctan\left[\frac{\pi R_S^2}{R(R + R_S) + \pi R_S^2}\right]$$

$$\eta = \frac{\pi}{2}\frac{\ell_\perp^2}{\lambda R_S}$$

$$F(\beta) = \left|\frac{\Omega_S}{\Omega_o}\right|\left[1 - \exp\left(-\frac{4\pi^2}{\lambda^2}\frac{T^2 L^2}{\ell_\perp^2}\sin^2\frac{\beta}{2}\right)\right]$$

$\overline{\Delta N_e^2}/\overline{N_e^2}$ = Variance of $\Delta N_e/N_e$ (per unit variation in electron density)

λ_N = Plasma critical wavelength

λ = Wavelength

R_S = Width of the scattering ionospheric layer along the line of sight

R = Range from the receiver to the bottom of layer R_S (or an average range through R_S), a function of altitude h_S and elevation angle E

$\left|\frac{\Omega_S}{\Omega_a}\right|$, $10\varphi_o$, β, L, T, $\ell_\perp$, and $\ell_{||}$ are defined in Fig. I-1.

Important assumptions are:

1. Single scattering
2. Gaussian correlation of $\Delta N_e/N_e$
3. $L \ll R_S$; $T > \lambda$
4. ψ is constant in scattering volume
5. Fluctuation level $\propto \int_V \sigma dV$, where σ is the scattering cross section in the scattering volume V
6. Receiver-to-blob range can be represented by an average range R
7. Transmitter is far enough above the ionospheric layer so that plane-wave conditions exist
8. Earth curvature effects are neglected.

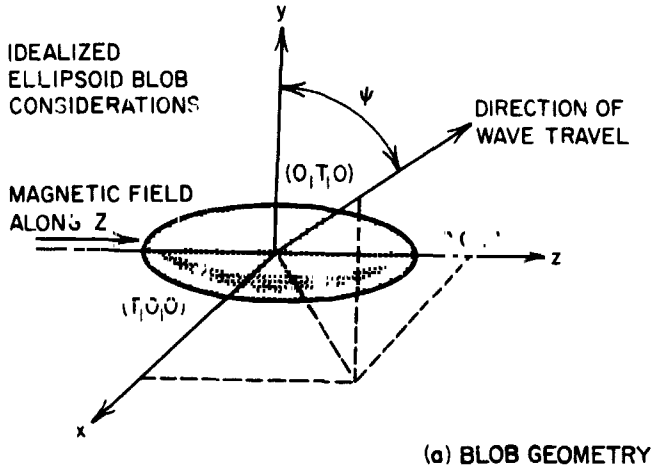

$\ell_{\parallel}$ –blob extent along the line of sight

$$\ell_{\parallel} = \frac{LT}{(T^2 \sin^2\psi + L^2 \cos^2\psi)^{1/2}}$$

$\ell_{\perp}$ –blob extent transverse to the line of sight

$$\ell_{\perp} = \frac{LT}{(T^2 \cos^2\psi + L^2 \sin^2\psi)^{1/2}}$$

(a) BLOB GEOMETRY

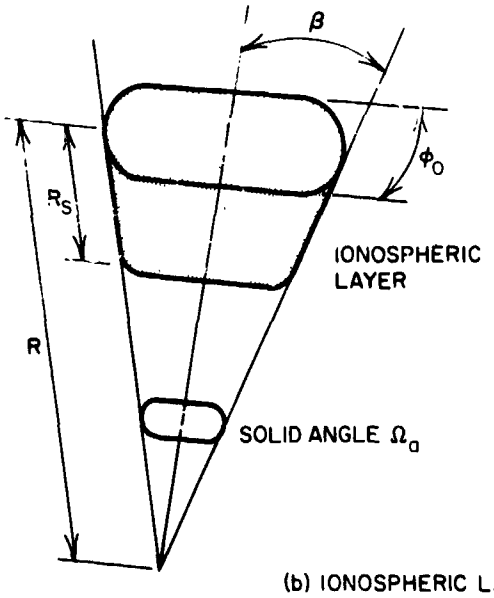

β, ϕ_0 define the beam of the receiving antenna

$\left|\frac{\Omega_s}{\Omega_a}\right|$ = beam coupling function

$\left|\frac{\Omega_s}{\Omega_a}\right| \equiv 1$ if $\Omega_s > \Omega_a$

where Ω_s is the larger of the solid angle extended from the scattering domain to the receiver and the solid angle defined by the satellite transmitting antenna.

(b) IONOSPHERIC LAYER GEOMETRY

TB-5067-41

FIG. I-1 GEOMETRIC CONSIDERATIONS OF SIGNAL FLUCTUATION CHARACTER FOR LINE-OF-SIGHT PROPAGATION THROUGH AN IONOSPHERIC LAYER

for narrow-beam antennas and when T and/or L becomes comparable to and less than d, the receiving aperture width--i.e.,

$$F(\beta) \approx \left|\frac{\Omega_s}{\Omega_a}\right| \pi^2 \left(\frac{\ell}{d}\right)^2 < \left|\frac{\Omega_s}{\Omega_a}\right| ,$$

provided $\ell \ll d$. The beam-coupling function $|\Omega_s/\Omega_a|$ is usually unity for narrow-beam receiving antennas when transmitter coupling is maximum and the scattering domain is extended.

Order-of-magnitude estimates of the scattering zones and scattering mechanisms in the E and F regions of the ionosphere are illustrated in Figs. I-2 and I-3. The $\ell_{||}2/\ell_{\perp}^2 \times \eta$ and $\overline{\Delta\alpha^2}$ levels are subjective and may differ from actual measurements. For example, E-region fluctuation level $\overline{\Delta\alpha^2} \approx 1$ may occur at a higher frequency during aurora.

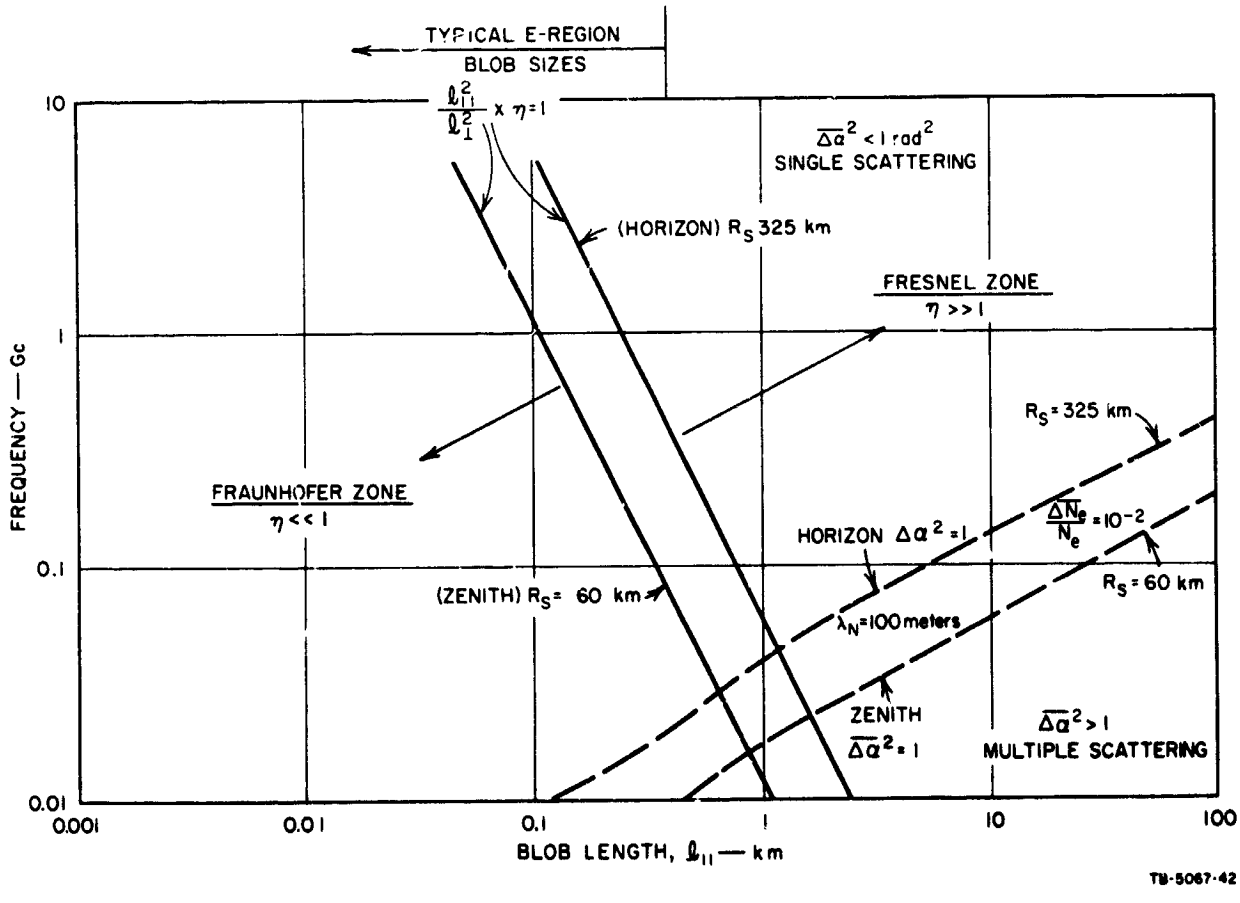

FIG. I-2 PROPAGATION ZONES FOR E-REGION BLOB STRUCTURE

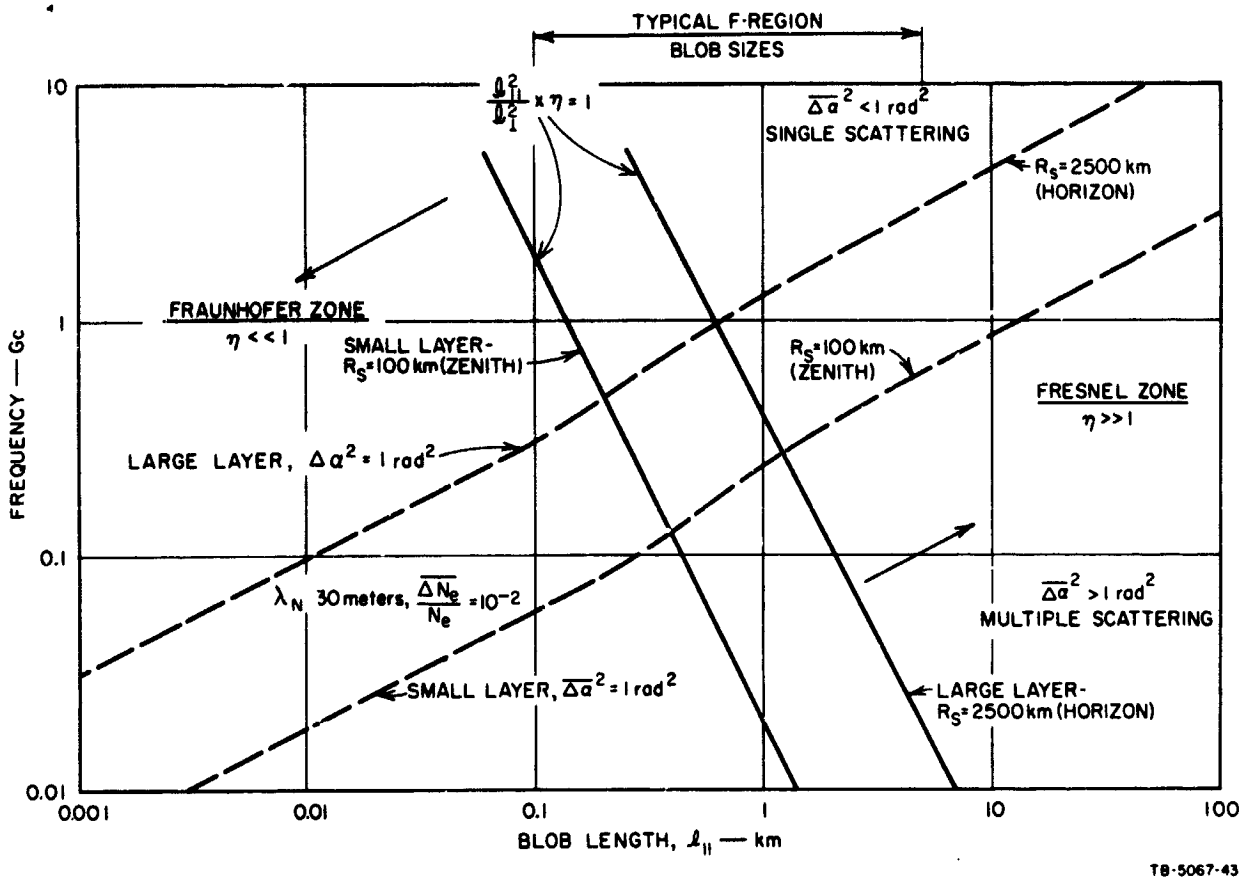

FIG. I-3 PROPAGATION ZONES FOR F-REGION BLOB STRUCTURE

In these figures, the solid lines are the boundaries, $\ell_{||}^2/\ell_\perp^2\eta = 1$, between the Fraunhofer scattering zone on the left and the Fresnel scattering zone on the right. For small elevation angles, the scattering layers are larger and therefore the corresponding boundary lies to the right of that for large elevation angles. The dashed lines are the boundaries, $\overline{\Delta\alpha^2} = 1$ rad^2, between the single-scattering region, $\overline{\Delta\alpha^2} < 1$ rad^2, and the multiple-scattering region.

The Fresnel zone predominates when propagation is transverse to the magnetic field (polar satellites, $\ell_{||}/_\perp\ell = T/L \lesssim 1$). Forward scattering is aspect-sensitive for transverse propagation and large blobs where the scattered signal is concentrated in a forward cone angle $\gamma/2\pi\ell_\perp \approx \gamma/2\pi L$. The fluctuation level, however, may be low if the scattering domain is discrete and elongated along the magnetic field. The fluctuation level will be larger (assuming equal blob sizes) for a

diffuse scattering domain elongated transverse to the magnetic field. Phase fluctuations are relatively insensitive to magnetic aspect angle ψ for near-transverse propagation where L cos ψ >> T sin ψ. However, amplitude fluctuations are seen to be very sensitive to ψ, being inversely proportional to ℓ_l^4.

When $\overline{\Delta\alpha^2} > 1$, multiple scattering exists and the fluctuation character is usually described by a Rayleigh probability distribution. Multiple scattering is characterized by large, unpredictable fluctuation levels and by fluctuation rates that may exceed the fluctuation rates associated with single scattering. Frequency scaling of fluctuation levels either ceases to exist or is very poor during multiple scattering.

It should be remembered that the total fluctuation level may be composed of contributions from several scattering domains. The variance of fluctuation level, at a given fluctuation frequency, for example, is expressed as

$$\overline{\Delta\alpha^2} = \sum_{s=1}^{N} \sum_{i,j=1}^{M_s} \Delta\alpha_{is}\Delta\alpha_{js} \qquad \text{(I-2)}$$

where M_s is the number of blob sets in the sth scattering domain and N is the number of scattering domains. The concept of Eq. (I-2) is important in that a number of scattering domains spread in range and containing a number of blob sets spread in size may be important to signal fluctuation character. Thus correlations of an ionospheric phenomenon with one domain and/or one blob set may be low in terms of composite signal fluctuation character determined by a multiplicity of domains and sets. The possible correlation between blob sets and scattering domains is implied in Eq. (I-2).

While irregular structure in the ionosphere may exist in all sizes, minimum bounds exist for those blob sizes important to electromagnetic wave propagation. The minimum bounds can be predicted by considering

the charged electrons and ions in the ionosphere. Along the magnetic field, the mean free path represents the minimum scale of electromagnetic irregularities. Typical electron mean free paths ℓ_e in the ionosphere are:

E-Region--80 km altitude, $\ell_e \approx$ 10 meters
140 km altitude, $\ell_e \approx$ 100 meters
F-Region--200 to 700 km altitude, $\ell_e \approx$ 0.5 to 2 km
1000 km altitude, $\ell_e \approx$ 10 km.

The scale of ionic irregularities is a factor of $4\sqrt{2}$ less than ℓ_e. Transverse to the magnetic field the minimum scale of irregularities approaches the minimum logitudinal scale. In the F-region, the minimum transverse scales are defined by the gyroradius of ions and electrons, $\approx 10^{-2}$ meters (electrons) and ≈ 5 meters (ions).

Blob anisotropy in the F-region, L/T, is often quoted as 5 to 1 for large blobs. In the E-region, anisotropy exceeding 10 to 30 is often quoted. These ratios naturally reflect resolution limitations and averaging processes.

The velocity of blobs is important to the spectrum of signal fluctuation character. A blob will contribute to a fluctuation frequency f_o, only if $f_o \ll V_o/\ell_o$. The inverse ratio ℓ_o/V_o is the correlation time, the time after which blobs of size ℓ_o in the structure are assumed to be capable of change. Velocities in the E-region will vary from a few meters per sec to $\approx$ 200 meters/sec. In aurora, velocities of 500 meters/sec have been measured. Ionospheric tides in the F-region have been observed at night to vary from 100 m/sec to 1 km/sec. These velocities are characteristic of the blob structure. The relative velocity of the line of sight along which the radio signal is transmitted can be larger than V_o (as in the case of satellite transmitters) and can predominate in determining the fluctuation frequency f_o.

The earth's magnetic field is believed to influence the translational velocity of blobs in the scattering domains. All observers of radio star scintillation report that the component of drift in the

north-south direction is small. Measurements indicate that drift is principally in the east-west direction (Ref. 85). The sense of direction has been observed to change from east-to-west before midnight to west-to-east after midnight (Ref. 90). These velocity signatures may, however, be masked in the proposed experiment due to the motion of the transmitter.

3. Limitations of the Communication Experiment

The measurement of pertinent ionospheric characteristics is limited by the design of the experiment. Of particular interest is the RF frequency, the transmitter and receiver orientation, the transmitter and receiver antenna directivities, and signal-processing parameters.

Frequencies of 2,4,8, and 16 Gc have been proposed for the communications experiment. Since ionospheric fluctuations become less effective with increasing frequency (and probably are completely negligible above 6 Gc in comparison to tropospheric fluctuations), the design of ionospheric experiments should be modeled to correlate with the character of the lowest communication frequency, 2 Gc.

A fundamental limitation of the communication experiment is that the spectral content of the measured amplitude and phase fluctuations is the result of two effects (Refs. 91-93). The first is the time fluctuation induced by the time variations inherent in the blobs in the scattering domains as seen in a coordinate system moving with the satellite-earth relative velocity. The second is Doppler shifting produced by the convection of the scattering structure by the satellite-earth relative velocity. These two effects are not readily separable. Thus the use of spectra data measured in the communication experiment to predict spectral characteristics for other transmitter-receiver configurations of differing satellite-earth relative velocity may be gross rather than detailed in description.

The relative orientation of the transmitting satellite, the receiving earth antenna, and the geomagnetic field is important. This is illustrated in Fig. I-4 for a typical overhead polar orbit over Oklahoma City (proposed site for experimental facilities). The magnetic aspect

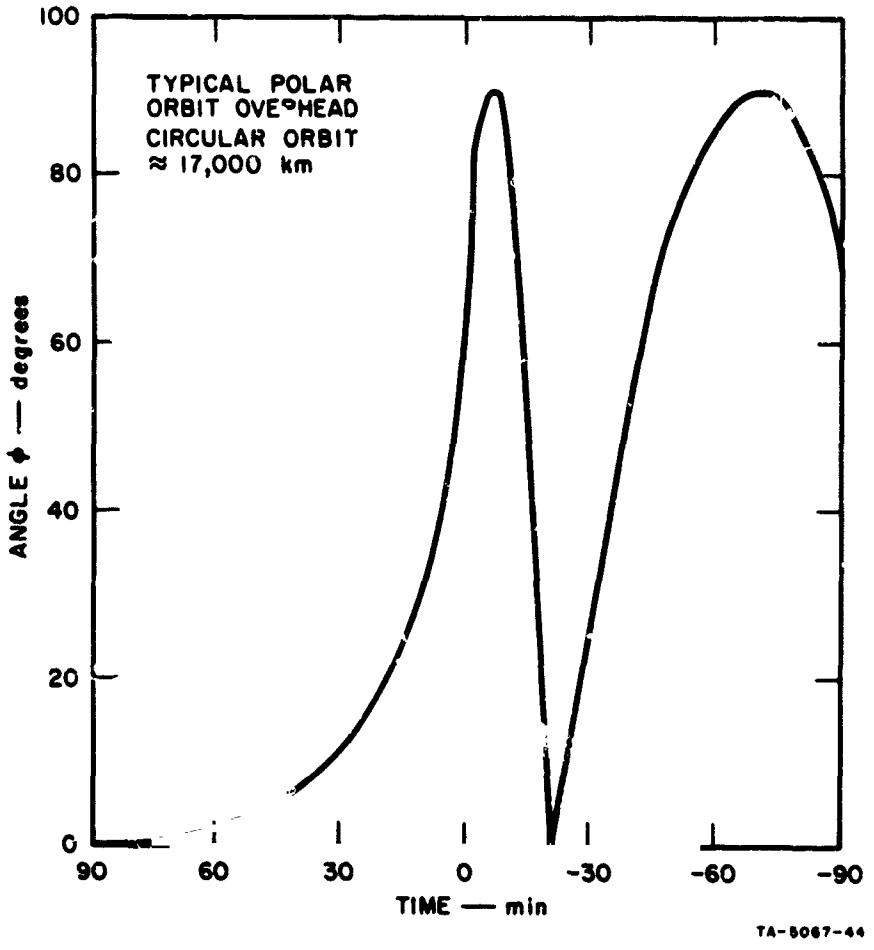

FIG. I-4 TRAJECTORY PROFILE FOR PREDICTING MAGNETIC ASPECT ANGLE
Typical polar circular orbit overhead, altitude ≈ 17,000 km

angle ψ is shown in Fig. I-1(a), (ψ is assumed to be constant in scattering domain). The angle ψ is seen to be asymmetrical during the viewing period. It is significant that, for a large part of the viewing time, transverse propagation predominates in the northern directions. It is expected that the geometry of any ionospheric experiments will have to be compared with the geometry of the communications experiment if useful correlations are to be expected.

While the effect of antenna directivity on signal level is recognized, other basic limitations are imposed by the receiving and transmitting antenna size. The receiving antenna diameter (4 meters) is an indication of the minimum blob size measured. The receiving antenna beamwidth specifies the portion of the ionosphere where high correlation

can be expected between ionospheric characteristics and RF signal characteristics. The beamwidth for a 4-meter antenna operating at 2 Gc is $\approx$ 52 mr. The beamwidth of a satellite transmitting antenna illuminating the earth at minimum proposed satellite altitudes is larger, $\gtrsim 21^{\circ}$. Thus it is expected that the beamwidth of the transmitting antenna will be sufficiently broad to allow maximum coupling between the scattering domains and the receiving aperture.

Signal-processing parameters are also important in regard to ionospheric characteristics. The high-frequency cutoff of 100 cps in the receiving system sets a lower bound on measurable blob fluctuations. Signals are to be processed for a period of 6 minutes at low spectral frequencies and $\approx$ 1 minute at high spectral frequencies. Ionospheric characteristics averaged over equivalent periods should be used in direct correlations. It is, however, conceded that data extrapolation and averaging of a number of power spectrum plots will allow evaluation of longer-term effects. Thus ionospheric characteristics of longer time constant, such as hourly, diurnal, and seasonal values, may be useful for correlation.

Correlation of small-scale blob structure with large-scale phenomena should be made with caution; and correlations may not be possible. Perhaps an indication of only small blob activity can be expected.

4. Ionospheric Measurements

a. Line-of-Sight-Signal Character at Frequencies Below 2 Gc

1) Frequency Scaling

A direct way to characterize the ionosphere at 2 Gc and above is to monitor its behavior concurrently at frequencies below 2 Gc. The signal source for such a monitoring facility would best be located on the satellite used in the experiment.

The ratio of phase fluctuation character at two different wavelengths is found from Table I-1 to be:

$$\frac{\overline{\Delta\alpha_1^2}}{\overline{\Delta\alpha_2^2}} = \frac{\lambda_1^2\varphi_1[1 + F(\eta_1)]F(\beta_1)}{\lambda_2^2\varphi_2[1 + F(\eta_2)]F(\beta_2)} \qquad \text{(I-3)}$$

provided $\overline{\Delta\alpha^2} \lesssim 1$ (single scattering). This ratio is independent of the Fresnel and Fraunhofer zone factor $[1 + F(\eta)]$ to a factor of two. The factor $F(\beta)$ can be assumed to be $|\Omega_s/\Omega_a|$ for practical applications where small blob sizes are filtered out by the receiving aperture. Usually φ_1 and φ_2 can be assumed equal to π and the phase ratio becomes

$$\frac{\overline{\Delta\alpha_1^2}}{\overline{\Delta\alpha_2^2}} = \frac{\lambda_1^2}{\lambda_2^2} \left| \frac{\Omega_s}{\Omega_{a1}} \right| \left| \frac{\Omega_{a2}}{\Omega_s} \right| \frac{\theta_1}{\theta_2} \quad . \qquad \text{(I-4)}$$

If the scattering domain does not exceed the receiving antenna beam coupling, the beam coupling functions become Ω_s/β^2 (circular beam, $\theta = \pi$ and $\Omega_a = \beta^2$) and

$$\frac{\overline{\Delta\alpha_1^2}}{\overline{\Delta\alpha_2^2}} = \frac{\lambda_1^2}{\lambda_2^2} \frac{\beta_2^2}{\beta_1^2} \quad . \qquad \text{(I-5)}$$

If ground effects on antenna patterns at λ_1 and λ_2 differ, the ratio β_2^2/β_1^2 is modified to include vertical and horizontal beamwidths--i.e., $\beta_{2v}\beta_{2h}/\beta_{1v}\beta_{1h}$, and φ_1 and φ_2 may differ. The phase ratio is then

$$\frac{\overline{\Delta\alpha_1^2}}{\overline{\Delta\alpha_2^2}} = \frac{\lambda_1^2\beta_{2v}\beta_{2h}\varphi_1}{\lambda_2^2\beta_{1v}\beta_{1h}\varphi_2} \quad . \qquad \text{(I-6)}$$

Equations (I-5) and (I-6) assume Ω_s is completely within the beamwidths of both receiving antennas. For extended scattering domains, the phase ratio is dependent on λ_1^2/λ_2^2 and perhaps φ_1/φ_2 (as $|\Omega_s/\Omega_a| \cong 1$ when $\Omega_s > \Omega_a$).

When both β_1 and β_2 are narrow beams, $\Omega_s < \Omega_a$, and $\varphi_1 = \varphi_2$, the phase fluctuation ratio is independent of wavelength and is proportional to the areas of the two antennas A_1/A_2.

The preceding statements assume that for practical purposes, the geometry factors relevant to the magnetic field are equivalent (for example, $\psi_1 \approx \psi_2$). If the geometry factors differ, the ratio will be a function of ψ_1 and ψ_2. It is also assumed that the wave paths through the scattering domain are equal (refractive variation between λ_1 and λ_2 are negligible). The wavelength dependence of $\overline{\Delta\alpha_1^2}/\overline{\Delta\alpha_2^2}$ may differ if refractive differences are sufficiently large and if multiple scattering exists ($\overline{\Delta\alpha^2} > 1$).

Scaling of phase fluctuation levels involves a maximum wavelength λ_2 below which multiple scattering effects can appear. Results from Project Wideband, where radio star fluctuation was measured through the auroral ionosphere, indicate that $\Delta\alpha^2 \approx \lambda^2$ (meters).[61] Thus a good choice of λ_2 would be 1 meter (f_2 = 300 Mc). With λ_2 designated, an upper limit on $\overline{\Delta\alpha_1^2}$ corresponding to single scattering at λ_2 is

$$\overline{\Delta\alpha_1^2}\ (\text{single scattering}) \lesssim \frac{\lambda_1^2}{\lambda_2^2} \approx \lambda_1^2 \qquad \text{(I-7)}$$

where extended scattering domains and/or broad-beam antennas are assumed. Thus at λ_1 = 0.15 meters (2 Gc) meaningful phase fluctuations scaled from λ_2 = 1 (300 Mc) would be roughly 10 degrees. If λ_2 is decreased, the upper limit on $\overline{\Delta\alpha_1^2}$ would increase with λ_1 fixed.

The ratio of amplitude fluctuation at two different wavelengths is:

$$\frac{\overline{\Delta A^2}}{\overline{A^2}} = \frac{\lambda_1^2}{\lambda_2^2} \left| \frac{\Omega_s}{\Omega_{a1}} \right|\left| \frac{\Omega_{a2}}{\Omega_s} \right| \left| \frac{\varphi_1}{\varphi_2} \right| \quad \text{(Fraunhofer zone scattering at } \lambda_1 \text{ and } \lambda_2\text{)} \tag{I-8}$$

$$\frac{\overline{\Delta A^2}}{\overline{A^2}} = \frac{\lambda_1^4}{\lambda_2^4} \left| \frac{\Omega_s}{\Omega_{a1}} \right|\left| \frac{\Omega_{a2}}{\Omega_s} \right| \left| \frac{\varphi_1}{\varphi_2} \right| \quad \text{(Fresnal zone scattering at } \lambda_1 \text{ and } \lambda_2\text{)} \; . \tag{I-9}$$

Ideally ground effects and beam-coupling effects cancel and the amplitude ratio varies between the square and fourth-powers of wavelength.

Under conditions where propagation mechanisms can be described by geometrical optics theory and by single scattering, the critical length defined by the crossover between ray theory and scattering theory allows the standard deviation of amplitude fluctuations to be scaled in frequency--i.e.,

$$\text{Standard deviation of amplitude fluctuations} \approx \frac{V_o}{\sqrt{R_s \lambda}} \text{ cps} \; . \tag{I-10}$$

The geometrical optics conditions require that $R_s < \ell_o^2/\lambda$. Thus scaling in the above manner is restricted to large blobs, small wavelengths, and thin scattering layers. If geometrical optics applies, the standard deviations at two frequencies scale as λ_1/λ_2.

2) Correlation

It is of interest to predict the correlations expected between signal fluctuation character measured at spaced frequencies. A theoretical measure of correlation is given in Fig. I-5. There is no effect of changing frequency in the extreme Fresnel limit as $\eta_2 \to \infty$. Correlation decreases for a given blob size when the frequency ratio f_1/f_2 and the

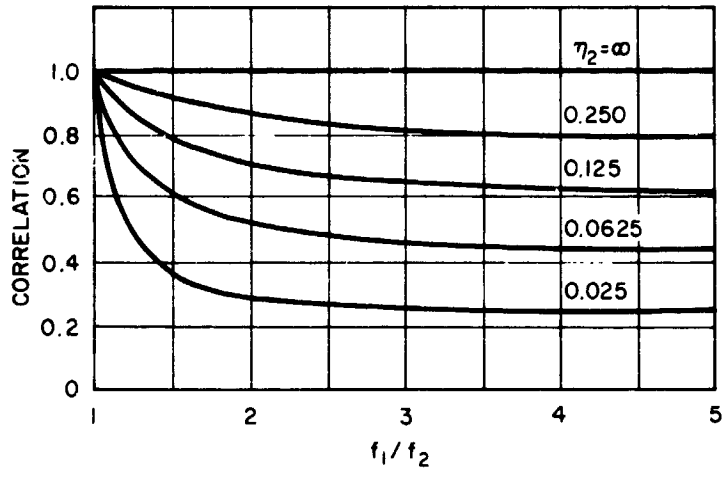

(a) PHASE CORRELATION

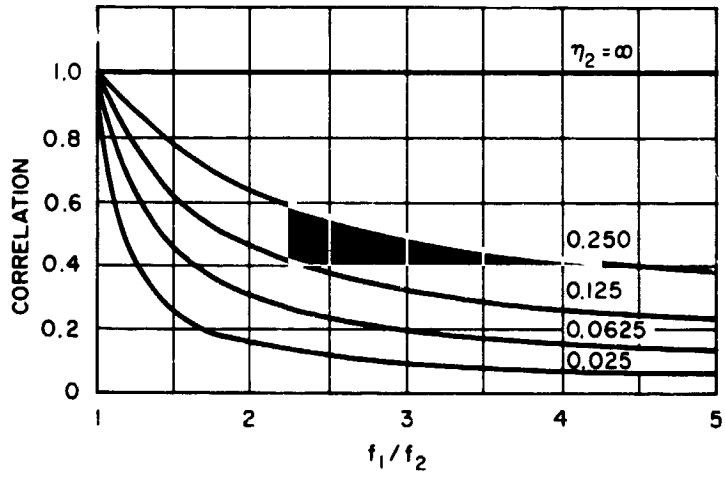

(b) AMPLITUDE CORRELATION

NOTE: $\eta_2 = \frac{\pi}{2} \frac{\ell_1^2}{\lambda R_s}$ and is a measure of whether one is in the near or far zone of blob scattering $\eta \to 0$ far zone, $\eta \to \infty$ near zone.

SOURCE: Ref. 95

TB-5067-45

FIG. I-5 CORRELATION OF SIGNAL FLUCTUATION CHARACTER AT SPACE FREQUENCIES

lower frequency f_2 decrease, and the scattering domain width R_s increases. Phase correlation is greater than amplitude correlation for a given η_2. Correlation ceases for turbulent, small blobs in the Fraunhofer limit where $\overline{\Delta\alpha^2} \approx \overline{\Delta A^2}/A^2$ as $\eta_1 \to 0$.

A theoretical measure of correlation between amplitude and phase fluctuations at a single frequency is given in Fig. I-6. Maximum correlation is ≈ 0.6. It is apparent that correlation between amplitude and phase is largest in the range of $0.1 \lesssim \eta \leq 10$ between the Fresnel and Fraunhofer limits. The low correlation in the Fresnel zone can be expected, in that amplitude fluctuations in the Fresnel zone are controlled by higher moments of the blob structure (Ref. 94) and may depend more strongly upon the range R (Ref. 35).

If phase correlation at spaced frequencies is to exceed 0.5, the value η_2 should exceed 0.1 and the product $\ell_\perp f_2$ should exceed $0.138\sqrt{R_s}$:

$$R_s = 100 \text{ km for small layers}$$
$$\ell_\perp f_1 \gtrsim 44$$
$$R_s = 1000 \text{ km for large layers}$$
$$\ell_\perp f_1 \gtrsim 138.$$

Thus for $f_2 \approx 100$ Mc (a possible beacon frequency for the satellite), correlation can be expected for blob sizes exceeding ≈ 440 meters for small layers and 1.4 kilometers for large layers. If f_2 is increased to 700 Mc, correlated blob sizes are greater than ≈ 60 meters (small layers) and ≈ 200 meters (large layers). Thus it is unlikely that correlation in the small eddy structure in the E-region will be measured using spaced frequencies.

Amplitude correlation at spaced frequencies for $\eta_2 = 0.1$ is predicted as 0.3 (e.g., f_1/f_2 = 2000 Mc/700 Mc). The factor of 3 (or less) separation in frequency for correlated measurements appears to be verified by radio star measurements.

The lower frequency f_2 is limited by multiple scattering when $\overline{\Delta\alpha^2} > 1$. Based upon Project Wideband data, f_2 is roughly 300 Mc. Thus

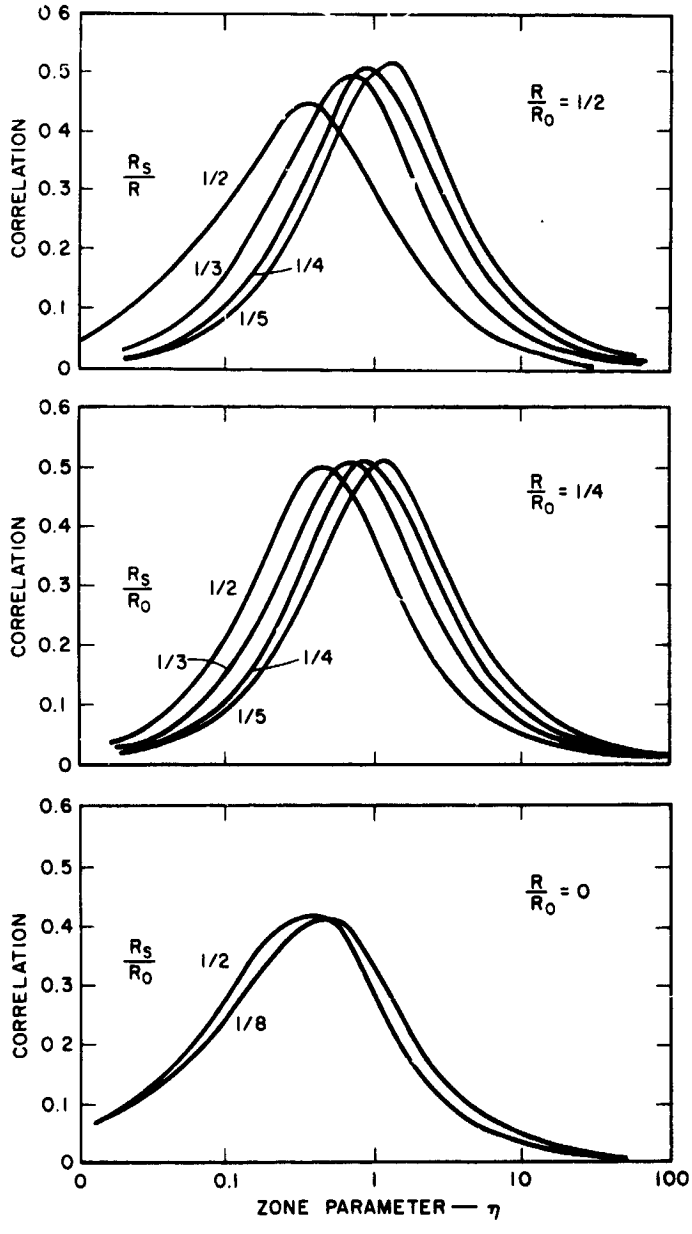

SOURCE: Ref 96

TB-5067-46

FIG. I-6 CORRELATION BETWEEN AMPLITUDE AND PHASE FLUCTUATION DATA

R_0 = Receiver-to-transmitter range

R = Range from receiver to scattering layer

R_s = Width of scattering layer

at frequencies below 300 Mc, multiple scattering effects can be expected and correlations will be poor. The effect of multiple scattering below 300 Mc on the fluctuation character spectra is illustrated in Fig. I-7 from published radio star data measured at 50 Mc and 200 Mc. The fluctuations are somewhat slower than what is expected in the communications experiment, and filtering limitations should be noted. However, the difficulty of correlating multiple scattering data is shown. Also illustrated in Fig. I-7 is the prediction of the fluctuation spectrum at a given time from a power spectrum measured 40 minutes earlier. Only the lower frequency components of the phase records appear to be predictable.

Measurement of ionospheric phenomena at HF and VHF has been shown to be complicated by multiple scattering mechanisms that result in poor correlation even within the HF and VHF bands as well as with higher frequencies where single scattering occurs. Measurements at HF and possibly VHF are further complicated by refraction, which is not simply related to multiple scattering. Order-of-magnitude frequency scaling of large signal character variations measured at HF and VHF does not necessarily indicate a serious disturbance at microwave frequencies. Single scattering measured at HF and VHF will probably not be significant at 2 Gc. Thus correlation measurements at HF and VHF should be viewed with caution.

3) Typical Monitoring Installations

It is proposed that telemetry signals on the satellite be measured. An alternative is to add a UHF frequency ($\approx$ 700 Mc) to the communication experiment. Typical telemetry parameters for 100-Mc and 700-Mc signals are compared in Table I-3 to parameters assumed for the communications experiment at 2000 Mc. Equal beam applications are preferred for similar coupling to the scattering regions.

The maximum power capability on the satellite limits high phase accuracy with broadbeam antennas. An equal beam application at 100 Mc requiring an 80-meter antenna installation is probably out of the question because of cost. The 700 Mc equal beam application is interesting as antenna sizes of 8 meter, 16 meter, and 32 meter have been proposed

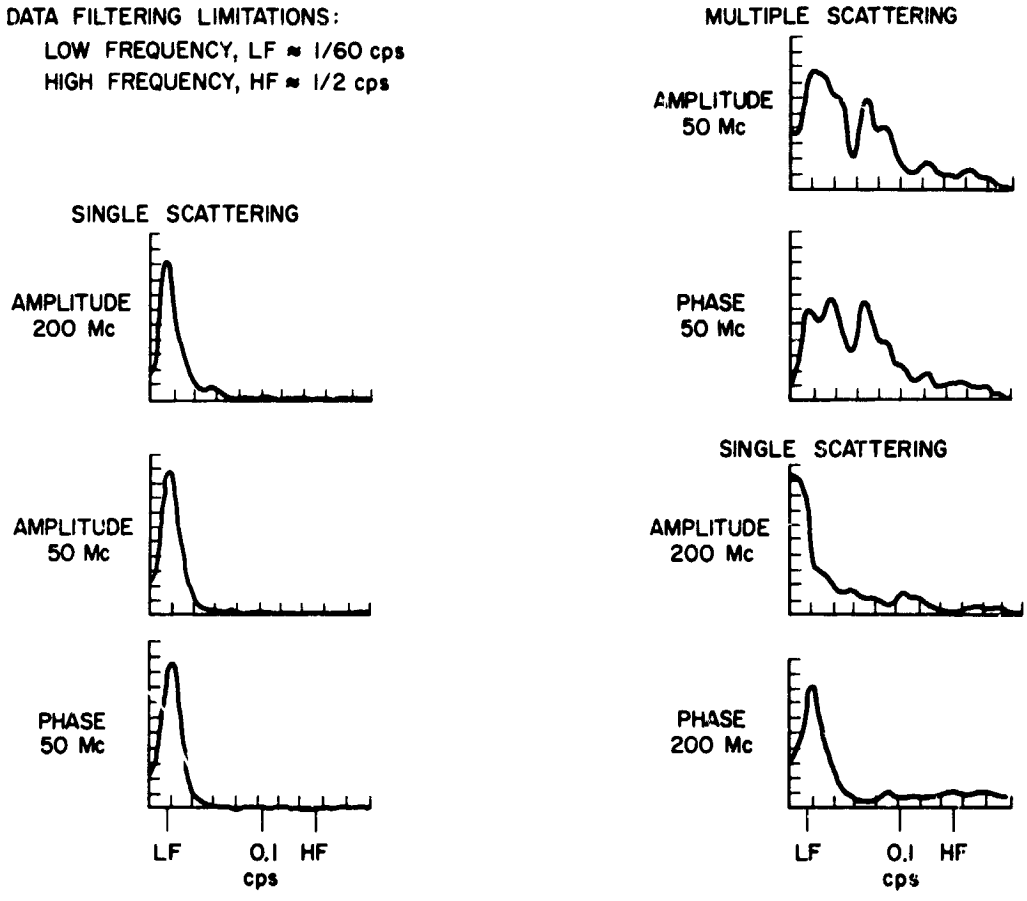

(a) COMPARISON OF SINGLE AND MULTIPLE SCATTERING

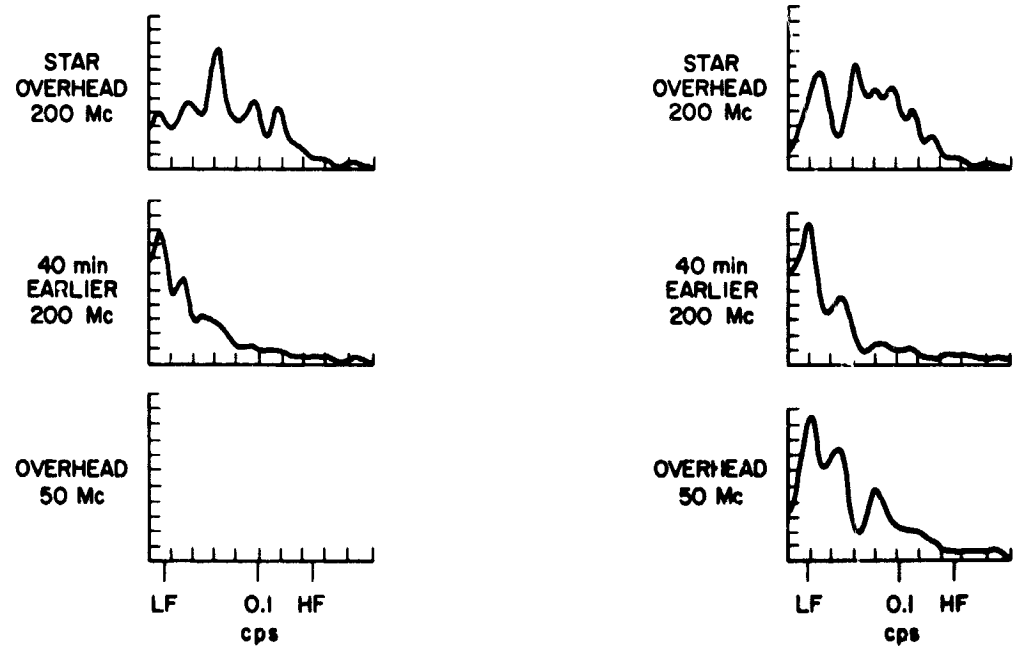

(b) COMPARISON OF SPECTRAL DATA SPACED IN TIME

SOURCE: Ref. 97

FIG. I-7 POWER SPECTRA OF RADIO STAR SCINTILLATION
Data-filtering limitations: Low frequency, LF ≈ 1/60 cps
High frequency, HF ≈ 1/2 cps

for the communications experiment--in addition to 4 meter antennas. Installation of a 700 Mc feed on the 8 meter and/or 16 meter antennas would then be justified.

The monitoring of the 100 Mc telemetry signal requires no modification to the satellite system. The 700 Mc telemetry signal requires an additional package in the satellite. Power supply requirements for the 700 Mc signal are reduced from those for the 2000 Mc communications signal in that RF power required is decreased by roughly 7 - 10 (equal beam application). Quite possibly the 700 Mc signal could be transmitted on the same satellite antennas as the 2000 Mc Communications frequency.

Numerous measurements of line of sight signal character through the ionosphere have been reported, especially for radio star measurements and for satellite telemetry signals.* The published data, however, does not reflect quantitative and detailed correlation of data. The simple correlation between fluctuation data and time plots of magnetic aspect angle ψ are significantly missing. Experimental limitations are generally vague and discussions of experimental accuracies are almost non-existent. In general, the transfer of information between uncoordinated experiments should be made with caution and only gross, if any, relations can be expected.

b. Backscatter Measurements

1) Blob Spectrum and Geometry Sensitivity

Measurement of backscatter using radar techniques has been a major tool in studying the irregular structure of the ionosphere. Measurements extend from ≈6 Mc. The anisotropic structure of the ionosphere causes backscatter signal character to be sensitive to aspect and magnetic field.

---

* References 85 and 98 contain extensive bibliographies where reference to individual publications can be obtained.

Table I-3

TYPICAL TELEMETRY PARAMETERS

	100-Mc Telemetry		700-Mc Telemetry		Communication Experiment
	Equal Beam	Broad Beam	Equal Beam	Broad Beam	
Radio Frequency (Mc)	100	100	700	700	2,000
Satellite Antenna Gain (db)	6	6	6	6	6
Ground Antenna Gain (db)	30	6	30	6	30
Ground Antenna Beamwidth (degrees)	3	~90	3	~90	3
Noise Temperature (OK)	30,000	30,000	600	600	600
Bandwidth	3 Kc	3 Kc	200 cps	200 cps	200 cps
Range (km)	30,000	30,000	30,000	30,000	30,000
17.5 mr Phase Accuracy					
Signal to Noise Ratio (db)	32	32	32	32	32
Satellite Transmitter Power	72 w	18 kw	4-5 w	1-1.25 kw	38 w
Reduced Phase Accuracy					
Signal to Noise Ratio (db)	12	12	12	12	12
Satellite Transmitter Power	0.7 w	179 w	40-50 mw	10-12.5 w	0.38 w

The required signal-to-noise ratio for phase-measuring systems is

$$S/N = 1/4\delta_{\alpha}^{2} \text{ for } S/N \text{ large}$$

where δ_{α} is the rms phase error in radians.
For a 17.5-mr phase accuracy,
the required S/N ratio is 32 db.

The scattering properties of ionospheric irregularities are given by:[99]

$$\sigma = 2^{3/2}\pi^3 \frac{\overline{\Delta N_e^2}}{\overline{N_e^2}} \frac{LT^2}{\lambda_N^4} e \frac{8\pi^2}{\lambda^2} (T^2 \cos^2 \psi + L^2 \sin^2 \psi) \sin^2 \frac{\theta}{2} \quad . \tag{I-11}$$

The angle θ is the angle between the direction of incidence and the direction of scattering ($\theta = \pi$ for backscatter along the direction of incidence). The scattering cross section is based upon a Gaussian space autocorrelation of $\overline{\Delta N_e}/\overline{N_e}$. The wavelength dependence of σ is determined by the blob dimensions, the aspect angle ψ and the scattering angle θ. Peak sensitivity of σ ($\theta = \pi$) occurs when $T = \lambda/2\sqrt{2\pi}$ for incidence transverse to the magnetic field, $\psi = 0^\circ$, and when $L = \lambda/4\pi$ for incidence parallel to the magnetic field, $\psi = 90^\circ$. The half-power width of blob filtering is roughly 0.7 to 2 times the ratio L(or T)/λ. Minimum wavelength is defined by the minimum blob dimension significant to the communication experiment, 4 meters, and is estimated as 25 meters (12 Mc) for $\psi = 0^\circ$ and 35 meters (8.5 Mc) for $\psi = 90^\circ$. These frequencies at times will not exceed the critical frequency of the F_2 ionospheric layer. Since scattering theory is not exact up to an order of magnitude, a decrease in wavelength can be envisioned--e.g., 3 to 6 meters.

The minimum-size blob character measured by backscatter should have low correlation with RF data. Thus, at best, backscatter would be compared with the RF data using threshold designations and histograms, indicating the thresholds of rapid fluctuations.

Transverse aspects, $\psi \approx 0^\circ$, are of primary importance. At these aspects ψ will not be zero at all angles of incidence for the radar beam (except for very narrow beams) and $(L/\lambda)\psi$ may predominate over T/λ in determining the magnitude of σ. Backscatter measurements at 400 Mc and 800 Mc using narrow-beam scanning antennas show a sensitivity to L/λ ratios of 10 to 20 at aspect angles $\psi < 17.5$ mr (Ref. 100).

2) Properties Measured

Properties of the ionosphere that are measured by backscattering (depending upon the radar wavelength, power, and resolution) can be classified as either regular fluctuating blob structure or disturbed phenomena--the aurora and ionospheric storms (Ref. 101).

Aurora and ionospheric storms are related to geomagnetic storms (and solar variations).

The primary particles causing the aurora are electrons and protons which radiate radio signals as they enter the atmosphere. Aurora echoes, whether discrete or diffuse, shift the frequency and broaden the spectrum of the echo signals. The spread in the spectrum is a noiselike broadening and is attributed to the random velocities of the auroral scatterers. The frequency shift is apparently caused by a mass motion of the aurora. The magnitude and sign of Doppler shifts are not always correlated with the measured changes in range of the auroral ionization as would be expected if the target were a moving sheet. The amplitude of auroral echoes fluctuates at a rapid rate following a Rayleigh probability distribution. The amplitude fluctuation and frequency spectrum are related. Rapid radio star scintillations in the direction of aurora have been observed. Due to absorption and increased fluctuation rates in aurora, radio star signals have disappeared for many minutes.

In periods of high geomagnetic activity ionospheric storms appear (Ref. 102). A longitude-independent or storm-time part shows a rise of the critical frequency of the F2 layer by some 10 percent at all latitudes throughout the storm but in moderate and high latitudes it is followed by a rapid decrease which troughs at about 30 percent some 24 hours after the storm commences. The general decrease in electron density has been seen at heights up to 1000 Km from the Alouette satellites. However, at latitudes above the auroral zone the trend is reversed and the storm causes a general increase of electron density with a maximum some three times normal at geomagnetic latitude 73^{0}. A remainder storm

component shows a diurnal variation in the critical frequency of the F2 layer increasing in amplitude with latitude and having a minimum soon after dawn and a maximum near midnight.

Whether ionospheric storms involve fluctuations that cause line-of-sight character to fluctuate has been neither experimentally verified nor disqualified.

3) Typical Backscatter Installations

Radar parameters for typical backscatter experiments are listed in Table I-4. A detailed description of the experiments can be found in the references.

As in the case of signal-monitoring experiments, radars with beamwidths equal to the beamwidth of the communication experiment receiving antennas, and slewed to common scattering domains, are preferable. Radars with equal beamwidths at HF require large antenna apertures, as indicated by the Stanford array (and by data in Table I-3).

These experiments using pulse techniques provide a measure of the range and location of scattering domains and a measure of the level of scattering. Measurement of Doppler rates would require a continuous-wave radar. Pulse radars would be better for ionospheric experiments than CW radars. Backscatter data from pulse radars is presented in a number of ways: range photos (A-scan), antenna-bearing-vs.-range photos (B-scan), and range-vs.-elevation photos. Range to scattering domains, measures of scattering level, and resolution and pointing of the radar are parameters especially important to a backscatter experiment in an ionospheric measurement program.

c. Sounding Measurements

Sounding measurements of the total interval reflection from ionospheric layers are used to map the electron density profile of the ionosphere. Ionograms also exhibit backscatter character, which is identified with the occurrence of spread-F and sporadic-E and other fine. irregular structure. Studies correlating spread-F and sporadic-E with line-of-sight amplitude fluctuations have been reported in the literature.

Table I-4

RADAR PARAMETERS FOR TYPICAL BACKSCATTER EXPERIMENTS

Frequency	15.3 Mc		
Transmitter Peak Power	100 ' w		
Antenna	8-element rhombic array, 2^0 beam-width in azimuth, slewable between 82^0 and 97^0 in one-degree steps, East-West looks, Size: 362 by 1600 feet.		
Receiver Bandwidth	3 kc		
Operating Pulse Length	0.4 msec		
Pulse Repetition Frequency	10 cps		
Source: Ref. 103			
Frequency	18 Mc		
Transmitter Peak Power	1 kw		
Yagi: Antenna Gain	6 db (assumed)		
Yagi: Antenna Beamwidth	≈90 degrees (assumed)		
Receiver Bandwidth	6 kc		
Operating Pulse Length	300 μsec		
Pulse Repetition Frequency	16-50 cps		
Source: Ref. 104			
Frequency (Mc)	216	398	780
Transmitter Peak Power (kv)	35	40	20
Dish: Antenna Gain (db)	30	36	42
Dish: Antenna Beamwidth (degrees)	6	3	1-1/2
Receiver Noise Figure (db)	8	5	8
Receiver Bandwidth (kc)	6		
Operating Pulse Lengths (μsec)	450-900		
Pulse Repetition Frequency (cps)	75-150		
Source: Ref. 105			

Sounders may be either fixed or swept in frequency. The fixed-frequency sounder is superior to the swept-frequency sounder to study the irregular structure of the ionosphere. With a fixed frequency, a rotatable, directional antenna can be used. A variable-frequency sounder using a directional antenna has the disadvantage of variable beamwidth. Antenna rotation with directional antennas has also the disadvantage of restrictions on rotating speeds if all frequencies are to be sensed in a given direction. A plan position indication (PPI) can be used with a rotating antenna. Only a range-vs.-time presentation (A-Scope) is available for a fixed antenna. The use of a fairly-high-gain directional antenna increases both the resolution and sensitivity of the sounder over another sounder using an antenna of lower gain.

The use of sounders in experimental studies would be useful in measuring the components of ionospheric storms. Sounders are limited, however, by broad beam coverage, lack of resolution, and ground clutter interference.

Sounders for correlation purposes have a number of other limitations:

(1) The sounding times when good correlation would be expected are limited (in zenith directions at experiment site).

(2) The extent of the sounding is limited--ground-based sounders are only good up to F-layer peak. Irregularities affecting phase fluctuations exist throughout the ionosphere.

(3) Spread-F exists in a number of modes, some of which are not directly associated with phase and amplitude fluctuations. Thus, sounding records require special analysis.

(4) A ground-based sounder by itself is unreliable for correlation purposes. The availability of long-term and numerous Alouette soundings when ground sounders, Alouette, and measurement satellite are in line is improbable.

A survey on the association between radio star scintillation and Spread-F and Sporadic-E phenomena has been discussed in Ref. 98. The following is quoted from pp. 38-64 of that reference:

"Most observers have expressed the opinion that the scintillation originates in the F2-region. A few interpret their results as indicating the E-region. For example, Dagg (Ref. 106), and Bolton, Stanley, and Slee (Ref. 107) have obtained a correlation with the occurrence of Sporadic-E, and Hartz (Ref. 108) has obtained a negative correlation. The diurnal variation for spread-F is similar to that for the scintillation index. A high correlation has been obtained in England. In Canada, Hartz reports insignificant correlation except for that between occurrence of scintillation and high F2 virtual heights, and even then the coefficient was small (+0.19). He suggests that, since the observations do not refer to the same latitude and the scales of the phenomena are quite different, little correlation may be expected."

d. Measurement of Magnetic Field (Refs. 109, 110)

The importance of the magnetic field in determining line-of-sight signal fluctuation character and backscatter characteristics has been pointed out. The gross structure of the magnetic field changes very slowly. At any given location the secular change usually amounts to less than 0.1 percent per year of the geomagnetic field over most of the earth's surface.

A minimum characterization of the ionosphere using the magnetic field would be to plot the angle ψ for the satellite trajectories. This information can be made available before the communication experiment is performed, by a knowledge of satellite trajectories and by using magnetic data obtained on isomagnetic maps (or by assuming a dipole model of the earth's field).

A close correlation has been found between the magnitude of the magnetic field and F-region drift velocities determined by measurements of radio star scintillation. The correlation is largest for the vertical H field. These correlations however are averaged over periods of hours. An occasional correlation between magnetic field and scintillation amplitude has also been found. Measurement of radio star installation at Accra, Ghana indicates that during sunspot maximum, the scintillation index is normal on quiet days but practically absent on magnetically

disturbed days (Ref. 111). This is a complete reversal of what happens at temperate latitudes, where scintillations are more probable on magnetically disturbed days.

A useful measure of the transient geomagnetic activity recorded by observatory magnetometers is available in the form of the "3-hourly range index" or K index--a figure indicating the magnetic character over a given 3-hour period. The K-index scale is defined for each observatory in terms of the amplitude of the magnetic variations during each 3-hour period. This index varies from 0 to 9, with K = 0 indicating magnetic quiet or calm, while K = 9 signifies great fluctuations in the geomagnetic field. The K index scales from the individual observatories are combined into a world-wide or planetary index, which is published periodically in a convenient form in the Journal of Geophysical Research.

The two most important transient variations in the magnetic field are the diurnal variations and the fluctuations produced during geomagnetic storms by hydromagnetic waves. The diurnal variation is reasonably predictable for a given location and usually involves field changes of the order of 0.1 percent of the total field. The diurnal variation is characterized by a minimum value for the field near local noon. Geomagnetic storms are disturbances that occur in the magnetic field with a frequency varying with the solar cycle. Storms are separated into two components, one dependent and one independent of longitude. A typical magnetic storm is illustrated in Fig. I-8. The prediction of magnetic storms can serve as a forewarning of large ionospheric effects.

A magnetometer (a small bar magnet suspended on a quartz fiber) is used to record the magnetic field at many magnetic observatories. This instrument does not fix the total field but measures variations in components. New instruments based on Larmar precession, in the magnetic field, of the magnetic moments of nuclei and atoms are in operation (Refs. 20, 113). These instruments are high-precision, and measurements may be transformed immediately into digital form and stored on magnetic tape for ease in data processing.

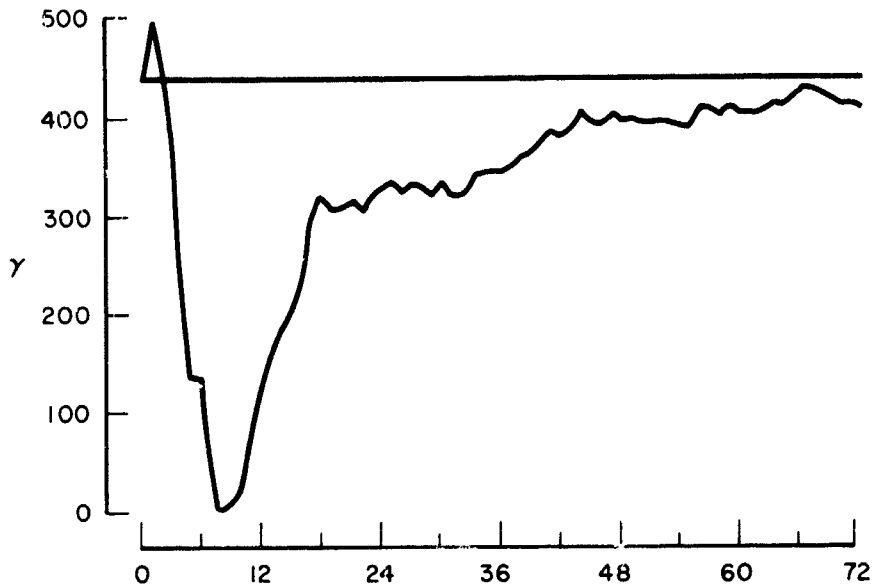

SOURCE: Ref. 112

NOTE: A large magnetic storm, the ...mponent. Storm time is started at the storm's sudden commencement. ...e initial phase is positive and 2 hr in length. The main phase with ...apid recovery lasts about 12 hr. The slow recovery takes several days. The scale at left is to show the magnitude of the variation.

TA-5067-48

FIG. I-8 TYPICAL IONOSPHERIC STORM RECORD

e. Reference to the Sun

The sun, being the primary source of energy for ionospheric irregularities, should be referenced in regard to time of day and sunspot cycle. Radar star scintillation has been observed to predominate at night (midnight) and at sunspot maximum. Reference to the sun can also be made using data from existing ionospheric facilities concerning solar flares, meteor activity, and cosmic noise levels.

The most useful index of solar activity is probably the sunspot number, which exhibits a strong 11-year variation. During sunspot maximum, solar flares occur with increased frequency. Some of these flares generate soft cosmic radiation and many of them emit radio noise.

f. Coordinated Measurements

Any extensive ionospheric measurement program would require coordinated measurements involving experimental sites removed from the receiving site used in the basic communication experiment. Most of the experimental sites that would be useful are in existence: world-wide geomagnetic and ionospheric sounding stations, solar observatories, ionospheric

research laboratories, etc. The use of data from these sites requires careful interpretation of the many parameters important to the characterization of the ionosphere as listed in Table I-1.

A coordinated program for measuring auroral characteristics has recently been reported (Refs. 114, 115). The program employed techniques of nuclear physics, of optical spectroscopy and of radio propagation using satellites, aircraft, and ground stations. This program is directed toward basic research on the understanding of ionospheric phenomena and coordinates measurements performed at earth orbiting observatories with measurements performed at aircraft and ground stations. In this program, a phase-coherent multifrequency beacon carried in the satellite and operating at 20, 40, and 120 Mc was monitored at ground and aircraft stations.

A relationship between disturbances in the ionosphere and in the troposphere should exist. Solar energy incident on the atmosphere creates disturbances in the ionosphere and subsequent changes in the meteorological characteristics of the troposphere. The processes involved are not fully understood and have not been measured. It is believed that disturbances measured in the ionosphere could be correlated with subsequent gross changes or disturbances in the troposphere. Monitoring of solar energy above the ionosphere would be especially important.

Appendix J*

NOISE-INDUCED ERRORS

* This appendix was prepared by W. H. Foy.

Appendix J

NOISE-INDUCED ERRORS

The voltage measurements of phase, path gain, and an angle of arrival obtained by a receiver of the recommended structure are given by Eqs. (5), Sec. III-E. In order to find quantitative estimates of the errors induced in these measurements by noise, we assume that the noise terms will be small and linearize to get

$$\varphi_M = \varphi + \varphi_{ns}$$

$$g_M \simeq K_o(1 + k_p) + K_o k_a + \frac{N_s}{a_o A_t}$$

$$\alpha_M \simeq \psi_a + \alpha_p - \alpha_e + \psi_a \cos(\varphi_\Delta - \varphi_{ns}) + \frac{2}{b_o A_p} n'_\Delta - \frac{\psi_a}{a_o A_p} N_s \qquad \text{(J-1)}$$

where

φ = Signal phase fluctuations

φ_{ns} = Phase variation induced on the sum signal by sum-channel noise, n_s

K_o = Average path gain

k_p = Fractional fluctuations in signal amplitude due to atmospheric path

k_a = Fractional fluctuations in transmitted signal amplitude

N_s = Error induced on the sum-channel envelope measurement by sum-channel noise, n_s

a_o = Summing hybrid voltage gain with respect to one pickup

A_t = Average transmitted signal amplitude

ψ_a = Average angle of arrival off boresight

α_p = Angle of arrival fluctuations caused by atmospheric path

α_e = Antenna-position-angle error

$\psi_\Delta = \psi_a + \alpha_p + \alpha_e$ = Angle off boresight

φ_Δ = Phase angle of difference channel with respect to sum channel

n'_Δ = Noise term resulting from mixing of difference-channel noise, n_Δ, with the phase-locked-loop VCO output, V_s

b_o = Voltage-per-unit-angle gain of the differencing hybrid with respect to one pickup

A_p = Amplitude of signal received by one pickup for arrival along axis of main lobe.

Start by examining the noise terms: φ_{ns}, N_s, and n'_Δ. Recall that we wrote the sum signal and difference signal as

$$\Sigma(t) = a_o A_p \cos(\omega_5 t + \varphi) + n_s$$

$$\Delta(t) = b_o A_p \Psi_\Delta \cos(\omega_5 t + \varphi + \varphi_\Delta) + n_\Delta$$

where ω_5 is the IF center-frequency. These will be narrow-band processes so we can write the noises in terms of in-phase and out-of-phase components,

$$n_s(t) = x_s(t) \cos \omega_5 t - y_s(t) \sin \omega_5 t$$

$$n_\Delta(t) = x_\Delta(t) \cos \omega_5 t - y_\Delta(t) \sin \omega_5 t \quad .$$

We assume that n_s, n_Δ are zero-mean normally distributed stationary random processes with power density spectra symmetrical about ω_5, and thus the correlation functions are related by

$$\langle n(t)n(t+\tau) \rangle = R(\tau)$$

$$= \langle x(t)x(t+\tau) \rangle = \langle y(t)y(t+\tau) \rangle$$

$$\langle x(t)y(t+\tau) \rangle = 0$$

where the $\langle\ \rangle$ brackets indicate ensemble averages. The sum signal can be written as

$$\Sigma(t) = (a_o A_p \cos \varphi + x_s) \cos \omega_5 t - (a_o A_p \sin \varphi + y_s) \sin \omega_5 t \quad .$$

Its envelope is

$$E(t) = \left\{(a_o A_p \cos\varphi + x_s)^2 + (a_o A_p \sin\varphi + y_s)^2\right\}^{1/2}$$

$$\simeq a_o A_p + x_s \cos\varphi + y_s \sin\varphi$$

and its phase is

$$\varphi_s(t) = \arctan \frac{a_o A_p \sin\varphi + y_s}{a_o A_p \cos\varphi + x_s}$$

$$\simeq \varphi + \frac{y_s}{a_o A_p} \cos\varphi - \frac{x_s}{a_o A_p} \sin\varphi$$

with approximations holding for large signal-to-noise ratios--i.e., when

$$\left|\frac{x_s}{a_o A_p}\right| \ll 1 \quad , \quad \left|\frac{y_s}{a_o A_p}\right| \ll 1 \quad .$$

Under the assumption that these approximations are valid, the phase error and envelope error induced by noise are

$$\varphi_{ns} \simeq \frac{y_s}{a_o A_p} \cos\varphi - \frac{x_s}{a_o A_p} \sin\varphi \qquad \text{(J-2)}$$

$$N_s \simeq x_s \cos\varphi + y_s \sin\varphi \quad . \qquad \text{(J-3)}$$

The noise n_Δ in the difference channel is mixed with V_s, the VCO output of the phase locked loop, where

$$V_s = \cos(\omega_5 t + \varphi + \varphi_{ns})$$

and the noise term in the mixer output is accordingly

$$n'_\Delta = 1/2\, x_\Delta \cos(\varphi + \varphi_{ns}) + 1/2\, y_\Delta \sin(\varphi + \varphi_{ns})$$

$$\simeq 1/2\, x_\Delta \cos\varphi + 1/2\, y_\Delta \sin\varphi \quad . \tag{J-4}$$

This approximation was obtained by neglecting noise-product terms such as $x_\Delta x_s$, $x_\Delta y_s$, etc. We shall be interested in the autocorrelation functions of φ_{ns}, N_s, and n'_Δ, and the form of the approximations in Eqs. (J-2) to (J-4) suggests that we consider the following function:

$$\begin{aligned} R_e(\tau) &= \Big\langle [x(t)\cos\varphi(t) + y(t)\sin\varphi(t)] \\ &\quad \times [x(t+\tau)\cos\varphi(t+\tau) + y(t+\tau)\sin\varphi(t+\tau)] \Big\rangle \\ &= \Big\langle x(t)x(t+\tau)\Big\rangle \Big\langle \cos\varphi(t+\tau)\Big\rangle \\ &\quad + \Big\langle y(t)y(t+\tau)\Big\rangle \Big\langle \sin\varphi(t)\sin\varphi(t+\tau)\Big\rangle \\ &= R(\tau)\Big\langle \cos[\varphi(t) - \varphi(t+\tau)]\Big\rangle \quad . \end{aligned}$$

The noise-term statistics thus depend on the statistics of the signal phase fluctuations; these statistics are to be determined by the proposed experiment. In order to go farther it is necessary to make some plausible assumption about the phase fluctuations; we suppose, therefore, that $\varphi(t)$ is statistically stationary and normally distributed with variance σ^2_φ and covariance function

$$\rho_\varphi(\tau) = \frac{1}{\sigma^2_\varphi} \Big\langle [\varphi(t) - \langle\varphi\rangle][\varphi(t+\tau) - \langle\varphi\rangle] \Big\rangle$$

and then compute

$$\Big\langle \cos[\varphi(t) - \varphi(t+\tau)] \Big\rangle = \exp\Big\{-\sigma^2_\varphi[1 - \rho_\varphi(\tau)]\Big\} \quad .$$

The variance of the error term, $R_e(o)$, will not depend on the phase fluctuations. Further, $R_e(\tau)$ should not depend strongly on the shape of

ρ_φ; almost all reasonable choices for an analytical approximation to $\rho_\varphi(\tau)$ should be equally valid, and so we choose

$$\rho_\varphi(\tau) = \frac{1}{\sigma_\varphi^2} \ln \left[1 + \left(e^{\sigma_\varphi^2} - 1 \right) \exp\left(-k \frac{\tau^2}{T_\varphi^2} \right) \right]$$

$$k = k(\sigma_\varphi) = \ln\left(e^{\sigma_\varphi^2} - 1 \right) - \ln\left[\exp\left(\frac{\sigma_\varphi^2}{e} \right) - 1 \right]$$

where the effective bandwidth of $\rho_\varphi(\tau)$ is given by

$$BW_\varphi = \frac{2}{\pi T_\varphi} \text{ cps} \quad .$$

Plots of $\rho_\varphi(\tau)$ for various values of σ_φ^2 are shown in Fig. J-1, which also shows that ρ_φ goes in the limit as $\sigma_\varphi^2 \to 0$ to the more conventional Gaussian shape. The ease of integration of exp (ρ_φ) and the fact that ρ_φ approximates the Gaussian shape quite closely are the reasons for assuming this form. We also need to choose a plausible form for $R(\tau)$, the noise autocorrelation function; since this will be set by the IF filter shape, we take it to be Gaussian:

$$R(\tau) = \sigma^2 \exp\left(- \frac{\tau^2}{T^2} \right)$$

where σ_s^2 , σ_Δ^2 = noise power in sum and difference channels, respectively, and the effective noise bandwidths of sum and difference channels are $2/\pi T_s$ and $2/\pi T_\Delta$, respectively. Now we can take the Fourier transform of $R_e(\tau)$ and so find the power density spectrum of the noise-induced error term.

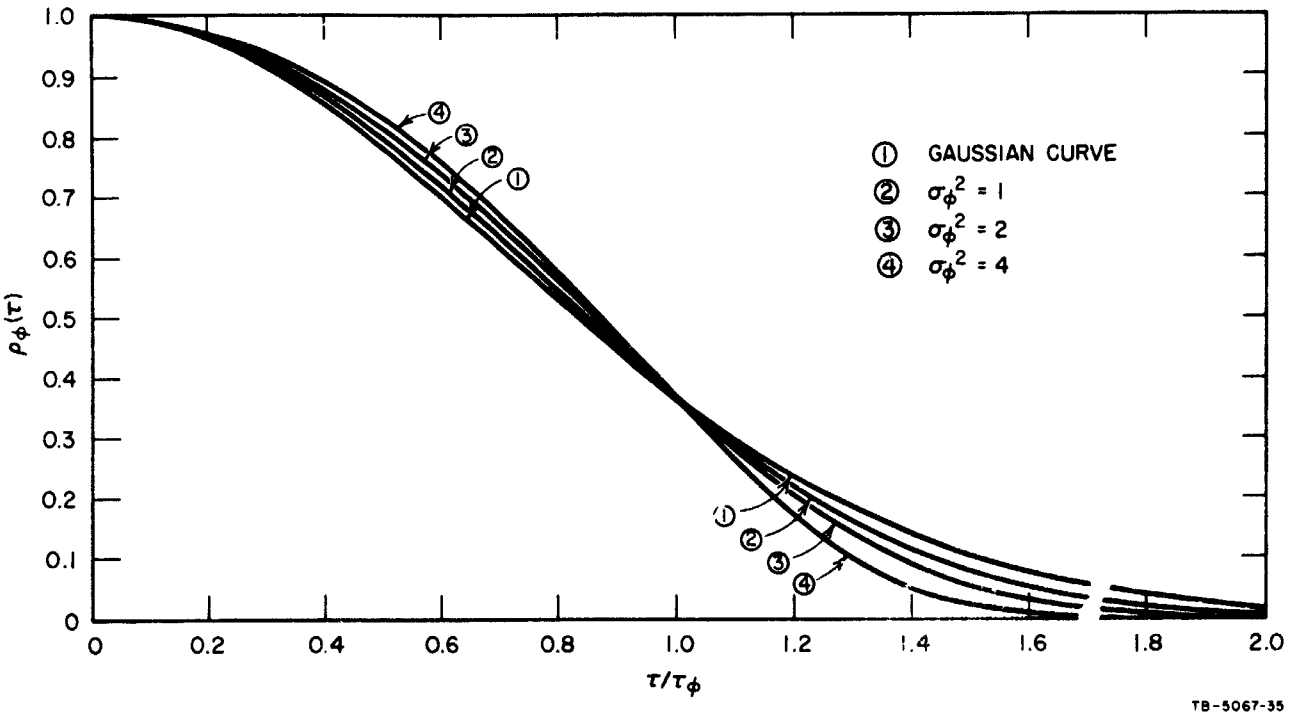

FIG. J-1 ASSUMED PHASE AUTOCORRELATION FUNCTION

$$G_e(f) = \int_{-\infty}^{\infty} d\tau R_e(\tau) \exp - (i2\pi f\tau) = G_e(f; \sigma^2, f_n)$$

$$= \frac{\sigma^2}{\sqrt{\pi} f_n} \left[e^{-\sigma_\varphi^2} \exp\left(- \frac{f^2}{f_n^2} \right) + \left(1 - e^{-\sigma_\varphi^2} \right) c_k \exp\left(- \frac{c_k^2 f^2}{f_n^2} \right) \right]$$

$$c_k = \left[1 + k \left(\frac{f_n}{f_\varphi} \right)^2 \right]^{-1/2} \qquad \text{(J-5)}$$

where

$$f_{ns} = \frac{1}{\pi T_s}; \quad f_{n\Delta} = \frac{1}{\pi T_\Delta}; \quad f_\varphi = \frac{1}{\pi T_\varphi} \quad .$$

For small σ_φ^2 or small f_φ, $G_e(f)$ approaches the simple Gaussian power density spectrum of the noise alone; the effect of increasing σ_φ^2 or f_φ is to spread the spectrum of the noise-induced error without changing its total power. This is illustrated in Fig. J-2, which shows G_e for $\sigma_\varphi^2 = 1$ and different values of the f_φ/f_n bandwidth ratio, and in Fig. J-3, where the bandwidth ratio is 1/4 and σ_φ^2 is varied. The noise-induced error terms of Eqs. (J-2) through (J-4) have power density spectra that can now be written in terms of this G_e spectrum as follows:

$$\text{Spectrum of } \varphi_{ns} \simeq \frac{G_e(f;\ \sigma_s^2,\ f_{ns})}{\left\langle a_o^2 A_p^2 \right\rangle} \qquad \text{(J-6)}$$

$$\text{Spectrum of } N_s \simeq G_e(f;\ \sigma_s^2,\ f_{ns}) \qquad \text{(J-7)}$$

$$\text{Spectrum of } n_\Delta' \simeq 1/4\ G_e(f;\ \sigma_\Delta^2,\ f_{n\Delta}) \quad . \qquad \text{(J-8)}$$

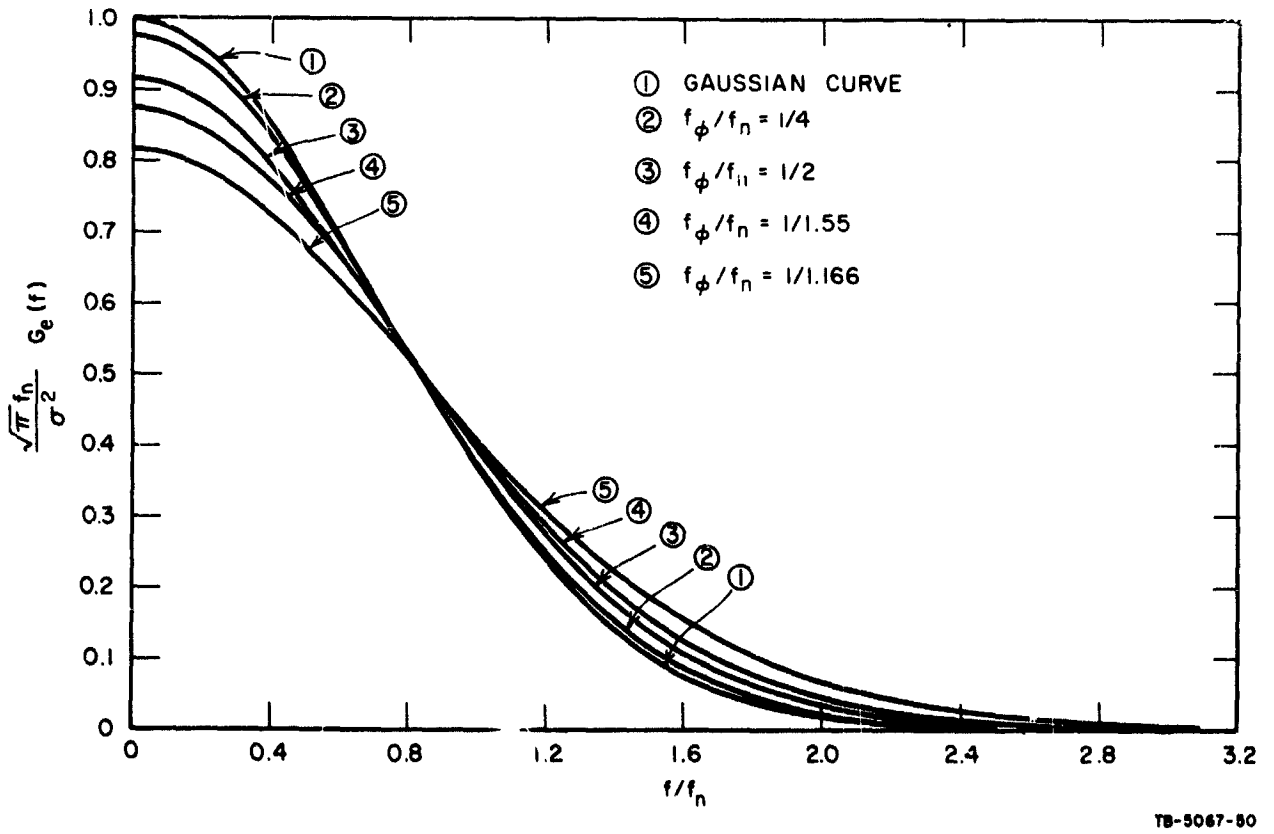

FIG. J-2 NOISE-INDUCED ERROR SPECTRA, $\sigma_\phi^2 = 1$

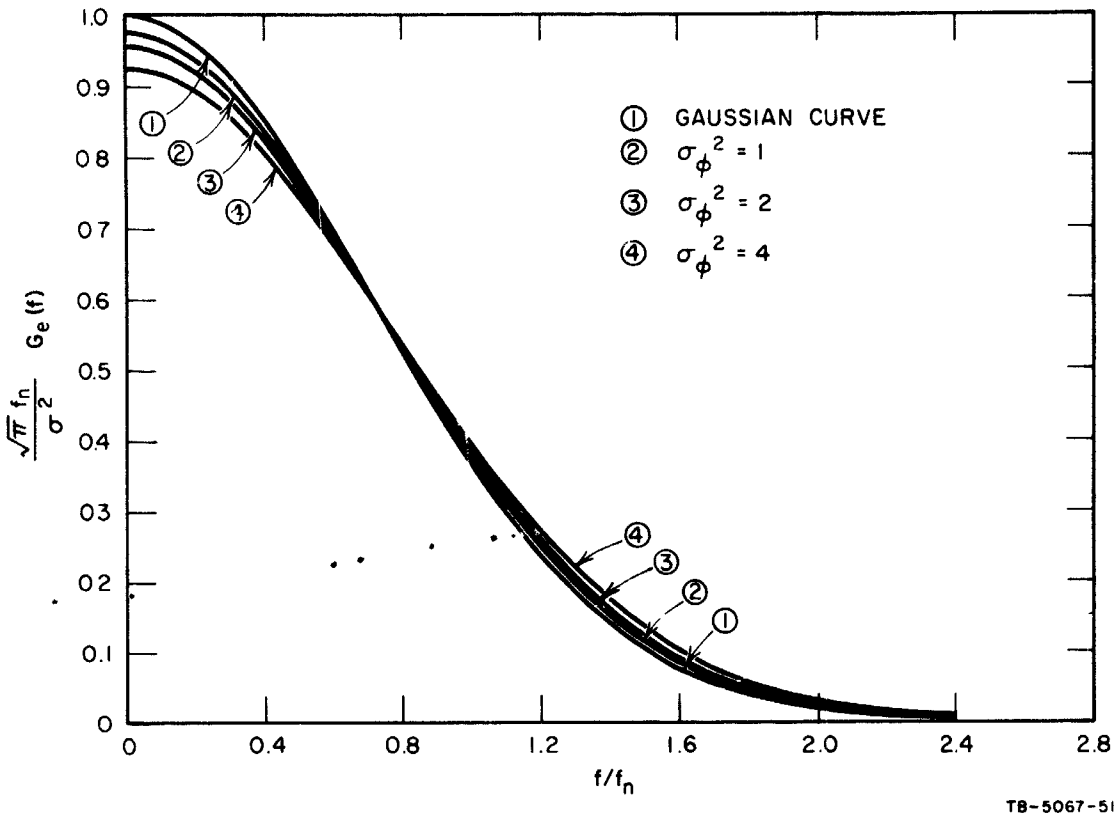

FIG. J-3 NOISE-INDUCED ERROR SPECTRA, $f_\phi/f_n = 1/4$

The corresponding mean-squared-error values are readily obtained directly from the autocorrelation functions. We assume that the noises in the sum and difference channels are statistically independent, and so obtain the following expressions for the noise-induced error terms in Eq. (J-7) when only first-order quantities are retained:

$$\left\langle \varphi_{ns}^2 \right\rangle \simeq \frac{\sigma_s^2}{a_o^2 \left\langle A_p^2 \right\rangle} = \frac{8}{a_o^2 \eta_s} \qquad \text{(J-9)}$$

$$\left\langle \frac{N_s^2}{a_o^2 A_t^2} \right\rangle = \frac{\sigma_s^2}{a_o^2 A_t^2} = \frac{8K_o^2}{a_o^2 \eta_s} \qquad \text{(J-10)}$$

$$\left\langle \left(\frac{2n'_\Delta}{b_o A_p} - \frac{\psi_a N_s}{a_o A_p} \right)^2 \right\rangle = \frac{\sigma_\Delta^2}{b_o^2 \langle A_p^2 \rangle} + \frac{\psi_a^2 \sigma_s^2}{a_o^2 \langle A_p^2 \rangle} = \frac{8}{b_o^2 \eta_\Delta} + \frac{8\psi_a^2}{a_o^2 \eta_s}$$

$$\left\langle \cos^2 (\varphi_\Delta - \varphi_{ns}) \right\rangle \simeq 1$$

where K_o is the average path voltage gain and η_s and η_Δ are ratios of maximum-available sum-channel signal power to the noise power of the sum and difference channels, respectively. These are basic design expressions. They relate noise-induced mean-squared errors to antenna signal-to-noise ratios and show how much rms error is reduced by an increase in transmitter power or a decrease in receiver noise temperature. Equations (J-9) and (J-10) define the noise for phase and path-gain measurements. For angle-of-arrival measurements we carry the analysis a bit farther; define the mean-squared noise-induced angle error as follows:

$$\sigma_m^2 = \left\langle \left[\psi_a \cos (\varphi_\Delta - \varphi_{ns}) + \frac{2}{b_o A_p} n'_\Delta - \frac{\psi_a}{a_o A_p} N_s \right]^2 \right\rangle$$

$$\simeq \frac{8}{b_o^2 \eta_\Delta} + \psi_a^2 + \frac{8\psi_a^2}{a_o^2 \eta_s} \quad .$$

It is convenient to normalize with respect to the antenna beamwidth, so we define α_n to be the angle between the maximum and the first null of the main lobe of one of the pickups. Then,

$$\frac{\sigma_M^2}{\alpha_n^2} \simeq \frac{8}{(\alpha_n b_o)^2 \eta_\Delta} + \frac{\psi_a^2}{\alpha_n^2} \left(1 + \frac{8}{a_o^2 \eta_s} \right) \quad . \qquad \text{(J-11)}$$

Useful values for a_o and b_o can be obtained by referring to the discussion of antenna patterns in Appendix F. It is assumed that the

pattern of a single pickup is $\frac{\sin x}{x}$ in shape, and that reasonable choices of offset angles lead to

$$a_o = 2.020$$

$$\alpha_n b_o = 3.845 \quad .$$

Thus, for small average angle errors (i.e., $\frac{\psi_a^2}{\alpha_n^2} \ll 1$), the mean-squared normalized noise-induced angle error will be

$$\frac{\sigma_M^2}{\alpha_n^2} \simeq \frac{0.540}{\eta_\Delta} \qquad \text{(J-12)}$$

which gives an estimation of this contribution to angle-of-arrival error.

REFERENCES

BLANK PAGE

REFERENCES

1. P. G. Smith, et al., "Analytical Study to Define an Experimental Program for the Evaluation and Optimization of Multi-Element Large Aperture Arrays," Final Report, Contract NAS 1-3780, Research Triangle Institute, Durham, North Carolina (October 1964).

2. "Investigation and Study of a Multi-Aperture-Antenna System," Final Report, Contract NAS 5-3472, Electronic Communications, Inc., Timonium, Maryland (April 1964).

3. R. B. Battelle, Ed., "Feasibility Analysis of a Deep-Space Receiving Terminal Array of Large Equivalent Aperture," Final Report, Contract NAS 1-3075, Stanford Research Institute, Menlo Park, California (May 1964).

4. J. E. Alder, et al., "The Design of an Experiment to Determine the Limitations Imposed on a Multiple-Aperture-Antenna System by Propagation Phenomena," Third Quarterly Report, Contract NAS 5-3974, Stanford Research Institute, Menlo Park, California (March 1965).

5. C. H. Dawson, "The Design of an Experiment to Determine the Limitations Imposed on a Multiple-Aperture-Antenna System By Propagation Phenomena," First Quarterly Report, Contract NAS 5-3974, Stanford Research Institute, Menlo Park, California (October 1964).

6. J. H. Bryan, et al., "The Design of an Experiment to Determine the Limitations Imposed on a Multiple-Aperture-Antenna System by Propagation Phenomena," Second Quarterly Report, Contract NAS 5-3974, Stanford Research Institute, Menlo Park, California (December 1964).

7. J. M. Stephenson, et al., "Design Criteria for a Large Multi-Purpose Tracking Antenna," Technical Report 1368, Philco Corporation, Western Development Laboratories, ASTIA No. AD 267147 (January 1961).

8. "Antenna Systems Prototype Research Project 854," Project Report, Rohr Corporation (1963).

9. M. Ryle, "A New Radio Interferometer and Its Application to the Observation of Radio Stars," Proc. Royal Society (London), Series A, Vol. 211, No. 1106, pp. 351-375 (March 6, 1952).

10. H. Penfield, "A Phase Tracking Interferometer," Proc. IRE 46, 1, pp. 321-325 (January 1958).

11. R. H. Dicke, "The Measurement of Thermal Radiation at Microwave Frequencies," Rev. Sci. Instr., 17, 7, pp. 268-275 (July 1946).

12. C. H. Mayer, "Improved Microwave Noise Measurements Using Ferrites," IRE Trans., MTT-4, 1, pp. 24-28 (January 1956).

13. R. E. McGavin, "Survey of the Techniques for Measuring the Radio Refractive Index," Tech. Note 99, National Bureau of Standards (May 1962).

14. R. T. H. Collis, F. G. Fernald, and M. G. H. Ligda, "Laser Radar Echoes From a Stratified Clear Atmosphere," Nature 203 (4951), pp. 1274-1275 (September 19, 1964).

15. R. T. H. Collis and M. G. H. Ligda, "Laser Radar Echoes from a Clear Atmosphere," Nature 203 (4944), pp. 508 (August 1, 1964).

16. K. A. Norton, et al., "An Experimental Study of Phase Variations in Line-of-Sight Microwave Transmissions," pp. 51-58, NBS Monograph 33, U. S. Government Printing Office (November 1961).

17. M. C. Thompson, Jr., H. B. Jones, and A. W. Kirkpatrick, "An Analysis of Time Variations in Tropospheric Refractive Index and Apparent Radio Path Length," J. Geophys. Res., 65, pp. 193-201 (January 1960).

18. A. P. Deam and B. M. Fannin, "Phase-Difference Variations in 9,350 Mc Radio Signals Arriving at Spaced Antennas," Proc. IRE 43, 9, pp. 1402-1404 (October 1955).

19. J. W. Herbstreit and M. C. Thompson, "Measurements of the Phase of Radio Waves Received Over Transmission Paths With Electrical Lengths Varying as a Result of Atmospheric Turbulence," Proc. IRE 43, 9, pp. 1391-1401 (October 1955).

20. G. S. Walters and P. D. Francis, "A Nuclear Magnetometer," Journal of Sci. Instruments, 35, pp. 88-93 (March 1958).

21. C. L. Hosler, and L. A. Gamage, "Cyclone Frequencies in the United States for the Period 1905 to 1954," Monthly Weather Review 84, 11, pp. 388-390 (1956).

22. C. H. Reitan, "Distribution of Precipitable Water Vapor Over the Continental United States," Bull. Amer. Meteor. Soc. 41, 2, pp. 79-87 (1960).

23. T. Fujita, "Index to the NSSP Surface Network," National Severe Storms Project Report No. 6, U. S. Weather Bureau, 32 pp. (1962).

24. D. C. Hogg and W. W. Mumford, "The Effective Noise Temperature of the Sky," Microwave Journal 3, 3, pp. 80-84 (March 1960).

25. H. C. Ko, "The Distribution of Cosmic Radio Background Radiation," Proc. IRE 46, 1, pp. 208-215 (January 1958).

26. G. H. Ball and D. J. Hall, "ISODATA, a Novel Method of Data Analysis and Pattern Classification," Technical Report, Stanford Research Institute, Menlo Park, California (April 1965).

27. R. H. Merson, "The Motion of a Satellite in an Axi-Symmetric Gravitational Field," The Geophysical Journal of the R.A.S., Vol. 4 (1961).

28. George Veis, "Geodetic Uses of Artificial Satellites," Smithsonian Contributions to Astrophysics, Vol. 3, No. 9 (1960).

29. J. P. Vinti, "Zonal Harmonic Perturbations of an Accurate Reference Orbit of an Artificial Satellite," Journal of Research N.B.S., Sec. B, Mathematics & Mathematical Physics, Vol. 67B, No. 4 (October-December, 1963).

30. D. Brouwer, "The Motion of a Particle with Negligible Mass Under the Gravitational Attraction of a Spheroid," Astronomical Journal, Vol. 51 (1946).

31. P. Musen, "Application of Hansen's Theory to the Motion of an Artificial Satellite in the Gravitational Field of the Earth," Journal of Geophysical Research, Vol. 64 (1959).

32. Samuel Pines, "Minivar, a Real Time Orbit Determination Program Based on the Kalman Filter," Analytical Mechanics Associates, Inc., on March 29-30, 1965.

33. Donald Proctor, "The Development of the GSFC Minivar Program," Sperry Gyroscope Co., presented at the GSFC-Contractor Astrodynamics Meeting at GSFC on March 29-30, 1965.

34. "Tropospheric and Ionospheric Refraction Effects," Smyth Research Associates, Report No. SRA - 91; ASTIA No. 217406.

35. V. A. Counter and T. P. Riedel, "Calculation of Ground-Space Propagation Effects at Radio Frequencies," Lockheed Report LMSD - 2461.

36. Space Programs Summary No. 37-25, Vol. III, Jet Propulsion Laboratory (January 31, 1964).

37. A. Cohen, "Antenna-Radome Profits," Microwave Journal (June 1964)

38. M. E. Tuiri, "Radio Astronomy Receivers," IEEE Trans., MIL-8, 3-4, pp. 264-272 (July-October 1964).

39. R. Manasse, "Maximum Angular Accuracy of Tracking a Radio Star By Lobe Comparison," IEEE Trans., AP-8, No. 1, pp. 50-56 (January 1960).

40. R. E. Hiatt and K. M. Siegle, "Forward Scattering by Coated Objects Illuminated by Short Wavelength Radar," Proc. IRE 48, 9, pp. 1630-1635 (September 1960).

41. M. I. Skolnik, An Introduction to Radar Systems (McGraw-Hill Book Co., New York, New York, 1962).

42. K. M. Siegel, "Bistatic Radars and Forward Scattering," National Aeronautical Electronics Conference Proceedings (1958).

43. H. G. Booker, The Use of Radio Stars to Study Irregular Refraction of Radio Waves in the Ionosphere," Proc. IRE 46, 1, pp. 298-314

44. A. R. Thompson and R. S. Colvin, "Experimental Investigation of the Coherence Distance of the Atmosphere for Microwaves," Final Report, Radioscience Laboratory, Stanford University, Stanford, California, Contract Number AF 19(604)-7249 (March 26, 1965).

45. S. L. Zolnay, "A Study of Scintillations at 2 KMc/sec Utilizing Solar Radio Emission," Report 1072-5, Ohio State University Research Foundation, Columbus, Ohio, Contract No. AF 30(602)-2166 (17 August 1962).

46. J. L. Pawsey and R. N. Bracewell, Radio Astronomy (Oxford; Clarendon Press, 1955).

47. R. N. Bracewell, "Radio Astronomy Techniques," Handbuch Der Physik, Vol. LIV, pp. 42-129 (1962).

48. R. S. Lawrence, "Investigation of the Perturbations Imposed Upon Radio Waves Penetrating the Ionosphere," Proc. IRE 46, 1, pp. 315-320 (January 1958).

49. E. U. Condon and H. Odishaw, Handbook of Physics, pp. 6-80 (McGraw-Hill Book Co., New York, N. Y., 1958).

50. J. Aarons, W. R. Barron, and J. P. Castelli, "Radio Astronomy Measurements at VHF and Microwaves," Proc. IRE 46, 1, pp. 325-333 (January 1958).

51. J. Aarons and J. P. Castelli, "Simultaneous Scintillation Observations on 1300 Mc and 3000 Mc Signals Received During the Solar Eclipse of October 2, 1959," IRE Trans., AP-9, 4, pp. 390-395 (July 1961).

52. E. J. Blum, J. F. Denisse, and J. L. Steinberg, "Radio Astronomy at the Meudon Observatory," Proc. IRE 46, 1, pp. 39-43 (January 1958).

53. J. L. Steinberg and J. Lequeux, Radio Astronomy (McGraw-Hill Book Co., Inc., New York, N. Y.).

54. H. A. von Biel, "Tropospheric Phase Fluctuations at S-Band," Technical Documentary Report No. RADC-TDR-63-408, Cornell Aeronautical Laboratory (October 1963).

55. W. O. Mehuron, "Passive Radar Measurements at C-Band Using the Sun as a Noise Source," Microwave Journal, Vol. V. No. 4, pp. 87-94 (April 1962).

56. G. Swarup, "Studies of Solar Microwave Emission Using a Highly Directional Antenna," Scientific Report No. 13, Contract AF 18(603)-53 Radioscience Laboratory, Stanford Electronics Laboratories (February 6, 1956).

57. L. Colin, "Limitations on Radio Receiver Sensitivity Imposed by Extra-Terrestrial Noise," Part I--Solar Radiation, Technical Memorandum RADC-TM-56-30, Rome Air Development Center (August 1956).

58. H. G. Weiss, "The Haystack Microwave Research Facility," IEEE Spectrum 2, 2, pp. 50-69 (February 1965).

59. R. S. Allen, J. Aarons, and H. Whitney, "Measurements of Radio Star and Satellite Scintillations at a Subauroral Latitude," IEEE Trans., MIL-8, 3 & 4, pp. 146-'55 (July-October 1964).

60. H. C. Ko, "Amplitude Scintillation of Radio Star at Ultra-High Frequency," Proc. IRE 48, 11, pp. 1871-1880 (November 1960).

61. W. A. Flood, "Project Wideband Final Report," RADC-TDR-64-461, CAL Report No. UB-1363-P-6, Cornell Aeronautical Laboratory, Inc., Buffalo, New York (November 1, 1964).

62. M. Schwartz, Information Transmission, Modulation and Noise, pp. 410-413 (McGraw-Hill Book Company, Inc., New York, N. Y., 1959).

63. W. A. Edson, "Noise in Oscillators", Proc. IRE 48, 8, pp. 1454-1466 (August 1960).

64. General Radio Experimenter, Vol. 38, No. 6 (June 1964).

65. R. J. Carpenter, et al., "A Prototype Vapor Frequency Standard," Proc. IRE, Trans. PGI-9, 2, pp. 132-135 (September 1960).

66. E. J. Baghdady, R. N. Lincoln, and B. D. Nelin, "Short-Term Frequency Stability: Characterization, Theory, and Measurement," Proc. of the Symposium on the Definitions of Short-Term Frequency Stability, Goddard Space Flight Center, Greenbelt, Maryland (November 1964).

67. M. J. Beran and G. B. Parrent, Jr., Theory of Partial Coherence pp. 7-11 (Prentice-Hall, Inc. Englewood Cliffs, New Jersey, 1964).

68. M. Born and E. Wolf, Principles of Optics (MacMillan Company, New York, N. Y., 1964).

69. L. V. Blake, "Tropospheric Absorption and Noise Temperature for a Standard Atmosphere," presented at the Antennas and Propagation International Symposium, Boulder, Colorado (July 1963).

70. D. C. Hogg and R. A. Semplak, "The Effect of Rain and Water Vapor on Sky Noise at Centimeter Wavelengths," Bell System Tech. J., Vol. 40, pp. 1331-1348 (September 1961).

71. K. L. S. Gunn and T. W. R. East, "The Microwave Properties of Precipitation Particles," Quart. J. Roy. Meteorol. Soc., Vol. 80, pp. 522-545 (October 1954).

72. N. E. Feldman, "Estimates of Communication Satellite System Degradation Due to Rain," Publication P-3027, The RAND Corporation, (October 1964).

73. A. S. Dennis and F. G. Fernald, "A Preliminary Analysis of Forward-Scatter Signals from Showers," Research Memorandum 5, Contract NASr-49(02), Stanford Research Institute, Menlo Park, California (October 1963).

74. A. S. Dennis, "The Scattering of SHF Radio Waves by Hail and Wet Snow," Final Report, Contract NASr-49(02), Stanford Research Institute, Menlo Park, California (June 1964).

75. J. S. Marshall and W. Hitschfeld, "Interpretation of the Fluctuating Echo from Randomly Distributed Scatterers. Part I," Canadian J. Phys., Vol. 31, pp. 962-995 (1953).

76. A. D. Whellon, "Relation of Radio Measurements to the Spectrum of Tropospheric Dielectric Fluctuations," J. Appl. Phys. 28, pp. 684-693 (June 1957).

77. H. C. van de Hulst, Light Scattering by Small Particles, pp. 28-39 (John Wiley and Sons, Inc., New York, N. Y., 1957).

78. B. J. Mason, The Physics of Clouds, pp. 84-99 (The Clarendon Press, Oxford, England, 1957).

79. R. C. McCarty and G. W. Evans II, "On the Estimation of the Marginal Probability Distribution from a Finite Single Sample Function," SRI Project 3857, Contract SD-103, Under ARPA Order 281-62, Project Code 7400, Stanford Research Institute, Menlo Park, California (November 1964).

80. O. Buneman, "Excitation of Field Aligned Sound Waves by Electron Streams," Phys. Rev. Letters, Vol. 10, pp. 285-287 (1963).

81. D. T. Farley, Jr., "Two-Stream Instability as a Source of Irregularities in the Ionosphere," Phys. Rev. Letters, Vol. 10, pp. 279-282 (1963).

82. D. T. Farley, Jr., "A Plasma Instability Resulting in Field Aligned Irregularities in the Ionosphere," J. Geophys. Res., 68, pp. 6083-6097 (1963).

83. A. Hewish, "The Diffraction of Radio Waves in Passing Through a Phase-Changing Ionosphere," Proceedings of the Royal Society, Vol. 209, pp. 81-96 (1951).

84. A. Hewish, "The Diffraction of Galactic Radio Waves as a Method of Investigating the Irregular Structure of the Ionosphere," Proceedings of the Royal Society, Vol. 214, pp. 494-514 (August-October, 1952).

85. H. G. Booker, "Use of Radio Stars to Study Irregular Refraction," Proc. IRE, Vol. 46, No. 1, pp. 298-314 (January 1958).

86. L. A. Chernov, "Wave Propagation in a Random Medium" (transl.), (McGraw-Hill Book Company, Inc., New York, N. Y., 1960).

87. D. A. deWolf, "Point-to-Point Wave Propagation Through an Intermediate Layer of Random Anisotropic Irregularities: Phase and Amplitude Correlation Functions," Trans. IEEE, AP-13, 1, pp. 48-52 (January 1965).

88. H. G. Booker and W. E. Gordon, "A Theory of Radio Scattering in the Troposphere," Proc. IRE 38, 4, pp. 401-412 (April 1950).

89. A. D. Wheelon and R B. Muchmore, "Line-of-Signt Phenomena--II. Scattered Components," Proc. IRE, 43, 10, pp. 1450-1458 (October 1955).

90. A. Maxwell and M. Dagg, "A Radio Astronomical Investigation of Drift Movements in the Upper Atmosphere," Philosophical Magazine, Vol. 45, PP. 551-569 (January-June, 1954).

91. R. A. Silverman, "Remarks on the Fading of Scattered Radio Waves," IRE Trans., AP-6, pp. 378-380 (October 1958).

92. R. A. Silverman and M. Balser, "Statistics of Electromagnetic Radiation Scattered by a Turbulent Medium," Phys. Rev. 96, 3, pp. 560-563 (November 1954).

93. R. A. Silverman, "Fading of Radio Waves Scattered by Dielectric Turbulence," J. Appl. Phys. 28, No. 4, pp. 506-511 (April 1957).

94. A. D. Wheelon, "Relation of Radio Measurements to the Spectrum of Tropospheric Dielectric Fluctuations," J. Appl. Phys. 28, 6, pp. 684-695 (June 1957).

95. R. B. Muchmore and A. R. Wheelon, "Frequency Correlation of Line of Sight Signal Scintillations," Trans. IEEE, AP-11, 1, pp. 48-51 (January 1963).

96. D. A. deWolf, "Propagation Through Random Anistropic Irregularities," Trans. IEEE, AP-13, 1, pp. 48-52 (January 1965).

97. S. Gruber, "Statistical Analysis of Radio Star Scintillation," J. Atmos. and Terrest. Phys. 20, pp. 59-71 (1961).

98. J. Aarons, Ed., Radio Astronomical and Satellite Studies of the Atmosphere (North Holland Publishing Company, Amsterdam, 1963).

99. H. G. Booker, "A Theory of Scattering by Non-Isotropic Irregularities with Application to Radar Reflections from the Auroras," J. Atmos. and Terrest. Phys. 8, pp. 204-221 (1956).

100. R. L. Leadabrand, "Electromagnetic Measurements of Auroras," in Auroral Phenomena--Experiments and Theory, M. Walt, Ed. (Stanford University Press, Stanford, California, 1965).

101. Proc. IRE 47, 2 (February 1959).

102. J. H. Piddington, "Geomagnetic Storms, Auroras, and Associated Effects," Space Science Reviews, Vol. 3, pp. 724-780 (1964).

103. J. R. Hofman, "Some Characteristics of F-Layer Irregularities Deduced from Backscatter Soundings Made with a Slewable Antenna Having a Two-Degree Azimuthal Beamwidth," Technical Report No. 36, Radioscience Laboratory, Stanford University, Stanford, California (26 June 1961).

104. B. R. Clemesho, "An Investigation of the Irregularities in the F-Region Associated with Equatorial Type Spread-F," J. Atmos. and Terrest. Phys. 26, pp. 91-112 (1965).

105. R. I. Presnell, R. L. Leadabrand, A. M. Peterson, R. B. Dyce, J. C. Scholobohm, and M. R. Berg, "VHF and UHF Radar Observations of the Aurora at College, Alaska," J. Geophys. Research 64, 9, pp. 1179-1190 (September, 1959).

106. M. Dagg, Diurnal Variations of Radio Star Scintillations, Spread F, and Geomagnetic Activity," J. Atmos. and Terrest. Phys. 10, pp. 204-214 (1957).

107. J. G. Bolton, O. B. Slee, and G. J. Stanley, Australian J. Phys., Vol. A-6, p. 434 (1953).

108. T. R. Hartz, Defense Research Board, Radio Physics Laboratory Project Report No. 23-2-3 (1958).

109. F. S. Johson, Ed., Satellite Environment Handbook (Stanford University Press, Stanford, California, 1961).

110. D. P. LeGalley and A. Rosen, Eds., Space Physics (John Wiley and Sons, Inc., New York, N. Y., 1964).

111. G. S. Kent and J. R. Koster, Nature, Vol. 191, p. 1083 (1961).

112. L. J. Cahill, Jr., "The Geomagnetic Field," in Reference 108, pp. 301-349.

113. K. A. Ruddock, "Optically Pumped Rubidium Vapor Magnetometer for Space Experiments," Proc. Second International Space Science Symposium, North Holland Publishing Company, Amsterdam, pp. 692-700 (1961).

114. J. E. Evans, "Coordinated Measurements on Auroras," in Auroral Phenomena--Experiments and Theory, M. Walt, Ed. (Stanford University Press, Stanford, California, 1965).

115. R. E. Meyerott and J. E. Evans, "Auroral Measurements and Upper Atmospheric Physics," AIAA Journal 2, 7, pp. 1169-1174 (July 1964).

STANFORD RESEARCH INSTITUTE

MENLO PARK
CALIFORNIA

Regional Offices and Laboratories

Southern California Laboratories
820 Mission Street
South Pasadena, California 91031

Washington Office
808–17th Street, N.W.
Washington, D.C. 20006

New York Office
270 Park Avenue, Room 1770
New York, New York 10017

Detroit Office
1025 East Maple Road
Birmingham, Michigan 48011

European Office
Pelikanstrasse 37
Zurich 1, Switzerland

Japan Office
Nomura Security Building, 6th Floor
1–1 Nihonbashidori, Chuo-ku
Tokyo, Japan

Retained Representatives

Toronto, Ontario, Canada
Cyril A. Ing
67 Yonge Street, Room 710
Toronto 1, Ontario, Canada

Milan, Italy
Lorenzo Franceschini
Via Macedonio Melloni, 49
Milan, Italy